COMPUTATIONAL APPROACHES TO OPTICAL MODELING NIR RADIATION PHENOMENA IN SLURRIES WITH ARBITRARY SOLIDS CONCENTRATION PROFILES

By

REZA MOHAMMADI ZIAZI

Bachelor of Science in Aerospace Engineering

Tehran Polytechnic University

Tehran, Iran

2009

Submitted to the Faculty of the
Graduate College of the
Oklahoma State University
in partial fulfillment of
the requirements for
the Degree of
MASTER OF SCIENCE
December, 2012

COMPUTATIONAL APPROACHES TO OPTICAL MODELING NIR RADIATION PHENOMENA IN SLURRIES WITH ARBITRARY SOLIDS CONCENTRATION PROFILES

Thesis Approved:

Dr. Frank W. Chambers

Thesis Advisor

Dr. Andrew S. Arena

Dr. Bruce J. Ackerson

ACKNOWLEDGEMENTS

It is like a dream come true for me pursuing my Master's degree in Mechanical engineering and doing critical research here in a fast developing school like Oklahoma State University. However, this dream was made true only because of continuous support, motivation, and kindness I received from my helpful advisor Dr. Frank W. Chambers.

I have had the opportunity and pleasure of working with and learning from an advisor who not only cares to share his precious knowledge, but also motivates the students with his endless new ideas. I express my gratitude toward Dr. Chambers who I have been most comfortable consulting and asking questions. His helpful suggestions and comments will remain with me for my life. So thank you, Dr. Chambers, for everything.

I would like to thank Dr. Andrew S. Arena Jr. and Dr. Bruce J. Ackerson for being in my thesis committee, guiding me through preparation of this thesis, and during my master's. Also, I appreciate their time and patience for reviewing the thesis document and attending my examination.

I also thank my lab partner Shyam, and thank all my friends specially Mehran, Amir, Nabil, and Hossein who supported me during the preparation of this thesis. I

Studying away from your family sometimes can get really hard, but one thing made it easier for me; my parents and my sister. Thank you for your love, support, and kindness.

Acknowledgements reflect the views of the author and are not endorsed by committee members or Oklahoma State University.

Name: REZA MOHAMMADI ZIAZI

Date of Degree: DECEMBER, 2012

Title of Study: COMPUTATIONAL APPROACHES TO OPTICAL MODELING NIR RADIATION PHENOMENA IN SLURRIES WITH ARBITRARY SOLIDS CONCENTRATION PROFILES

Major Field: MECHANICAL ENGINEERING

Abstract:

Near infrared sensors project light into particle-laden flows and use light returned via diffuse reflectance and scattering phenomena to measure solids concentration and chemical composition. An important measurement parameter is the depth of penetration returning the light used in the measurements. In this work several optical modeling approaches were evaluated for predicting the depth of penetration of near-infrared (NIR) light in slurry flow in a pipe. The goal was to find a model suitable for predicting the depth of penetration for slurry flows with arbitrary solid concentration profiles. The models which were considered fall in two categories; continuum and discontinuum theories. Continuum models consider the sample as one integral layer while discontinuum models divide the sample into layers one particle thick. Hence, discontinuum models are well suited for slurries with varying concentrations which can be adjusted layer by layer. The continuum theories used were Shuster, Kubelka–Munk, radiation transfer, three flux, and diffusion. The discontinuum theories used were plane parallel layer, assembly of sheets, and representative layer theory. Discontinuum models were applied to cases which included uniform, hypothetical, and realistic concentration profiles predicted using Computational Fluid Dynamics (CFD). For the CFD predictions, the slurry was xylene liquid and ADP solid flowing in a 50.8 mm diameter horizontal pipe at mean velocities between approximately 1.8 and 4.0 m/s, corresponding to Reynolds numbers between $1.2x10^5$ and $2.8x10^5$. Monodisperse spherical slurry particles with diameters ranging from 38 to 150 microns were considered with solid volume fractions ranging from 5% to 35%.

Numerical versions of the optical models were created for the theories using MATLAB R2012a. Each model simulated the passage of NIR radiation through the sample based on light fractions. Light fractions were computed for each layer of the discontinuous models, and the depth of penetration was evaluated. Validation was performed with results in the literature for optical experiments for similar cases. Comparisons of the results suggest that the discontinuum theories are more accurate than continuum theories for these applications, with representative layer theory used with Stokes formula providing the best results. It is concluded that the models are suitable for predicting the depth of penetration for NIR measurements.

TABLE OF CONTENTS

Chapter Page

Chapter Page

LIST OF TABLES

LIST OF FIGURES

Figure Page

Figure Page

Figure Page

NOMENCLATURE

A	Absorption fraction
a	Symbolic representation of the fraction of incident light absorbed by a layer
A(R,T)	Absorption/remission function
B	Apparent remission coefficient
b	Symbolic representation of fraction of incident light remitted from the surface of a particle
C	Concentration of particles inside the slurry sample computed from CFD
$(bd)_i$	Symbolic representation of remission power of the material comprising particles in layer i
D	Diffusion coefficient in radiative transfer model
d	The thickness of a sample or a layer of sample through which light is passing
d_i	Symbolic representation of thickness of a particle inside a layer known as i
E	Irradiance
E_a	Absorption coefficient obtained from radiative transfer equation
E_s	Scattering coefficient obtained from radiative transfer equation
g	Cosine of scattering angles
$(E_a + E_s)$	Extinction coefficient based on terminology of radiative transfer equation
I	Intensity of incident light inside the sample

I_0	Intensity of incident radiation
J	Intensity of reflected beam inside the sample
J_0	Intensity of reflected beam out of sample
K	Absorption coefficient
k	Absorption power of material
K_i	The effective absorption coefficient for
L	Radiance
m	Mass of the particle or layer of sample
N	Refractive index
Q	The radiant energy in Joules
r	Reflectance of a layer inside the material
r_i	Reflectance of a particle inside a layer of material
r_0	Reflectance from a surface of material based on Fresnel law
R	Remission fraction
R_∞	The reflectance of a layer so thick that further increase in thickness fails to change the reflectance
s	Kubelka-Munk scattering coefficient
s_p	Symbolic representation of cross sectional surface fraction that belongs to particles

S_i	Cross sectional surface in a sample comprised of particle type i
t	Transmission fraction of a layer of material
v_p	Volume fraction of particles
v_0	Void fraction
Vol	Volume of a particle or a layer of the sample
w_p	Weight fraction of a particle
X	Distance from the edge of the sample

Greek symbols

α	Absorption coefficient used in Mie, and three flux approximation and the
α	Absorption probability for representative layer theory
β_i	Fraction of incident light absorbed by a layer
Δ	Sum of fractions of light inside a sample used in Stokes formula
ε	Fraction of radiation absorbed per unit pathlength in the sample
μ	The cosine of the angle between the direction of solid angle and the surface normal of the sample
Ω	Solid angle
Ω	Ratio of fractions of light inside a sample used in Stokes formula

Φ	Photon fluence rate or radiant flux with the unit of Joules per second
Ψ	A parameter for calculating integral fractions of light inside a sample used in Stokes formula
ρ_i	Symbolic representation of density of particle type i
ϑ	The angle of incidence with the surface normal
σ	Fraction of radiation scattered per unit pathlength in the sample
ξ	The average path length of light when passes through

Subscripts

i	Type of particles
d	Properties of a layer of thickness d
f	Of the fluid
p	Of the particles
j	Number of particles in a layer
s	Measured quantity
1	Initial conditions; initial fraction of light for discontinuum theories and lower boundary of integration for continuum theories

CHAPTER I

INTRODUCTION AND BACKGROUND

1.1 Introduction

One of the main goals of the thesis is to answer the fundamental question "How far does light penetrate into the slurry fluid flow in a pipe during Near-Infrared (NIR) irradiation by a NIR sensor?" For a particular case, a quick answer to this question would be to run an experiment. Moreover, an experiment requires an equipped laboratory with imaging instruments, probes inside the pipe, and other facilities to visualize the flow field. This might not be affordable. Since numerical approaches allow solutions for many cases, it is preferred to use a computational approach to simulate the travel of light inside the pipe using the newest and the most efficient theoretical approaches. By choosing the numerical method, a model is built based on the characteristics of the fluid at rest. Then the results from the model can be compared to the NIR diffuse reflectance theories. Calculating the penetration depth requires answers to related questions: "What is the concentration of particles inside the field and how is it going to be predicted through optical theories?", and "What is the light distribution in terms of fractions of the incident radiation inside the particulate slurry?" There are related works in the literature, however, most of them are experimental techniques to measure concentrations of slurries either online or offline using optical NIR sensors. However, almost none of the theoretical approaches have been applied to predict light interactions with particles inside a slurry sample. It means that the theories found in the literature have not yet been applied to the case of a slurry sample. However,

experimental methods to model light interaction with slurries are available in the literature. Study and research in the field of optical size and concentration monitoring of slurries have been performed using analytical methods, which required some parameters from experiments. But, there are approaches that do not need any experiment. Those methods use experiment-dependent models which require some input parameters that must be provided through an experiment. In this thesis, the details of both of these two types of methods along with their experimental requirements, assumptions, and mathematical models will be reviewed.

1.2 Motivation

In recent years, near-infrared (NIR) optical modeling has gained extensive acceptance in different scientific and industrial areas by means of its advantages over other analytical techniques. This type of spectroscopy is prominent because of its ability to record spectra for solid and liquid samples. Modern applications of near-infrared use it to measure the composition of unknown samples using techniques invented by scientists at the United States Department of Agriculture (Workman and Weyer, 2008). It has become a very popular technique in a wide variety of industries due to its speed, precision, broad applicability and avoidance of extraneous chemicals. It is widely used in agricultural, chemical, pharmaceutical, combustion products, textile and many other industries. Moreover, advances in instrumentation have caused the manufacture of spectrophotometers capable of rapidly providing spectra that are flexible enough for use in different applications. NIR spectroscopy requires some input parameters such as the intensity of radiation, the fractions of diffuse light in the medium, and the characteristics of the slurry fluid. A wide range of theories has been developed to support experimental capabilities of methods that use NIR diffuse reflectance and transmittance.

There are a number of distinct mathematical models capable of characterizing near-infrared light diffusion in one-phase mediums or one phase with a mixture of two or more types of different components. These models are different, however, most of them implement the fundamental technique

of applying near-infrared radiation to monitor different materials. The applications of NIR spectroscopy are summarized in Table 1.1.

Table 1.1 Description of different fields and applications of near-infrared radiation has already been used in the previous works

Field	Applications	Model/Technique
Clinical sector	Human blood cells, In vivo imaging Human body tissues, Optical topography of brain	Monte Carlo Simulation, Diffusion approximations, Steady state diffusion theory, Transport theory, Addding doubling method, Delta-Eddington approximation,
Astronomical sector	Astrophysics, Detection of infrared galaxies, Interstellar molecules	Dual field interferometry
Agriculture	Agricultural products monitoring, Analysis of food crops, Analysis of processed food like baking products, and Analysis of non-food agricultural products like paper, wool, etc.	Representative layer theory, Kubelka-Munk theory, Diffuse reflectance theory, Schuster's theory
Remote monitoring	NIR spectroscopic imaging, Hyperspectral imaging in the remote investigation of plants and soils	Experimental techniques to collect data from airplanes or satellites to investigate the soil chemistry on the ground
Material Science	Film thickness measurements	Near-infrared measurement in the diffuse reflectance mode
Particle measurement	Slurry flow, granular flow, fluidized beds, powders and ground materials	Continuum theories of diffuse reflectance such as classical Kubelka-Munk theory, Beer-Lambert's law, etc., Monte-Carlo Simulation
Industrial uses	Study of industrial chemicals, Process control applications, Rapid laboratory measurements, Real-time online analyses	Particle-Laden slurry transport in mines, Process control for food, agricultural, combustion, textile, and pharmaceutical products,

Before examining the techniques shown in Table 1.1 in detail consider a brief introduction to NIR models. Based on the foundations of near-infrared models there are two different paths indicated by these theoretical treatments: continuum theories and discontinuum theories. These two types of theories are separated by the two distinct types of mathematical models on which they are based. For example, the theory of representative layers is applicable in many industrial processes. Among the

theories of diffuse reflectance, the representative layer theory is the latest efficient method to model near-infrared phenomena inside particulate, turbid, in vivo, powdered, and generally uniform and non-uniform mediums using discontinuous mathematics. As it was depicted in the Table 1.1, none of the near-infrared theoretical treatments have analyzed slurries with discontinuum mathematical techniques. Reviewing the literature, discontinuous mathematical methods have not yet been used for slurries. Continuum theories are imperfect due to their weakness in exhibiting the light interactions with particles in real non-uniform mixtures that scatter light and are not continuous. On the other hand, the only method that addresses light propagation inside a slurry has been found in the work of Rabhi, Mason, Roze, Dussouillez, and Bottero (2010) that uses an experimental-theoretical algorithm and some parameters such as refractive index to find particle size distribution (PSD), and the slurry concentration to be fed into a simulation. Hence, their approach is not pure theoretical. Meeten and Wood (1993) introduced another approximation for measuring the diffuse reflectance of fluids using optical fiber methods, but the classic Kubelka-Munk theory is applied to interpret the experimental data. Kubelka-Munk theory is a powerful tool to describe light diffusion but is only applicable to continuous mediums: it underestimates the optical properties of a real discontinuous sample. This introduction presents the approaches that are going to be discussed in the present thesis. In the following chapters the latest approach has been used to characterize the optical properties of slurries that naturally have discontinuity in their composition.

1.3 Background

Near-infrared technology and slurry mixtures are two separate academic, technological, and industrial areas for which at first it may seem very difficult to find a connection, but after a brief introduction one may see the relationship between them. Hence, studying an overview about the Near-Infrared and the slurry is essential to reading and understanding this thesis.

1.3.1 Near Infrared Technology

Near-infrared is the electromagnetic radiation with a spectrum of wavelengths just beyond visible light. Near-infrared is a part of infrared radiation which usually is divided into three spectral regions: near-, mid- and far-infrared. However, another categorization is done by Center for Measurement, Vegetation, and Health [MVH] (2006) at the University of New Hampshire: the infrared region is divided into five parts: near, short-wave, mid-wave, long-wave, and far-infrared . This spectrum is shown in Figure 1.1.

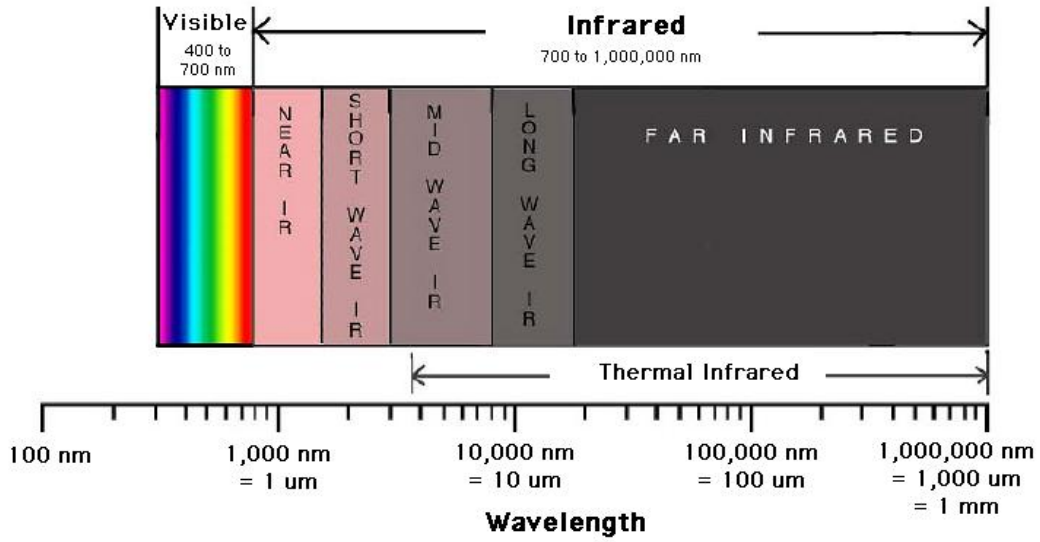

Figure 1.1 Schematic representation of divisions of the infrared electromagnetic spectrum. The near infrared region corresponds to a wavelength range of between 700 and 2500nm. The mid-infrared region is further divided into short, mid and long wave infrared and corresponds to a wavelength range of 2500 – $5x10^4$ nm. Finally the far infrared region corresponds to a wavelength range of $5x\ 10^4$ – $1x10^6$ nm. (MVH, 2006)

The boundaries between near, mid- and far-infrared regions are not agreed upon and can vary. The main factor that decides which wavelengths are included in each of these three infrared regions is the type of detector technology used for gathering infrared beams of light. The infrared region of light has longer wavelengths than visible light, making it invisible to the human eye, however, the near-infrared spectrum has shorter wavelengths with proximity to visible light. Spectroscopy is defined as the study

of the wavelength spectrum of radiated energy interacts with matter – it is transmitted, reflected or absorbed. Although a theoretical analysis underlies NIR spectroscopy, it is mostly known as an experimental branch of NIR technology. Theoretical techniques have been developed to interpret the data gathered from the spectrum. Modeling is absent in the spectroscopic techniques. On the other hand, theories of diffuse reflectance provide an opportunity to model the near-infrared penetration of light inside a sample. Recently, more sophisticated theorems have been applied to model the near-infrared phenomena.

The earliest application of Near-Infrared spectroscopy goes back to the 1800's, when organic compounds were investigated by NIR photography. Thus, the first application of NIR technology was studying chemicals in compounds. In the 1940s, the availability of new commercial instruments led to one of the first industrial applications of NIR in chemical and polymer industries. Until that time applications were confined to academic or research projects (Workman and Weyer, 2008). Norris in USDA in 1949 was the first person who began to apply NIR in the food industries. During the 1950s and 1960s, progress in this field of chemical monitoring became stagnant, however, diffuse reflection theories propelled NIR spectroscopy to a wide range of applications in agriculture, pharmaceuticals, and many other industries. With the advent of new instrumentation and methods, the interest in NIR industrial applications has become greater. Infrared technology is not limited to physical applications monitoring materials in samples; it can be applied in astrophysics and astronomical observations. NIR observations have been made from ground based observatories since the 1960's. They are done in much the same way as visible light observations for wavelengths less than 1 micron, but require special infrared detectors beyond 1 micron. Mid- and far-infrared observations can only be made by observatories which can get above our atmosphere because space-borne telescopes are very sensitive to heat. The reason is that the telescope itself has a certain temperature and continually radiates heat that would interfere with the measurements taken by a NIR sensor. Far infrared waves are thermal, therefore, we experience this type of infrared radiation every day in the form of heat. The heat that we

feel from sunlight, a fire, an oven or a warm coffee is infrared. These observations require the use of special cooled detectors containing crystals like germanium whose electrical resistance is very sensitive to heat. Despite all of the mid- and far infrared applications, NIR is more popular among industries.

Industries strive to produce quality commercial products at the lowest cost and in the shortest time. Introducing analytical methods that offer technical and cost-saving advantages over conventional approaches can lead to business-related improvements in the manufacture of chemical products. In recent years, near-infrared (NIR) spectroscopy has been incorporated into several analytical protocols for obtaining qualitative and quantitative information on incoming materials, mixtures, and products. One of the most important applications in industries is slurries. NIR spectroscopy is used in these industries to monitor composition and control the process. Therefore, NIR light and slurries are connected through this widespread application.

1.3.2 Slurries

Despite much progress in techniques of conveying materials discovered in mines, the semi-industrial transport of minerals out of mines had been an issue until the early sixteenth century, when a solution was found. Hydraulic conveying over short distances for alluvial mineral separation was documented in the sixteenth century. The hydraulic term refers to the technique of transporting those minerals; the process that is performed with the stream of fluid inside pipelines. The particulate medium by which the hydraulic transport of minerals took place has an academic name; a slurry. Particle-laden slurry transport through pipelines is one of the important industrial applications of slurries.

The scientific interpretation of the word introduces the slurry as a solid-liquid mixture. The slurry has been categorized in the group of multiphase mixtures. Another meaning states a thick suspension of solids in a liquid. Therefore, this type of flow can be categorized in the group of dispersed phase and separated flows. When there is more than one phase participating in a fluid

mixture, the combination is known as a multiphase mixture. As shown in Table 1.2, there are four types of multiphase flows (Crowe, 2012). Due to the presence of two phases, this flow is more complex than single phase flows. Two-phase flows consist of discrete elements such as droplets in a gas or solids in a liquid. Thus, they are not attached to each other, therefore, in a separated flow, two phases are dispersed by a line of contact.

Table 1.2 Examples of single and multi-component, multiphase fluids

	Single Component	**Multi-component**
Single-phase	Water, Oxygen	Air, Emulsions
Multiphase	Steam-Water, Freon-Freon Vapor	Air-Xylene, Slurry

Slurries are applicable in many engineering, industrial, chemical, and fossil energy areas like transport of bulk quantities of materials such as coals and ores or flow of mud. The significance of particle deposition results from its key role in industrial processes such as filtration, separation, particle transport, combustion, air and water pollution, metallurgical processes and many others (Hossain, Naser, and Imteaz, 2011). The fluid that carries the particles through the pipe may be Newtonian or non-Newtonian, and usually influenced by turbulence, drag, hindered velocity, virtual mass effects, phase interaction, crossing-trajectories, and particle inertia (Chen, 1994). Moreover, the process of transporting solid-liquid mixtures through pipelines is common in the mining and petrochemical industries. Furthermore, turbulent slurry flows with high solid volumetric concentrations are an important part of many chemical or mineral applications. In addition, the need to measure the pressure drop and concentration profiles in pipelines made researchers study this kind of fluid and build more accurate models (Lahiry and Ghanta, 2010). Slurry transportation in the horizontal direction may be classified into three major flow patterns: (1) pseudo-homogeneous slurry (or homogeneous); (2) heterogeneous and sliding bed slurry (or moving bed), and (3) saltation and stationary bed slurries, as described by Ling et al. (2003). A pseudo-homogeneous slurry is a pattern

in which particles are uniformly distributed along the cross-section of the pipe since the velocity is so high to prevent the particles from accumulating in the bottom of pipe cross-section due to gravity effects. This process is practical since the high flow rates prevent the particles from falling due to the influence of gravity. However, heterogeneity happens in a slurry flow when the flow rate cannot overcome the transportation of the particles to the lower part of the cross-section. By further decreasing the velocity, the particles will accumulate in the bottom of the pipe cross-section. This region is called a moving bed layer (Ling et al., 2003). This phenomenon occurs in the saltation and stationary bed flows. In conclusion, when one thinks about the combination of a liquid with insoluble solids inside, there are many different examples.

1.4 Statement of the Problem

The main goal can be expressed in this form: the near-infrared region of a light beam is chosen to penetrate into a slurry for detecting the slurry particles by sensing the fractions of light in each section through the sample depth, with reflectance or transmittance to a NIR sensor. The problem is to estimate the fractions of light at each distance inside the sample to answer the question of the depth inside the slurry at which the particles will be detected by the sensor. Therefore, the fractions of light at each possible point inside the sample must be known to estimate the layer within the media where the light is able to be transmitted to the detector or is blocked by the heavy concentration of particles.

As it is depicted in Figure 1.2, when the generated light reaches the surface of the medium, a portion is transmitted into the sample, and the rest is reflected. Then the transmitted light goes through the sample, which may be represented as many layers of particulate slurry. The reflectance, transmittance, and abrorptance occurs in each layer, until the remaining transmitted portion of light is detected by the detector. This geometry can be shown with another configuration where the detector is located in the same place as the generator, detecting the reflectance of the light instead of transmission.

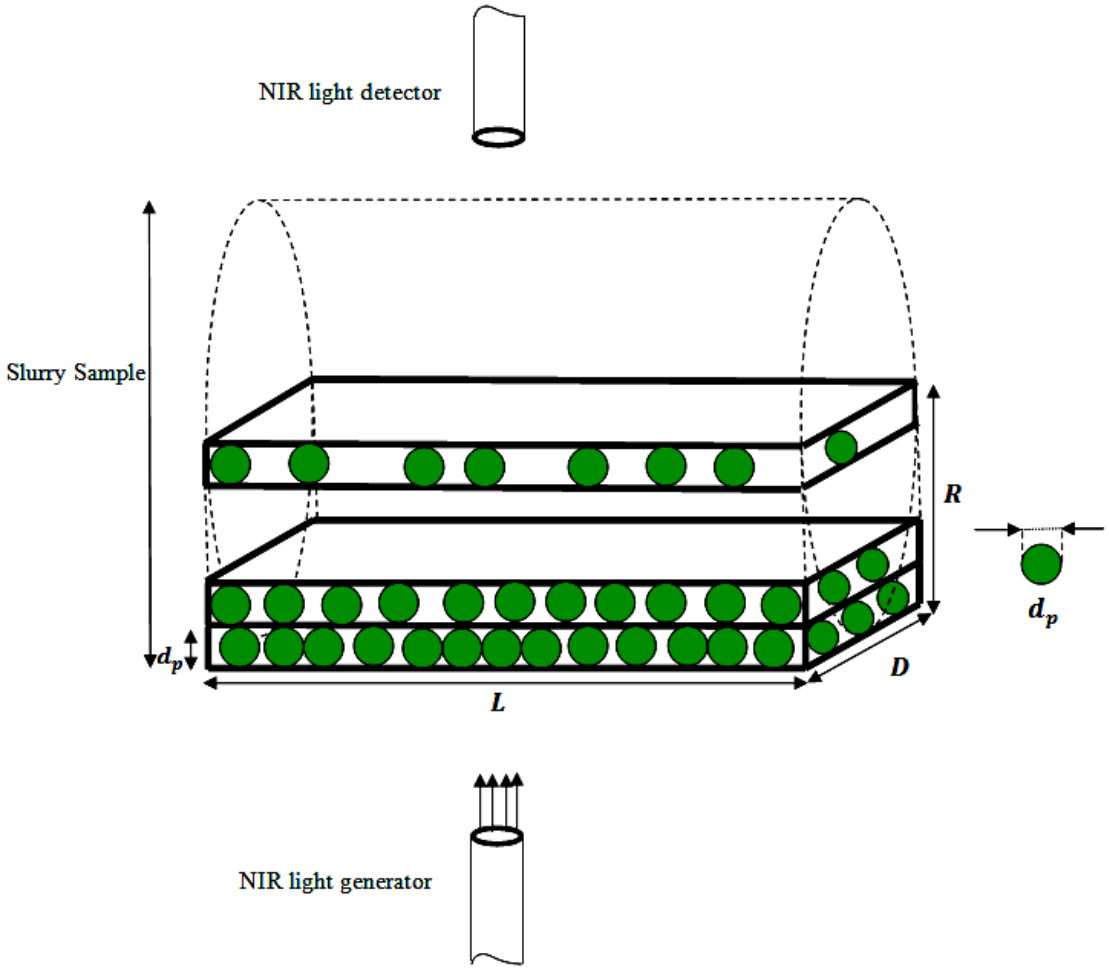

Figure 1.2 The geometry of the light generator, detectors, and the sample

Now, the problem is to predict the amount of the light through the sample and the penetration depth of light inside the slurry. Transmission, reflection, and absorption inside the sample gives us information about the concentration of particles inside the sample. Moreover, it can predict the shape of particle accumulation in each layer inside the slurry.

1.5 Goals

The primary goal of this thesis is to permit accurate estimates of how much light is detectable by the sensor, and what portion of the sample contributes to the signal. Answering these two fundamental

questions will describe the sample from a spectroscopic perspective. This information will help us choose the best location for installing the NIR sensor outside of an slurry sample.

Tools for modeling the NIR light interactions with particles inside a slurry are theories of diffuse reflectance. These theories were applied to the problem with their limitations and assumptions considered. The purpose for using different theories to model the optical interaction is to compare them and find the most computationally efficient approach for modeling the NIR diffuse reflectance phenomena in slurries. Moreover, the problem is divided into two groups of NIR diffuse reflectance theorems based on their mathematical treatments: continuous and discontinuous functions. Each of these two groups requires different arrangements for the configuration of the sample. Therefore, they have different results. Continuum theories aim to find the light fractions integrally inside the sample, so the accumulative fractions are estimable without using any other theory in any distance from the boundaries of the sample where the light first was encountered. This means that continuum theories directly calculate the cumulative fractions of light in each distance from the edge of the sample, and the methodology of these theories is different from discontinuum ones in which the light fractions are estimated locally, so one must combine them with another method to find light fractions at each depth inside the sample. The details of these methods will be discussed in the following chapters. The purpose of implementing discontinuous theories is to find the same fractions but locally. This gives us an opportunity to have an estimation about optical properties of each possible point and layer inside the sample when the effects of other layers are not present. It means that the reaction of each particular layer to the incident beam is considered in isolation and only based on the local configuration of the particles inside each particular layer of the sample.

The main goal is achieved by considering these objectives and steps: **(i)** for continuum mathematical approaches such as plane parallel mathematics, Kubelka-Munk theory, Schuster's theory, three flux approximation, and diffusion theory, and **(ii)** for discontinuum mathematical

approaches such as the theory for plane parallel mathematics, assembly of sheets, representative layer theory, and combined representative layer theory and the Stokes formulas.

In order to meet the goals discussed above, the following tasks must be done: **(i)** reviewing all of the theoretical approaches appropriate for the case of this problem in terms of assumptions, limitations, advantages, etc, **(ii)** implementing the theories by developing a mathematical model based on them, and **(iii) c**omparing the results of the models.

The first task will be done in Chapter 2, where continuum and discontinuum diffuse reflectance theories are introduced. In Chapter 3 the models created based on these two groups of theories are discussed respectively according to the mathematics of the methods. In Chapter 4, the results are compared with each other. Hence, the most compatible model will be introduced based on the results. Finally, in Chapter 5, the conclusions and recommendations are presented.

CHAPTER II

PAST CONTRIBUTIONS

2.1 Introduction

Optical methods for modeling NIR radiation phenomena inside a medium, whether it is composed of one-phase continuous components, one-phase powdered sample, or multiphase elements are available in the literature which will be addressed in this chapter. Although, this work connects the fluid dynamics of a slurry flow to an optical phenomena that is the interaction of light with particles in a slurry sample, most of the work has been concentrated on optical theories to model the NIR radiation inside a slurry. Hence, this chapter is dedicated to surveying the theoretical methods pertaining to optical modeling inside slurries. Before describing the approaches, one needs to know what has been done in past contributions to NIR technology in analyzing samples. Then, acquiring a preliminary knowledge about the definitions of fundamental expressions and terms that are related to optical models and are mostly used in this thesis is essential. After introducing the optical nomenclature, NIR optical methods are reviewed. These approaches are gathered by reviewing these major concepts in the available literature: near-infrared spectroscopy, online and offline measurement of slurries, NIR diffuse reflectance and transmittance, particle size analysis, slurry concentration measurements, and theories used in optics.

All of the optical methods examined in this study have certain fields of application based on their assumptions. The assumptions make constraints, however, by simplifying the analytical model

one may produce a new model consistent with the restrictions. Therefore, measuring the capabilities of each theory in the literature through a thorough study may facilitate the choice of the approach which best matches the requirements of our problem. In this part optical methods are briefly introduced and then their assumptions and basic concepts, as well as the mathematics beyond those concepts will be discussed.

2.2 History of past contributions

History of past contribution to the theories of diffuse reflectance helps to a better understanding of the theorems. A summary is gathered in Table 2.1. Bouguer in 1760, and scientists start the works on diffuse reflectance and engineers have been involved in the measurement of light since the early experiments and instruments described by him. Pierre Bouguer (1729) and Johann Lambert (1760) developed the principle underlying the model for the absorption of light that relates the absorption to the properties of the material through which the light is traveling (Dahm & Dahm, 2007). This law will be introduced in detail in this chapter.

Moreover, Bouguer's elementary mirror hypothesis (1729) represents an application of the absorption by glass and water for various thicknesses (Darrigol, 2012). Darrigol also reviewed the absorption law pointed out by Bouguer stating that the successive equal layers of a homogenous transparent medium absorb a constant ratio of light that they receive. Kortum (1969) delineated Bouguer's elementary mirror hypothesis which has been employed to explain diffuse reflection from surfaces. Lambert's inverse square law, additivity law, and extinction laws are all based on Bouguer's work. Lambert's hypotheses were more accepted than Bouguer's findings since there were some contradictions in Bouguer's observations in the laws of diffuse reflection. In fact, Bouguer's model of diffuse reflection was found to fail later (Darrigol, 2012).

Table 2.1 Overview of the development of modeling techniques for diffuse reflection.

1760	P. Bouguer described diffuse reflection by elementary mirror hypothesis for surfaces with random orientations
1860	G.G. Stokes produced a two-flux theory of diffuse reflectance. The theory considers individual particles as plane parallel layers, and provides an analytical tool to the mathematics of plane parallel layers.
1887	E. Lommel and R.V. Seeliger developed a complicated theory of diffuse reflection concerning interactive irradiation of distinct elements inside a sample.
1905	A. Schuster proposed a special part of diffuse reflection based on continuous mathematics by publishing "Radiation through a foggy atmosphere", which involves particles in sample.
1908	G. Mie devised a novel method involving the scattering of light by isolated spherical particles, which uses the mathematics of complex variables and numbers.
1926	T.H. Gronwall proposed an article that emphasized on a simplified version of plane parallel mathematics.
1931	Kubelka and Munk published their classic paper that demonstrates the Kubelka–Munk equation, derived using continuous mathematics. They displayed that the reflection which is calculated by the absorption/remission formula from an infinitely thick sample, is equivalent to the ratio of absorption to remission coefficients for a medium. Their work produced many controversies over the failure of their model at certain conditions, and confusion over the effects of: direct and diffuse illumination; front surface reflection; and the relationship of the absorption and scattering coefficients of a sample to the coefficients of the material making up the sample. (Chalmers & Griffiths, 2002)
1946	F. Benford produced a very complete theory describing the mathematics of plane parallel layers. His work was very creative, novel, and independent of previous contributions.
1963	N.T. Melamed published a paper proving his method for modeling diffuse reflectance inside particulate samples, which is independent from plane parallel mathematics.
1966	Wendlandt and Hecht published the first "handbook of diffuse reflection" in 1966, which was the first handbook in the field of spectroscopy.
1969	G. Kortum published 'Reflectance Spectroscopy', a book which is heavily mathematical and covers continuum and discontinuum theories rather thoroughly. (Chalmers & Griffiths, 2002)
1970-1975	E.L. Simmons proposed several articles including simplified version of plane parallel mathematics to model particles inside a sample, and a modified particle theory (Chalmers & Griffiths, 2002). He proved the proportionality of the discontinuous and continuous theories in the case of two-flux approximations.
1997	T. Burger *et al*. presented a method in their publication pointing out application of the radiation transfer model to characterize diffuse reflectance through more advanced methods such as using three (or more) fluxes to separate absorption and scattering coefficients.
1995-2000	Dahm and Dahm conducted a carefully planned research that results in: a method to use plane parallel mathematics to separate absorption and remission coefficients; presenting an absorption/remission function which is constant for all sample thickness; and an equation relating the absorption and remission of one thickness of sample to that of any other thickness. They clarified the confusions over Kubelka–Munk theory, developed the representative layer theory that models a complex sample by defining layers, each one representative of the sample. They also developed a simple particle model.

The calculation of the amounts of light absorbed, transmitted and remitted by several layers is a very complicated process. Some fraction of light will be absorbed by a layer, which reduces the transmitted fraction to the next consecutive layer. In addition, some may return to the first layer as the result of reflection from the next layer, which again a portion may again be absorbed, transmitted, or remitted back to the next consecutive layer. The mathematics that is able to model this complex physical situation is called mathematics of plane parallel layers, which was developed by Sir George Stokes in 1860. Dahm and Dahm (2007) assert that Stokes theory is an exact estimation for plane parallel particles.

The Lommel – Seeliger reflectance law is a time honored-law, which has been used until today. It is based on a model, which is founded based on diffuse reflection by considering the optical characteristic of every single element inside the sample. Therefore, this model was very complex comparing to similar ones in that ages. However, it has some limitations such as predicting only the scattering of only collimated incident light (Fairbairn, 2004).

Schuster proposed a method of scattering and absorption within a sample by visualizing a dilute suspension of particles in which the particles were luminescent, absorbing, and scattering. He published a paper in 1905 describing a particle theory that developed to determine a solution for particular problems (Griffiths & Dahm, 2008). He developed his particle theory using continuous mathematics.

Gustav Mie designed a solution to Maxwell's equations to describe the scattering of electromagnetic radiation by a sphere. The solution is in the form of an analytical infinite series. The Mie scattering solution finds exact solutions for Maxwell's equations by separating equations for radial and angular dependence of the solution in the problems dealing with scattering (Bohren & Huffman, 1998). Thomas Hakon Grönwall published a paper in 1926 about new method in geometrical optics and presents a simpler method than the plane parallel mathematics.

Kubelka and Munk (1931) published their classic paper in the field of optics, which revealed a formulation for the scattering, and absorption of infinitely thick samples. Kubelka and Munk published their paper which is a two-flux version of a multi-flux method of solving radiation transfer problems. This method is popular because of its simple analytical equation, which is known as the Kubelka-Munk equation. However, this theory has some assumptions that limit the cases to which it can be applied.

Benford (1946) described mathematics of plane parallel layers, which is very complete and novel. In 1946, he published a detailed analysis of the absorption and scattering of light in the article of 'Radiation in a diffusing medium. He used discontinuous mathematics and assumed that the sample was divided into a series of plane parallel layers (Dahm & Dahm, 2008). Benford's calculations were developing a system of relations that can be used to compute the reflection, absorption and transmission fractions for a sample if the number of layers and those fractions for each are known.

Melamed proposed a complete statistical theory for the absolute diffuse reflectance of powders about a half century ago (Mandelis, Boroumand, & Bergh, 1990). In the past half century many spectroscopists performing quantitative diffuse reflectance spectroscopy of powdered materials have used the Melamed model. Melmad's theorem was successful in the field of modeling diffuse reflectance since unlike other discontinuum mathematics, Melamed applied statistical summations on the sample consisting of discrete particles reflecting light diffusely. The laws of geometrical optics (Mandelis et al., 1990) limited his model. Mandelis et al. deduced that Melamed's statistical approach had prominence over other theories that are based on plane parallel mathematics but with some limiting assumptions. Proceeding Melamed's unique theory, Wendlandt and Hecht (1966) published the first handbook in the field of spectroscopy. In 1969, Kortum presented his book in the field of reflectance spectroscopy that is a breakthrough in using

cumbersome mathematics to embellish continuum and discontinuum theories of diffuse reflectance (Griffiths & Dahm, 2008).

Simmons has used a simplified particle model (plane parallel mathematics) to relate diffuse reflectance to some optical parameters of the model without the use of heavy equations, which result from the more modified Melamed's theory (Mielenz et al., 1977). A more recent study in the field of diffuse reflectance was done by Burger et al. (1995) who developed a diffuse reflectance model using three or more fluxes (Griffiths & Dahm, 2008).

Dahm and Dahm (1999) presented a more complete method to study the diffuse reflection phenomena inside samples containing non-homogeneous particles. They used the plane parallel layer model of Benford (1946) to develop a more accurate approximation to calculate the fractions of light for each layer. This accuracy is a result of relating the physical properties of the elements of the medium to the optical properties of the sample. They also developed an equation for relating absorption/remission of one layer to that of the sample. This equation is comparable to the Kubelka-Munk function but is a descriptive tool for more complex samples (Griffiths & Dahm, 2008). Moreover, throughout their systematic work, they presented a series of explanations about the Kubelka-Munk theory and its controversies.

2.3 Fundamental Definitions

In this section fundamental definitions are presented that are necessary for the appreciation of the concepts proposed not only in this chapter but also in the following chapters. There is a chain of prerequisites for conveying the information about topics from basic elementary components in optics to more rigorous concepts. Some of the definitions are not found in the theories but introducing them is essential since these fundamental terms have used in some more advanced definitions. Hence, they

are explained before separately. Each part is described sufficiently for applying the theorems into models.

2.3.1 Geometrical Optics

Geometrical optics is the study of light without diffraction or interference (Greivenkamp, 2004). It is essential to explain the fundamental definition of geometrical optics to briefly introduce this significant part of classical optics. Geometric optics refers to the ray optics and describe the light propagation in terms of rays. In this part of classical optics, the rays are explained to spread out in rectilinear path in a homogenous medium. Rays are able to be bent, transmitted by splitting in two or more parts at the interface between two distinct media, may be refracted in a medium where the refractive index changes, or are absorbed and reflected. Geometrical optics provides rules, which depend on the wavelength of the electromagnetic wave, for propagating these rays through an optical system. Therefore, geometric optics is a crucial simplification of optical sciences that fails to account for some optical phenomena such as diffraction and interference. It provides an outstanding estimation about the travel of light into materials, however, when the wavelength is very small compared with the size of objects or materials with which the light interacts. Geometric optics can be used to describe the geometrical aspects of imaging, including optical aberrations.

2.3.2 Wavefront and Ray

In physics, a wavefront is the locus of points having the same phase: a two dimensional line, curve, or surface for a wave propagating in 3D space (Schuster, 1904). Greivenkamp (2004) reported a very concise description about the geometrical optics based on the optical path length. Optical path length is proportional to the time required for light to travel between two points (Greivenkamp, 2004). The relation is:

$$OPL = \int_a^b n(s)ds \tag{2.1}$$

where n is the refractive index which varies along the path. If it is constant the integration is not required. Mouroulis and Macdonald (1997) suggested that the propagation of waves is commonly described by means of wavefronts.

In geometrical optics the concept of wavefront is fundamental. Because of the higher frequencies of the waves such as infrared, optical, x-ray and gamma-ray, the temporal component of electromagnetic waves is usually neglected for the corresponding wavelengths, therefore, the phase of the spatial oscillation is the only parameter that is described. Moreover, most optical system and detectors are indifferent to polarization, so this property of the wave is also usually neglected. Maxwell's equations are a powerful descriptor for the optical system electromagnetic waves, and linear propagating waves such as sound waves that have similar wave equations. There are also geometrical wavefronts which are described similar to the physical wavefronts but are not propagating and are frozen in space (Mouroulis & Macdonald, 1997).

Introducing the wavefront is essential to define another fundamental element in optical physics which is the ray. Rays are defined as the lines normal to a family of wavefronts. The direction of electromagnetic propagation as suggested by Mouroulis and Macdonald (1997) is given by the Poynting vector, which is the cross product of the electric and magnetic field vectors. This direction of energy flow is conveniently described by rays. One might think that a very narrow beam of light is a ray but it is not. The divergance in the beams of light contributes the idea that the cross-section of beams are not constant in their lengths.

In this thesis, it has been assumed that the media is isotropic and our definition of rays is consistent with this assumption. However, there are some materials in which the direction of electromagnetic waves such as visible or near-infrared light is not always normal to the wavefronts such as crystals or non-linear media where it is possible for the wave to exit the material at a different wavelength from which it entered.

2.3.3 Radiant Energy

McCluney (1994) stated that radiation is the scattering of energy in several forms through space. Following this definition, the radiant energy can be described as the quantity of energy propagating onto, through, or emerging from, a specified surface of given area in a given period of time. For estimating the energy, all the wavelength spectrum contained in the radiation are must be included. The radiant energy is known by Q and its unit when a limited wavelength range is to be considered is shown in joule. Near-infrared light has a radiant energy calculated by integrating the radiant flux over time.

2.3.4 Solid Angle

Solid angle is a two dimensional angle in three dimensional space and is described by a closed curve and a point in space. According to Figure 2.1 (a), the solid angle is the projection of curve C in space, and curve C subtends solid angle Ω at point P at the center of a unit sphere. It extends the two dimensional concept of a plane angle to three dimensions. The magnitude of this angle is calculated by projecting the area of a closed curve in space on a sphere of unit radius, therefore, the solid angle of an object is equivalent to the area of the segment of a unit sphere, centered at the angle's vertex or center of sphere, that the object covers. Another relation that has been set forth by Palmer and Grant (2010) is the ratio of projected area of the closed curve on a sphere with arbitrary radius, dA_{sphere}, over the square of the sphere radius. This defining the solid angle along with the corresponding relationships have been presented schematically by Figure 2.1 (b). The unit of this angle is measured by steradian. The relationship associated with solid angle is:

$$\Omega = \frac{dA_{sphere}}{r^2} \tag{2.2}$$

where Ω is the solid angle, dA_{sphere} is the segment of the projected area on the sphere, and r is the radius of sphere.

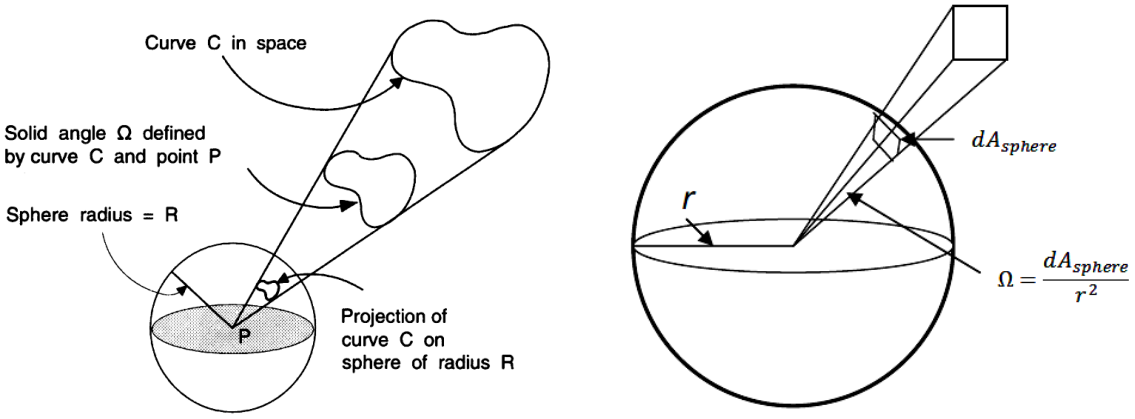

Figure 2.1 (a) Schematic representation of solid angle. (McCluney, 1994); (b) Solid angle relationships

Hemispherical solid angle is another important definition. The three solid angles are directional, conical, and hemispherical. McCluney (1994) distinguished between these three types and claimed that the directional one refers to an infinitesimally small solid angle in a particular direction from arbitrary point p in space like Figure 2.1 (a) and (b). Directional solid angles are only used in mathematical models of reflectance and transmittance but are not applied in experiments and measurements since the associated flux with this infinitesimal angle is unmeasureable in quantity. Conical solid angles are measures of intermediate-sized solid angles in the shape of circular cones. The mostly used solid angle is the hemispherical one that has the size of 2π steradians. The shape of this angle is the same as a hemisphere.

2.3.5 Radiant flux

The radiant flux is the time rate of flow of radiant energy with the unit of watt. This flow of radiation is characterized by the quantity of energy transferring through a region in space or usually a surface per unit of time. The defining equation is:

$$\Phi = \frac{dQ}{dt} \tag{2.3}$$

where Q is the radiant energy in Joules and Φ is the radiant flux with the unit of Joules per second or watt (McCluney, 1994). According to this definition, the radiant flux is radiated from a source over optical wavelengths, which are defined to be from 3×10^{11} to 3×10^{16} Hz. This region is equivalent to the electromagnetic spectrum commonly referred to as ultraviolet, visible, and infrared.

2.3.6 Radiance

We started defining the fundamental quantities with radiant energy Q which has as its unit the joule (J). Radiant power introduced as radiant flux is energy per unit time ($\frac{dQ}{dt}$) with the symbol Φ and is measured in Watts. Palmer and Grant (2010) deduced that these two definitions are not informational about the spatial distribution of power in terms of area or direction. Hence, another parameter is required that is an elemental quantity in radiometry, and is defined as the power per unit area, and per unit projected solid angle. It is known as radiance (Palmer & Grant, 2010). Since the radiance can be integrated along a beam, it is possible to calculate it in any location of an optical system. The radiance depends upon the direction and it can come from many points on a surface. Moreover, it can exist everywhere since it applies to a field quantity. The defining equation is (Palmer & Grant, 2010):

$$L = \lim_{\Delta s, \Delta\omega \to 0} \left(\frac{\Delta \Phi}{\Delta s \, cos\theta \Delta \Omega} \right) = \frac{d^2 \Phi}{\mathrm{d}s \, cos\theta \Delta \Omega} = \frac{d^2 \phi}{ds \, d\Omega} \tag{2.4}$$

where, L is the radiance, Ω is the solid angle, Φ is the radiant flux and s is the surface.

2.3.7 Irradiance

Irradiance (radiant incidence) is defined as the power of electromagnetic radiation per unit area. Described by McCluney, irradiance is the area density of radiant flux, the radiant flux per unit area in a specified surface that is incident on, passing through, or emerging from a point in the specified surface. The defining equation is:

$$E = \frac{d\Phi}{ds_o} \tag{2.5}$$

where $d\Phi$ is an element of radiant flux and ds_o is an element of area in the surface. It is essential to mention that radiance and irradiance are quite different. Radiance is the angular distribution of radiation emitted per unit area into a cone having unit solid angle, while irradiance sums up all this angular distribution over a specified solid angle Ω. Hence, the relation associated with the summation over the solid angle comes from the following integration:

$$E = \int_{\pi} L d\Omega \tag{2.6}$$

where, L is the radiance and Ω is the solid angle.

2.3.8 Radiant Intensity

McCluney (1994) characterized radiant intensity, I, as the density of solid angle or flux of energy radiated per unit solid angle (steradian) incident on, passing through, or emerging from a point in space. The defining equation is:

$$I = \frac{d\Phi}{d\Omega} \tag{2.7}$$

where $d\Phi$ is an element of radiant flux and $d\Omega$ is the element of a solid angle in the specified direction. The intensity is a strong function of direction from or toward the point for which it is defined. Also, it changes with distance from its source except for a collimated beam (Dahm & Dahm, 2007). Intensity can be derived from radiance by integrating over area:

$$I = \int_{A} L dA \tag{2.8}$$

2.3.9 Refractive Index

Index of refraction is a very fundamental parameter in optics, and it can be measured with a very high accuracy of 10^{-8} (Chartier, 2005). Refractive index is a property of a substance which is a number indicating the level of electromagnetic wave propagation in a medium. Before introducing the relation

for refractive index, it is essential to know about the source of this concept. Fundamental equations of wave propagation into a medium are known as Maxwell's equations. Using Maxwell's equations for a dielectric medium and then simplifying the integral forms and implementing some mathematical operations and manipulating, one can obtain the general wave equations for the propagation of a periodic disturbance, which is shown below (Hecht, 2002):

$$\nabla^2 \vec{E} = \epsilon_0 \mu_0 \frac{\partial^2 \vec{E}}{\partial t^2} \tag{2.9}$$

$$\nabla^2 \vec{B} = \epsilon_0 \mu_0 \frac{\partial^2 \vec{B}}{\partial t^2} \tag{2.10}$$

where E is the electric field vector, B is the magnetic field vector, ϵ_0 is the electric permittivity of free space, and μ_0 is the permeability of the free space. The phase velocity of Maxwell's equations is:

$$\upsilon = 1/\sqrt{\epsilon\mu} \tag{2.11}$$

Therefore, based on the Wendlandt and Hecht (1966) analysis, the refractive index, defined as the phase velocity in a vacuum which is equal to the speed of light compared to that in a given medium, is:

$$n = \frac{c}{\upsilon} = \sqrt{\frac{\epsilon\mu}{\epsilon_0\mu_0}} \tag{2.12}$$

where c is the speed of light or phase velocity in vacuum and υ is the phase velocity in the material. ϵ and μ are permittivity and permeability of the material, while ϵ_0 and μ_0 are permittivity and permeability of the vacuum. When light passes through a medium, some part of it will always be absorbed. This can be conveniently considered by introducing a complex index of refraction:

$$\tilde{n} = n + i\kappa \tag{2.13}$$

where the real part of the refractive index n indicates the phase speed, whereas the imaginary part κ is the amount of absorption loss when the electromagnetic wave propagates through the medium.

2.3.10 Diffraction

Diffraction appears as a limitation to the rectilinear propagation of light (Chartier, 2005). Diffraction is a complicated process, and occurs when a light beam collides with an obstacle. After collision, some parts of the light deviate in different directions. In classical physics the diffraction is described as the apparent bending of waves around small obstacles and the spreading out of waves past small orifices. Diffraction is observed for any kind of propagating phenomenon. All types of waves can be diffracted. Pedrotti et al. (2007) have presented a compelete study on this important phenomenon in classical optics. They suggested a simple defintion for this term that is any deviation from geometrical optics which results from the obstruction of wavefront of the light. The diffraction is observed even if the obstacle is not opaque and the transmitted wavefronts are affected by change of amplitude and phase.

2.3.11 Refraction

Refraction is the change in direction of a wave due to a change in its medium. This phenomenon occurs because of an inhomogeniety and discontinuity of the interface atoms which reflects light backward or transmit it forward through the medium. Hence, the fact that the incident rays are bent is called refraction (Hecht, 2002). Wendlandt and Hecht (1966) pointed out a simpler definition for refraction. They supposed that the electromagnetic radiation starts its path through a medium with a specific index of refraction while it reaches to another medium with a different refractive index. Whenever it encounters the separating region between two different media, a part of the beam is reflected back into the first medium, however part continues into the second medium, but with an altered direction of propagation. Hence, the refraction is essentially a surface phenomenon.

Electromagnetic radiation is an element in the refraction process, hence the governing equations of electromagnetic radiation are valid when the light refracts from one medium to another. When the

light passes through the medium, the phase velocity of the wave is changed but its frequency remains constant. The refraction occurs for any type of electromagnetic wave; from light to any other electromagnetic waves such as sound. Refraction is described by Snell's law, which constructs an expression based on the law of refraction for the relationship between the two incident and refraction angles and the properties of the wave which passes through the boundary of two different isotropic materials. The formula is derived for a given pair of media and a wave with a specified frequency stating that the ratio of the sines of the angle of incidence θ_i and angle of transmitted wave after refraction θ_t is equivalent to the ratio of phase velocities (v_i / v_t) in the two media. This ratio is also equivalent to the opposite ratio of the indices of refraction (n_i / n_t):

$$\frac{sin\theta_i}{sin\theta_t} = \frac{v_i}{v_t} = \frac{n_t}{n_i} \tag{2.14}$$

To prove the expression above, one can start from sketching the refraction phenomenon at an interface like Figure 2.2 by drawing the wavefronts at an instant of time. Each of them is a surface that has a constant phase. Because of the change in the phase velocity at the interface, the waves bend (Hecht, 2002). In fact, Figure 2.2 is a representation of several exposures of a single wavefront that shows it in equal time intervals of Δt.

When the wavefront *OB* reaches the interface, it refracts at point *A*. Assuming that it takes Δt for the wavefront *OAB* to get to the surface *RED* with phase velocity of v_i, different points on the surface of the wave traverse with different phase velocities after this time interval because one portion of the wave is in the incident medium with phase velocity v_i and another part is in the transmitting medium with phase velocity of v_t.

In this thesis, the analysis is done on the two-phase flow of Xylene as the liquid and ADP particles as the solids. Near-infrared radiation is employed as an electromagnetic wave that penetrates the solid-liquid mixture by a sensor which is located in air outside of the mixture. The refractive index of

xylene and ADP are greater than the air ($n_{Xylene+ADP} > n_{Air}$)or the phase velocity in air is greater than that in a liquid-solid mixture ($v_{xylene+ADP} < v_{Air}$).

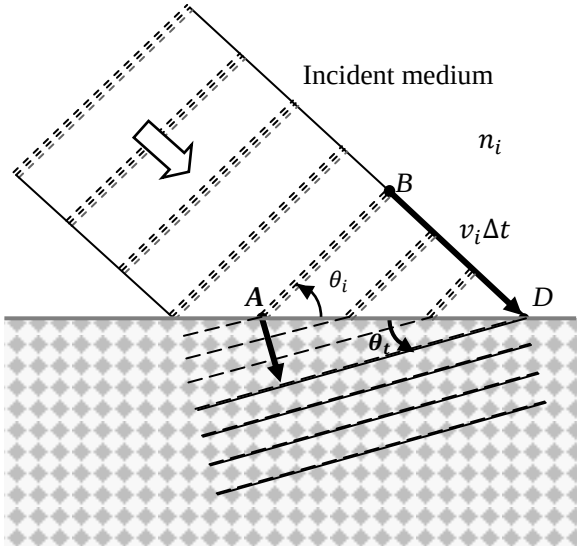

Figure 2.2 Geometric description for the refracted waves approached the interface at equal time intervals

Hence, according to Figure 2.2, for the case of near-infrared waves in air as the incident medium striking on the xylene-ADP sample as the transmitting medium, the vector *BD* is longer than *AE* because $v_i > v_t$ and time intervals are equal. In Figure 2.2, the two triangles *ABD* and *AED* share a common hypotenuse which is *AD*. Therefore,

$$\frac{\sin\theta_i}{BD} = \frac{\sin\theta_t}{AE} \tag{2.15}$$

where, $BD = v_i\Delta t$ and $AE = v_t\Delta t$, so

$$\frac{\sin\theta_i}{v_i} = \frac{\sin\theta_t}{v_t} \tag{2.16}$$

By multiplying both sides by *c* and since $n_i = \frac{c}{v_i}$ and $n_t = \frac{c}{v_t}$, one has:

$$n_i \sin\theta_i = n_t \sin\theta_t \tag{2.17}$$

The equation above is the general law of refraction or Snell's law.

2.3.12 Reflectance (reflection) and reflectivity

Introducing this important concept in optics, demands an understanding of the difference between three distinct terminologies which are common for all light fractions. As pointed out by Siegel and Howell (1981) there are differences between the fractions ending *–itivity* and *–ance*. It is common to refer the ending *–ivity* to intensive, coherent, or bulk properties of matter. The ending –ance is used to assign for the extensive properties of a material.

Reflection is a phenomenon by which a part of the light rays that are incident on the medium or particle leave it from the same side or scatter backward. This was a preliminary definition of reflectance that was addressed by Rea (2000). Hecht (2002) explained that reflection occurs when a beam of electromagnetic radiation impinges on a surface of material some light will scatter backward. Reflection, usually refers to a surface reflection not internal or external reflections within the medium. Hecht also clarified this issue for the gradual change in the mediums. In this situation, there is a continuous change of interface and very small amounts of reflection will be observed since the interface is effectively vanished. In contrast, any abrupt change in the interface exerts a discontinuity to the light intensity since a portion is reflected. Internal and external reflections will be discussed later in this section. There is no difference between the concept of reflection and reflectance in the literature, and it is possible to use reflectance in place of reflection or vice versa. However, in some of the references the meaning of reflectance and reflection are separated. For instance, Rea (2000) clearly delineated their boundaries by defining the reflectance as the ratio of reflected flux to the incident flux, while the reflection is a general term for the process by which the incident flux leaves a medium from the incident side or with a reflection angle less than 90 degrees, and without any change in frequency. According to CIE (1987), reflectance is the ratio of the reflected radiant to the incident flux that is radiated on the sample. Reflectivity is generally known as reflectance since it refers to the

incident electromagnetic power that is reflected at an interface. However, there is a slightly difference. The bureau of CIE (1987) specified a definition for reflectivity which is distinguished from reflectance. They suggested that reflectivity is the reflectance of a layer of the material with a thickness that does not change the reflectance if it is increased. This means that the sample or object is thick enough that the reflectance is not influenced by adding more thickness to it. This definition for reflectivity includes both internal scattering and surface reflectance. In other words, reflectivity is the restrictive value of reflectance as the surface becomes thick; it can be attributed to the inherent reflectance of the surface. McCluney (1994) claimed that sometimes it would be desirable to limit the definition of reflectivity to include only interface effects. By interpreting this definition, one can say that reflectivity is property of material, while reflection is the property of a particular sample of that material or surface.

Dilaura (2011) deduced that reflection is affected by the geometry, wavelength, and polarization of the incident flux. There are three types of surface reflections depend on the radiation flux; specular, mixed, and diffuse reflection. Specular reflection happens on a polished material when the beams are reflected specularly. Specular reflection, also called regular reflection, occurs when all the parallel incident flux is reflected with reflection angles equal to the incidence angle (McCluney, 1994). Hecht (2002) pointed out that the specular reflection process occurs when the light remitted by millions of atoms combines as a single beam. As is obvious from Figure 2.3, what is important is that the scattering effects are absent in the specular reflections. In this Figure, specular angle and incident angles are shown. Specular angle is the angle between the reflected ray and the normal to the surface. For regular (specular) reflections these two angles are equal. Perfectly specular reflections have no diffuse element.

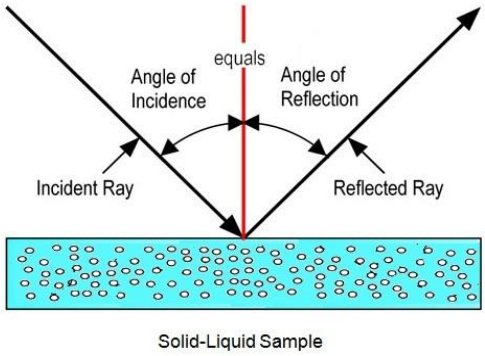

Figure 2.3 The geometry of the light generator, detectors, and the sample

Another type of reflectance is diffuse reflection. Diffuse reflectance or irregular reflection occurs on samples and materials that consist of particles and crystals or have rough surfaces. Each incident ray encounters an infinitesimal particle which obeys the basic definition and rule of reflection. However, since the shapes of particles in a solid-liquid mixture may not be uniform, there are some particles that do not have flat surfaces. Therefore, the reflected rays leave the particle surface in other planes with many different reflection angles and distinct directions. This process is depicted in Figure 2.4(a) where the incident beam strikes a particulate sample but it reflects diffusely in many different angles and in different planes. The intensities of reflected rays are not constant as is shown in Figure 2.4(a) and (b). The illuminated spot has the most energy and the reflected ray from this point has the greatest intensity, then it diminishes as the viewing angle to any side increases (Juds, 1988). Moreover, some of the energy of the incident illumination is attenuated by being transmitted through the sample or being absorbed by the liquid or solid particles inside the slurry which changes into heat and rises the temperature. A beam of parallel rays incident on a surface or medium that has a diffusely reflecting characteristic will be converted to a collection of rays distributed over a hemispherical solid angle. The diffusivity of materials are different. Some produce strong forward scattering whereas others diffuse the light almost in all directions. McCluney (1994) emphasized that if the reflection radiance is constant for all directions, then the surface type is called a Lambertian surface. The term diffuse can also be used for the non-Lambertian surfaces. Perfectly diffuse reflectance is special case

for the diffuse reflections. This phenomenon occurs when the density and distribution of reflected beams are higher near the surface normal and decreases as the cosine of the angle of the reflected direction. An important point is that perfect diffusion does not mean perfect reflection; it does not mean that the reflection is 1.0.

Most surfaces have a mixture of diffuse and specular characteristics. Rea (2000) described this feature on some special surfaces which diffuse most of the light in all directions except for a ray that reflects specularly. Therefore, this type of reflection is partly regular (specular) and partly diffuse. In real situations, a specularly reflecting material has less quantified capability to diffuse the light than reflect it specularly. On the other hand, a diffusely reflecting material reflects the light specularly less than the amount that it diffuses, quantitatively (McCluney, 1994).

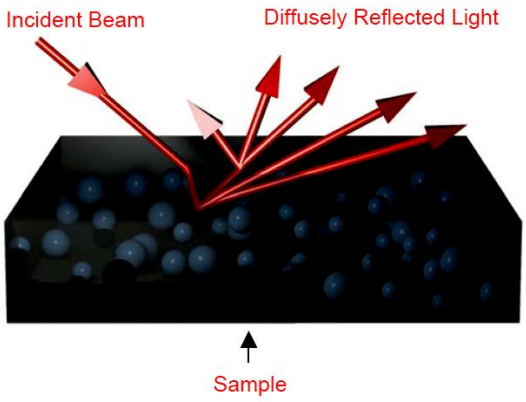

(a)

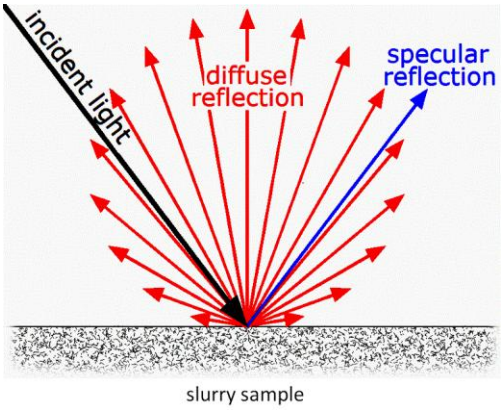

(b)

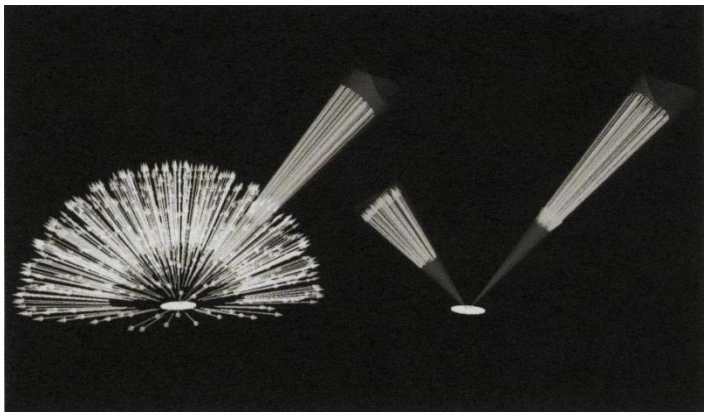

(c)

Figure 2.4 (a) Diffuse reflection from a sample composed of particles (SPECAC Limited, n.d.); (b) Specular versus diffuse reflectance on the surface of a slurry fluid. (c) Diffuse and specular reflectance. Diffuse reflectance (left) sends beams in all directions regardless of the uniform parallel incident rays. Specular reflectance (right) incident cone is preserved (Dilaura, 2011)

All types of reflections which occur at interfaces including specular, diffuse, and mixed reflections, are external reflections. Total reflection has two categories; external and internal reflections. Considering the passage of an incident beam from medium 1 (incident medium) to medium 2 (transmitting medium), one can construe the occurrence of an external reflection when the refractive index of the first medium is less than the one for the second or transmitting medium. The reason is that the light is initially traveling from a less to a more optically dense medium. This phenomena happens since the compression of atoms in a dense material does not allow the photons to find a way through the medium, hence the reflection at the interface is strong. In fact, specular and diffuse reflections which are surface reflections are categorized as external reflections. On the other hand, internal reflection occurs when the light going from a region with high refractive index to a region with lower index. Dahm and Dahm (1999) also defined internal reflections as light that has been transmitted through one or more particles, returned from an internal particle, and transmitted through any particle encountered on the way back to the detector. In some occasions, neither reflection nor transmission takes place when incident beam encounters the interface. From a two dimensional perspective, the beam reflects exactly at the line of the interface or in a 3-D view it will be reflected in the plane of the interface (Pedrotti et al., 2007).

In this thesis the remission is used as the reflection in agreement with the notation used in the literature. Remission is the summation of external reflection, internal reflection, and backward scattering (Dahm & Dahm, 1999). The remission fraction is the ratio of the remitted intensity to incident light; the light that strikes a particle (Dahm & Dahm, 2007).

2.3.13 Scattering

Scattering is a form of propagation of electromagnetic waves in a way that energy is attenuated through the scattering medium and remission to many directions (Pedrotti, 2007). Therefore, the scattering will be a result of deviation of light from the medium. Scattering is also called diffuse

scattering by Dahm and Dahm (1999). They referred to a process in which light interacts with a particle and changes its path in many directions regardless of the orientation of particle surface. This light is capable of being absorbed or remitted immediately. Mie theory is a powerful tool to exactly predict the scattering. The intensity of scattered light relies on the particle geometry (Dahm & Dahm, 1999).

For inferring the difference between scattering and diffuse reflection, Kortum (1969) clarified this very important issue. Before going through the difference, a concise explanation about the dependency of particle size and wavelength is required. Reflection, refraction, and diffraction are three different elements by which the interaction of the wave with a particle is characterized. These three phenomena occurs differently if the particle size is greater than the wavelength of the electromagnetic wave. However, if the dimension of the particle is less than or comparable to the wavelength of light, then it would be impossible to separate the contribution of the concepts of reflection, refraction, and diffraction during the collision of waves with particles. This phenomenon is known as scattering (Kortum, 1969). In contrast, diffuse reflection is the isotropic angular distribution of light in densely packed materials.

Single and Multiple Scattering

It is very important to introduce two different phenomena about scattering; single and multiple scattering. Single scattering happens when radiation is scattered locally by a local center. If the numbers of scattering centers are high, the scattering will occur many times which is called multiple scattering. The difference between the single and multiple scattering is that single scattering is similar to a random phenomenon; however, multiple scattering is less random. The location of single scattering center is not determined, therefore, it tends to depend on the incident trajectory, which looks random to an observer. Single scattering is described by probability distributions (Bohren, 1998).

The reason that multiple scattering is less random than single scattering is because of the averaging of a large number of scattering events. Hence the final path of the radiation appears to be a deterministic distribution of intensity. This is exemplified by a light beam passing through thick fog. Multiple scattering is analogous to diffusion. Optical scattering centers designed to produce multiple scattering are thus known as diffusers.

Forward and Backward Scattering

Forward and backward scattering are two types of scattering events. Forward scattering refers to the scattered beams that leave a sample travelling in a direction that produces a component with the same direction as the incident beam. Backward scattering is defined as the scattered light that leaves a sample in the opposite direction of the radiation.

2.3.14 Reflection (remission) Coefficient

Reflection coefficient is defined as the difference between the propagation velocities of the two media forming the interface (Guenther, 1990). He offered the following equation for the reflection coefficient between two media:

$$b = \frac{n_t - n_i}{n_t + n_i} \tag{2.18}$$

where b is the reflection coefficient and n_i and n_t are the index of refractions for the incident and transmitted media, respectively. Or, Pedrotti et al. (2007) suggested the following formula which is the same as Equation 2.18:

$$b = \frac{1 - n}{1 + n} \tag{2.19}$$

where *n* is the relative refractive index. Dahm and Dahm (2007) suggested the following definition for the apparent linear remission coefficient of a sample which is the fraction of light remitted from a small thickness of the material divided by the magnitude of that small thickness.

$$B = \lim_{d \to 0} \frac{R_d}{d} \tag{2.20}$$

where R_d is the remission fraction for light that is reflected from a small thickness of material. Chartier (2005) defined the reflection coefficient as a complex number where its modulus is equal to unity. He deduced this definition based on doing some calculation on Fresnel formulas. For modeling purposes in this thesis the formulation of Dahm has been used since it is consistent with the number of different layers.

2.3.15 Absorptance (absorption)

In physics, absorption of an electromagnetic wave is a phenomenon in which the energy of a photon in the ray is taken up by the material. This energy is consumed in a nano scale by the electrons of an atom. The activities of the electrons due to radiation heat up the matter. In spectroscopy, absorptance, absorbance or absorption, also called optical density of a material is the logarithmic ratio of the radiation strike on a material to the radiation transmitted through a material. In the literature, the absorption of light through a material has been also called attenuation. When speaking of the linear absorption, the dependency of the attenuation is independent of the intensity of the beam, but in certain conditions, the medium changes its transparency due to the intensity of waves going through, and nonlinear absorption happens (Venkatram, Rao, & Akundi, 2005). McCluney (1994) defined the absorptance as the ratio of the absorbed radiant to the incident flux which has the symbol α.

Absorbance measurements are often carried out in analytical chemistry. Considering a light beam having an intensity I_0 impinging on a sample and an intensity I_d incident on the detector, Dahm and Dahm (2007) suggested that absorbance function is the negative logarithm of the fraction of the incident intensity that strikes a detector. According to this definition the following formula is derived:

$$A = \ln \frac{I_0}{I_d} \tag{2.21}$$

where A is the absorption fraction I_0 is the incident intensity, and I_d is the intensity exits the sample. Sometimes it is said that the absorbance is defined for the case of transmission through non-scattering sample as $\ln(1/T)$, where T is the transmission fraction (Dahm & Dahm, 2007). In contrast, the absorption function has certainly been useful in the field of near-infrared reflectance spectroscopy in which it is defined as $\log(1/R)$, where R is the remission fraction of light. But what is suggested by Dahm and Dahm (2007) and is used in this thesis is the meaning of absorbance function for the case of transmission. The reason for using this interpretation of absorption is because of instruments which use log-based absorbance. Dahm and Dahm (2007) stated different usages of log-based transmission and reflection cases. In a transmission measurement, since the fraction of light transmitted is calculated from $\mathrm{T} = I_d/I_0$, absorbance function can be written in the form of $\log(\frac{1}{T})$. In the experiments that are based on remission, the absorbance is calculated in terms of remission in the form of:

$$A = \log(\frac{1}{R}) \tag{2.22}$$

where R is the remission fraction measured from incident light. However, the exponential form of the absorption fraction is used for quantitative purposes. This form will be introduced completely in Chapter Three.

2.3.16 Absorption Coefficient

The traditional definition for the absorption coefficient is the ratio of absorbed light by a thin layer in the material to the length of that small thickness (Dahm & Dahm, 2007). The following equation represents the absorption coefficient for a linear type of material:

$$K = \lim_{d \to 0} \frac{R_d}{d} \tag{2.23}$$

K is the absorption coefficient, d is the thickness of the small layer of sample, and A is the absorption fraction of light inside the medium. An important point about the absorption is related to nonlinear

situations. When a specific thickness of the sample for which the absorption fraction is calculated is thick – the thickness criterion is explained in detail in Chapter Three – then the absorption fraction is not a linear function of the depth of the layer. Dahm and Dahm (2007) asserted that as the thickness of the layer under measurement gets smaller, the absorption fraction falls in the linear regions. If the sample is a small layer of material, the absorption is called linear and the value will be linearly proportional to the sample thickness. Dahm and Dahm (1999) also described this linearity for the material through their proposed hypothesis. According to their descriptions, the absorption is linear if all internal parts of the material are equally illuminated.

Dahm and Dahm (2007) asserted that absorption coefficient is another definition for the absorption power of the material while there is no scattering in the sample. In a homogeneous sample any particular thickness which absorbs light, has a limit of capacity for absorption. The amount of absorption is in constant or linear proportion to the intensity of radiation. This fraction is independent of: the absolute value of intensity; and the location of that special thickness or layer of the sample. This rule is known as Bouguer-Lambert Law in optical physics. The formulation is:

$$\frac{I_d}{I_0} = T = \exp(-kd) \tag{2.24}$$

where k is the absorption coefficient, T is the transmitted intensity, I_0 is the intensity of the light a which passes the thickness of the material in the location of line 0 which is shown in Figure 2.5, and I_d is the intensity of light at the point d, d is the distance between two lines, and d is the absorbing power of the material. Penetrating through the sample, some portion is absorbed and some will be transmitted. Pierre Bouguer (1760) discovered the law of absorption of light through the material, and later it was developed by Johann Lambert (Dahm & Dahm, 2007). This law describes the absorbed light by a homogenous material as a linear fraction of intensity on such a layer. The limitation of this technique is its homogeneity.

The absorbing power of material is known as the negative of the natural log of the intensity transmitted through a particular distance *d* of the sample (Dahm & Dahm, 2007). The absorbing power of a material is the same as the absorbance of a homogeneous sample of the material of unit thickness. For example, the absorbing power of a material is the same as the absorbance of a homogeneous sample of the material that is 1 cm thick:

$$k\ \mathrm{cm}^{-1} = \ln\left(\frac{I_0}{I_{d=1\mathrm{cm}}}\right) = \ln\left(\frac{1}{T_{d=1\mathrm{cm}}}\right) \tag{2.25}$$

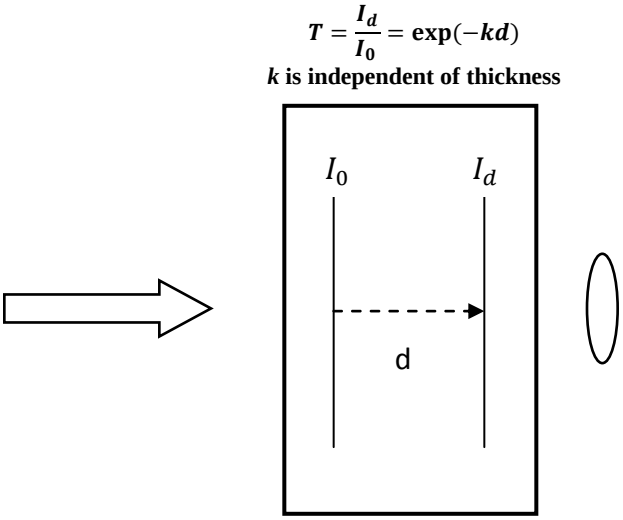

Figure 2.5 Illustration of Bouguer-Lambert law

Therefore, the absorbing power of the material or *k* is calculated by the absorbance of the homogeneous sample of the material. It should be noticed that *kd* does not have any units. If one divides the relation above by the distance that light travels, *d*, the result will be the absorption power which is derived from the following equation:

$$k = \frac{\ln\left(\frac{I_0}{I_d}\right)}{d} = \frac{\ln\left(\frac{1}{T_d}\right)}{d} \tag{2.26}$$

For a portion of sample that is under direct illumination, the absorbing power of the material is the ratio of the amount of light that would be absorbed if every absorption portion were under incident intensity equal to the incident ray, to the intensity of the incident beam (Dahm & Dahm, 2007).

The thickness of the layers is calculated in the units of cm^{-1}. In this thesis K will refer to the absorption coefficient of a sample and k is the absorption coefficient of a material which is also known as absorption power of material.

2.3.17 Transmittance (transmission)

Transmittance is the fraction of electromagnetic wave at a specified wavelength that passes through a sample. A more concise definition is the movement of light through a sample of material without being absorbed (Dahm & Dahm, 1999). The important point about transmission is that it is incorporated with the fact that suggests the amount of light that is not absorbed, is reflected or transmitted. The only difference between the reflection and transmission is the angle of incidence and the angle that light makes with the normal to the surface of interface. If the light is transmitted through the medium with an angle less than the critical angle – at which the remitted beam falls exactly on the interface line – the light is transmitted, whether internally within the layers of sample or externally outside of the medium. In this situation the light is refracted and it is transmitted to the other layers inside the sample or it is coming out of the sample. However, when the incident light strikes the sample at an angle more than the critical angle, the beam that is leaving the medium is said to be reflected. Therefore, the boundary between the reflectance and transmittance is very close.

Dahm and Dahm (2007) pointed out that the transmission fraction is calculated from the following equation which is derived based on the Bouguer – Lambert law for transmission. The law says that the fraction of light beam transmitted through the sample while moving through the distance d inside a continuum medium is calculated from:

$$T = \exp(-kd) \tag{2.27}$$

where *k* is the linear absorption coefficient in the absence of scattering inside the sample. Considering this limiting assumption, one can conclude that this expression is designed for the samples with high concentration of particles. The reason is that by increasing the number of particles the chance of light scattering will increase, which is not consistent with the assumption of this law. But fortunately this equation is valid for the small particles according, as shown in Figure 2.6.

The straight line in Figure 2.6 is a tangent line to the relation $\exp(-kd)$ that represents the deviation of transmission curve from the line C with the relation *kd*. This line can be used instead of the exponential function in the linear region. The linear region is essential to be found since the validity of some theories such as Bouguer-Lambert law and plane parallel layers are dependent upon this assumption. In Chapter Three, this linearity assumption is introduced. Furthermore, least squares method to find threshold for the minimum deviation from the straight line is presented not only for transmission but also for absorption.

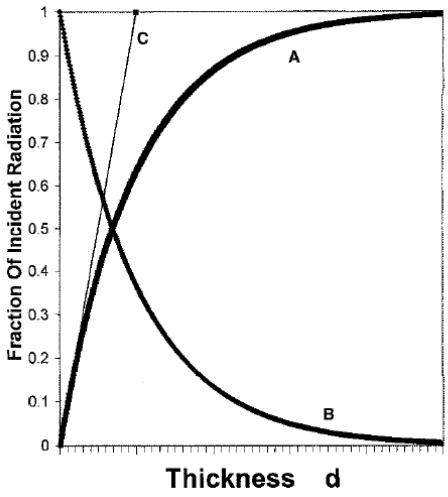

Figure 2.6 (A) Absorption fraction; (B) transmission fraction (e^{-Kd}); (C) straight line representing *Kd* which lies on the transmission curve in smaller thicknesses of the sample or layer of the sample which is illuminated (Dahm & Dahm, 1999)

2.4 Continiuum Theories of Diffuse Reflection

2.4.1 Introduction

Near-infrared (NIR) diffuse reflection (DR) has become extensively applicable for the quantitative analysis of many products and commodities since it 40 years ago when it was first used in spectroscopy. As was mentioned in Chapter 1, mid-infrared diffuse reflectance is used more for investigating and characterizing than for the determining the quantity of particulate samples. Considering the mentioned cases, investigating the diffuse reflectance process is useful if the very large amount of information is to be collected from the spectrum. Those theories of diffuse reflectance that use simple mathematics has connections with the reflectance of a sample which is known by $R(\tilde{v})$. In this situation, the assumption which says all light being reflected from both a sample and a a standard reflecting reference with 100% reflectance can be measured (Chalmers & Griffiths, 2002). Chalmers and Griffiths (2002) suggested that the relative diffuse reflectance $R'(\tilde{v})$ can be measured by estimating the ratio of the spectrum of the radiation received by the detector from a particulate sample and the corresponding spectrum which can be estimated experimentally after reflection from a non-absorbing reference matter. In the cases which the material thickness is large, any change in the thickness does not influence on the power of the radiation which is going to be received by the detector. Therefore, the power will not change. The measured spectrum is called the reflectance spectrum at infinite depth, $R_{\infty}(\tilde{v})$ (Chalmers & Griffiths, 2002).

Chalmers and Griffiths (2002) asserted that all algorithms for multivariate analysis obtain the most accurate calculations about the concentration when the intensity of each spectral parameter is proportional to the concentration of the anlayte in a linear fashion. Hence, diffuse reflectance will be changed into the linear form if an ideal standard for the analysis of diffuse reflectance is required by applying theories. In the linear condition, the dependence of intensity of the spectrum on the concentration of each analyte is linear which is analogous to the conversion of transmittance spectra to

absorbance for considering Beer's law (Chalmers & Griffiths, 2002). For many cases in near-infrared diffuse reflectance spectrometry, a conversion which is equivalent to what is mentioned is performed. For instance, before applying the theorems to the sample and model the light interactions, one may require to change the R_∞ spectrum in to the form of –log R_∞ or log $1/R_\infty$. It is significant to mention that most NIR/DR spectra is usually estimated using log1/R which, for thick samples, is the same as logR_∞ (Chalmers & Griffiths, 2002). Fortunately, for many materials the concentration of the sample under anlysis will not change most of the time by even a factor of two. Therefore, the linear assumption is valid and the deviation from linearity is not considerable. Hence, Chalmers and Griffths (2002) concluded this approach usually have excellent results.

Applying the parameter of log 1/R as the preferred ordinate for near-infrared diffuse reflection is in opposite side to what most physical scientists would consider appropriate for experimental part of a diffuse reflectance measurement (Griffiths & Dahm, 2008). The theory of Kubelka and Munk is one of the mostly used theories of diffuse reflectance spectroscopy. In this Chapter, this theory is introduced with a summary of other continuum theories of diffuse reflection. The assumptions of the theories are very important since they produce limitations. These constraints only affect the accuracy of the results. However, all of these methods have been validated through experiments. The last part of this thesis contains a discussion of some studies and measurements about the depth of penetration of light. The information and models are investigated based on the available theories in the literature. Modeling the penetration depth in a two-phase flow of xylene and ADP is achieved using the theorems, which are to be discussed in this Chapter.

2.4.2 Lambert Cosine Law

The diffuse reflectance phenomenon is a widely applicable usages of near-infrared radiation, which is easily noticed in everyday life. Griffiths and Dahm (2002) made an example for the intensity of radiation reflected from a completely matte surface. The reflected or remitted radiation has equal

intensity in all directions. Also, it is not important to know what is the angle of incidence or angle of observation of light from the surface. This experiment made Lambert to be the first person who created a mathematical formula and theory based on the diffuse reflectance of light (Chalmers & Griffiths, 2002). He assumed that the reflected flux which is known by I_r, in an area $f\ cm^2$, and solid angle ω steradians (sr), is proportionate to the cosine of the angle, which the incident beam builds with the normal to the surface, α, and the angle of observation ϑ that are shown in Figure 2.7. This is obtained from the Equation 2.28:

$$\frac{dI_r/df}{d\omega} = \frac{CS_o}{\pi} cos\alpha\ cos\vartheta = B\ cos\vartheta \tag{2.28}$$

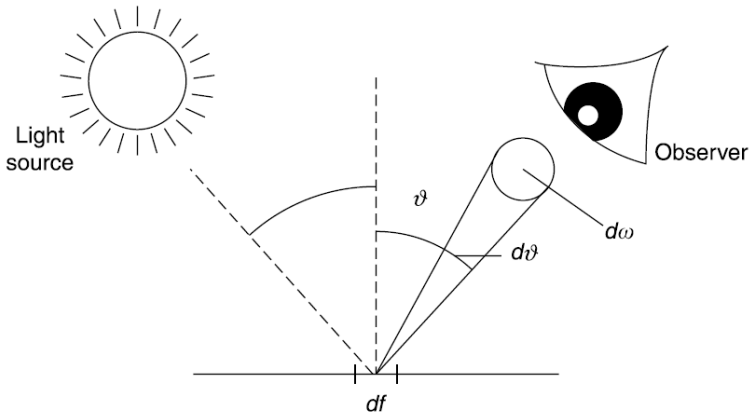

Figure 2.7 Diagram showing the variables used in the Lambert cosine law (Griffiths & Olinger, 2002)

where B is the radiation density or surface brightness in W$cm^2\ sr^{-1}$, S_o is the irradiation intensity in W cm^2 for normal incidence, and the constant C is the fraction of the reflected intensity of radiation. C is less than unity because some portions of radiation flux are always absorbed with the surface. Equation 2.28 is famous since it is known as the Lambert cosine law (Chalmers & Griffiths, 2002). Kortum (1969) suggested that the Lambert cosine law can be derived from the second law of thermodynamics, although this opinion was not held by Wendlandt and Hecht (1966). Kortum (1966) pointed out that it is rigorously valid only for a material which has the characteristics of a black-body.

These black body radiators acting as an ideal diffuse reflector. Griffiths and Dahm (2008) pointed out that the angular distribution of the reflected or remitted light is not dependent of the angle of incident radiation. This fact is in contradiction with tehe features of black-body radiator since ideal diffuse reflectors has some different characteristics. This contradiction is made since all incident radiation is absorbed by a black body, however, an ideal diffuse reflector does not absorpb all the radiation. An ideal diffuse reflector is not realistic and has never been found in practice. Hence, the Lambert cosine law is an ideal descriptor of diffuse reflection which always there are deviations from that. According to what Chalmers and Griffiths (2002) stated, there are many authors that have reported the results of experimental investigations that were prepared to prove or disprove this law. They found that in the law is only valid when both the angle of incidence α and the angle of observation ϑ are small.

2.4.3 Mie Scattering

One of the most applicable and more accepted theories of the scattering of light was developed around by Mie. Mie scattering theory models the travel of light into the isolated particles, and predicts the absorption by and scattering from that particle. Only a very brief introduction is given here. Kortum (1969) has pointed out a summarized description about Mie scattering theory. Mie developed and derived a model to predict the following factors: **(i)** the angular distribution of the intensity, and **(ii)** the angular distribution of polarization of scattered radiation for a plane wave which is scattered once through a phenomena called single scattering by a particle (Griffiths & Dahm, 2008). These two phenomena can be both dielectric and absorbing. Mie assumes that the particle is spherical, and there is no limit on its size. He presented that the angular distribution of scattered radiation for single scattering will not be isotropic. The basic equation of Mie scattering theory is:

$$\frac{I_{\theta s}}{I_0} = \frac{\lambda^2}{8\pi^2 R^2}(i_1 + i_2) \equiv q(\theta_s) \tag{2.29}$$

where $I_{\theta s}$, is the scattered intensity at a distance R from the center of the sphere; I_0 is the intensity of the incident radiation, and I_0 is the wavelength of the incident radiation (Chalmers & Griffiths, 2002). The variables i_1 and i_2 are functions of the angle of the scattered radiation θ_s, the refractive index difference between particle and medium, and the ratio of the particle circumference to wavelength. The ratio of the refractive index of the sphere to its environment is known by *m*, and the ratio of the particle circumference to wavelength is known by p (Chalmers & Griffiths, 2002). Equation 2.29 applies only to the case of a dielectric nonabsorbing particle. If the particle absorption is high, the complex refractive index must be used in the determination of i_1 and i_2.

Mie theory is general for spherical particles of any size. However, it is valid only for single scattering, therefore, is applicable only to systems in which particles are well separated (Chalmers & Griffiths, 2002). For instance, when the particles in the atmosphere scatter light, the special case of Mie theory is obtained where the particle is much smaller than the wavelength of incident radiation. Most analyses in the range of mid-infrared and near-infrared spectroscopy the multiple scattering is a definite assumption since it happens in real samples (Chalmers & Griffiths, 2002). Theissing (1950) improved Mie theory by assuming that the multiple scattering from particles which nonetheless are still supposed to be sufficiently well dispersed and separated in the medium. Therefore, the interference and phase differences between the scattered fluxes from the particles are not important and can be neglected. The number of times when a photon is scattered and distributed in the medium is defined as the scattering order (Chalmers & Griffiths, 2002). By increasing the order of scatter the value of forward scattering in the sample is doing an opposite behavior and will decrease, therefore, the angular distribution of scattered light does not change with direction and in all directions is isotropic. He also discovered that the if the ratio of particle circumference to wavelength is larger the order of scattering must increase to generate an isotropic scattering. For example, if p is 0.6 and m is 1.25, twofold scattering is required for an isotropic distribution of the reflected radiation. However,

while p = 5 and m = 1.25, a scattering order of 8 is needed for isotropic reflection of radiation (Chalmers & Griffiths, 2002).

In the NIR region, band absorptions are so low that large particle sizes, of the order of 100 microns, can be calculated using Mie theory (Griffiths & Dahm, 2008). Hence, *p*, the ratio of the particle circumference to wavelength, is large. In this case, the order of scattering must also be large in order to have an isotropic variation of the scattered radiation. In the mid-infrared range, this feature is changed where it is quite common for *p*. Hence, it will be approximately around 1 (Griffiths & Dahm, 2008). If the number of particles in a sample is large, multiple scattering does take place for most samples of the type used for infrared reflection analysis, therefore, the diffusely reflected radiation has an isotropic distribution that should at least be reached. Hence, to predict multiple scattering in a densely packed medium is required to model the variation of reflectance with the change in concentration (Griffiths & Dahm, 2008).

In most of the samples for which the near-infrared diffuse reflection can be used, the scattering density is large, the ratio of particle circumference to wavelength is higher than 1, and the concentration of particles are high enough that phase relations and interferences between scattered beams do exist (Chalmers & Griffiths, 2002). Hence, in this case, there is no solution to the problem of multiple scattering in the sample. Therefore the scientist must resort to the phenomenological analysis may be required.

2.4.4 Radiation Transfer Treatments

Theories that have been developed to predict the diffuse reflection of radiation are built based on the radiation transfer equation. A radiation transfer equation can be written as if one simplify it:

$$-dI = \kappa\rho I\, ds \tag{2.30}$$

Equation 2.30 is a description of the change in intensity *dI* of radiant flux in a specific wavelength in a sample with the density ρ and with the pathlength of *ds*. κ describes the attenuation coefficient for the total radiation loss. This dissipation can be due to scattering or absorption. The radiation transfer equation that is used in the derivation of most phenomenological analyses considers only plane parallel layers of particles within the sample and can be written as:

$$\mu \frac{dI(\tau,\mu)}{d\tau} = -I(\tau,\mu) + \frac{1}{2}\omega_o \int_{-1}^{1} P_0(\mu,\mu')I(\tau,\mu')d\mu' \tag{2.31}$$

where μ' is the cosine of the angle ϑ with respect to the outward surface normal; *m* is the cosine of the angle ϑ with respect to the inward surface normal; $d\tau$ is the optical thickness and is equal to $\kappa\, \rho\, dx$, where *dx* is the distance between the boundaries of one plane-parallel layer; I is the intensity of the beam of radiation striking the layer; $\omega_o = \frac{\sigma}{(\sigma+\alpha)}$ is the albedo for single scattering, with the scattering and absorption coefficients σ and α (Chalmers & Griffiths, 2002). The scattering phase function $P_0(\mu,\mu')$ is the probability for scattering from direction μ' into μ. If each beam scatters isotropically, $P_0(\mu,\mu') = 1$ and is not dependent to the angle between the incident radiation and the scattered radiation. The phenomenological analyses that have been developed can be deemed as continuum theories or discontinuum theories (Chalmers & Griffiths, 2002). In continuum theories, the absorption and scattering coefficients are the properties of the irradiated material. However, in discontinuum theories a layer of the material is made up of several partial layers whose thickness is limited by the size of the scattering and absorbing particles. It means that based on the size of particles the thicknesss of the layers must change (Chalmers & Griffiths, 2002). Optical constants can then be found from the scattering and absorption of these particles. This section only considers a sample as a continuum.

In our modeling, we have used the method of approximation for the radiation transfer equation proposed by Patterson, Schwartz, and Wilson (1989). Figure 2.8 is an experimental apparatus that they used in their method. When the light reflects diffusely from the tissue containing a dye, the

changes in the reflectance is identified by the concentration of dye. In Figure 2.8, the measurement setup is shown. In this figure, an experiment based on radiative transfer approximation is illustrated.

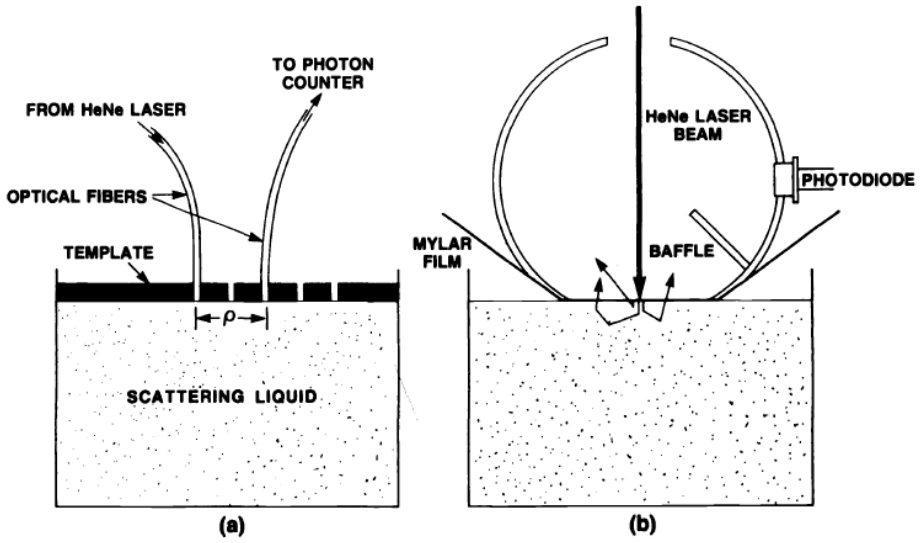

Figure 2.8 (a) Experimental apparatus for the measurement of R(ρ), the local diffuse reflectance (b) Apparatus for the measurement of R, the total diffuse reflectance (Patterson et al., 1989)

2.4.5 Schuster's Theory

Schuster' theory was one of the earliest theories of diffuse reflectance. He was interested in astrophysical problems that were related to radiation transfer. From the general laws of radiation, Schuster suggested that an atmosphere is required for a star to show emission lines of light instead of absorption lines. The characteristics of this atmosphere is that the scattering overcomes the absorption. As mentioned by Nobbs (1985), the approach adopted by Kubelka and Munk was first introduced by Schuster in 1905 and was developed to calculate the radiation from the self-luminous opaque dust cloud surrounding a star. This theorem will be modeled with details in Chapter Three.

2.4.6 Kubelka-Munk Theory

Kubelka-Munk is a widely used theory in the field of diffuse reflectance. The theory was basically developed in the field of spectroscopy. However, recently there were many debates on the revisions

over it to increase its accuracy and the number of different applications. The theory developed by Kubelka and Munk is obtained based on solutions to the radiative transfer problem. This theorem was first used to investigate the optics of paint layers. Kubelka and Munk developed their models based on the remission, not scattering. Kublka – Munk equations are produced from radiative transfer and are in the form of differential equations. The Kubelka-Munk equation is a two flux version of a multi-flux method used to solve the radiation transfer problem (Nobbs, 1985). Kubelka and Munk made several assumptions in their derivation of a simplified solution to the radiation transfer equation. Note that none of them are exactly the same as the corresponding parameters defined by Schuster. Figure 2.9 shows the type of system for which Kubelka and Munk derived their solution.

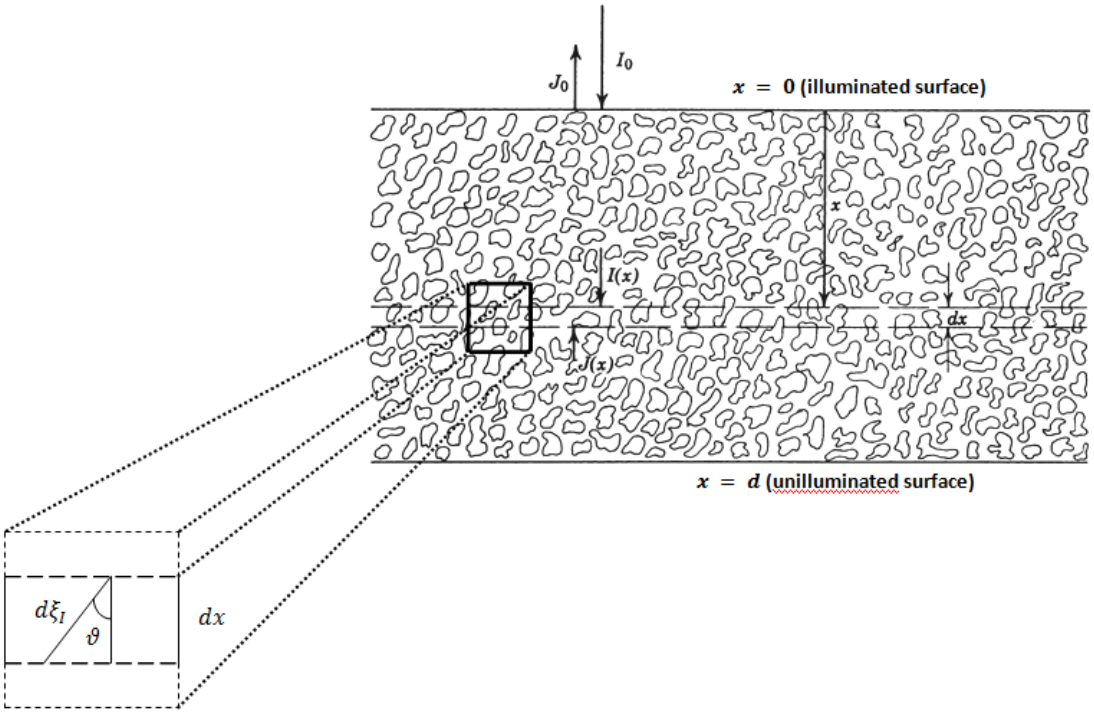

Figure 2.9 Schematic representation of a layer of absorbing and light scattering particles

The assumptions are listed below:

- The radiation fluxes (I and J) travel in two opposite directions.

- The sample is illuminated with monochromatic radiation of intensity I_0.
- The distribution of scattered radiation is isotropic so that all regular (specular) reflection is ignored.
- The particles in the sample layer (defined as the region between x = 0 and x = d) are randomly distributed.
- The particles are very much smaller than the thickness of the sample layer *d*.
- The sample layer is subject only to diffuse irradiation.
- The breadth of the macroscopic sample surface (in the yz plane) is great compared to the depth d of the sample and the diameter of the beam of incident radiation (to discriminate against edge effects).
- The scattering particles are distributed homogeneously throughout the entire sample.

Either an exponential or hyperbolic solution may be developed, although only the exponential derivation is shown here. A detailed description of the hyperbolic solution is given elsewhere.

Kubelka and Munk arrived at the two fundamental differential equations which, once solved, give the simplified solution to Schuster's fundamental function. As it is feasible that the angle through dx, ϑ, which the radiation might follow could be between 0° and 90°, the average pathlength for radiation passing through d*x* in the +*x* direction can be found by the integral:

$$d\xi_I = dx \int_0^{\frac{\pi}{2}} \left(\frac{\partial I}{I \partial \vartheta}\right)\left(\frac{d\vartheta}{cos\vartheta}\right) \equiv u dx \tag{2.32}$$

After some mathematical operations and manipulations, which are discussed in detail in Chapter Three, one can find the two fundamental differential equations for Kubelka-Munk theory:

$$-dI = -\varepsilon u I dx - \sigma u I dx + \sigma v J dx \tag{2.33}$$

$$-dJ = -\varepsilon v J dx - \sigma v J dx + \sigma u J dx \tag{2.34}$$

2.4.7 Diffusion Theory

Kienle et al. (1998) presented a different approach to investigate the radiation transfer equation. This approach is applicable in biomechanics and biomedical engineering. In the paper that is published by Kienle et al. (1998), the diffusion approximation is used to determine the optical properties of biological tissue. Griffiths and Dahm (2008) pointed out that the propagation of photons in a thick sample with scattering coefficients which are larger than the absorption coefficients, are described by diffusion approximation. The details of this approach are described in Chapter Three and the results are discussed in Chapter Four.

2.5 Discontinuum Theories of Diffuse Reflection

2.5.1 Representative Layer Theory

A layer is representative of a sample if each one of the particles in the sample provide the same volume and surface area fractions in each layer as in the sample (Dahm & Dahm, 2007). The reason for using the volume fraction of the particles is because the absorption fraction of the particle is completely related to volume. On the other hand, the remission is strongly dependent on the surface area fraction of the particle.

The important question is what makes a layer be representative of a sample. Dahm and Dahm (2007) demonstrated three reasons for a layer to be representative. First, the thickness of the layer should have no more than the thickness of one particle since one of the assumptions of representative layer theory was related to the scattering and absorption properties of the layer by combining the mentioned properties for each particle in the layer. Therefore, it would be more suitable to use the thickness for the layer to be nowhere more than one particle thick.

Second, another feature of the representative layer introduced by Dahm and Dahm (2007) is that the volume fraction of each particle in the layer is the same as the sample. One of the most

important assumptions of representative layer theory is related to the voids. Thus, the media that represents the voids does not absorb or scatter light. This means that if the media is a fluid its absorption and scattering must be neglected. Moreover, the void fraction of the representative layer must be the same as the sample.

Finally, the third reason is that the surface area fraction of each particle in the layer will be the same as the sample. Surface area fraction is a property that is more difficult to work with than volume fraction because the shape and size of the particles are required to estimate the total surface area fraction.

In the model of the representative layer that we present here, a particle is of a different type from another if it differs in size and/or composition. Each particle type is characterized by its composition (as represented by its absorption and remission coefficients), its volume, and the average cross-sectional surface area that it presents to the incident beam. We will picture a particle as having two flat ends, each perpendicular to the incident beam. While the shape of the cross-section is not important for our model, it may be pictured as a square. Thus, a representative layer is made up of voids and of particles (shaped as boxes) of varying size. The ends of the boxes are perpendicular to the incident beam. The representative layer is of non-uniform thickness, but is nowhere more than a single particle thick. The layer is representative if:

- The volume fraction of each particle type is the same in the layer as in the sample as a whole.
- For all particle types, the cross-sectional surface area in the layer is in the same proportion as the surface area of the particle type in the sample as a whole.
- The fraction of the cross-sectional surface area that is made up of voids is the same as the void fraction of the sample as a whole.
- Surface area and volume fractions for a given particle type can be computed from weight fractions and particle densities as follows (subscript *i* denotes a specific particle type and *j* is

an index denoting a summation over all particle types). Also, the variables used in the following equations are introduced in Table 2.2.

Table 2.2 Variables used in the development of representative layer theory

Definition of terms			
ρ_i	**Density of a particle**	s_i	**Fraction of particle surface area**
v_i	**Fraction of occupied volume by particle i**	S_i	**Fraction of cross-sectional surface area**
V_i	**Fraction of total volume**	w_i	**Weight fraction**
v_o	**Void fraction**	d_i	**Thickness of a particle**
K_i	**Absorption Coefficient**	b_i	**Remission Coefficient**

$$v_i = \frac{\left(\frac{w_i}{\rho_i}\right)}{\sum\left(\frac{w_j}{\rho_j}\right)} \tag{2.35}$$

$$s_i = \frac{\left(\frac{w_i}{\rho_i d_i}\right)}{\sum\left(\frac{w_j}{\rho_j d_j}\right)} \tag{2.36}$$

$$V_i = (1 - v_0)v_i \tag{2.37}$$

$$S_i = (1 - v_0)s_i \tag{2.38}$$

The following formulas assume that the amount of transmitted light lost by an interaction with a single particle to either absorption or remission is small. According to the assumption of our model, for a single particle, the fraction of light absorbed is given by the cross-sectional area and the Bouguer–Lambert law, and the remission fraction is given by the cross-sectional area and $b_i d_i$. Thus, for a representative layer, Equations 2.39 – 2.40:

$$A_1 = \sum S_i[1 - \exp(-k_i d_i)] \tag{2.39}$$

$$R_1 = \sum S_i\, b_i d_i)] \tag{2.40}$$

The model used to form the layer assumes that the absorption coefficient is independent of remission. For the case of low absorption, an additional simplification may be made. It has been shown experimentally by Kortum (1969) that b_i is proportional to $1/d_i$. This observation is attributed to the fact that the surface area to volume ratio of a particle is proportional to 1/di; the observation is thus consistent with the assumption that remission is a surface phenomenon. This implies that the product $b_i d_i$ is a property of the composition of the material making up the particle but is independent of particle size. Thus, we term $(bd)_i$ the remitting power of a material. For this case, the following approximation is reasonable. Therefore in Equation 2.41 we have:

$$R_1 = \sum S_i\,(bd)_i \tag{2.41}$$

In the linear region, where, for a given absorbing power of a material, the absorption fraction of a particle is proportional to its thickness, the following conditions will be observed.

1. The contribution of a particle type to absorption is proportional to the volume fraction (including voids) of the particle type and to the absorption coefficient of the material making up the particle.
2. The contribution of a particle type to remission is proportional to the cross-sectional surface area of the particle type in the representative layer and the remission power of the material making up the particle.
3. In a mixture of two or more particle types of similar remitting power, the absorption/remission function of each particle type is represented in the absorption/remission function of the sample weighted in proportion to surface area to volume ratio of the particle type.

In regions of higher absorption, the coefficients obtained from the plane parallel mathematics depart significantly from those of the material under consideration and the assumptions about the shape of the particles and the direction of light travel become more important. The regions of extremely high absorption tend not to be of value for compositional analysis. Here, the contribution of a particle to the absorption of a layer is proportional to the surface area fraction of the particle type and not dependent on its thickness. The representative layer model would still be useful in applications such as image analysis.

In the representative layer theory, the remission coefficient is taken as the remission fraction of a single, real layer that is one particle thick divided by the effective thickness of the layer. (The representative layer does not necessarily have a uniform thickness, but its total volume V and a front surface area S can be determined, and V/S can be termed its effective thickness.) The idea behind this is that such a layer has every particle exposed to the full intensity of the incident beam, just as every molecule is exposed to the full intensity of the beam in a sample of infinitesimal thickness. This consideration is not of particular importance to the spectroscopist, but it is brought up to point again out that the coefficients are only approximations to the quantities which we would like to measure.

CHAPTER III

OPTICAL MODELING

3.1 Overview and Organization

Optical modeling of the near-infrared radiation traversing through a medium containing a slurry flow with varying and non-uniform concentration profiles requires investigating different optical theories that are capable of predicting the light scattering and absorption through a particulate medium. These models are chosen based on their applications found in the literature. These theories are applied to similar cases such as powdered samples, which are used in the food product industries or multiphase flow of slurries in oil and gas industries. The validity of methods applied to this problem have been measured through experiments. Hence, only those theoretical methods were chosen which had some experimental results consistent to the two-phase flows or at least particulate solid materials such as coal ore. Detailed study of six broad areas of applied optics results in choosing the most applicable models to the case of solid-liquid mixture of ammonium dihydrogen phosphate (ADP) as the solid phase and the xylene as the liquid phase.

Doing research for choosing best models that matches the case of the proposed study has mostly been focused on the application of models and their assumptions. The applications of models are crucial since they reveal the physics of the operational environments known as mediums, as well as the experiments conducted to test these models. Moreover, the assumptions play another important

role since there are some restrictions such as the shape of particles, homogeneity of the medium, the distribution of the light inside the sample, scattering level of the light, the absorption power of the sample, etc. The next priority was dedicated to choice of a model that has been applied to near-infrared radiation. The wavelength of the light has a relation to the particle sizes in some of the models. Therefore, knowledge about the average particle size in the slurry is required. Some models such as Kubelka-Munk and Mie Scattering theories have been applied to several cases. The theory proposed by Kubelka and Munk is not founded on rigorous mathematics and there have been many controversies in the world of optics over the modifications made on the Kubelka-Munk theory to build up a more advanced model. However, Mie scattering is the most accepted theory and a powerful tool to predict the radiation scattering and absorption phenomena on isolated particles, and is restricted to only spherical ones. Therefore, the choice of model was a very important process. The details of the assumptions and restrictions are described in this chapter. Based on applications, all of the categories that are studied are gathered into the following major areas:

Near-infrared spectroscopy of mixtures consisting of opaque materials and fluids such as paint or blood with applications in biotechnology such as monitoring blood vessels is a major category of this study. Other liquid-liquid mixtures such as milk and solid-liquid mixtures such as oil and sand slurries are the working fluids of some experiments that that have been performed to validate the results of theorems. These theorems are Kubelka-Munk, diffusion theory, and Mie scattering theories.

Near-infrared spectroscopy of uniform powdered samples is applied to many industrial uses. This area consists of several studies which have been performed on some theories to be compared with the experiments. These theories are representative layer theory, simplified version of Kubelka-Munk theory;

Optical modeling of light transport in tissue is another important area in near-infrared radiation. This area contains many papers used to estimate the penetration of light inside the human

tissue. These papers apply experiments to compensate the lack of information for the input data required for modeling the phenomena. For instance, Monte Carlo simulation is a popular method for this purpose. In addition, diffusion theory is used to predict the light fractions through the medium.

Optical modeling of non-uniform powdered samples is the third category of applicable models that were studied in this research. In this situation the light is absorbed or scattered by a mixture of solid particles of different types. The sample then is non-uniform. These models even are able to be applied to the cases of light through samples containing multiphase flows such as two or more types of solids in a liquid. The representative layer theory is the most recent theorem that models this type of complex mixture since it was developed in 1999.

These models, which have been reviewed to be implemented in this study, have some common restrictions such as the homogeneity. However, the representative layer theory is not restricted to homogeneous samples. The optical theories that are modeled have been chosen wisely to solve the problem of near-infrared light penetration through different depths inside the slurry sample.

The aims of this chapter are: introducing the development process of the models in terms of the formulation; then applying those formula, as well as the assumptions to build algorithms of models, also introducing different scenarios for some of models which require input data to be fed from an external source such as computational fluid dynamics (CFD); and showing the process of computerizing the algorithm in MATLAB 7.10.0.499 (R2010a) and FORTRAN 2003. In this Chapter, before making the algorithms the assumptions and the mathematics of the theories are investigated. Since the mathematics of each theory suggests a specific configuration and is based on a unique geometry, the arrangement of the elements is studied to make the building of algorithm easier. In this chapter the development of different parts are as follows: **(i)** optical models: in this section the mathematical formulas are gathered or derived for making the algorithms, **(ii)** designing the algorithms: algorithms of codes are introduced in this section, **(iii)** code development: in this section

the values of some input parameters for different scenarios of the methods are addressed. Finally, after writing the interactive software code based on the models, the results are will be presented in Chapter 3. A detailed description about the results is presented in Chapter 4.

3.2 Development of Continuum Optical Models

Optical models introduced in the previous chapter are derived and modified based for the case of two-phase slurry of xylene and ADP. Methods are developed here in two parts: continuum and discontinuum theories. We kept this categorization since some elements in developing algorithms of models are different from continuum to discontinuum theories. These elements are concerned with adjustments that have been made to discontinuum models, which are required as inputs for algorithms. For instance, one of the most important adjustments has been done is for the representative layer theory to make it compatible to the case of a slurry fluid by being fed with the computational fluid dynamics models of Reynolds stress and k-epsilon. Uniform and non-uniform concentration profiles were those elements that were used as inputs for the adjusted model of representative layer. These concentration profiles are modeled separately. Complete details of computational approaches for optical models are discussed in this section.

Models that are discussed here are continuum models or are based on particle treatments. Continuum models are mostly developed by deriving solutions to the radiatiative transfer equation and applying approximations to them. Continuum models that are developed are: Schuster's theory, Kubelka-Munk theory, radiative transfer treatment, three-flux approximation, and diffusion theory. Most continuum models are much easier to apply than discontinuum ones because of their mathematical operations. However, their simplicity includes many differences with other models of diffuse reflectance or particle theory such as Mie scattering theory. These continuum theories are not as powerful as Mie scattering to predict the scattering and absorption in particles. In this section,

models are developed. Moreover, restrictions for the case of slurry fluid flow will be discussed concisely.

3.2.1 Schuster's Model

In Chapter Two a brief discussion about Schuster's theory is reviewed from literature. In this section, his formulas to solve the radiation transfer equation will be implemented. He has built a very simple model. In this study, the purpose is to apply it to this novel case of a slurry sample, and to compare its results with other theories of diffuse reflectance.

As stated by Chalmers and Griffiths (2002), in 1905, Schuster was the first scientist who tried to find a simplified solution of the radiation transfer equation. He assumed that the light penetrates the slurry sample through two oppositely incident radiations in direct illumination. This was a very simple assumption since the incident beam encounters the sample with an intensity I, and reflects back with an intensity J. Hence, these two different fluxes that are in opposite directions symbolize a very simple case in dealing with the particular problem of radiation transfer. With this simplification, Schuster derived the following two differential equations:

$$-\frac{dI}{d\tau} = (k+s)I - sJ \tag{3.1}$$

$$\frac{dJ}{d\tau} = (k+s)J - sI \tag{3.2}$$

when

$$k = \frac{2\alpha}{\alpha+\sigma} \tag{3.3}$$

$$s = \frac{\sigma}{\alpha+\sigma} \tag{3.4}$$

where α is the true absorption coefficient of single scattering, σ is the scattering coefficient for single scattering, and τ is the penetration depth through the sample. In Equation 3.4, s used by Schuster is identical to the albedo ω_o for single scattering. As it was introduced in Chapter Two, albedo is a

parameter that refers to diffuse reflectivity or reflectance power of a surface. It has been defined as the fraction of reflectance intensity from the surface to incident radiation upon it. Albedo is a dimensionless fraction like reflection or absorption that states the extent to which it reflects light. The albedo number for a black surface is zero and for perfect white surface is one. As it stated by Chalmers and Griffiths (2002), these coefficients relate to the reflectance measured as if particles in the model were separated so far apart so that only single scattering is able to happen. It means that these coefficients, can be applied to the individual particles in the case of single scattering.

If the boundary conditions are set as:

$$I = I_o \text{ at } \tau = 0 \tag{3.5}$$

$$I = I_{(\tau)} \rightarrow 0; \qquad J = 0 \text{ at } \tau = \tau \text{ for } \tau \rightarrow \infty \tag{3.6}$$

These boundary conditions can be interpreted to the following expressions:

1. The intensity of flux *I* is equivalent to the incident intensity at zero penetration depth, and;
2. At an infinite depth into the sample the intensity of both rays *I* and *J* is zero, therefore there will be no change in the diffuse reflection.

the differential Equations 3.1 and 3.2 is solved to represent the reflectance at infinite depth, i.e. the depth which a sample must be in order to have no further change in the measured diffuse reflectance:

$$R_\infty = \frac{J_{(\tau=0)}}{I_o} = \frac{1 - (k/(k+2s)^{1/2}}{1 + (k/(k+2s)^{1/2}} \tag{3.7}$$

where R_∞ is the reflectance of the light that returns to the sensor above the sample. This can be written as:

$$\frac{(1-R_\infty)^2}{2R_\infty} = \frac{k}{s} = \frac{2\alpha}{\sigma} \tag{3.8}$$

Equation 3.8 is known as Schuster's equation. It gives the reflectance for isotropic scattering when two radiation fluxes that are assumed in the direction of the surface normal and are opposite to each other encounter the sample. In Section 3.2.2, it will be seen that Kubelka and Munk derived an expression similar to Schuster's solution. The difference between the scattering and absorption coefficients in Kubelka-Munk and Schuster's theories is only related to the definition of two constants *k* and *s*. Schuster defined these constants in terms of the absorption and scattering coefficients for single scattering, while, Kubelka and Munk presented *k* and *s* in their equations as the absorption and scattering coefficients for the densely packed sample as a whole. Dahm and Dahm (2007) pointed out that the Schuster's scattering and absorption coefficients have the following relations with the scattering and absorption coefficients in Kubelka-Munk equations:

$$k = 2\alpha, \quad s = \sigma \tag{3.9}$$

where k and s are absorption and scattering coefficient similar to Kubelka-Munk function. As mentioned by Dahm and Dahm (2007), since Schuster's theory deals with isotropically scattering particles, even if the direct illumination strikes the sample, it becomes diffuse as it scatters within a sample.

According to the Schuster's paper for the "foggy atmosphere", which is a sample of particles, it can be imagined that the atmosphere is divided into layers, each containing a number of particles. Therefore, Griffiths and Dahm (2008) stated that in the limit of infinite dilution, there will be one particle in such a layer. For such a condition, there can be no multiple scatter between particles in the same layer. Equations 3.1 to 3.4 represent an implicit assumption that the fraction $(\alpha + \sigma)$ is insignificant compared to 1. This limitation is somewhat improved by the following discontinuous solution:

$$f(R_\infty) = \frac{(1 - R_\infty)^2}{2R_\infty} = \frac{k}{s} = \frac{\alpha(2 - \alpha - \sigma)}{\sigma} \tag{3.10}$$

which is the discontinuous form of Schuster's equation for isotropic scattering. The Dahm equation is an exact solution to diffuse reflectance using discontinuum approaches. Dahm's equation is also valid for anisotropic scattering and does not assume that $\alpha + \sigma$ is insignificant compared to 1. For modeling Schuster's theory, the equation above is modified to account for the void fraction and to be implemented in the model produced by representative layer theory that uses the concentration profiles obtained from CFD.

$$f(R_\infty) = \frac{(1-R_\infty)^2}{2R_\infty} = \frac{k}{s} = \frac{\alpha(2-\alpha-\sigma)}{\sigma} = \left(\frac{2}{1-v_0} - \alpha - 2\beta\right)(1-v_0)\alpha/\beta \qquad (3.11)$$

3.2.2 Kubelka-Munk Model

Kubelka-Munk (K-M) theory has been introduced in Chapter Two. It is a two dimensional theory in the field of diffuse reflectance. Kubelka-Munk equations are derived here in this section following the approach of Wendlandt and Hecht (1966). Nobbs's (1985) clarification of the model is also applied to the developed model. He has used plane parallel layers to develop the Kubelka-Munk equations, improving the accuracy.

This method has provided the most widely adopted approach to determine the characteristic of light in diffusing media by solving simultaneous first order differential equations. These equations describe the reduction of light in a sample due to scattering and absorption.

Configuration of model:

1. By considering a layer composed of absorbing and light scattering particles that are uniformly or randomly distributed, one can start using diffusion theory.
2. The dimensions of particles are smaller than the layer thicknesses.
3. The width of the layer has been extended to infinity. Consequently, the effect of edges can be neglected.

4. According to Figure 3.1, d is the thickness of the layer, and the positive x direction is downward such that $x = 0$ is the illuminated surface and $x = d$ is the unilluminated surface. The radiant flux in the positive x direction is I while the reflection in the negative x direction is J. Also, the incident beam has the intensity of I_0.
5. It can be approximated that only the two directions of the incident and reflected beams are considered in this theory and that they are perpendicular to the surface of the layer. This assumption introduces a small error compared to ideal diffuse reflection.

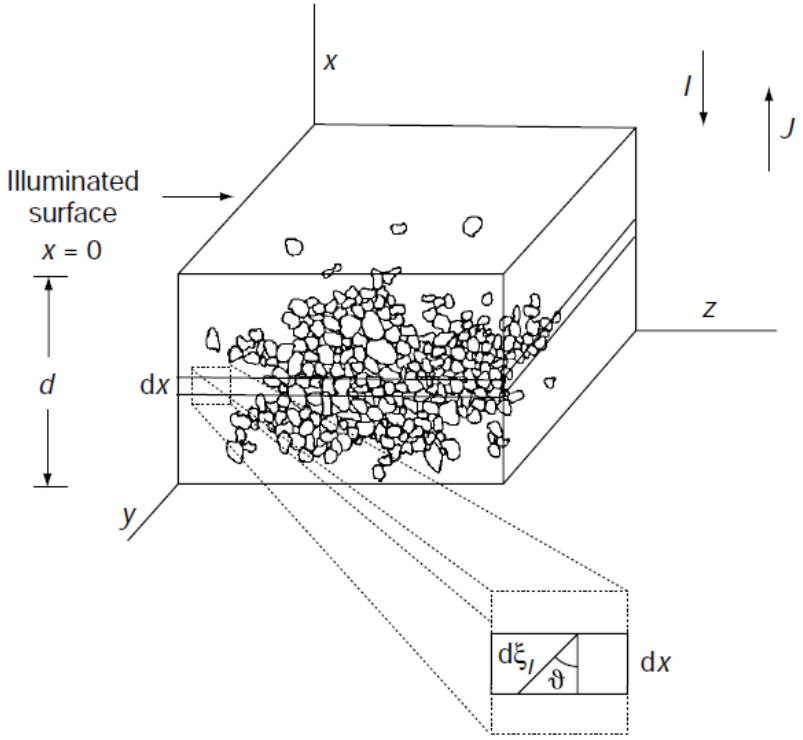

Figure 3.1 Diagram of a sample of slurry representing the Kubelka-Munk model. There is a random distribution of particles. (Chalmers & Griffiths, 2002)

If the illuminated beam has an angle ϕ from the surface normal, as it goes through an infinitesimal layer dx. But the path is not dx and is $dx/cos\phi$. Hence, to calculate the average path length, $d\xi_I$, of light when it passes dx in downward direction we have:

$$d\xi_I = dx \int_0^{\pi/2} \frac{\partial I}{I \partial \Phi} \frac{d\Phi}{cos\Phi} \equiv u dx \tag{3.12}$$

where $\frac{\partial I}{\partial \Phi}$ is the angular distribution of the intensity in the positive x direction. The average path-length of light passing through infinitesimal layer dx in the reverse direction toward the illuminated surface of sample can be estimated through the following relation:

$$d\xi_J = dx \int_0^{\pi/2} \frac{\partial J}{J \partial \Phi} \frac{d\Phi}{cos\Phi} \equiv v dx \tag{3.13}$$

All of the variables used in this model are explained in Table 3.1. These variables are also used in Schuster's theory.

Table 3.1 Variables used in the development of Kubelka and Munk's simplified solution to the radiation transfer equation. (Neither ε or σ are exactly the same as the corresponding parameters defined by Schuster)

Field	Description
d	sample layer thickness
$+x$	downward direction through the sample
$-x$	upward direction through the sample
$x = 0$	illuminated surface
$x = d$	unilluminated surface
I	radiant flux in $+x$ direction
J	radiant flux in $-x$ direction
ϑ	angle at which a particular ray traverses through dx
dx	an infinitesimal layer
$dx/cos\vartheta$	pathlength of a particular ray traverses through dx
$d\xi_I$	Average pathlengtth of radiation passing through dx in the $+x$ direction
ε	Fraction of radiation absorbed per unit pathlength in the sample
σ	Fraction of radiation scattered per unit pathlength in the sample

Let ε be the absorption coefficient that means the fraction of light absorbed per unit path length. Moreover, σ is the scattering coefficient that is defined by the fraction of scattering

coefficient to the unit path length. Now, consider when the flux is penetrating the sample in the positive x direction. According to the theory of diffuse reflectance, it is easily seen that any reduction in intensity, when light passes through the element of dx is:

$$(\varepsilon + \sigma)Id\xi_I = (\varepsilon + \sigma)uIdx \tag{3.14}$$

where $\varepsilon uIdx$ is the amount of light that is absorbed and $\sigma uIdx$ is the part which is scattered. Inversely, if the infinitesimal thickness of dx is illuminated by J component – when the light is reflected back to the illumination surface – the corresponding expression for the decrease in the intensity can be obtained by:

$$(\varepsilon + \sigma)Jd\xi_I = (\varepsilon + \sigma)vJdx \tag{3.15}$$

According to the discussion above, for the whole dx there are two different illuminations of light reflected or absorbed by the thickness dx. Therefore, the differential equation describing the reduction in the intensity of the flux in both directions of I and J through that infinitesimal layer dx is:

$$dI = -(\varepsilon + \sigma)uIdx + \sigma vJdx \tag{3.16}$$

and,

$$dJ = +(\varepsilon + \sigma)vJdx - \sigma uIdx \tag{3.17}$$

According to the equations above, the signs have been chosen to be compatible with this principle that by increasing x, I and J decrease. In an ideal diffusing medium, the radiation has the same intensity in all directions. The angular distribution of the flux through a plane in a given direction for example in x direction is (Hecht, 1966):

$$\frac{\partial I}{\partial \Phi} = I \sin 2\Phi \tag{3.18}$$

Moreover, for the negative x direction, the change of the intensity in angular direction is:

$$\frac{\partial J}{\partial \Phi} = J \sin 2\Phi \tag{3.19}$$

By substituting the Equations 3.18 and 3.19 into 3.16 and 3.17 respectively, then the values of u and v in the Equations 3.16 and 3.17 can be obtained using the following formula:

$$u = v = \int_0^{\pi/2} \frac{sin2\phi}{cos\phi} d\phi = 2\int_0^{\pi/2} sin\phi \, d\phi = 2 \tag{3.20}$$

The reason for integrating over the range of $\phi = 0$ to $\phi = 90$ is because of the angle of the incident light through the sample. The angle $\phi = 0$ corresponds to the beam normal to surface and $\phi = 90$ is parallel to the surface. Therefore, by substituting the magnitude of u and v from the integration above into Equations 3.16 and 3.17, the differential equations for I and J are:

$$\begin{aligned} dI &= -(k+s)Idx + sJdx \\ dJ &= +(k+s)Jdx - sIdx \end{aligned} \tag{3.21}$$

where $k = 2\varepsilon$ and $s = 2\sigma$. The Equations of 3.21 are only valid for the ideal diffusion of light in the layer which is under consideration (Wendlandt & Hecht, 1966). The ideal diffusion means that the intensity of light is the same in all directions. In the case of diffuse incident radiation or the case of parallel light, these two equations are also valid. For example, for the case of diffuse illumination at incident angle of 60 degrees, u and υ are again equal to 2 since $cos\phi = \frac{1}{2}$. According to experiments discussed by Bull (1990) as well as Dahm and Griffiths (2008), the equations seem to be valid for powdered samples. By solving this system of differential equations, the radiation flux for ideally diffusing medium can be obtained through the following general solutions:

$$\begin{aligned} I &= A(1-\beta)e^{\kappa x} + B(1+\beta)e^{-\kappa x} \\ J &= A(1+\beta)e^{\kappa x} + B(1-\beta)e^{-\kappa x} \end{aligned} \tag{3.22}$$

where,

$$\kappa \equiv \sqrt{k(k+2s)} \tag{3.23}$$

and,

$$\beta \equiv \frac{\kappa}{k+2s} = \sqrt{\frac{k}{k+2s}} \tag{3.24}$$

A and B are constants that must be determined by the boundary conditions of the sample at *x=0* and $x = d$, if we integrate over the entire thickness of the sample. Therefore, the boundary conditions are:

$$\begin{aligned} I &= I_0 \quad for \quad x = 0 \\ I &= I_{x=d}\,, J = 0 \quad for \quad x = d \end{aligned} \tag{3.25}$$

Solution for A and B under these conditions gives:

$$\begin{aligned} A &= -\frac{(1-\beta)e^{-\kappa d}}{(1+\beta)^2 e^{\kappa d} - (1-\beta)^2 e^{-\kappa d}} I_0 \\ B &= \frac{(1+\beta)e^{\kappa d}}{(1+\beta)^2 e^{\kappa d} - (1-\beta)^2 e^{-\kappa d}} I_0 \end{aligned} \tag{3.26}$$

Now, we can use geometric optics to find the relations for the reflection and transmission fractions. The transmission and reflection are:

$$\begin{aligned} T &= \frac{I_{x=d}}{I_0} = \frac{4\beta}{(1+\beta)^2 e^{\kappa d} - (1-\beta)^2 e^{-\kappa d}} \\ R &= \frac{J_{x=0}}{I_0} = \frac{(1-\beta^2)(e^{\kappa d} - e^{-\kappa d})}{(1+\beta)^2 e^{\kappa d} - (1-\beta)^2 e^{-\kappa d}} I_0 \end{aligned} \tag{3.27}$$

These formulas also can be written in the form of hyperbolic functions which have been derived by Kubelka (Wendlandt & Hecht, 1966).

$$\begin{aligned} T &= \frac{I_{x=d}}{I_0} = \frac{2\beta}{(1+\beta^2)\sinh \kappa d + 2\beta \cosh \kappa d} \\ R &= \frac{J_{x=0}}{I_0} = \frac{(1-\beta^2)\sinh \kappa d}{(1+\beta^2)\sinh \kappa d + 2\beta \cosh \kappa d} I_0 \end{aligned} \tag{3.28}$$

If there is no scattering within the layer, then $s = 0$ and from Equations 3.23 and 3.24, $\kappa = k$ and $\beta = 1$. Substituting into Equation 3.27, the transmittance of the layer is calculated similar to the Beer-Lambert law, and is $T = e^{-\kappa d}$. Wendlandt and Hecht (1966) defined the reflectance of infinite layers as R_∞, which refers to the infinite thickness of sample or $d = \infty$, therefore, $T_\infty = 0$. The following formula is derived for the reflectance of an infinitely thick sample:

$$R_\infty = \frac{1-\beta}{1+\beta} = \frac{1-[k/(k+2s)]^{1/2}}{1+[k/(k+2s)]^{1/2}} \tag{3.29}$$

R_∞ is the reflectance of a layer so thick that further increase in thickness fails to change the reflectance. Absorption and scattering coefficients of Kubelka-Munk model for a special case of xylem and ADP is obtainable with an experiment. However, Nobbs (1989) proved that the plane parallel mathematics can be used with the Kubelka-Munk theory. In this situation, Kubelka-Munk functions are derived with a discontinuum approach using the layers shown in Figure 3.2. The incident and reflected intensities are obtained for each layer. Then, they are applied to calculate the light fractions to find absorption and scattering coefficient in each layer. According to this formula one can apply them in the optical model code by using the plane parallel layers. It means that the form of Equations 3.29 is only applicable to a thick layer of the sample. However, one must transfer it into the form of discontinuous layers and make it possible to be applied to several layers. Figure 3.2 represents the reflectance and transmittance of a thin layer of material. This has been done by Nobbs (1985).

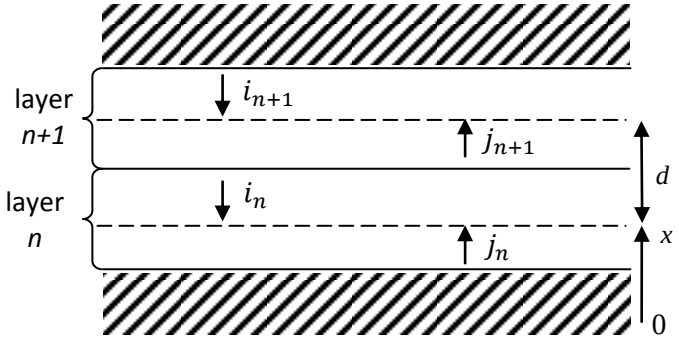

Figure 3.2 Reflectance and transmittance of a thin layer of thickness *d* within a sample

The reflectance and transmittance of a thin layer of thickness d is characterized by the following formula (Nobbs, 1985):

$$I_{n+1} - I_n = \left[\left(\frac{1}{t}\right) - 1\right] I_n - (\frac{r_0}{t}) J_n$$
$$J_{n+1} - J_n = [t - 1 - ({r_0}^2/t)] J_n - (\frac{r_0}{t}) I_n \quad (3.30)$$

where r_0 and t are the reflectance and transmittance of a single layer, respectively. In this form of the Kubelka-Munk model, the scattering and absorption coefficients are defined as follows: $S.d$ is the reflectance and $(1 - K.d - S.d)$ is the transmittance that can be substituted as $r_0$and t in Equations 3.30.

$$S = (\frac{r_0}{d})_{d \to 0} = (\frac{dR_0}{dx})$$
$$K = (\frac{a}{d})_{d \to 0} = -\left(\frac{dT}{dx}\right) - (\frac{dR_0}{dx}) \quad (3.31)$$

Therefore, the diffuse reflectance of an infinitely thick sample can be achieved using Equations 3.30 and 3.31 considering this fact that the $R_\infty = (\frac{J_n}{I_n})$. Hence,

$$R_\infty = \frac{(1 + {r_0}^2 - t^2) - [(1 - {r_0}^2 - t^2)^2 - 4{r_0}^2]^2}{2r_0} \quad (3.32)$$

The reflectance of a sample over an ideally black background,R_0, and the transmittance will be written as:

$$R_0 = \frac{R_\infty (1 - e^{-2Z})}{(1 - {R_\infty}^2 e^{-2Z})} \quad (3.33)$$

$$T = \frac{(1 - {R_\infty}^2) e^{-Z}}{(1 - {R_\infty}^2 e^{-2Z})} \quad (3.34)$$

where,

$$Z = [K + S(1 - R_\infty)]x \quad (3.35)$$

or,

$$Z = [K(K + 2S)]^{1/2}x \tag{3.36}$$

where x is the depth through the sample, K is the absorption coefficient and S is the scattering coefficient. K and S are reflectance and transmittance coefficients of a thin layer. They are proportional to the concentrations of absorbing and scattering particles present in the material. A separate model is required to relate K and S to the fundamental optical properties of the material, or absorption coefficient, ε, or scattering coefficient, σ. The relationship between ε and K is calculated by Kubleka when the light traverses the infinitesimal distance du is εdu. The average pathlength for diffuse light is explained through an integral in Equation 3.20. However, for the relationship between scattering coefficient S and σ, there is no straightforward method. The simple approach that was developed by Kubelka assumes that the light was isotropically scattered. Therefore, only half of the total scattered will be into the upper half hemisphere and contribute to the reflectance of the layer.

3.2.3 Radiation Transfer Approximations

There are several models developed to simplify radiation transfer theory for different spectroscopic applications. The model used here is an approximation of radiation transfer equation developed by Patterson, Schwartz, and Wilson (1989). This model was introduced in Chapter Two, and in this section the formulation used in the model will be discussed.

This model is developed based on a measurement. The schematic view of the experiment was shown in Figure 2.8. In this setup, light is projected on the surface of the tissue by an optical fiber sensor and scattered light is detected by a second sensor also positioned on the surface at a distance from the source. The steady-state solution to radiation transfer equation, which for a homogeneous medium, results in a differential equation for the photon fluence rate $\phi(r)$

$$-\mathrm{D}\nabla^2\Phi(\mathrm{r}) + \mu_\mathrm{a}(\mathrm{r}) = \mathrm{S}(\mathrm{r}) \tag{3.37}$$

where D is the diffusion coefficient and can be determined from the following equation:

$$D = \{3[\mu_a + (1 - g)]\mu_s\}^{-1} \tag{3.38}$$

where, *S(r)* is the photon source, g is the mean of the cosine of scattering angles, μ_a is the linear absorption coefficient, and μ_s is the linear scattering coefficient. The solutions to radiation transfer equation are somewhat unwieldy to use, therefore it is difficult to derive useful analytic expressions for the quantities of interest in reflectance spectroscopy. Some assumptions is made to simplify the model and to find expressions that are approximate.

Patterson et al. (1989) introduced an accurate approximation of radiation transfer equation, which incorporates based on a refractive index mismatch at the surface of the material. This approximation is achieved by solving the reflectance when a set of parallel beams is incident on the surface. A one dimensional version of Equation 3.37 is determined from the following equation:

$$-D\frac{d^2\Phi(z)}{dz^2} + \mu_a\phi(z) = S(z) \tag{3.39}$$

where S(z) represents a source of first scattered photons:

$$S(z) = (1 - g)\mu_s \exp\{-[\mu_a + (1 - g)\mu_s]z\} \tag{3.40}$$

and the differential equation is solved based on the boundary condition. Equation 3.41 shows the empirical relation of the internal diffuse reflection coefficient that is related to refractive index of the material (Patterson et al., 1989):

$$r_d = -1.44n^{-2} + 0.71n^{-1} + 0.668 + 0.0636n \tag{3.41}$$

where n is the refractive index, and r_d is the internal diffuse reflection. Finally, the total diffuse reflection is derived using the boundary condition at the surface ($z = 0$):

$$R = \frac{a'}{1 + 2k(1 - a') + (1 + \frac{2k}{3})\sqrt{3(1 - a')}} \tag{3.42}$$

where a' is the transport albedo:

$$a' = \frac{(1 - g)\mu_s}{\mu_a + (1 - g)\mu_s} \tag{3.43}$$

and,

$$k = \frac{1 + r_d}{1 - r_d} \tag{3.44}$$

Patterson et al. examined Equation 3.42 with Monte-Carlo simulation and suggested that the diffuse reflectance obtained from this relation is accurate to within 2% for values of μ_a, μ_s, and g. Moreover, Equation 3.42 is applicable to soft tissues in the red, and near-infrared wavelengths.

3.2.4 Three Flux Model

This model is developed based on two methods: that developed by Burger, Kuhn, Caps, and Fricke (1997) and another which is a diffuse reflectance approximate model based on the radiative transfer equation proposed by Burger, Ploss, Kuhn, Ebel, and Fricke (1997). The equation of radiative transfer for diffuse reflectance and transmittance is analytically solved by using a three flux approximation. In the studies performed by Burger et al., combined transmittance and reflectance measurements allow one to derive both the scattering and the absorption coefficients. Therefore, their studies are not pure theoretical (experiment is required) since they measured these two coefficients.

The radiation transfer through a scattering and absorbing non-homogeneous medium can be described by the equation of radiative transfer (ERT). For a plane-parallel sample, the change of intensity I at an optical depth τ along the path dx in a direction Ω is given by:

$$\mu \frac{dI}{dx} = -(E_a + E_s)I + \frac{E_s}{4\pi}\int_{4\pi} p(\Omega, \Omega')\, I(\Omega') d\Omega' \tag{3.45}$$

where μ is the cosine of the angle between the direction Ω and the surface normal of the sample. Intensity losses are caused by scattering and absorption processes. An intensity increase caused by scattering from all directions is evaluated by the probability of such scattering events. This probability is defined as the phase function or $p(\Omega, \Omega')$.

3.2.5 Diffusion Model

The diffusion model is a totally distinct method to describe and anlayze the radiation transfer through materials. The diffusion approximation is a technique, which is often used in biomedical applications. Griffiths and Dahm (2008) pointed out that the scattering of the light beams in a medium with sufficient thickness can be predicted by a diffusion of radiation. The feature of this diffusion process is the scattering coefficient which should be greater than the absorption coefficient. A similar approach to Equation 3.32 is designed to calculated the diffuse reflectance of the sample of slurry fluid with an large optical thickness. Hence, $R\infty$ can be described as a function of the ratio α/σ. This ratio is the absorption to scattering coefficient defined by Schuster (1905). The diffuse reflectance for directional sample illumination yields (Chalmers & Griffiths, 2002):

$$R_\infty = \frac{1}{1 + 3(\alpha/\sigma) + 5/3(3(\alpha/\sigma)^2 + 3(\alpha/\sigma))^{1/2}} \tag{3.46}$$

The result of applying the two radiative transfer approximations such as three-flux model and diffusion approximation, which predict the diffuse reflectance of an optically thick sample are compared with the Kubelka-Munk results in Chapter Four. Chalmers and Griffiths (2002) stated that three models of diffusion theory, the three-flux theory, and the radiative transfer approximation were computed for both directional and diffuse illuminations, however, for the K-M theory, only diffuse illumination is considered. It is essential to recall that the directional illumination applies to samples which are illuminated by a perpendicular direction of light and diffuse illumination occurs when beams. The data according to the K–M theory (Equation 3.32) were obtained for diffuse sample

illumination. The differences between the K–M theory and the other models are because of the direction of sample illumination. In addition, the definition of Schuster's and Kubelka-Munk's scattering and absorption coefficients cause discrepancies between the results of diffuse reflectance in the continuum models. Giovanelli (1955) proposed an approach to solve radiation transfer equation. His model is an exact solution to the radiation transfer equation, and the three-flux approximation is in very good agreement to the results of Giovanelli (1955). However, in the model of diffusion approximation large deviations from the exact solution is appeared for larger ratios of absorption to remission coefficients. It is essential to mentioned that in all the models described in previous sections, specular reflection when the light first encounters the boundary of the sample is neglected. Hence, these models are only valid for the slurries which does not have high concentrations or have to be used with care for other samples (Griffiths & Dahm, 2002).

3.3 Development of Discontinuum Optical Models

3.3.1 Model of Plane Parallel Layers

The strategy of the plane parallel layer treatment is to divide a sample into distinct layers. Radiation entering a given layer may be absorbed, may be transmitted forward into the next layer, or may change direction and be remitted (the word we use to describe the summation of regular and diffuse reflection) into the previous layer. A layer having a thickness d absorbs a particular fraction A_d of the radiation, transmits a particular fraction T_d, and remits a particular fraction R_d, with $A_d + R_d + T_d = 1$. Note that the thickness d is simply a label that designates the layer to which the symbol applies and does not affect the calculation. The fractions of incident light absorbed, remitted, and transmitted (which we refer to as the A, R, T fractions) from a particular layer, i, of unknown thickness can be equally well represented by the symbols A_i, R_i, and T_i.

The remainder of this section presents mathematics used to represent a sample as a combination of layers. This mathematics are valid regardless of the number of fluxes, or any other aspect of the model used

to determine the properties of an individual layer. If an incident beam first encounters layer *i* and then a second layer, *j*, a fraction of the incident intensity T_i enters layer *j*, and a fraction T_iT_j will be transmitted through both. A fraction T_iR_j will be remitted by the second layer back into the first. It may, then, either be transmitted through the first layer (and recorded as part of the total reflected light), absorbed in the first layer, or remitted back into the second layer. This remission back and forth between layers in a sample can continue indefinitely, as illustrated in Figure 3.3.

Assume a sample is composed of two layers, i and j (where i is closest to the incident beam) and the A, R, and T properties for each individual layer are known. The properties for the sample as a whole (indicated by the label i and j) are given by the following equations:

$$\begin{aligned} T_{i+j} &= T_i T_j/(1 - R_i R_j) \\ R_{i+j} &= R_i + T_i^2 R_j/(1 - R_i R_j) \\ A_{i+j} &= 1 - T_{i+j} - R_{i+j} \end{aligned} \tag{3.47}$$

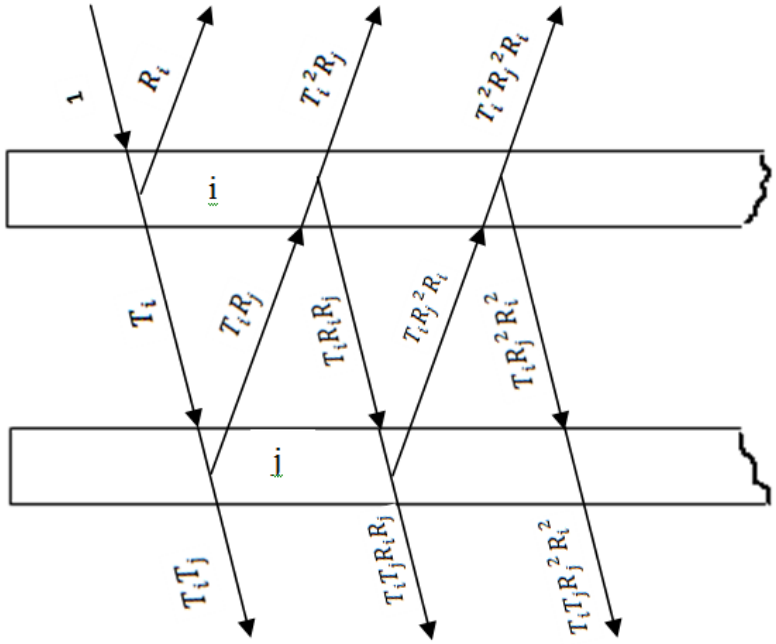

Figure 3.3 Absorption, reflection and transmission possibilities for a sample composed of two layers

Note that Equation 3.41 does not require that the properties of the material in layer *i* are the same as those in layer *j*. For materials composed of multiple identical layers, the properties of a sample consisting of $n+1$ such layers can be derived from the properties of a sample consisting of n layers, using Equation 3.48:

$$\begin{aligned} T_{n+1} &= T_n T_1/(1-R_n R_1) \\ R_{n+1} &= R_n + {T_n}^2 R_1/(1-R_n R_1) \\ A_{n+1} &= 1 - T_{n+1} - R_{n+1} \end{aligned} \tag{3.48}$$

For a sample of a homogeneous material twice as thick as a sample of thickness *d*, Equation 3.49:

$$\begin{aligned} T_{2d} &= T_d T_d/(1-R_d R_d) = {T_d}^2/(1-{R_d}^2) \\ R_{2d} &= R_d + \frac{{T_d}^2 R_d}{1-{R_d}^2} = R_d\left(1+\frac{{T_d}^2}{1-{R_d}^2}\right) = R_d(1+T_{2d}) \\ A_{n+1} &= 1 - T_{2d} - R_{2d} \end{aligned} \tag{3.49}$$

3.3.2 Model for Assembly of Sheets

Model for the assembly of sheets considers a layer of the sample and applies the model formulation on that layer. This layer is called a sheet. A sheet is a three dimensional layer of material with two large, flat, smooth, parallel surfaces with two dimensions much larger than the third (Griffiths & Dahm, 2008). The third dimension is the thickness of the sheet. It is assumed that the sheets are under directed illumination. It means that the sheets are subjected to a directed beam from a direction perpendicular to the other two dimensions which are larger than the thickness. The radius of the beam is much smaller than the front surface area of the sheet that it encounters. When the incidence is directional, the reflectance from the surface of a sheet, r_0, may be estimated from the index of refraction of the material, n_1, and the index of refraction of the dispersing medium, n_0, based on the Fresnel equation (Dahm & Dahm, 2007):

$$r_0 = \frac{(n_1 - n_0)^2}{(n_1 + n_0)^2} \tag{3.50}$$

This formula does not study the effect of absorption on remission. It is important to mention that in the near-infrared region, the absorption is small. Hence, the refractive index, and consequently the reflectance of a surface should not change dramatically with absorption fraction of light (Griffiths & Dahm, 2008). However, in the mid-infrared region, the effect of absorption on reflectivity should be considered. Moreover, in this region, the refractive index changes significantly across the band. In these situations, it has been suggested by Griffiths and Dahm (2008) that the effect of absorption must be considered before using the Fresnel equations.

Inside a sheet, the transmission is dissipated due to absorption since the light is absorbed based on the absorption power of the material. The loss of transmission due to absorption can be calculated from the Bouguer–Lambert law using the expression $[1 - exp(-kd)]$, where k is the linear absorption coefficient of the material making up the layer and d is the thickness of the sheet. Therefore, when a portion of the light incident on the back surface is absorbed, and the reflection from it is correspondingly reduced. The fraction of incident light the total transmittance through a layer, T_1, and the fraction of light absorbed by a layer, A_1, and the fraction remitted by a single sheet, R_1 can be estimated from the Equations 3.51.

$$\begin{aligned} R_1 &= r_0 + \frac{(1 - r_0)^2 r_0 \exp(-2kd)}{1 - {r_0}^2 \exp(-2kd)} \\ T_1 &= \frac{(1 - r_0)^2 \exp(-2kd)}{1 - {r_0}^2 \exp(-2kd)} \\ A_1 &= 1 - R_1 - T_1 \end{aligned} \tag{3.51}$$

The reflectance from a layer, R_1, describes a very important physical meaning. The expression $exp(-2kd)$ is an exponential function always between zero and one, and is located in a negative term

in the denominator. Hence, for the case of a constant reflectivity, if the absorption increases, the remission is affected in a sense that it will be reduced from the total intensity that has penetrated into a single sheet of the material. Hence, if the surface reflections and absorptions are independent from each other and are not influenced by the reduction of one fraction, it is possible to find a condition under which the layer's absorption and remission depends on each other. Therefore, the remission from a sheet of material or a particle inside a medium, which has both a front and rear surface and has absorbing characteritics, does depend on absorption.

In this model it is assumed that refractive index of particles and medium is a constant value in the range of near-infrared spectrum. Hence, because of this assumption the constant reflectivity, r_0, which depends on a constant refractive index, is a reasonable assumption in the NIR region. However, in higher wavelengths such as the mid-infrared, the conditions are more complicated since the refractive index varies in the spectrum, where there are strong absorption bands. Therefore, increases r_0. In this situation, it is probable that the remission from an absorbing layer or particle depends on absorption.

The equations that govern the travel of light through a sample composed of several sheets are complicated, but they are solved and computed with a computer program. Here in the following equations, *x* represent the distance into the sample analogous to the thickness of a single sheet. For example if *x* is equal to 2, it is twice the thickness of a single sheet, and if *x* is 1/2, it is half the thickness of a single sheet (Griffiths and Dahm, 2008). These equations are used to integrally calculate the fractions of light inside the medium. From the fractions of a single layer (given by A_1, R_1, and T_1), we can calculate the fractions for a distance *x* (with $A_x + R_x + T_x = 1$) by Equations 3.52. The fractions of light calculated from the following equations are their total value from the surface or boundary of medium to the point represented with the value of *x*. The algorithm of this model is illustrated in Figure 3.4.

$$T_x = \frac{\Omega - \Omega^{-1}}{\Omega\Psi^x - (\Omega\Psi^x)^{-1}}$$

$$R_x = \frac{\Psi^x - (\Psi^x)^{-1}}{\Omega\Psi^x - (\Omega\Psi^x)^{-1}} \tag{3.52}$$

$$A_x = 1 - T_x - R_x$$

where Ω ,Ψ, and Δ are defined as:

$$\Omega = \frac{1 + R_1 + {T_1}^2 + \Delta}{2R_1}$$

$$\Delta = \sqrt{(1 + R_1 + T_1)(1 + R_1 - T_1)\,(1 - R_1 + T_1)(1 - R_1 - T_1)} \tag{3.53}$$

$$\Psi = \frac{1 + R_1 + {T_1}^2 + \Delta}{2T_1}$$

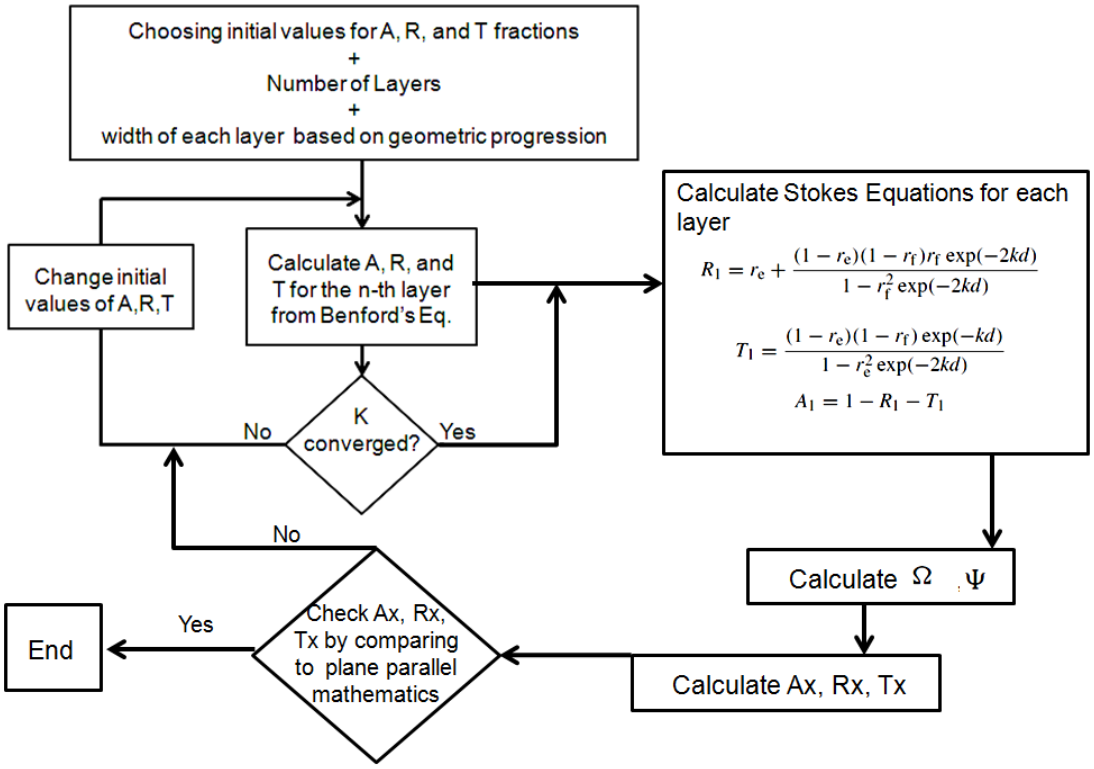

Figure 3.4 The flow chart of the model of assembly of sheets

In Figure 3.4 the algorithm of the assembly of sheets is described. In this model one may use the Equations of 3.51 independently to calculate the fractions of light without using plane parallel mathematics. But it is essential to mention that in this situation, the absorption and remission coefficients of the particles and the medium to be measured, however, plane parallel layers is used to calculate the these coefficients. The convergence is based on the absorption coefficient. This algorithm is used for the representative layer after small modifications.

3.3.3 Representative Layer Model

Representative layer model has rigorous mathematics that can calculate the fractions of locally for each layer of material by relating the physical properties of the slurry with optical properties of the sample. There are many assumptions that must be presented before presenting the main theory (Dahm & Dahm, 1999). These assumptions are described in the following.

1. One assumption relates to the fractions of remission and absorption. It is assumed that the absorption domain is molecular and therefore may be described as a continuum. The remission domain will not be well represented as continuum by using the continuous functions since remission is defined to have a domain which is particular.
2. A second assumption is that the sample is composed of the combination of identical layers, each characterizing the sample as a whole.

Generally, the representative layer theory builds a bridge between the sample properties shown by its representative layers and the properties of the individual particles. Each sample can be divided into several layers to apply plane parallel mathematics to those layers and find the properties of each layer in terms of absorption, remission, and transmission fractions. The representative layer theory can also be applied to such samples. The properties of the representative layer are described by the following:

1. The absorbing power of material (related to the absorption coefficients of the materials in the sample)

2. The remission power (related to the index of refraction of the particle making up the sample)
3. The volume of the particles in the layer.
4. The cross-sectional area of the particles of which the layer is comprised.

There are some exceptions in specific conditions in which the fractions of light do not depend on the four major properties described above. For instance, in the absence of absorption, the fraction of incident light remitted by a layer is independent of the thickness of the layer and is dependent only on the remission power and the cross-sectional surface area of the particles in the sample.

The representative layer theory is used to model the fractions of light into the sample. The geometry of the sample can be determined based on the location of the sensor and the direction of illumination. We have assumed that the direction of illumination is perpendicular to the surface of the sample, hence there will be no deviation in the direction of the light before striking the sample. This assumption makes the use of two flux models easier. A code is developed for numerical computations of the light fractions on representative layer. MATLAB 7 release 2010b is used to implement the algorithm to the computer. Then, all the assumptions of representative layer theory have been applied to this model.

These assumptions are:

1. The geometry consists of plane parallel layers each no more than one particle thick.
2. The volume fraction of each particle in the layer is calculated from the local concentration of particles in that particular depth inside the sample. This concentration can be result of CFD calculations.
3. The thicknesses of all the layers are equal.
4. The particles are assumed to be spherical.
5. The void fraction of the layer is obtained by subtracting the concentration from hundred percent concentrations.

6. The absorption is assumed not to be high; therefore, it is possible to use the linear absorption region in Figure 3.4 which is derived based on plane parallel mathematics.

It is essential to mention that in the regions of extremely high absorption, the plane parallel math is unreliable and instead, the contribution of a particle to the absorption of the layer is proportional to the surface area fraction of the particle, and is not dependent on its thickness. Light fractions are shown in the Figure 3.4 for a sample case.

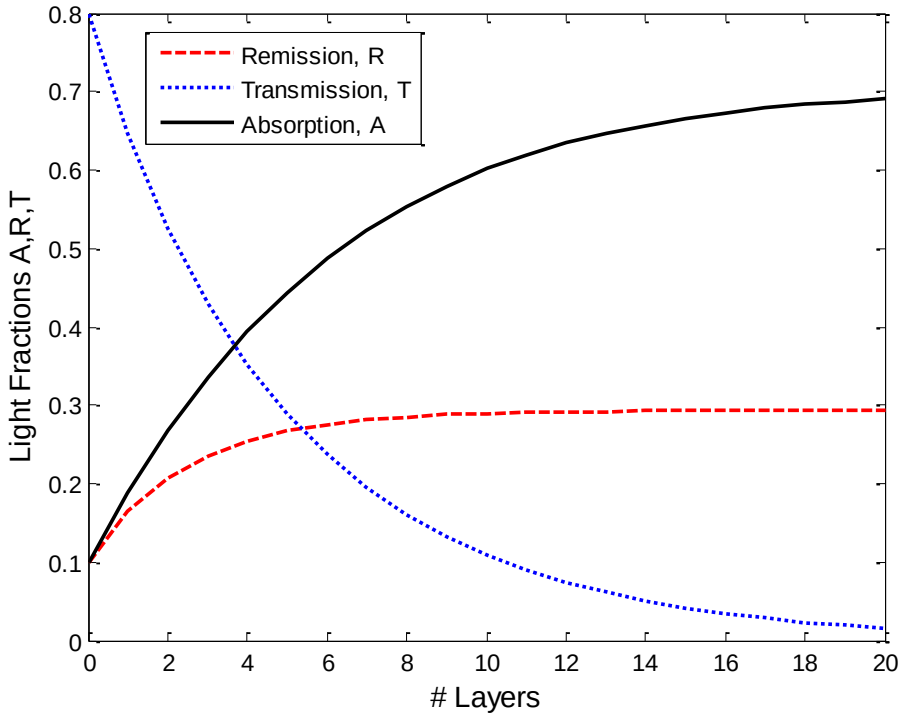

Figure 3.5 Absorption (A), remission (R), and transmission (T) fractions as a function of thickness for the case $A_1 = 0.1$, $R_1 = 0.1$, $T_1 = 0.8$

The purpose of using the linear region for our model is mentioned above. However, finding the limit between the linear and non-linear regions for the absorption fraction of light is also important. In the linear region, compositional analysis of plane parallel mathematics is used to model the fractions of light, however, in no-linear regions the plane parallel mathematics is less reliable.As shown in Figure 3.5, this linear region starts from the first layer where the incident ray encounters the

medium, and would finish when the linear absorption line intersect with the absorption curve derived from plane parallel mathematics.

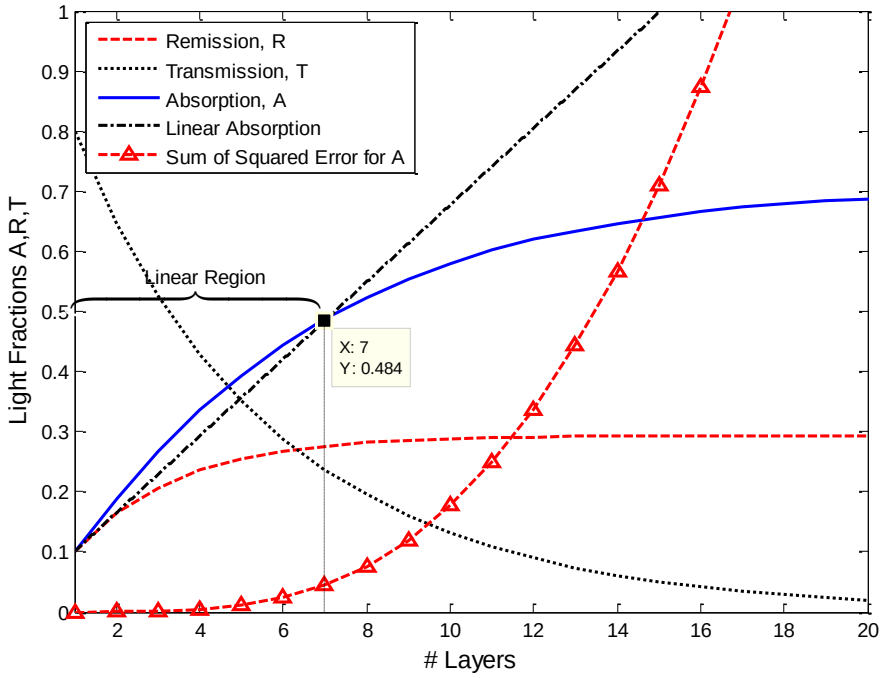

Figure 3.6 The most linear region for absorption fraction based on the least square error between linear absorption with equation A = K.d and absorption curve derived from plane parallel mathematics

7. The number of layers is chosen as to maintain the first assumption. It means that each layer occupies only one particle in depth, so the thickness of a layer is equal to the thickness of a single particle.

Absorption/Remission function for a representative layer:

The absorption fraction in a representative layer can be calculated by summation of the absorption of each particle in that layer. The contribution of an individual particle to absorption is a function of two parameters: the absorption fraction of the particle and its volume fraction in the layer. Moreover, to calculate the remission fraction of a representative layer, it is possible to estimate the

remission fraction and surface area fraction of each particle. Thus, the absorption fraction of all the particles can be achieved by multiplying the absorption fraction of each particle by the volume fraction of the particles.

$$\text{Absorption}_{\text{ all particles}} = (\text{Absorption fraction of one particle}) \times (\text{volume fraction of particles})$$

By generalizing, the fraction of light absorbed by the representative layer, A_1, is introduced as:

$$A_1 = \sum V_i \alpha_i \tag{3.54}$$

where α_i is the absorption coefficient for a particular type of particle i, and V_i is the volume fraction of the same type of the particle. On the other hand, the total remission fraction of the layer can be obtained by multiplying the remission coefficient of each particle by the surface area fraction instead of the volume fraction. Hence, the total amount of light remitted by the representative layer, R_1, is:

$$R_1 = \sum S_i \beta_i \tag{3.55}$$

where S_i is surface area fraction of particles of type i, and β_i is the fraction of incident light remitted from the surface of a particle of type i. This terminology is used by Dahm and Dahm (2007). The important fact is that A_1/R_1 is a function of volume fraction to surface area fraction which can be simplified as the fraction of d (dimension of each particle) by assuming cubic particles.

$$A_1/R_1 = \frac{\sum V_i \alpha_i}{\sum S_i \beta_i} \propto \frac{\sum V_i}{\sum S_i} \sim \frac{d^3}{d^2} \sim d \tag{3.56}$$

Hence, the bigger the particle the higher the absorption fraction of the particle.

The absorption/remission function relates the fraction of light absorbed, the fraction of light remitted, and the fraction of light transmitted by a representative layer. If one can measure the fraction

of incident light absorbed, remitted, or transmitted by a sample, the Dahm equation for Absorption/remission function is introduced as:

$$A(R,T) = \frac{\left[1 - {R_s}^2\right] - {T_s}^2}{R_s} = \frac{A_d(2 - A_d - 2R_d)}{R_d} \tag{3.57}$$

where the subscript *s* refers to a measured quantity and subscript *d* represents properties of a layer of thickness d (Dahm and Dahm, 2007).

Some principles and formulas related to representative layer theory:

Two different kinds of samples can be expressed as non-scattering and particulate samples (Dahm & Dahm, 2007).

In a non-scattering sample we have:

- the absorbing power of the sample can be determined easily,
- the absorbing power of a material making up a sample is the same as that of the sample as a whole, and
- the contribution of a component in a material to the absorbing power of that material is proportional to its concentration.

In a scattering (particulate) sample:

- determination of linear absorption coefficient requires measurement and calculation,
- the absorbing power of material is not as easy to determine as the non-scattering samples which is obtainable from linear absorption coefficient,
- the contribution of a component in a material that make up a particle to the absorbing power of the material is proportional to its concentration, and
- the properties of the particle such as shape and size, would be helpful to determine the relationship between the absorption coefficient of a sample and the absorbing power of a material.

In the samples that have no scatter, a principle relationship fundamental to spectroscopy can be introduced as:

$$\text{Absorbance} = \log\left(\frac{I_0}{I_t}\right) \tag{3.58}$$

where I_0 is the intensity of incident light radiation, and I_t is the intensity of transmitted radiation. This relationship depends on the Bouguer-Lambert Law, which describes the fraction of a light beam absorbed, A, and transmitted, T, when moving within a homogeneous material with negligible remission. The results are:

$$\begin{gathered} Transmission\ Fraction:\ T = exp(-kd) \\ Absorption\ Fraction:\ A = 1 - exp(-kd) \end{gathered} \tag{3.59}$$

The symbol k denotes the linear absorption coefficient of the material in the absence of scatter. This can be referred to as the absorbing power of the material.

When a sample scatters and absorbs light, the situation is more complicated. Consider a plane parallel sample that has a uniform thickness and is directly illuminated, with the direction of light perpendicular to the surface. All fractions of the incident beam can be divided into three fractions: absorption, A; remission, R; and transmission, T. Consider a case with a sample divided into two different layers x and y. Suppose all of the fractions of A, R, and T for each layer are known. Benford (1946), proposed that the properties of each individual layer for the sample named as x+y are the following:

$$\begin{gathered} T_{x+y} = T_x T_y/(1 - R_x R_y) \\ R_{x+y} = R_x + {T_x}^2 R_y/(1 - R_x R_y) \\ A_{x+y} = 1 - T_{x+y} - R_{x+y} \end{gathered} \tag{3.60}$$

In the equations above there are just two identical layers. If there were n+1 identical layers, the following equations may be derived for the sample of n+1 layers:

$$T_{n+1} = T_n T_1/(1 - R_n R_1)$$

$$R_{n+1} = R_n + T_n{}^2 R_1/(1 - R_n R_1) \tag{3.61}$$

$$A_{n+1} = 1 - T_{n+1} - R_{n+1}$$

If the thickness of the sample is twice as thick as a sample with thickness d, the following equations may be derived by using the terminology of Dahm and Dahm (2007). The following formulas are derived for two parallel identical layers of thickness d.

$$T_{2d} = T_d T_d/(1 - R_d R_d) = T_d{}^2/(1 - R_d{}^2)$$

$$R_{2d} = R_d + \frac{T_d{}^2 R_d}{1 - R_d{}^2} = R_d\left(1 + \frac{T_d{}^2}{1 - R_d{}^2}\right) = R_d(1 + T_{2d}) \tag{3.62}$$

$$A_{n+1} = 1 - T_{2d} - R_{2d}$$

Also, the assumption of uniformly distributed material holds here. Finally, if the thickness of the sample is half as thick as a sample with thickness d, by changing d into d/2 it is possible to derive the following equations:

$$R_{2d} = R_d(1 + T_{2d}) \;\Rightarrow\; R_d = \frac{R_{2d}}{(1 + T_{2d})} \xrightarrow{\text{d to d/2}} R_{d/2} = R_d/(1 + T_d)$$

$$T_{2d} = \frac{T_d{}^2}{1 - R_d{}^2} \;\Rightarrow\; T_d{}^2 = T_{2d}\left(1 - R_d{}^2\right) \xrightarrow{\text{d to d/2}} T_{d/2} = \sqrt{T_d[1 - R_{d/2}{}^2]} \tag{3.63}$$

$$A_{d/2} = 1 - T_{d/2} - R_{d/2}$$

These equalities may be expressed in a form known as the Absorption/Remission function, A(R,T), which is constant for any thickness of a sample. These relationships may be summarized in the Dahm equation (Dahm, 1999) as:

$$A(R, T) = \frac{[1 - R]^2 - T^2}{R} \tag{3.64}$$

By expanding the numerator of Equation 3.64, one has:

$$A(R, T) = \frac{[1 - R]^2 - T^2}{R} = \frac{(1 - R - T)(1 - R + T)}{R} \tag{3.65}$$

Also, we had the following equation for the relationship between A, R, and T:

$$\mathrm{A} = 1 - \mathrm{R} - \mathrm{T} \tag{3.66}$$

By substituting Equation 3.66 into 3.65 the following equation will be derived:

$$\mathrm{A(R,T)} = \frac{(1 + T - R)A}{R} = \frac{(1 + T - R)A}{R} \tag{3.67}$$

Now, by taking T from equation 3.66 and substituting into 3.67, we have:

$$\mathrm{A(R,T)} = \frac{(1 + (1 - R - A) - R)A}{R} = \frac{(2 - A - 2R)A}{R} \tag{3.68}$$

The Absorption/Remission function is also proportional to the ratio of both the linear absorption, *K*, and remission, *B*, coefficients for the sample and the fraction of light absorbed, A_0, and remitted, R_0, by a sample of infinitesimal thickness.

$$\mathrm{A(R,T)} = \frac{2\mathrm{K}}{\mathrm{B}} = 2\frac{\mathrm{A_0}}{\mathrm{R_0}} \tag{3.69}$$

Equations 3.68 or 3.69 are known as Dahm equations which are equivalent to Kubelka-Munk absorption to remission function.

There are many reasons for the absorption coefficient to be different from the absorbing power of the material of which the sample is comprised. According to Dahm and Dahm (2007), the reasons are the voids, surface reflection, and the distance that the light traveled

1. *Voids*: A scattering sample is likely to contain voids.
2. *Surface reflection*: Each particle reflects a fraction of the light that strikes the surface, thus this amount cannot be absorbed.
3. *The distance that the light travels*: The absorption coefficient of the sample is dependent on the distance that the light travels through a sample. This is different from the distance through a homogeneous material since the scattered light moves through the sample in all directions. Moreover, light is remitted frequently between internal surfaces of the particle.

Stokes Formulas

After finding the properties of one layer from representative layer theory, one is able to apply those properties to Stokes formulas. The Stokes formulas approximate the passing of light through a sample composed of several parallel sheets. If we assume that x represents the distance into the sample compared to the thickness of a single sheet we have:

$$T_x = \frac{\Omega - \Omega^{-1}}{\Omega\Psi^x - (\Omega\Psi^x)^{-1}}$$

$$R_x = \frac{\Psi^x - (\Psi^x)^{-1}}{\Omega\Psi^x - (\Omega\Psi^x)^{-1}} \tag{3.70}$$

$$A_x = 1 - T_x - R_x$$

where Ω and Ψ is obtained from the following:

$$\Omega = \frac{1 + R_1 + {T_1}^2 + \Delta}{2R_1}$$

$$\Psi = \frac{1 + R_1 + {T_1}^2 + \Delta}{2T_1} \tag{3.71}$$

in which Δ is obtained from the following relation:

$$\Delta = [(1 + R_1 + T_1)(1 + R_1 - T_1)(1 - R_1 + T_1)(1 - R_1 - T_1)]^{1/2} \tag{3.72}$$

R_1, T_1, A_1 are the initial fraction of light. For instance, if x is equal to 2, it means that the x is twice the thickness of a single sheet. On the other hand, if x=0.5 it represents a distance that is one half the thickness of a single sheet. Since in our model we have assumed that the thickness of a sheet is equal the thickness of a single particle (Dahm & Dahm, 2007) then the number of sheets are obtained by dividing the thickness of the whole sample over the thickness of a single sheet. Figure 3.7 illustrates the flow chart of the combined model of representative layer and Stokes formulas.

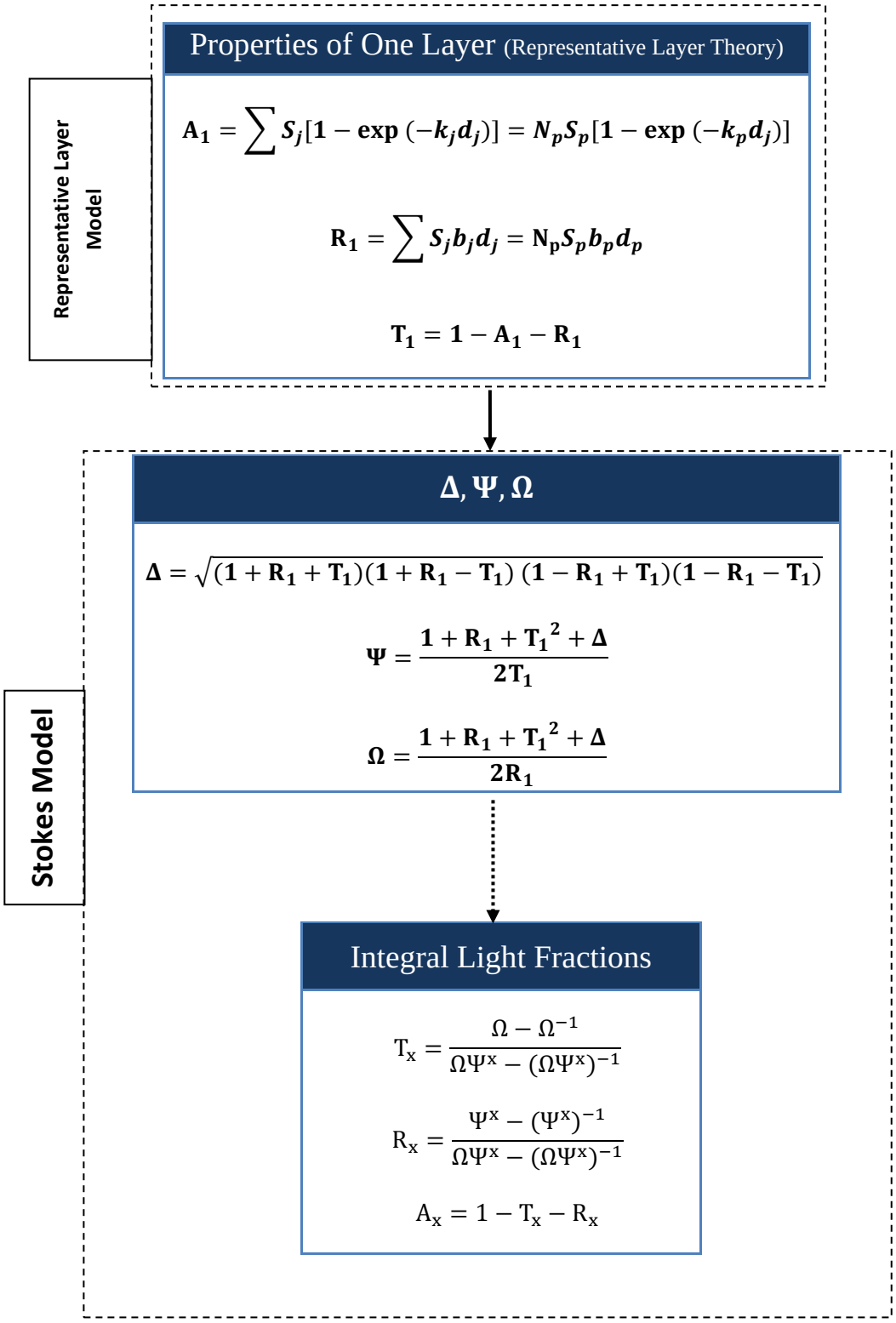

Figure 3.7 Schematic of the algorithm used to computerize the representative layer theory and the Stokes formula for the integral light fractions

In Figure 3.7, the algorithm of the assembly of sheets is introduced. The representative layer theory is the input for the model, where all of the fractions of light are calculated based on their initial condition, volume fraction of particles and layers, surface area fraction of particles and layers, number of layers, and number of particles.

After calculating the first block of the integrated model, the fractions of light for each layer are determined and imported to the second block in Figure 3.7. Now, the model is changed into Stokes model. Hence, the formula based on the Stokes model is the governing equation of the Stokes block. The convergence criterion is the absorption coefficient. In this model Ω, Ψ, and Δ are calculated using A_1, T_1, and R_1. Then, Stokes formulas are applied to estimate the fractions of light in any depth through the sample.

3.4 Code Implementation

MATLAB is used as a program to facilitate the calculations. The program requires inputs to calculate light fractions for each layer. The inputs are:

1. Concentration of three different particle sizes (38, 75, and 150 μm) is imported from Fluent CFD results into MATLAB. The profiles are shown in Figure 3.8.
2. The geometry of each rectangular layer including its length and width is entered.
3. The number of the layers and the density of the particles must be adjusted by the user.

The structure of the program is composed of a main code and three different subroutines for three different sizes. In these three subroutines the data from Fluent is loaded and a curve is fit to this data to give us a function for the concentration of the particles at each point inside the sample. Then, for three initial concentrations of 5%, 20%, and 30%, the following relations are computed in loop:

$$Vol_{particles} = C \times Vol_{layer} \tag{3.73}$$

where C is the concentration.

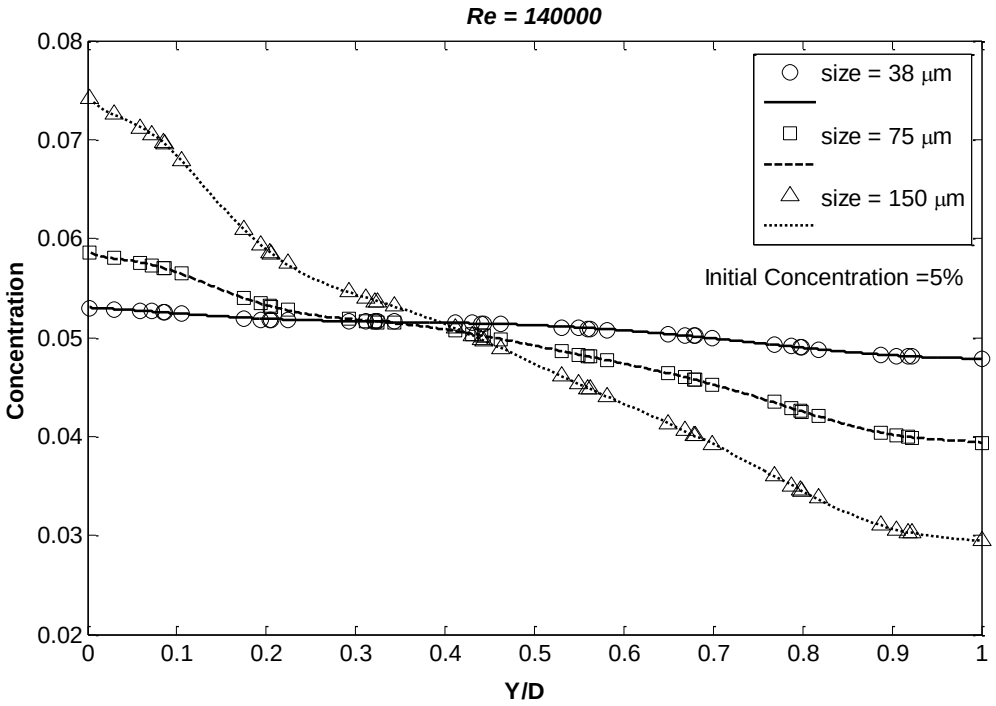

Figure 3.8 Concentration profiles derived from Fluent simulation for the initial concentration of 5% and Reynolds number of 140000 for three particle sizes of 38, 75, and 150 μm

With the equation above, one is able to calculate the total volume of the particles in the sample.

$$Vol_{fluid} = (1 - C) \times Vol_{layer} \tag{3.74}$$

where, C is the concentration. The relation calculates the total volume of fluid in the layer. Then the number of particles is calculated based on the sphericity assumption through the following equation:

$$N_{particles} = \frac{Vol_{particles}}{\pi d^3/6} \tag{3.75}$$

where, d is the average diameter of the particles. By substituting volume of particles from Equation 3.73 into the Equation 3.75, it is possible to compute the number of particles. Moreover, the mass of each particle is:

$$m_{particles} = Vol_{particles} \times \rho_{particles} \tag{3.76}$$

where, ρ is the density of the ADP particles. The aim to use the mass of the particles to compute the weight fraction of the particles through the following relation:

$$w_p = \frac{m_{particles} \times g}{(\rho_p Vol_p + \rho_f Vol_f) \times g} \tag{3.77}$$

where g is the gravity. The subscript p refers to any particle inside the layer. The weight fraction is defined as the fraction of each particle weight to the total weight of the layer. Weight fraction, number of particles, volume of the particles in the sample, volume of fluid, and mass of each particle helps us to initialize the materials needed to use in the Dahm equations for developing the representative layer theory, which is going to be discussed in this chapter. Another helpful relation is the volume fraction of particles:

$$v_p = \frac{w_p/\rho_p}{\sum w_p/\rho_p} = \frac{w_p/\rho_p}{N_p(\frac{w_p}{\rho_p})} \tag{3.78}$$

where the v_p is the volume fraction of a particle type which is proposed by Dahm in his paper (Dahm, 1999), N_p is the number of particles in the representative layer, w_p is the weight fraction of the particle which has been calculated in Equation 3.77, and finally ρ_p is the density of the particle. Also, fraction of particle surface area that belongs to a particle type inside the layer is determined by substituting the weight fraction from 3.66 into the following relation:

$$s_p = \frac{w_p/(\rho_p d_p)}{\sum w_p/(\rho_p d_p)} = \frac{w_p/(\rho_p d_p)}{N_p(\frac{w_p}{\rho_p d_p})} \tag{3.79}$$

where the s_p is the surface area fraction of a particle type, N_p is the number of particles in the representative layer, w_p is the weight fraction of the particle which has been calculated in Equation

3.77, d_p is the diameter of a particle, and finally ρ_p is the density of the particle. In addition, the next step is to calculate the fraction of total volume composed of particle type:

$$V_j = (1 - v_0)v_p = (1 - (1 - C))v_p \tag{3.80}$$

where *j* refers to number of particles in the layer, v_p is the volume fraction of a particle type, v_o is the void fraction, and C is the concentration of the particles at that particular layer. Also, fraction of cross sectional surface area comprised of particles of this type is:

$$S_j = (1 - v_0)s_p = (1 - (1 - C))s_p \tag{3.81}$$

Equations 3.73 to 3.80 are computed for three different initial concentrations as well as 3 different particle sizes.

The main code then calls the three subroutines for these three particle sizes. On the other hand, the absorption and scattering coefficients must be provided for the main code. This can be achieved through plane parallel mathematics and by computing the following equations for n layers of the sample:

$$\begin{aligned} \mathrm{T_{n+1}} &= \mathrm{T_n T_1}/(1 - \mathrm{R_n R_1}) \\ \mathrm{R_{n+1}} &= \mathrm{R_n} + \frac{\mathrm{T_n}^2 \mathrm{R_1}}{1 - \mathrm{R_n R_1}} \\ \mathrm{A_{n+1}} &= 1 - \mathrm{T_{n+1}} - \mathrm{R_{n+1}} \end{aligned} \tag{3.82}$$

the purpose to calculate these fractions of light is just to find the scattering and absorption coefficients for each layer through the following relations:

$$\begin{aligned} \mathrm{k_{n+1}} &= \mathrm{A_{n+1}}/d_p \\ \mathrm{b_{n+1}} &= \mathrm{R_{n+1}}/d_p \end{aligned} \tag{3.83}$$

Although the fractions of light that are obtained from plane parallel mathematics are different from what is derived from representative layer theory, the absorption and reflection coefficients are

calculated just from the plane parallel math to be fed into the model developed based on representative layer theory. Hence, we will use K and B that are estimated for each layer based on Equations 3.83, and then one can use them to substitute into the light fraction relations derived from representative layer theory:

$$\mathrm{A}_1 = \sum S_j[1 - \exp(-k_j d_j)] = N_p S_p[1 - \exp(-k_p d_j)]$$

$$\mathrm{R}_1 = \sum S_j b_j d_j = \mathrm{N_p} S_p b_p d_p \tag{3.84}$$

$$\mathrm{T}_1 = 1 - \mathrm{A}_1 - \mathrm{R}_1$$

where *j* refers to a particle inside a layer and *p* refers to an individual particle inside one layer. Since the particles are assumed to be identical the absorption fraction summation over the whole layer is a derived by finding the absorption fraction for one particle which is identified by subscript p and multiplying by the number of particles. For the equations above, the unknowns are the absorption A_1, remission R_1, and T_1 fractions, as well as b_j and k_j, that are two other unknowns which have already been estimated from Equation 3.83 (plane parallel mathematics). S_j and d_j are the fractions of cross-sectional surface are comprised of particle type and the average diameter of particles, respectively.

CHAPTER IV

RESULTS AND DISCUSSION

4.1 Brief Recapitulation

It has been discussed in the preceding chapters that characterizing the light movement in a multiphase flow involving solid particles within a liquid phase may be achieved through: **(i)** studying and investigating different mathematical models in the field of diffuse reflectance, **(ii)** investigating their compatibilities with modeling particles in a fluid and simulating the near-infrared phenomena in a slurry, **(iii)** developing programs in MATLAB to build computational algorithms based on mathematical models obtained from optical theories in the field of diffuse reflectance. The motivation is to build a novel method for predicting the depth of penetration of light through the slurry by calculating the fractions of light. Also, it has been considered that Computational Fluid Dynamics can provide the required varying concentrations of particles as input for mathematical predictions of optical phenomena. Uniform concentrations are constant through the cross-section of pipe, while varying concentrations are not constant. In the current study CFD results for the flow of a chemical slurry in which 2-Amino-4, 6-dimethylpyrimidine (ADP) are the particles and Xylene is the liquid were used. Many different cases of CFD simulations have been applied from the available models in previous research databases to feed concentration profiles to discontinuum theory optical models which are demonstrated in this chapter. The schematic representation of the problem depicted in

Figure 4.1 (has been shown previously, however, it is worth repeating here. This picture helps to understand the geometry of the model and the light beam direction through the sample.

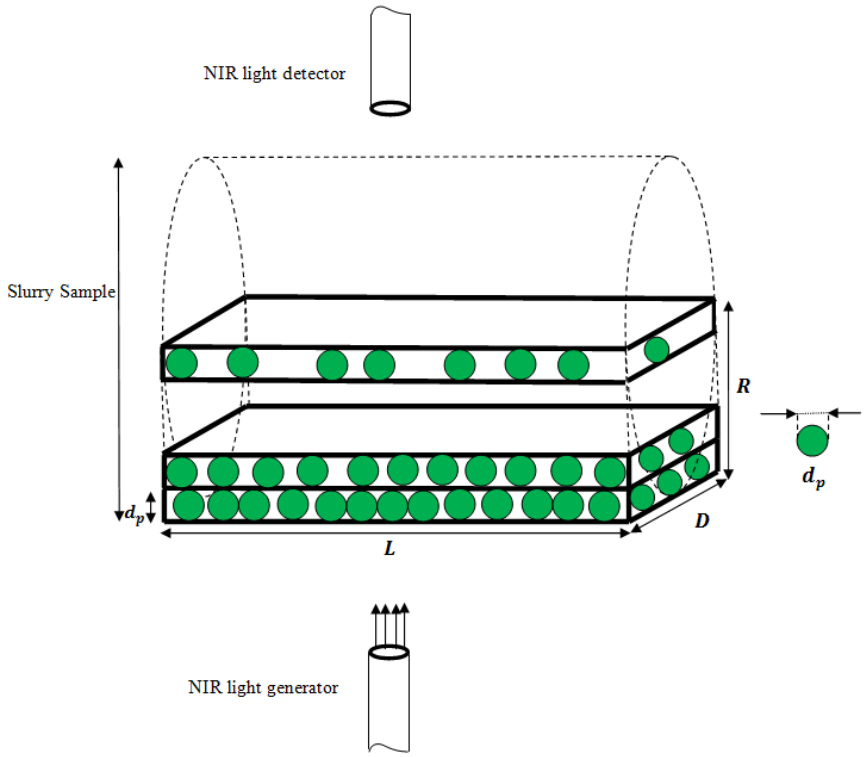

Figure 4.1 The geometry of the light generator, detectors, and the sample

The optical properties associated with a beam of diffuse light with a particular intensity striking the very first layer of the sample will be changed because portions of light will be absorbed, transmitted, or remitted. The fractions of light which are called initial fractions for this simulation are considered as inputs for all of the discontinuum and some of those continuum theories which use simple discontinuous mathematics to divide the sample into layers and apply their continuous method for each infinitesimal layer inside the sample. These models are discussed in this chapter and their results are compared with the literature. Kubelka-Munk theory is a continuum approach. However, in some special applications such as powdered samples, it has been improved by being added to the model of plane parallel mathematics. This work has been done by Nobbs (1985). Hence, it is capable of

predicting a freely suspended layer inside a sample containing a lot of other layers with more complicated and accurate mathematics (Nobbs, 1985). The effects of initial fractions of the light – absorption, remission, and transmission – that enters the medium will be discussed in this Chapter. By adjusting some of the parameters such as refractive index, scattering and absorption power, concentration of particles, and initial fraction of light to the case of slurry sample of xylene and ADP, one is able to make the models compatible to the geometry of problem. For continuum theories initial fraction refers to the boundary of integration applied for solving differential equations. For discontinuum theories the initial fraction of light pertains to the property of the first layer where the light encounters the sample. In this Chapter the results of different models are explained in detail.

This Chapter aims at presenting the important findings of the current research which focuses on the application of optical theories to model near-infrared phenomena inside slurries. The arbitrary solid concentration profiles are used in representative layer theory as input data on the composition of the sample. Concentration profiles are the results of different CFD simulations done separately in other research in this project using ANSYS Fluent 13.0 and 12.0 CFD software packages. Different turbulence models including K-ε and Reynolds stress were applied to determine profiles of solid concentrations. In this analysis, the penetration of light was considered spatially, and since the light monitors the sample with much higher speed than the flow field velocity, it is assumed NIR transmittance to and reflectance from the pipe happens instantaneously, so that the slurry is stationary relative to the light during this momentary process. Fluctuations due to fluid and particle motion are not considered. Optical models were created based on the fundamentals of each theory. They were developed using Fortran 2003 and MATLAB R2012a software programs as two different computational tools. The codes are available in the Appendix B. Each model simulated the passage of NIR radiation through the sample based on light fractions. Computing light fractions was performed for each layer, so the depth of penetration has been evaluated based on the value of these fractions at each depth through the sample. In this Chapter, the results of different models are discussed; they are

validated with the optical experiments performed for similar cases in the literature. Moreover, results of continuum and discontinuum theories are compared through investigating similar cases for the input data. Also, the depth of penetration of light is estimated for each scenario.

This Chapter is divided to two major parts, one for continuum theories and the other for the discontinuum ones. In the continuum part the results of five different approximations and theories are presented and discussed. In the discontinuum part, the results of the three different complicated models are reviewed and analyzed. Finally, the results of two groups are compared and the advantages and disadvantages of each group are investigated.

4.2 Results of Continuum Optical Models

In this section the continuum model results are presented. The first one is Schuster's theory which is a very old model of diffuse reflection with very simplified mathematics which may help to understand and estimate the light through the medium. Kubelka-Munk is a more advanced model than Schuster's approximation. Hence, the results of these two theories are compared in section 4.4. Kubelka-Munk theory is used for optically thick samples. The three flux model is another model applied to solve the radiative transfer equation using an approximate method. This model is compared to Giovanelli's theory, published in 1955, in Section 4.4. As it was mentioned in previous chapters, the radiative transfer model is based on one equation that treats the extinction of a flux of radiation in a particular direction. The intensity inside the layers, penetration depth of light or the distance that light travels, density of medium, and the scattering and absorption coefficients are the components that vary in the proposed models. The diffusion model is the last theory whose results are comparable to other continuum theories, however, it treats the scatter as photons taking a random walk through a concentration gradient until the path of light is discontinued by absorption in the medium (Dahm & Dahm, 2007).

4.2.1 Schuster's Model

Schuster's particle theory uses continuum mathematics. The process for deriving equations presented in Chapter Three is similar to Kubelka-Munk theory. The difference between these two models will be discussed later in this chapter. As is illustrated in Figure 4.2, the parameter R_∞ which is known as reflectance at infinite depth is an essential element in continuum theories. This parameter is the reflectance of a layer of material which is optically thick. This means that whenever the light

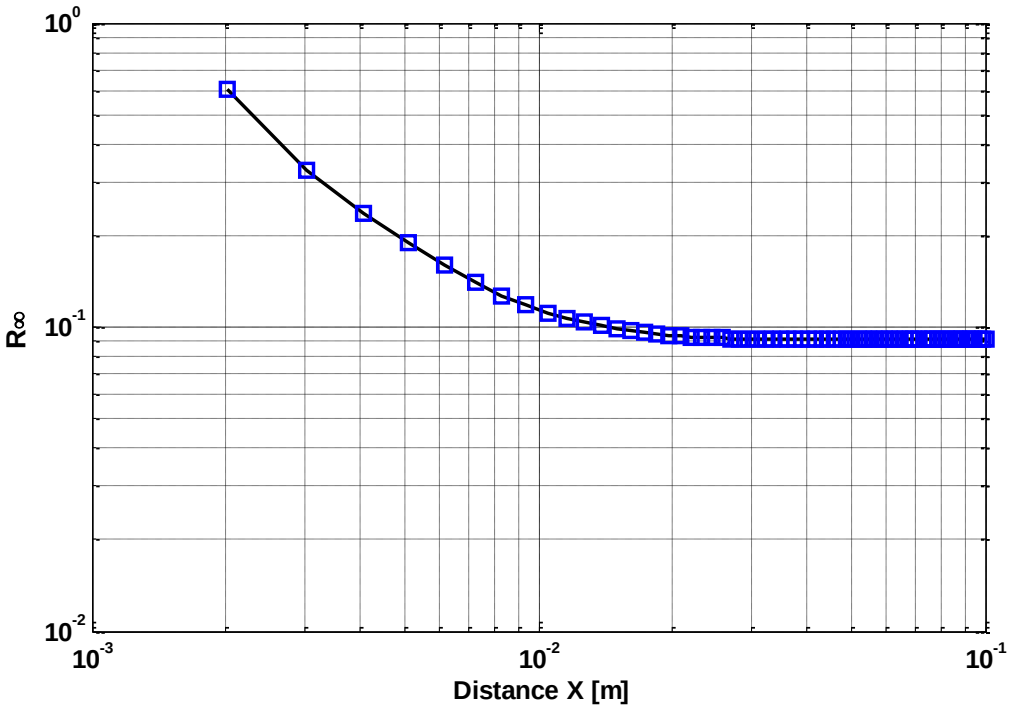

Figure 4.2 Illustration of diffuse reflectance of thick layers at different depths through the sample. X values represent the distance from the edge of the sample through its depth.

penetrates a sample of finite thickness, it will be reflected in each depth that it travels through the sample. The gradient of reflection through the sample will continue until a depth where any increase in thickness does not change the reflection. Therefore, the change in the depth of the sample will not affect the reflectance. Each point greater than X = 0.02 in Figure 4.2 represents a depth in the sample at which the reflectance is saturated. For this simulation of Schuster's theory, the sample thickness is assumed to be 10 cm. According to the Figure 4.2, the reflectance reached the constant value very

quickly at about the 3 cm depth. By increasing the sample thickness the reflectance does not change significantly. This phenomenon depends on the sample thickness; scattering and absorption coefficients; and the intensity of the light beam. Hence, the reflection from the material is a function of those elements. The scattering and absorption coefficients are characterizing the power of material in reflecting and absorbing the light. Note the assumptions of this theory are very restrictive. The reflectance function derived by Schuster (1905) involves two oppositely directed radiation fluxes which are in the direction of surface normal. Hence, the direction is not inclined and there will not be any angular distribution of light after striking the sample.

Kubelka and Munk (1931) developed a more accurate two-flux model than Schuster's. This model is similar to Schuster's solution, with the primary difference being the definition of two coefficients of absorption and scattering. These two constants are known as k and s. On the other hand, Schuster defined similar constants in terms of absorption and scattering for a sample containing a material which has a property of single scattering. Kubelka and Munk derived their model for a densely packed sample which has the properties of absorbing and scattering the light ideally. These materials are called ideally diffusing mediums. However, Schuster's model applied to a foggy atmosphere where the concentrations of particles are not very high. These two differences are shown in Figure 4.3, where Kubelka-Munk absorption to scattering coefficient is higher than the one developed by Schuster. The reason is the assumption of Schuster's theory which only applies to samples with small concentrations and consequently small amounts of absorption. According to Section 3.2.1, the ratio of coefficients k over s is exactly twice as great as the ratio of absorption to scattering α/s. As illustrated in the figure, the thickness of layers decreases when the distance through the sample increases. It is because of the linearity of light fractions in the smaller depths through the sample. Absorption, reflection, and transmission are linear until their rate of change is decreased. Hence, larger depths need more resolution, and for this, the number of data points increased in the large depths. Each point in Figure 4.3 can also represent a unique sample. For each point, the value on

the horizontal axis illustrates the distance through a specific sample at which the maximum reflection occurs.

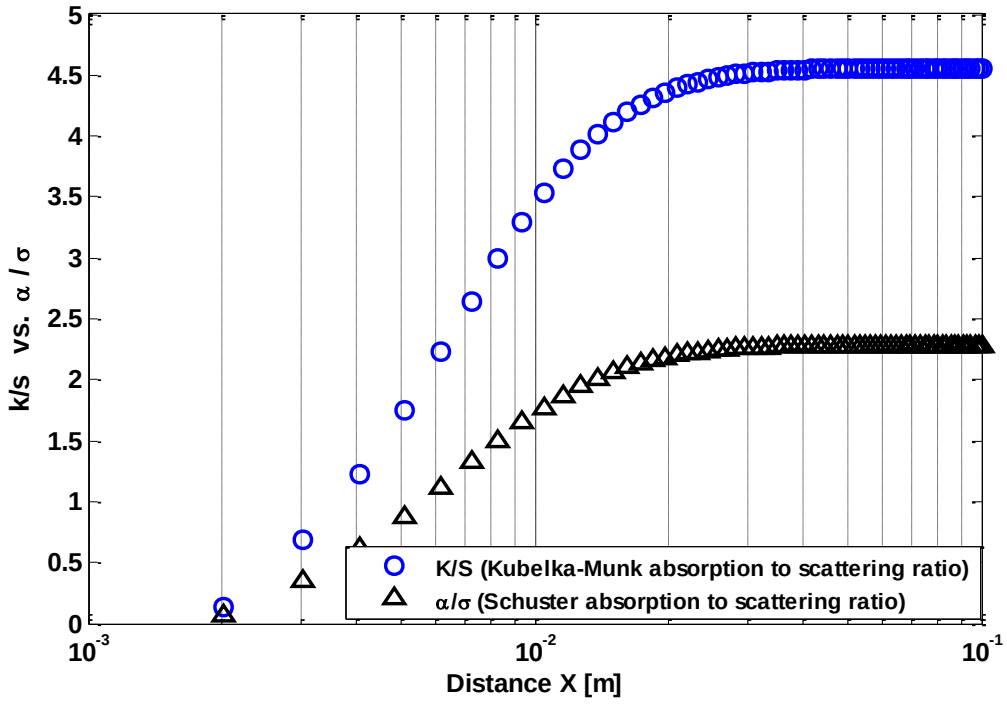

Figure 4.3 Scattering and absorption coefficients for the models of Schuster and Kubelka-Munk. X values represent imaginary thickness inside the sample.

The difference between multiple and single scattering is very important for the case of Schuster's theory. The reason stems from the fact that single scattering is effective for a random media, where the interaction of light with particles is not deterministic. Therefore, for the Kubelka-Munk model which is used for a denser medium than Schuster's model, the single scattering assumption does not work well. In addition, Schuster's theory is a simple two-flux theory that refers to reflection and transmission of light. It can be concluded from this discussion that Shuster's model is very simple to apply to the cases of complex non-homogeneous samples where the concentration varies. In a sample with low concentration of particles, the probabilities of light striking the medium are used to predict the fractions of light. As mentioned in Chapter Two, in the limit of infinite dilution, Schuster's assumption suggests that one particle may be present in each layer. Considering the discontinuous

interpretation of Schuster's theory, the level of dilution will be solved easily through the discontinuous solution of Schuster's equations.

Another important factor that affects the reflectance of light is its initial fraction. The initial fraction of the light beam is defined as the lower boundary of integration or one of the boundary conditions of the differential equations that are discussed in Chapter Three. As illustrated in Figure 4.4, small variations in the boundary conditions will have significant influence on the total remission fraction of light.

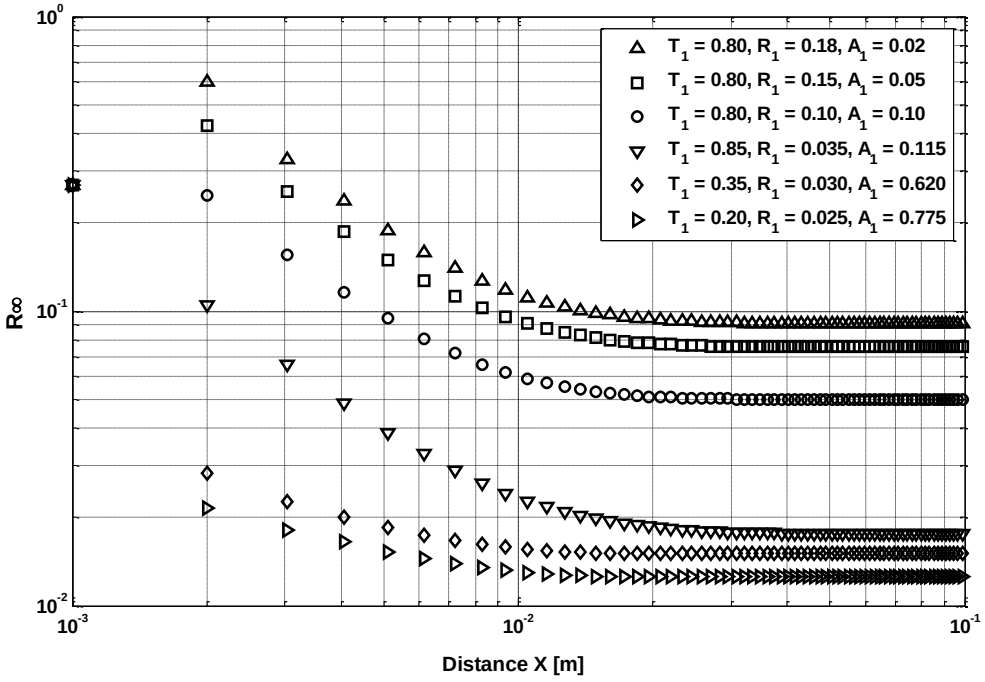

Figure 4.4 Total diffuse reflectance for different initial fraction of light as a boundary condition for the sample.

In Figure 4.4, the values associated with symbols T_1, R_1, and A_1 are called initial fractions of light or boundary condition for solving the differential equation of Schuster's model. It is obvious that the diffuse reflectance is a strong function of initial reflection. The other important fact about this diagram is related to the reduction of remission in the case of constant transmission. What is evident is that the

total diffuse reflectance is not influenced by increases in absorption. This effect is shown in more detail in Figure 4.5. In this graph, four different cases are investigated. The first and second cases consider constant transmission, where the absorption increases, while remission is slightly reduced. These two cases have the behavior that was just described. Transmission is constant and the remission is decreased, hence, diffuse reflection is also decreased, however, as was mentioned before, the absorption does not affect the total reflection.

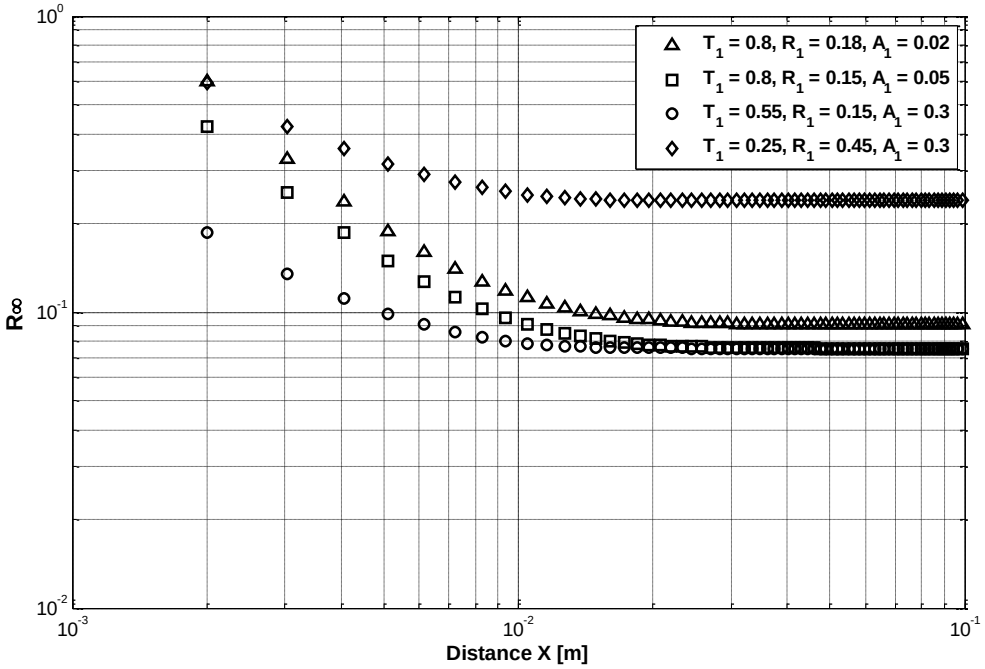

Figure 4.5 Diffuse reflections for four different cases of initial fraction of light.

The next case involves the comparison between the cases shown in Figure 4.5 with initial fractions of T_1 = 0.8, and T_1 = 0.55. In these two cases the remission is constant, hence, only transmission and absorption are changed. In Figure 4.5, the effects of initial reflection and transmission are studied in this Figure. The result was expected since by increasing absorption six times the diffuse reflection has been decreased. Thus, diffuse reflectance is dependent directly to initial remission. The other case is related to the initial fraction of light when the absorption is

constant and equal to 0.3, while remission is increased. This case proves that the total remission is a strong function of the initial remission fraction, while it is a weak function of initial transmission, and is not affected by the initial absorption.

4.2.2 Kubelka-Munk Model

The Kubelka-Munk model was developed as a solution to the radiation transfer problem. This theory is very similar to Schuster's formula derived in Chapter Three, however, unlike Schuster, Kubelka envisioned using the solution for dense systems with high concentrations. Another discrepancy between the Kubelka-Munk model and Schuster's theory is related to the different scattering effects that are assumed by the two theorems. The Kubelka-Munk model solved the differential equations for the case of remission, not the isotropic scattering assumed by Schuster. Isotropic scattering refers to the distribution of reflected or transmitted radiation which is the same in all directions.

As discussed by Kubelka and Munk, the relationship between the scattering and absorption coefficients is defined for the whole thick sample. As was pointed out by Nobbs (1985), these two coefficients are also calculated through the reflectance and transmittance of a thin layer inside the sample. Therefore, by limiting the boundaries of integration to one layer of material, one is able to predict all fractions of light, as well as absorption and scattering coefficients for that layer and then expand the model to the whole material to calculate the optical properties for each layer. This approach of solving a differential equation for an infinitesimal thickness inside the sample is more accurate than integrating over the whole sample since the composition of each infinitesimal layer is determined by one particle thickness. This is one of the fundamental assumptions of K-M theory. Figure 4.6 shows the reflectance from and transmittance through an isolated layer of material. The layer is imagined to be freely suspended and illuminated from above by diffusely incident light of intensity I. The layer reflects the amount $I.R_o$ and transmits the amount $I.T$. Moreover, R_o and T are the reflectance and transmittance of the layer respectively for incident light. If the layer is diffusely

illuminated from the opposite direction by an intensity J, then the amounts reflected or transmitted are $J.R_o$ and $I.T$, respectively.

Figure 4.6 is representative of a layer in a sample. It might be confusing since the Kubelka-Munk theory is a continuous method, however, using the approach proposed by Nobbs (1985) made our model more accurate because the fractions of light are calculated for each infinitesimal thickness, which may help to assume that the scattering effects within the infinitesimal layer are negligible.

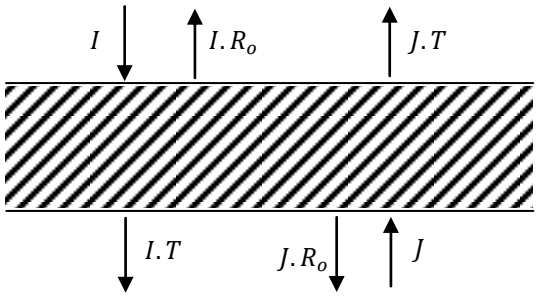

Figure 4.6 Reflectance and transmittance of a thin layer of thickness *d* within a sample

Kubelka – Munk function is a powerful tool that predicts the diffuse reflectance of an infinitely thick sample. According to Figure 4.7 and Figure 4.8 the intensity of light is decreasing whether it is a reflected beam or a incident beam. The intensity is different from the light fraction. Here intensity ratio is the ratio of reflected J or transmitted I intensity to the reference intensity J_0 or transmission I_0 which implies reflectance (I/I_0) and transmittance J/J_0 , respectively. The reflectance and transmittance are almost similar for all of the initial fractions. Reflection is a transmission but in opposite direction, hence both will decrease in the sample. Before calculating this function, the fractions of light must be determined throughout the method developed in Chapter Three. According to the equations the remission, transmission, and absorption are found for a sample of 100 units of thickness. These thicknesses are similar to layers in the discontinuum theories, however, they are different.

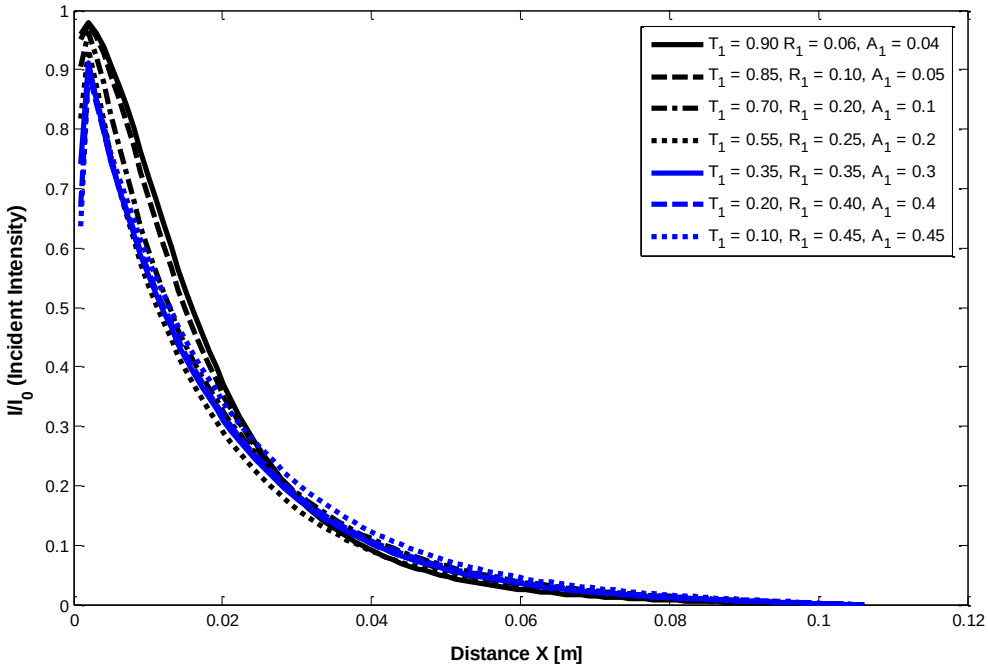

Figure 4.7 Intensity of incident beam through the sample at different initial boundary conditions

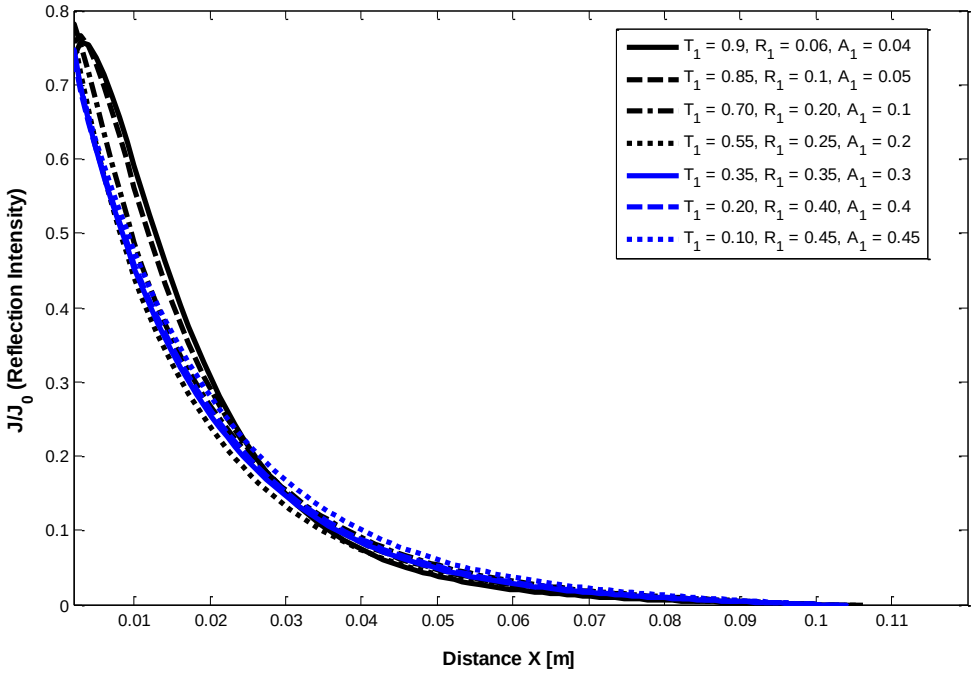

Figure 4.8 Intensity of reflected beam from the sample at different initial boundary conditions

The approach used here is a continuous method but the numbers in the horizontal axis correspond to a depth inside the sample. The numbers on the horizontal axis refers to number of layers. Since K-M theory is continuous and layers are not used, each number is representative of a fictitious layer that does not exist. According to Figure 4.9 the rate of growth of remission per unit thickness is much faster than the absorption or transmission. The absorption reaches the maximum after 25 unit thicknesses, while remission reaches the maximum after 10 unit thicknesses. On the other hand, transmission decays very much slower than the last two fractions. When the transmission reaches zero, the absorption and remission are meaningless since the model is saturated. Because of the simplicity of the model, in which the concentrations of particles are not considered, it is impossible to predict the real depth at which there is no transmission. Here, the model assumes the sample is a homogeneous mixture of xylene and ADP. The absorption and remission coefficient for the xylene and ADP must be measured from an experiment. However, in this model, the absorption and remission coefficients are found from Equation 2.20 and 2.23

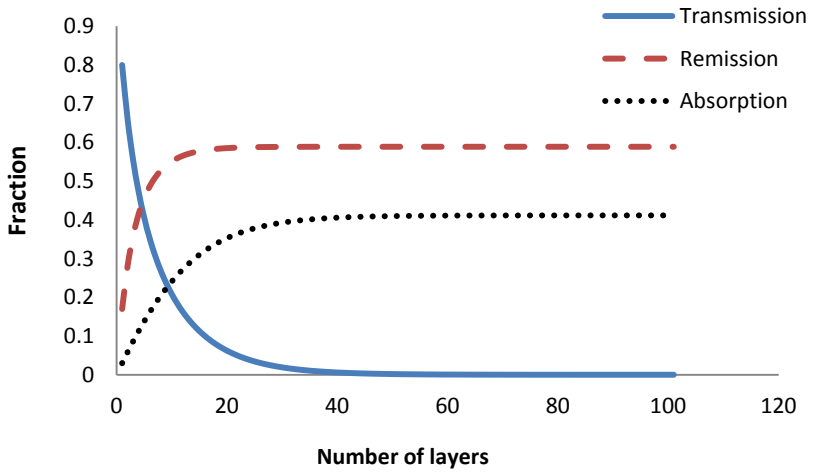

Figure 4.9 Absorption, remission, and transmission fractions calculated from Kubelka-Munk function

The Kubelka-Munk equations apply these absorption and scattering coefficients. Moreover, according to one of the assumptions the absorption by infinitesimal particles is small. This is obvious from

Figure 4.9 which represents a limited amount for absorption, however, xylene has considerable power of absorbing light. This is a limiting assumption that proves basic K-M theory is not a powerful tool for the slurry sample of xylene and ADP.

The Kubelka-Munk function is derived from continuous mathematics by making several assumptions. These assumptions which were introduced in Chapter Three are based on the experimental arrangement and configuration of the sample. If the geometry is not compatible with the assumptions the model will fail. Isotropic scattering is an important assumption. For instance, if there is specular reflection, there may be preferential directions of travel of light through the sample, which violate the diffuse radiation assumption (Griffiths & Dahm, 2008).

Effect of sample particle size on reflectance:

The model developed by Bull (1990) is a simplified version of the Kubelka-Munk model. By a making the constraint that the particle size is much greater than half the coherence length of the radiation and must be greater than the radiation wavelength, it is possible to use the simplified model to predict the contribution of particle size on the reflectance in the sample. The model is discussed in previous chapters. In order to relate the reflectance of the sample to the particle size using the equations derived in Chapter Two, it is necessary to determine the relationship between particle size and absorption and reflectance of individual particles. Let us use the parameter which is known as $\frac{1}{e}$, penetration depth, with the symbol τ. It was proven by Bull (1990) that the fraction A/R is equivalent to particle size since according to the Beer Lambert law and the Kubelka-Munk function $A/R = [1 - \exp(-{}^{x}/_{\tau})]/2r$ which gives ${}^{x}/_{\tau} \cong 2(A/R)r$, where r is the reflectance of a single layer. Therefore, as it is shown in Figure 4.10, the log of inverted diffuse reflection, called reciprocal reflectance, increases with the particle size. This means that the reflection is decreasing as the particle size increases since the vertical axis is $1/R_{\infty}$ not R_{∞}. This graph is derived for different cases of initial fractions of light. In this diagram, it is obvious the lower the reflectance, the higher the log of

reciprocal reflectance. The reflectance and transmittance had the most effects on the diffuse reflection. According to Figure 4.10, if the reflection fraction in a particular area of the sample is low the particle sizes in that region are small.

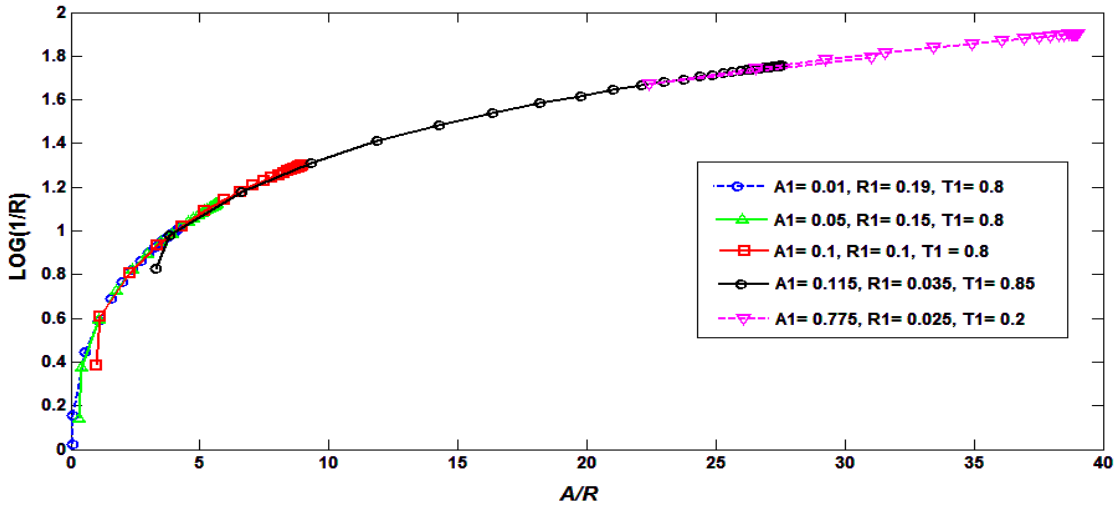

Figure 4.10 The log of reciprocal reflectance plotted as a function of the A/R fraction.

The model proposed here for the Kubelka-Munk model is compared to the similar result proposed by Bull (1990). The model of Bull was applied to a powdered sample of wheat to derive the reflectance. As is clear from Figure 4.11 the diffuse reflectance has the same trend, which is ascending. The discrepancy in the values of reflection is related to the difference between two samples. By comparing these two figures, it is clear that similar results are obtained from our model.

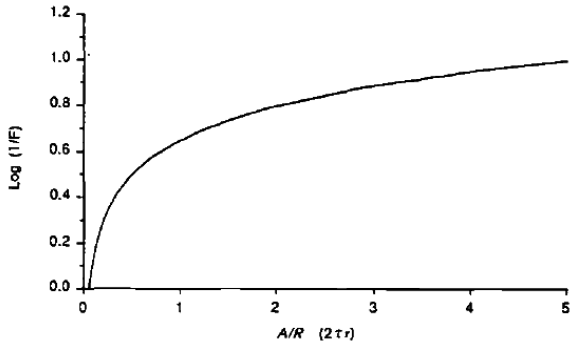

Figure 4. 11 The log of reciprocal reflectance plotted versus A/R fraction derived by Bull (1990)

Finding a numerical regression for the diffuse reflectance is important since it is possible to use the absorption to remission or even the particle size of the sample for predicting the total reflection from each layer in the sample or from the whole sample. In Figure 4.12, a polynomial curve fit is used.

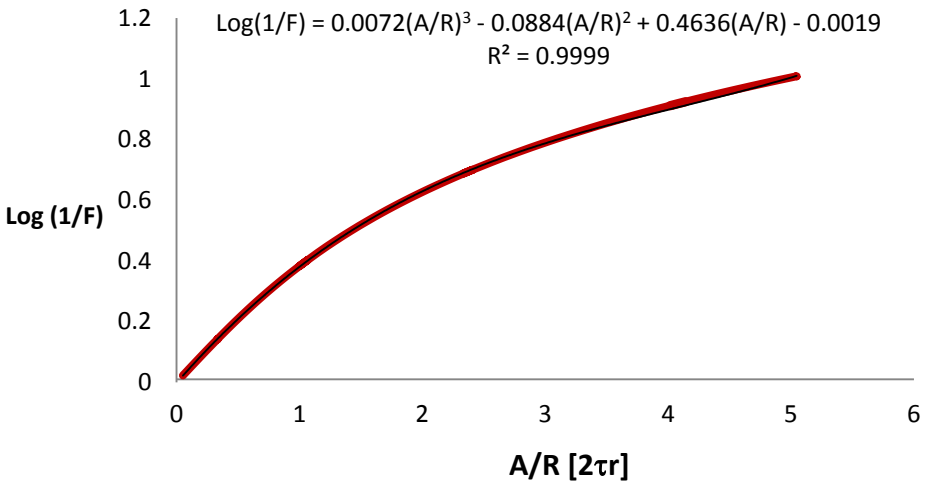

Figure 4.12 Polynomial curve fitted to the log of reciprocal reflectance versus equivalent particle size in units of $2\tau r$

In Figure 4.13, a simpler formula is derived to predict the reflectance by inserting particle size or A/R.

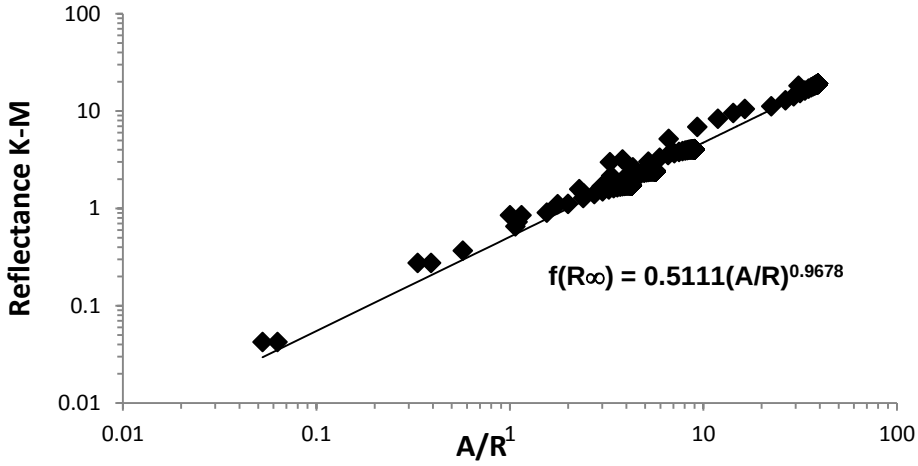

Figure 4.13 Exponential curve fitted to the log of reciprocal reflectance

4.2.3 Radiation Transfer Approximations

The radiation transfer approximation is developed based on the model proposed by Patterson et al. (1989). The model has been applied to the case of diffuse reflection from tissue. This is a simple model of light propagation which allows quantitative prediction of diffuse reflection. For this model the absorption, remission, and transmission must be obtained from an experiment. In the experiment, the optical properties of the layers of material such as absorption and scattering coefficients are obtained. In this model the cosine of scattering angle is applied for two cases. The first case is for an isotropic scattering, which suggests the cosine of scattering angles must be zero. However, for a case of forward scattering the value of cosine of scattering angles must be derived from an experiment. Different values are chosen for the cosine of scattering angles, and they are shown in Figure 4.14. It has been illustrated that for isotropic scattering ($g = 0$), diffuse reflection is maximum, but the minimum

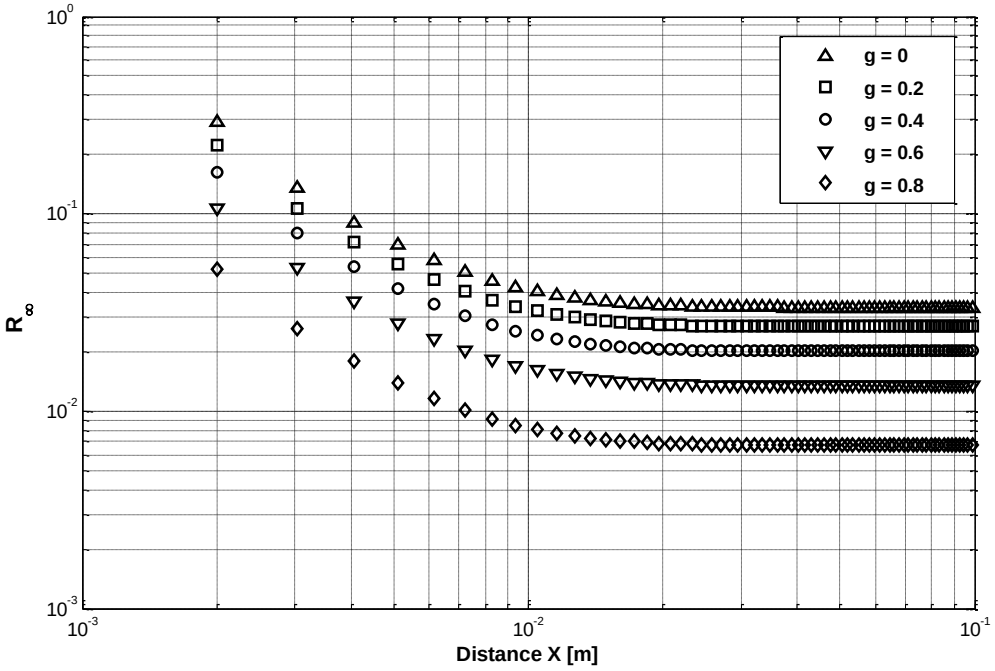

Figure 4.14 Diffuse reflection of radiative transfer approximation for different cosine of scattering angle

occurs when the value of g approaches 1. This Figure provides information about the whole range of scattering; from isotropic to completely forward scattering. In this thesis, the wavelength of light is in the near-infrared region, from 0.75 μm to 1.4 μm. Therefore, the sizes of particles in this research are assumed to be in the range of 38 μm to 750 μm, much larger than the wavelength of radiation. Thus the slurry sample in this study shows significant scattering in the forward direction since the particle sizes are much greater than the wavelength of the light. The values near 1 may be more realistic for the NIR radiation in the slurry of xylene and ADP, however, for an accurate estimation about the radiation through a sample, this model requires an experiment to find the absorption and scattering coefficients. In our model, the absorption and scattering coefficients are derived from the absorption and reflection fractions of light which were obtained from the approximate solution of radiation transfer equation. Figure 4.15 is derived from the following equation, previously discussed in Chapter Three.

$$R_\infty = \frac{\frac{(1-g)\mu_s}{\mu_a+(1-g)\mu_s}}{1+2(1+r_d)/(1-r_d)\left(1-\frac{(1-g)\mu_s}{\mu_a+(1-g)\mu_s}\right)+\left(1+\frac{2(1+r_d)/(1-r_d)}{3}\right)\sqrt{3\left(1-\frac{(1-g)\mu_s}{\mu_a+(1-g)\mu_s}\right)}} \quad (4.1)$$

where all of parameters have been discussed in Chapter Three. Patterson et al. suggested the Equation 4.1. The relation above uses the scattering and absorption coefficient, as well as the cosine of scattering angle to provide an estimation of diffuse reflection. It is derived from a more advanced model of radiative transfer equation, the Kubelka-Munk theory and provides better and more reasonable results.

In Figure 4.15 the radiative transfer approximation is used to investigate the effect of boundary conditions on the diffuse reflection from the sample. As is obvious, the remission is the most powerful parameter that determines the diffuse reflection strength. As before, transmission has less effect on the total reflection from a sample, however, absorption does not change the diffuse reflection. The reason that transmission and reflection affects the total reflectance is because of their

similarities. As in Chapter Two, reflection is transmission but in an opposite direction. Therefore, some theories such as Mie scattering uses scattering instead of the reflection and absorption. Mie scattering is a particle theory which studies the light on single particles not layers.

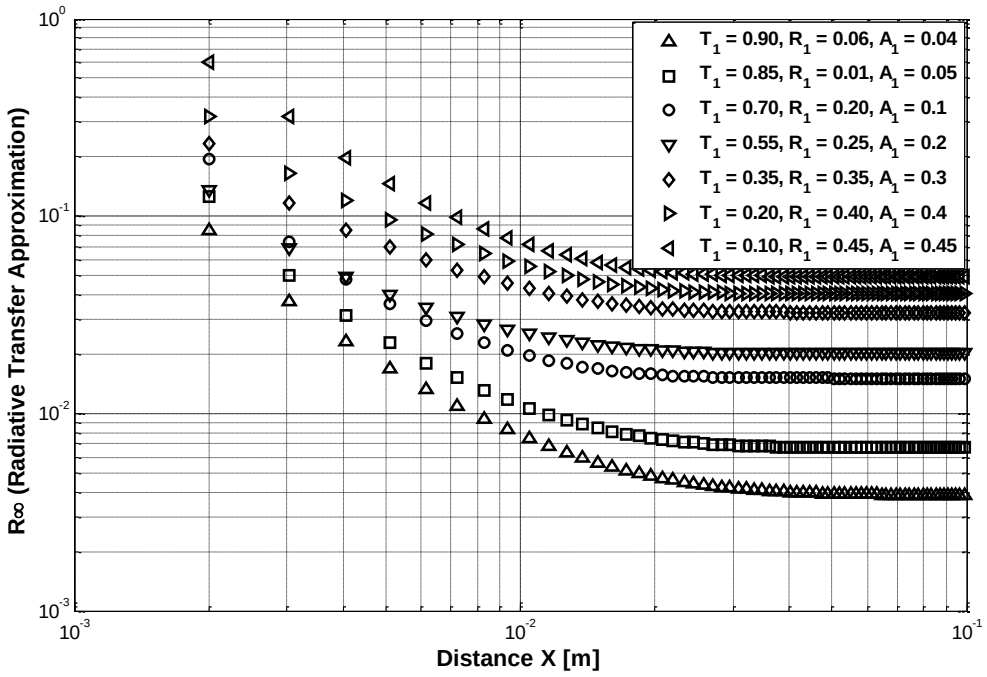

Figure 4.15 Diffuse reflection of radiation transfer model of Equation 4.1 for seven different cases of initial fraction of light. Model of Patterson et al. (1989).

Figure 4.15 implies another important fact about the diffuse reflection at small distances. Diffuse reflection for different initial fractions of light varies from the smaller distances to larger distances inside the sample. In distances between 0.001 m to almost 0.01 m, diffuse reflection changes from 0.08 to 0.6 for different initial fractions, however, in larger depths through the sample, an expansion for the various diffuse reflections happens. When light encounters the sample in the very first distances through the sample, it diffuses, however, at first the diffusion is not high since the medium is just changed. Minor varaiance for different initial fractions in this stage belongs to the

sensitivity of the model to the initial conditions. In longer distances through the sample the diffusion strength is higher, therefore, one can see the divergence of the total reflections.

Another approximation of the radiative transfer equation by Griffiths and Dahm (2008) suggests the following formula which was derived in Chapter Three. It uses coefficients of single scattering developed by Schuster (1905).

$$R_{\infty} = \frac{1}{1 + 3\left(\frac{\alpha}{\sigma}\right) + \left(\frac{5}{3}\right)\sqrt{3\left(\frac{\alpha^2}{\sigma^2}\right) + 3\left(\frac{\alpha}{\sigma}\right)}} \tag{4.2}$$

Figure 4.16 uses this equation to illustrate different results for the same initial fractions used in Figure 4.15. By comparing this Figure and Figure 4.16, it is concluded that the diffuse reflection in the model of Patterson et al. (1989) is smaller than the values of diffuse reflection in Figure 4.16. The diffusion of reflectance throughout the sample is lower than the model of Figure 4.15.

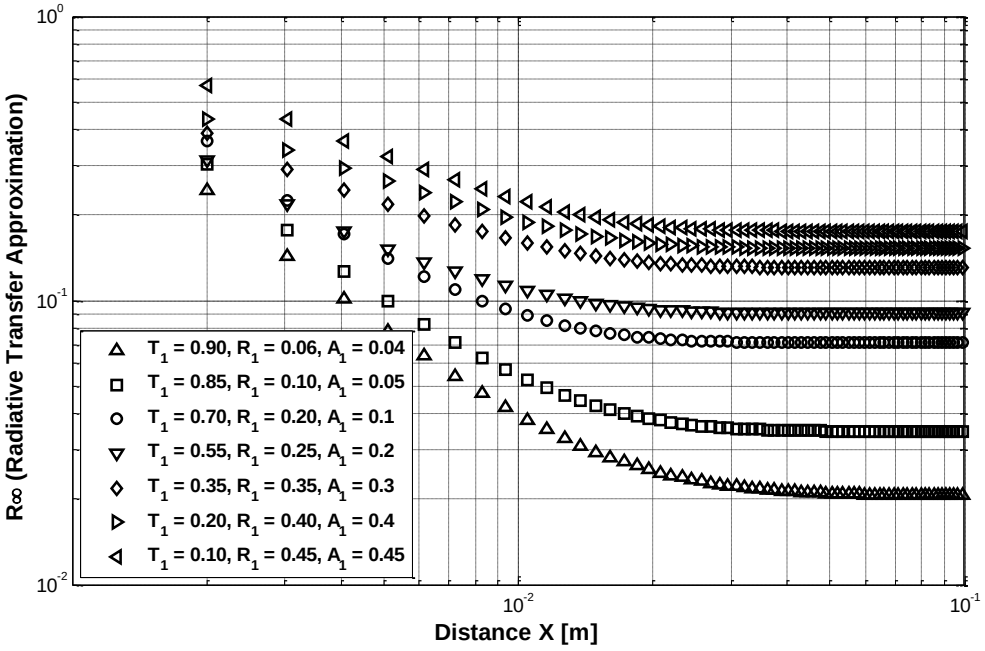

Figure 4.16 Diffuse reflection of radiation transfer model for seven different cases of initial fraction of light based on the radiative transfer approximation proposed by Griffiths and Dahm (2008).

4.2.4 Three Flux Model

This model was proposed by Burger, Kuhn, Caps and Fricke (1997). The model solves three simultaneous differential equations that are developed based on the solution to the radiative transfer equation (RTE). This equation is solved analytically for diffuse reflectance and transmittance. The isotropic scattering of an optically thick sample is derived based on the parameter that is called albedo, ω_0, which is the ratio of scattering to extinction coefficient. The equation of radiative transfer describes the influence of scattering and absorption coefficient within a medium (Kuhn et al. 1993). In the model proposed by Burger et al. the difference between the directional and diffuse illumination is considered. However, the directional illumination is the only part that is modeled here since it has been assumed that the sensor directly illuminates the light into the sample. Table 4.1 can be plotted as Figure 4.17, which illustrates the difference between diffuse and directional illuminations.

Table 4.1 The total reflectance and ratio of absorption and scattering coefficients of radiative transfer equation ($\frac{Ea}{Es}$) which is calculated based on a three flux approximation by Burger et. al (1997)

	Directional illumination			Diffuse illumination		
ω_0	R_∞	$\left(\frac{Ea}{Es}\right)_{\text{Giovanelli}}$	$\left(\frac{Ea}{Es}\right)_{3-\text{flux}}$	R_∞	$\left(\frac{Ea}{Es}\right)_{\text{Giovanelli}}$	$\left(\frac{Ea}{Es}\right)_{3-\text{flux}}$
0.1	0.01639	9	8.8182	0.0217	9	8.2696
0.15	0.03524	4	3.9271	0.04626	4	3.6869
0.3	0.05721	2.3333	2.2976	0.07445	2.3333	2.1574
0.4	0.08336	1.5	1.4811	0.10934	1.5	1.3603
0.5	0.11521	1	0.9907	0.14653	1	0.9321
0.6	0.15541	0.6667	0.6623	0.19471	0.6667	0.6245
0.7	0.20867	0.4286	0.4278	0.25655	0.4286	0.404
0.8	0.28526	0.25	0.2507	0.34187	0.25	0.2376
0.85	0.33966	0.1765	0.1775	0.40017	0.1765	0.1686
0.9	0.41495	0.1111	0.1121	0.47802	0.1111	0.1069
0.95	0.53555	0.0526	0.0533	0.59667	0.0526	0.0511
0.99	0.75275	0.0101	0.0103	0.79457	0.0101	0.01
0.99	0.91285	0.001	0.001	0.92971	0.001	0.001
1	1	0	0	1	0	0

In Figure 4.17 the diffuse illumination is calculated based on the results of the radiation transfer equation presented by Burger et al. (1997). In the diffuse illumination, there is a slightly deviation from the directional illumination. Therefore, for the simplified model proposed by Burger et al. (1997), the diffuse illumination is not well determined since the scattering and absorption coefficients are dependent on the cross sections and phase functions of Mie scattering theory. The following equation which was derived in Chapter Three, is a tool to relate the Kubelka-Munk scattering and absorption coefficients to the radiative transfer coefficients (Burger et al, 1997). This helps to compare the results of this three flux model with Kubelka-Munk's results. It relies on two basic coefficients, a_0 and a_1, which must be derived from Legendre polynomials for the case of diffuse illumination. However, they suggested a simplified coefficient for isotropic diffuse illumination that is a limiting assumption for the case of a slurry fluid.

$$K/S \approx \frac{2}{(3a_0 - a_1)/4} . \frac{E_a}{E_s} \tag{4.3}$$

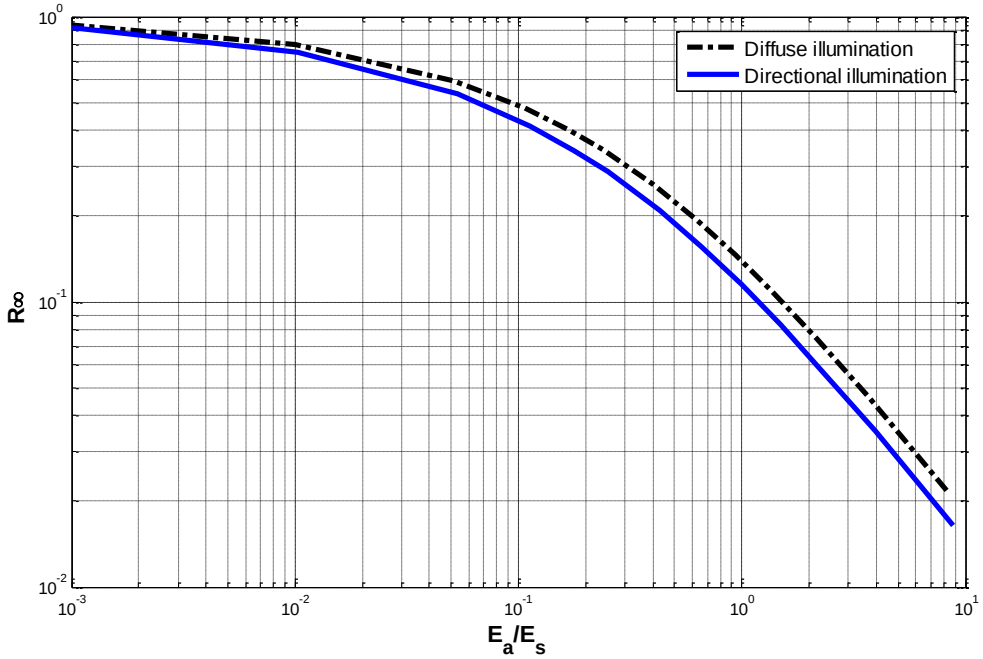

Figure 4.17 Diffuse reflectance for the direct and diffuse illuminations plotted versus the ratio of absorption to scattering coefficients of RTE approximate model developed by Burger (1997).

These two coefficients are derived for different cases of particle shapes by Mudgett and Richards (1971). The nearest case to the slurry was calculated for sphere disks. He suggested the values for the coefficients presented in Table 4.2.

Table 4.2 The values of two coefficients of Legendre polynomials for spherical disks suggested by Mudgett and Richards (1971).

a_0	a_1
1.000	**1.5560**

By applying these values into Equation 4.3, one can plot Figure 4.18. By comparing to Figure 4.17, one can conclude that in Figure 4.18, in the regions far from the wall, the reflectance for diffuse illumination is about 0.02, and for directional illuminations is about 0.03-0.08 higher than Figure 4.17. The reason is related to the conversion from radiation transfer coefficients $\frac{E_a}{E_s}$ to the Kubelk-Munk terminology, *K/S*. Now, we can use Figure 4.17 for comparing with Kubelka-Munk's results.

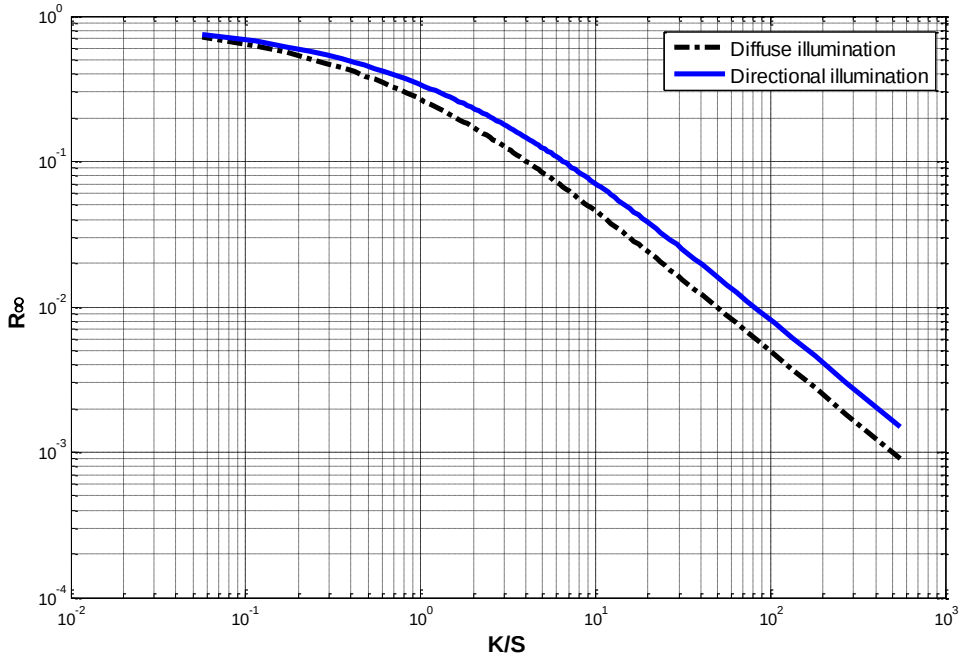

Figure 4.18 Diffuse reflectance of direct and diffuse illuminations plotted versus the ratio of absorption to scattering coefficients of K-M theory for particles with the shape of spherical disks.

To avoid using the assumption of spherical disks, only the directional illumination is applied. In Figure 4.19 the proposed model is compared with the values suggested in the three flux model of Burger et al. (1997). The discrepancy occurs because Burger's model applied the absorption to scattering coefficients $\frac{E_a}{E_s}$ that are used in the radiative transfer equation, however, the model of the three flux approximation proposed here uses the Kubelka-Munk terminology. The terminology of the radiative transfer equation has not been used here because one needs to conduct an experiment to measure the absorption and scattering coefficients as inputs for the three flux model. Another reason for not using the diffuse illumination is because of the properties of xylene in absorbing the light. Xylene absorbs the light significantly; therefore, the diffusion is not very much higher than absorption in xylene and ADP mixture. The reason for the small bump in the model of Burger is not clear since the data for the model of Burger et. al (1997) is directly derived from their results in their paper.

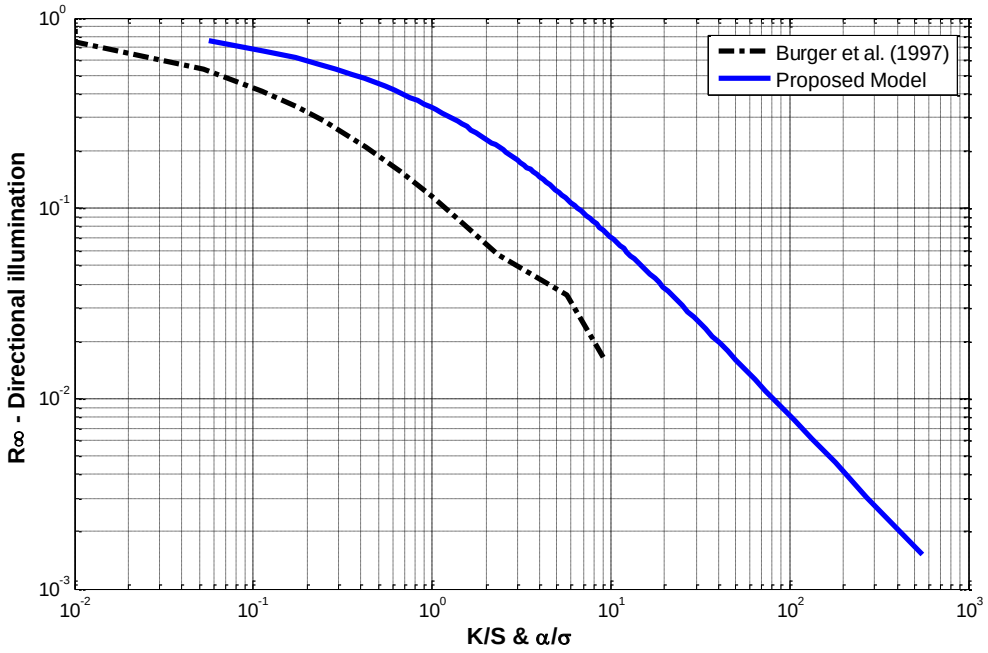

Figure 4.19 Diffuse reflectance of three different models of diffuse reflectance derived by Griffiths and Dahm (2008).

It has been noted by Burger et al. (1997) that the results of three flux approximation show a maximum relative error of about 2% for $R_\infty = 0.016$. This error causes a jump in the directional total reflectance in Figure 4.19. The differences between the Kubelka-Munk, the three flux approximation, and diffusion theories are discussed in Section 4.2.5.

4.2.5 Diffusion Model

In this thesis, the diffusion model is studied briefly for the purpose of comparing its results with other continuum theories. This model is a summary of work done by Griffiths and Dahm (2008) which is another approach to investigate the radiation transfer equation. One important assumption about this model, mentioned in the previous Chapter, is related to the scattering and absorption coefficients. It has been assumed that the scattering is much larger than absorption, therefore, it is described through a diffusion process. This assumption is sufficient not to consider this theory for our modeling because xylene absorbs light considerably, so the diffusion is not much higher than absorption in our sample. Figure 4.20 illustrates the diffuse reflectance of four different optical theories in the cases of continuum mathematics which was derived by Griffiths and Dahm (2008).

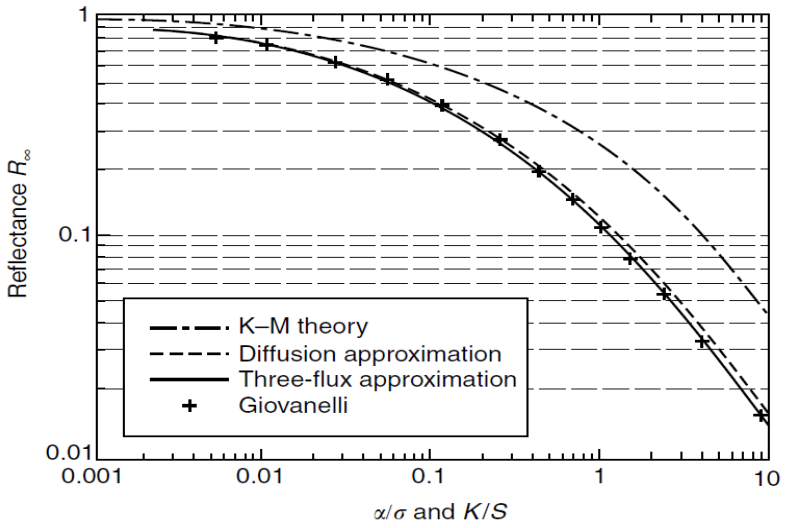

Figure 4.20 Diffuse reflectance of three different theories of diffuse reflectance derived by Griffiths and Dahm (2008).

Figure 4.21 presents the difference between these three models. The diffuse reflectance is modeled by diffusion approximation. As discussed by Burger et al. (1997), Kubelka-Munk theory deviates from the other two models due to its limitations and simplicity. The relative error for R_∞ in Kubelka-Munk compared to Giovanelli's calculations is more than 8% for small R_∞ and below 5% for larger R_∞. Diffusion and three flux approximations shows less errors (Burger et al., 1997). This observation is in accordance with the results of Kortum (1969), who pointed out the crucial deviation of K-M theory with experimental results for $K/S > 0.13$.

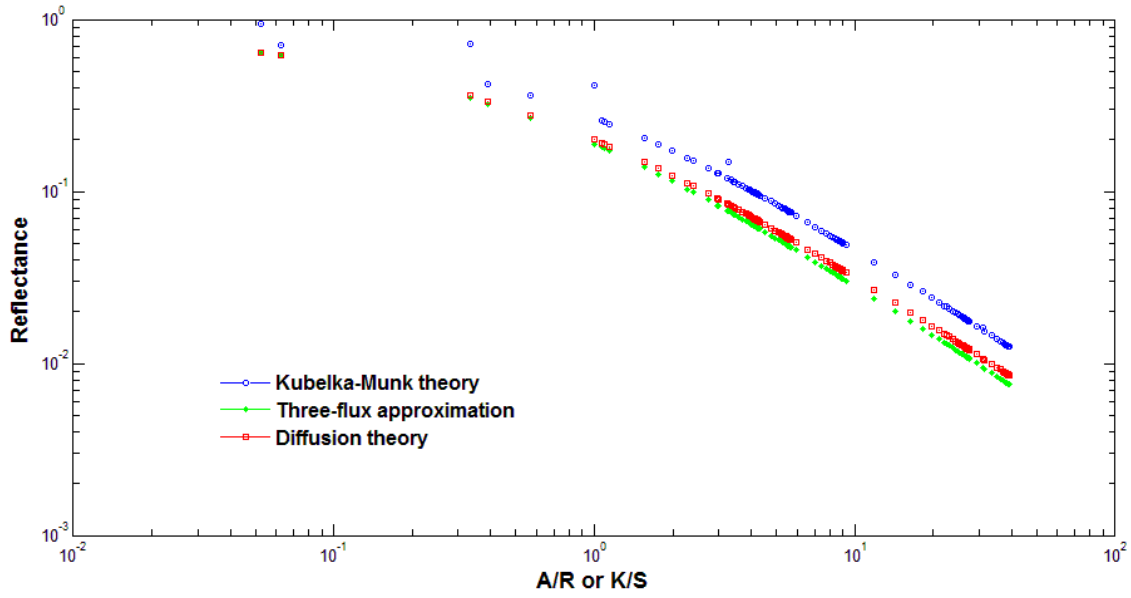

Figure 4.21 Diffuse reflection of an isotropic, optically thick sample according to the three flux approximation, the diffusion approximation, and Kubelka-Munk different models continuum theories.

4.3 Results of Discontinuum Optical Models

Continuum models are investigated in detail in Section 4.2. In the present section, the results of discontinuum optical models are reviewed and discussed. Discontinuum optical theories are discussed in detail in Chapter Two and the models were built in Chapter Three. Discontinuum models are more

appropriate for mixtures than continuum ones since they suggest a more advanced description of the sample. Discontinuum models describe the light interaction phenomena with individual particles and the whole sample throughout more visible functions that are hidden in the assumptions of continuum theories (Griffiths & Dahm, 2008). This feature is achieved by treating the sample through defining multiple layers which divide one thick sample into many smaller samples in size which maintain the properties of the whole sample. Each layer is a collection of infinitesimal particles. Hence, the size of particles controls the thickness of the layers and consequently, the scattering and absorption properties of the layers are determined by particles and the surrounding medium. Dahm and Dahm (2007) have recently proposed a novel approach in applying discontinuum theory to the two-flux results of radiative transfer equation. This method is known as representative layer theory and results are shown in this Section. The model of plane parallel layers is applied to compute the fractions of light discontinuously throughout the sample. Other discontinuous models also use descriptions similar to the fundamental formulation of plane parallel layers. Discontinuum theories use a definition for the initial fraction of light which is different from continuum theories. These models assume that the sample is divided into several layers each one particle thick. When the light beam encounters the sample, the first layer will be interacted. Some portion of the light is transmitted to the next layer, T_1, some is reflected out, R_1, and some is absorbed, A_1. The fractions of R_1, T_1, and A_1 are known as initial fractions of light for the following sections discussing discontinuum models. The plane parallel layers, assembly of sheets, and representative layer model, combined with Stokes formulas, are discussed.

4.3.1 Model of Plane Parallel Layers

The plane parallel layer model is used to predict the absorption, remission, and transmission locally for each layer in the sample. The sample is divided into a finite number of layers. Each one has different thickness relative to the other layers. According to Figure 4.22, the light beam approaches

the sample in a layer recognized as $n+1$. The light beam has three possible options, whether being transmitted to the layer *n*, being reflected out of the sample, or being absorbed by the same layer. If it is transmitted to the next layer, the probability of this phenomena is T_{n+1}, however, if it reflects back from the sample it comes out with the possibility of R_{n+1}. The absorption is unknown, however, and will be calculated from reflection and transmission probabilities since the total probability is equal to one; $R_{n+1} + T_{n+1} + A_{n+1} = 1$. This is the phenomena for the first layer being illuminated by the incident beam. The transmitted beam from the layer $n+1$ is considered as a incident beam for the second layer but its intensity is T_{n+1}, not 1.

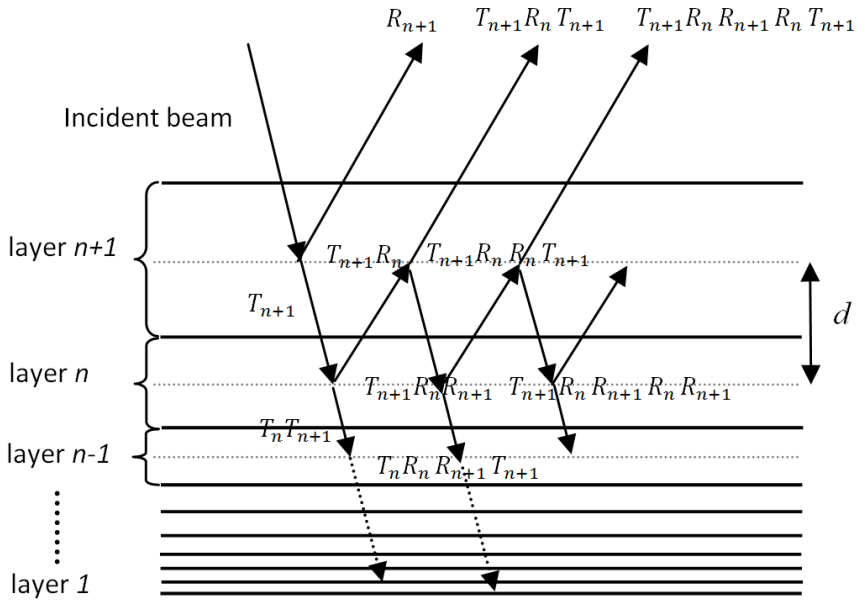

Figure 4.22 Absorption, reflection and transmission probabilities in two layers of a sample consisting of *n*+1 layers with different thicknesses changing sequentially based on a geometrical progression.

This process also occurs for the other layers as a sequential phenomena, and finally it will be absorbed by the sample or reflected to the sensor or transmitted to the other side of the sample. The intensity may approach zero without being absorbed after several reflections or transmissions. It is hard to predict all these probabilities without modeling. In our model, a geometric progression is applied as a

scheme that requires more accuracy from the layers that are far from the sample edge where the incident beam was first encountered. This accuracy is achieved by decreasing the thickness of the layers gradually as depicted in Figure 4.22.

Absorption, remission, and transmission fractions at different layers of the sample with a total thickness of 1.5 cm are shown in Figure 4.23. This Figure is plotted for a sample that has a high remission. In this sample, there are 50 layers. The thickness of the layers starts from 0.01 m and decreases with a rate of 1.01 that finally approaches a thickness of 0.015 m after passing through 50 layers. The rate of decay in transmission is much faster than the rate of growth in the other two fractions. The reason stems from the convergence criterion which has been met very fast. The convergence in this model is determined from the absorption coefficient. Dahm and Dahm (1999) pointed out that the absorption coefficient is a parameter that converges faster than other coefficients such as remission coefficient. In this model the absorption and remission coefficients for each layer

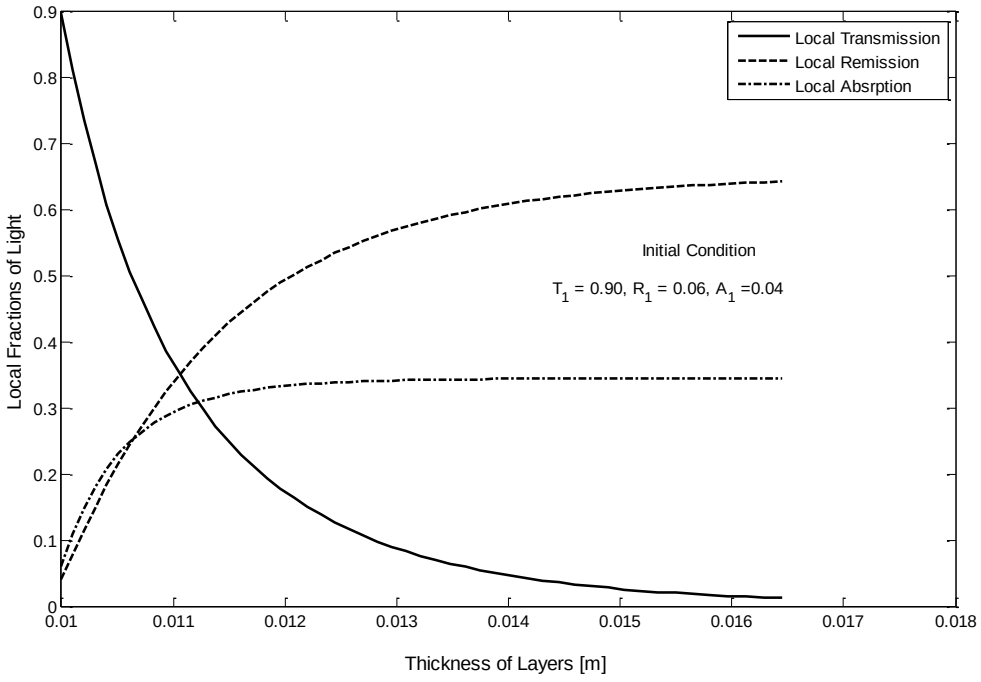

Figure 4.23 Local absorption, reflection and transmission probabilities in the sample for initial condition of $A_1 = 0.04, R_1 = 0.06, T_1 = 0.9$

are evaluated from the ratio of absorption fraction to the thickness of that infinitesimal layer. Therefore, the absorption coefficient is controlled in each iteration. The control process is achieved by controlling the absolute values of the absorption coefficients between two consecutive iterations. In this model, this absolute value of this difference is chosen to be less than $\frac{1}{10000}$. Hence, one can be certain about the convergence of the equations. Also, there are other parameters that increase the accuracy. One parameter which increases the accuracy is the thickness of the layers. Increasing the number of layers will increase the accuracy of model since the fraction of light is calculated for a small thickness. However, by increasing the thickness of layers, the model get closer to a continuum one in the limit, so the accuracy decreases and the convergence criterion which is based on absorption coefficient does not approach the accuracy of 0.01 for this model. .

Dahm and Dahm (1999) pointed out that the plane parallel layer is not a descriptor for regions of high absorption. In higher absorption samples they suggested that the representative layer theory is a more powerful descriptor. Therefore, the linear absorption region is better to be determined from absorption fraction and absorption coefficient (Dahm & Dahm, 1999). The linear region is obtained by using a least squared regression technique for absorption fraction. In the model of representative layers, a similar approach to the plane parallel model is used to obtain the absorption and remission coefficients. Therefore, these coefficients are calculated by dividing the absorption fraction over the thickness of the layer. The linear region in Figure 4.24 is determined by a least squared tolerance of 5% error. In this Figure, it has been shown that this amount of error is achieved when the light passes the layer number 7. At this point the absorption fraction is A = 0.484. Another line plotted that is obtained from the equation $A = Kd$, where K is the absorption fraction and d is the thickness of the layer. This equation is an approximation of the Beer-Lambert law.

The Beer-Lambert law suggests the absorption and transmission in a sample with the property of negligible remission (Dahm & Dahm, 1999). This law suggests that the transmission and absorption

through a sample of thickness d in a material for which K is a linear absorption coefficient can be determined from the following equations:

$$A = 1 - e^{-kd}$$
$$T = e^{-kd} \tag{4.4}$$

These two equations are very important since they have been used in more rigorous models such as representative layer theory. Therefore, the equation $A = Kd$ is an approximation of linearity since for small absorption fractions, the absorption is proportional to sample thickness $A \approx Kd$. The absorption fraction curvature is very close to the line of kd in the first seven layers of the sample. Initial fractions of light for this simulation are assumed to be $A_1 = 0.04, R_1 = 0.06,$ and $T_1 = 0.9$. It must be noted that regions of extremely high absorption will not be considered in this report since these regions are not compatible with the compositional analyses discussed in Section 3.3.3 (Dahm & Dahm, 1999).

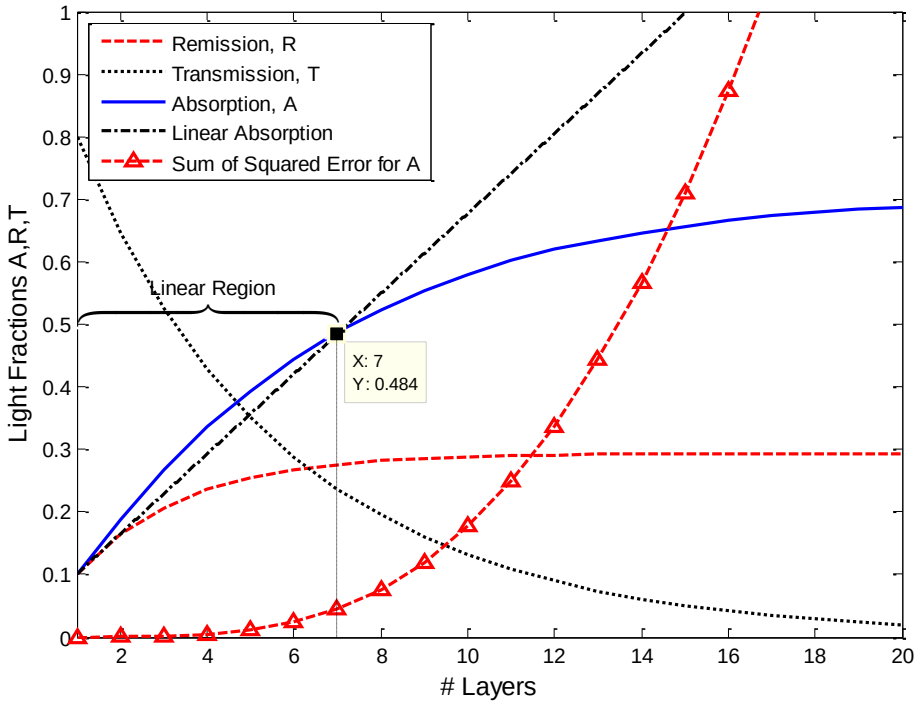

Figure 4.24 The illustration of linear region in the model of plane parallel layers determined from sum of squared regression.

Figures 4.25 and 4.26 illustrate the results of plane parallel layers and the Beer-Lambert law for absorption and transmission fractions. The variations of *A* and *T* with different initial fractions are remarkable.

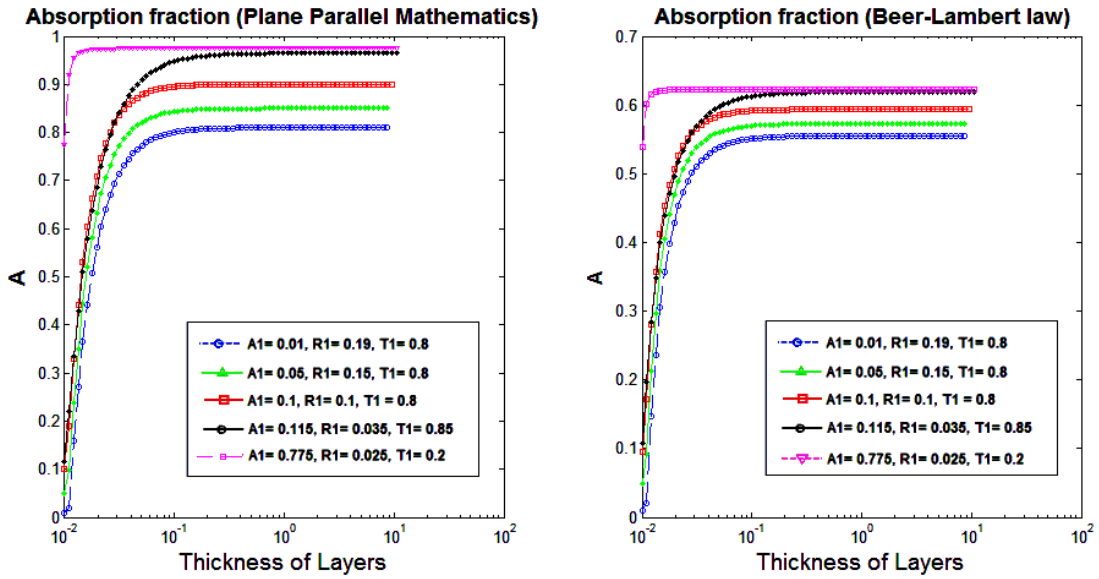

Figure 4.25 Local absorption fraction for different initial conditions

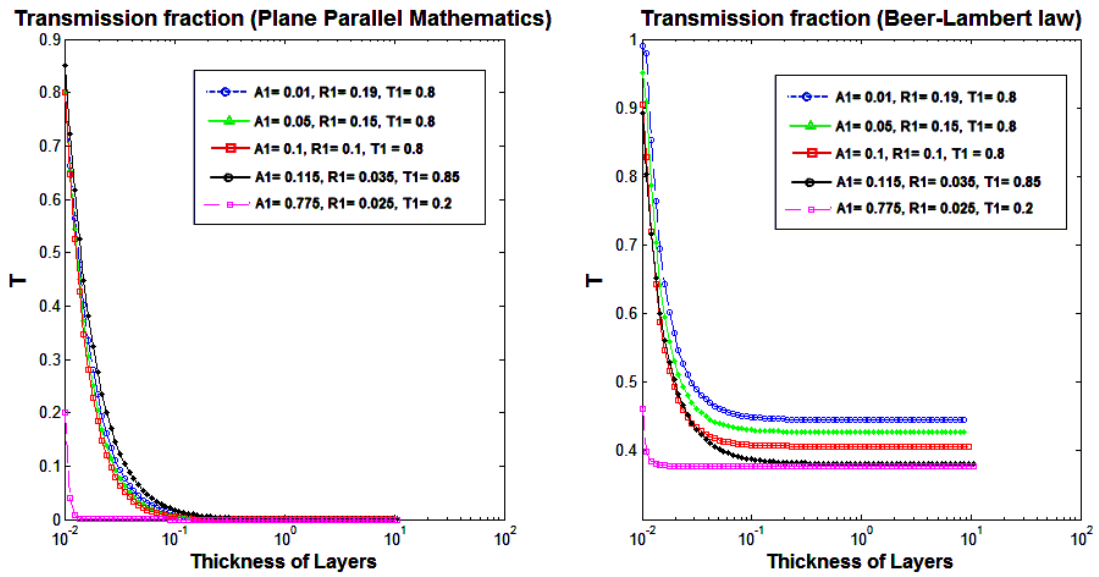

Figure 4.26 Local transmission fractions for different initial conditions

A careful observation of these Figures reveals that the Beer-Lambert law converges faster than plane parallel mathematics since the equations used by Beer-Lambert law are exponential. Moreover, one can notice that the curve corresponding to highest initial absorption fraction with the values of $A_1 = 0.775, R_1 = 0.025,$ and $T_1 = 0.2$ has a different behavior than other 4 curves. The reason is that the initial absorption fraction in this figure is much higher than the others.

Application to the system of slurry flow (xylene and ADP)

The plane parallel model is a good approximation for layers with discontinuities since it can predict the fractions of light in layers that are exactly one particle or any integral number of particles thick. Hence plane parallel layer is an accurate descriptor of systems that consist of several particles. In our model the xylene is a liquid and primary medium. The ADP particles are the secondary phase of the sample with their own optical properties. The initial fractions of light are crucial components representing the optical properties of the sample in a plane parallel layer model. These fractions for the sample of xylene and ADP must be determined through experiment. Chalmers and Griffiths (2002) suggested the initial fraction of light for a real sample that consist of particles. These fractions are $A_1 = 0.1, R_1 = 0.05,$ and $T_1 = 0.85$. Table 4.3 illustrates the result of applying this real fraction of light to our model of plane parallel layers.

Using Equation 3.41 which is another interpretation of plane parallel layers, one can use geometric progression in the inverse direction. In this method of using plane parallel layers, the initial fractions of light are known from experiment, however, the fractions of light are unknown inside the sample. By the aid of inverse geometric progression and applying plane parallel layers, one can determine the fractions of light in all of the layers of material as shown in Table 4.3. The first row in Table 4.3 is the known initial fraction of the sample, however, the fractions for other layers were unknown. The extrapolation is a powerful technique that has been applied to plane parallel layers. It enables us to use the fractions of the first layer and expand the calculations to find the fractions for other layers.

Table 4.3 Description of computing absorption and remission coefficients by extrapolating from a known sample of thickness d to a sample of infinitesimal thickness.

Thickness (d is thickness of known sample	A_n Absorption fraction	R_n Remission fraction	T_n Transmission fraction	B Remission coefficient (units are those of d $(the\ thickness)^{-1}$)	K Absorption coefficient (units are those of d $(the\ thickness)^{-1}$)
d	**0.100000**	**0.050000**	**0.850000**	**0.050000**	**0.100000**
d/2	0.051355	0.027027	0.921618	0.054054	0.102711
d/4	0.026021	0.014065	0.959914	0.056259	0.104084
d/8	0.013097	0.007176	0.979727	0.057410	0.104775
d/16	0.006570	0.003625	0.989805	0.057997	0.105122
d/32	0.003290	0.001822	0.994888	0.058295	0.105295
d/64	0.001647	0.000913	0.997440	0.058444	0.105382
d/128	0.000824	0.000457	0.998719	0.058519	0.105426
d/256	0.000412	0.000229	0.999359	0.058556	0.105447
d/512	0.000206	0.000114	0.999680	0.058575	0.105458
d/1024	0.000103	0.000057	0.999840	0.058585	0.105464
d/2048	0.000051	0.000029	0.999920	0.058589	0.105466
d/4096	0.000026	0.000014	0.999960	0.058592	0.105468

4.3.2 Model for Assembly of Sheets

The assembly of sheets model has been introduced in Chapters Two and Three. In this Section the results of the model are discussed. This model uses Stokes formulas to solve the problem of remission from and transmission through a sample of parallel sheets. As was mentioned in the previous Chapter, a sheet is an object with two large smooth flat surfaces which are parallel to each other. The theory uses the reflectance of a surface that is obtained using the Fresnel equation which relates the refractive indices of the primary phase and secondary phase. The formulas and the assumptions of this model are discussed in detail in Chapter Three. Dahm and Dahm (2007) have pointed out that the model of assembly of sheets is also called a series of Stokes sheets. The procedure for modeling is discussed in Chapter Three, but a brief recapitulation is given here. The remission, transmission, and absorption fractions of light are first calculated based on the assembly of sheets formulas presented in Chapter Three. These fractions are for one layer of material, however, the Stokes formulas are used to predict the light fractions for different distances through the sample. The refractive indices in this model are shown in Table 4.4. The reflection is obtained from the Fresnel law, Equation 4.5 is reviewed here.

According to this equation, the reflection is obtained based on the values of Table 4.4. The reflection value is 8.8x10E-5.

In the near-infrared region, the refractive index of ADP does not change considerably. According to the Figure 4.27, the refractive index of ADP changes less than 0.03 in the range of 0.7 to 1.4 μm. According to Figure 4.27, an arbitrary value of 1.5242 is chosen. The refractive index of xylene is an average in the NIR spectrum which was shown in Table 4.4.

$$r_0 = \frac{(n_1 - n_2)^2}{(n_1 + n_2)^2} \tag{4.5}$$

Table 4.4 Refractive index of xylene and ADP

Refractive index of xylene	Refractive index of ADP
1.49582	1.52424

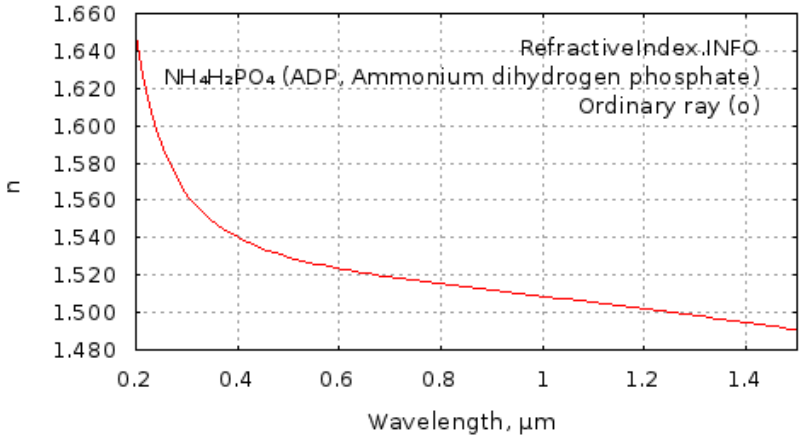

Figure 4.27 Refractive index of ADP as a function of wavelength. The data is collected from Refractive Index Database (N.d.)

Now consider the results of applying the model. The remission is plotted against the distance through the sample. This model is achieved by applying the refractive index to Stokes formulas. In Figure 4.28, the total absorption fraction through the layers for different initial fractions of light have been plotted. It is noticeable that the absorption for this model almost is the same for different initial

fractions of light. This phenomenon must be proved analytically. According to the complex formula of the model of assembly of sheets, the absorption is dependent on the other two fractions of light; remission and transmission. Since absorption does not change by changing the initial fractions of light, one can think of the equation of absorption $A = 1 - R - T$. According to this equation, if the absorption is constant for initial fractions of light, the sum of remission and transmission will be constant for various initial conditions. Another reason stems from the refractive indices that are used in this model. The optical properties of xylene suggest a considerable absorption in the range of near-infrared radiation. Having this discussion in mind, one can conclude that the absorption fraction is much higher than the other two fractions of light. Hence, the variations in those small fractions of light such as remission and transmission do not affect the total absorption very much.

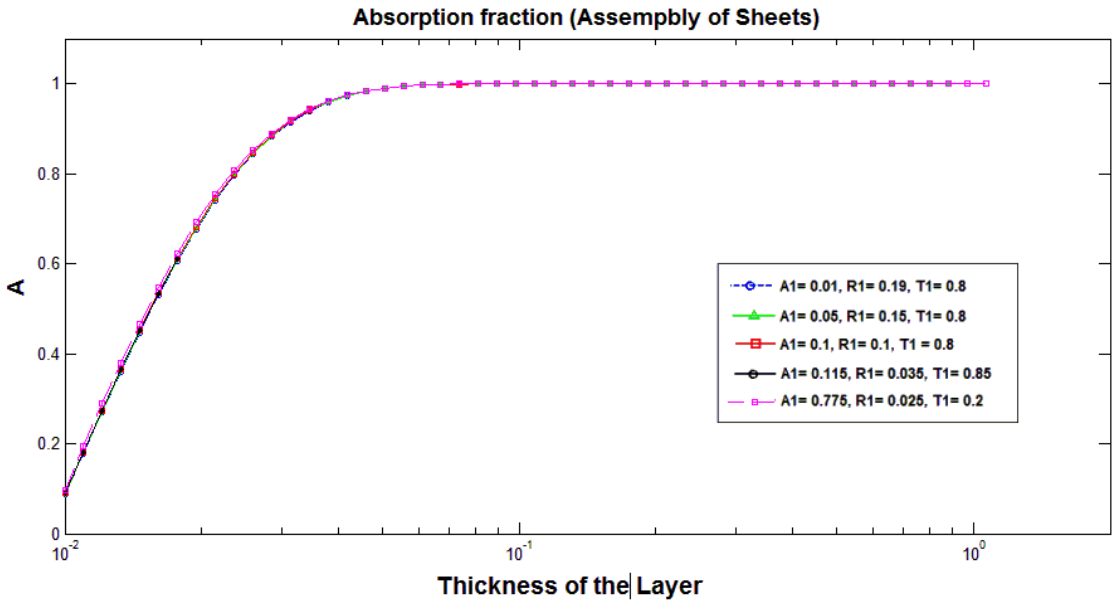

Figure 4.28 Total absorption fraction through the layers of the sample for different initial conditions.

Figure 4.29 presents the remission fraction through a sample of xylene and ADP that is modeled by using the assembly of sheets. As expected, the remission from this sample is not as considerable as the absorption. Therefore, one can conclude that unlike other theories of diffuse reflectance investigated so far (except representative layer theory), the theory for the assembly of

sheets is the most applicable theory to the case of a two-phase sample of xylene and ADP. Theory for assembly of sheets predicts the fractions of light not only locally but also integrally through the sample. Figure 4.29 shows that the effect of other fractions of light on remission is not considerable since the initial absorption fraction is changed from 0.01 to 0.775, and the effects on the remission are negligible. It can be concluded that the initial remission has the greatest effect on the total remission computed from model of assembly of sheets.

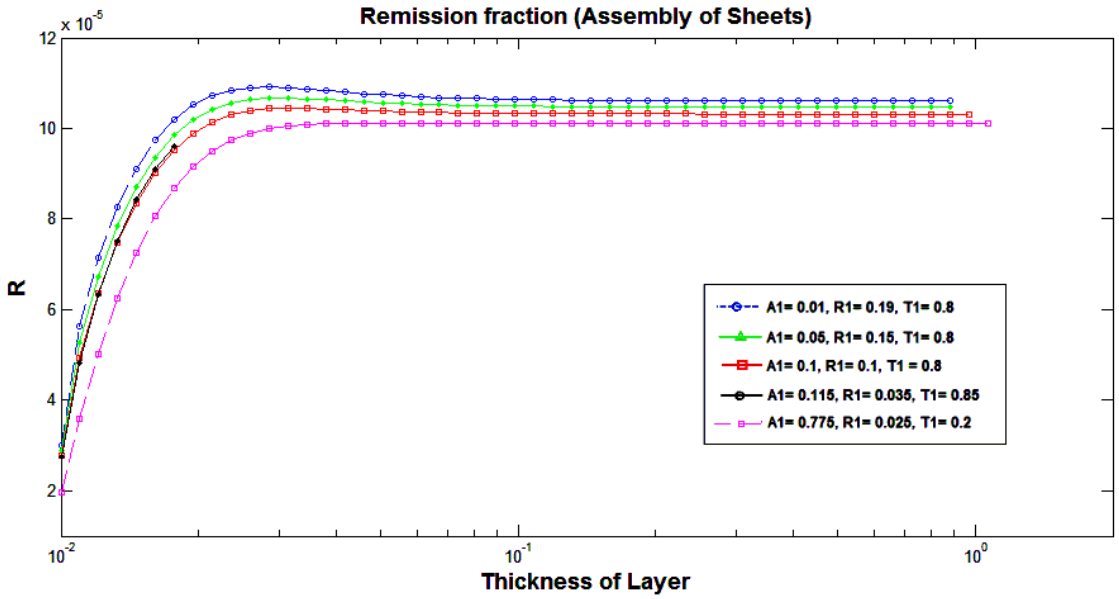

Figure 4.29 Total absorption fractions through the layers of the sample for different initial conditions

4.3.3 Representative Layer Model

Representative layer theory (RLT) is the last theorem in this study. It is the newest theory in the field of diffuse reflectance that is studied in this thesis. In fact, representative layer theory is an approximate method that builds a bridge between the properties of the particles in a layer of a sample and the properties of the whole mixture. This theory is capable of modeling particles of different types with different size and composition (Chalmers & Griffiths, 2002). In the model of the representative layer that we present, hypothetical arbitrary concentration profiles also are used. Computational Fluid

Dynamics (CFD) is used to predict the concentration of particles in the sample in the direction perpendicular to the axis of pipe. The algorithm and the procedure used to implement the CFD results in the model is discussed in detail in Chapter Three. For describing the theoretical scope of representative layer theory, one can assert that this theorem is a combination of plane parallel layers, Beer-Lambert law, Stokes formulas, and even Kubelka-Munk theory. In this model, each particle is characterized by its composition, the cross - sectional surface area that it presents to the light beam incident on the sample, its volume, and the density. We assume that the particle cross section is circular since the RLT does not have any restriction about the particle shape.

Modeling for Arbitrary Concentrations

One important point about the representative layer model used in this section is the geometry of the model. As shown in Figure 4.1, the representative model applied is to a rectangular sample. The cross section of this rectangle is a square with sides equal to D. The reason for changing the circular cross-section of the pipe into a square is because of the assumption of direct illumination in the representative layer model. This assumption makes us build a geometry in which the layers are parallel to each other and perpendicular to the incident beam. Before applying CFD concentration profiles to the model, six different cases of hypothetical arbitrary concentrations are used. The aim is to investigate the results for arbitrary concentration profiles.

In Table 4.5, hypothetical concentrations are divided into three groups of uniform, linear, and parabolic concentrations. These concentrations have been applied to the sample of xylene and ADP with the particle sizes of $75\mu m$. The uniform concentration profiles are shown in the left side of Figure 4.30. On the right side of Figure 4.30, one can see the linear and parabolic concentration profiles. The equations for the linear and parabolic concentrations are chosen arbitrarily, however, the two lines of on the right side of figure start from 0.2 and 0.3 to compare with uniform concentrations.

Table 4.5 Different cases of hypothetical concentrations

Hypothetical Concentrations	*Particle Diameter $d_p = 75\ \mu m$*		
	Uniform Concentrations (C)	***Linear Concentrations***	***Parabolic Concentration***
	C = 0.05	C = -0.1(Y/D) + 0.3	C = -0.4(Y/D)^2 + 0.25(Y/D) + 0.25
	C = 0.2	C = -0.15(Y/D) + 0.2	
	C = 0.3		

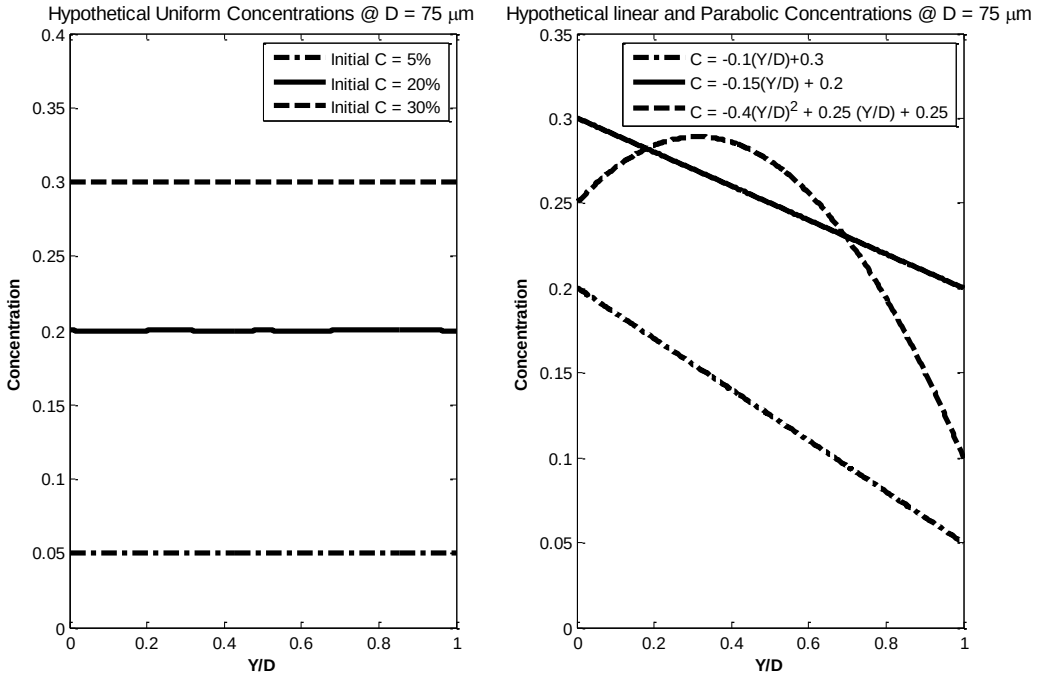

Figure 4.30 Hypothetical concentration profiles in a sample with particles of 75 micron

Figure 4.31 illustrates the local and integral absorption fraction of light for uniform concentrations. As it was expected, local absorption will remain constant since the concentration of particles in each layer is constant. In the diagram on the left, there is a small variation in the very near the wall region which occurs because of the numerical convergence of the code. However, this small

bump does not appear in the integral absorption since the absorption fractions for the layers are summed up layer by layer. Therefore, one can see the starting point of the integral absorption in the very near wall region is higher than the constant value of local absorption. For example, for the initial concentration of 20%, the constant value of local absorption is A = 0.1, while its integral absorption starts from the value of A = 0.15 for the first layer. This phenomenon occurs because of the very small variations in local absorption in the layers adjacent to wall, shown in Figure 4.31.

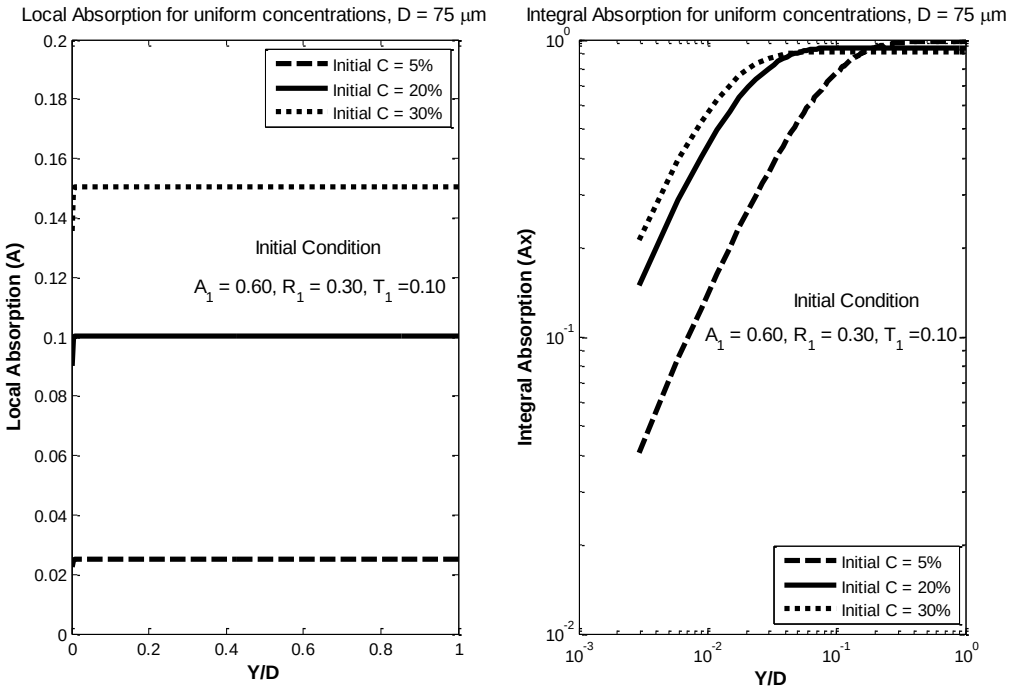

Figure 4.31 Local and integral absorption fraction for the case of uniform concentrations

Remission fraction of light is plotted in Figure 4.32. In the left side of the figure, the local remission is plotted, while in the right, the integral remission shows the variation for this fraction. It can be noticed that unlike absorption fraction, the local remission does not show variations in the very near wall region. The absorption equation is an exponential function. The function takes the exponent of negative values of absorption coefficient, according to Equation 3.84. Therefore, the absorption fraction is a nonlinear function of the layers. In addition, the convergence criterion of the model is

based on the absorption coefficient which is illustrated in Equation 3.83. Convergence criterion in the model representative layer theory is the same as plane parallel layers which checks the absolute values of absorption coefficients for convergence of the model. This value must be optimized for different initial conditions since it is a very strong function of boundary conditions. For these reasons, the jumps in the local remission fraction are very small or negligible for lower initial concentrations to higher ones, as shown in Figure 4.32.

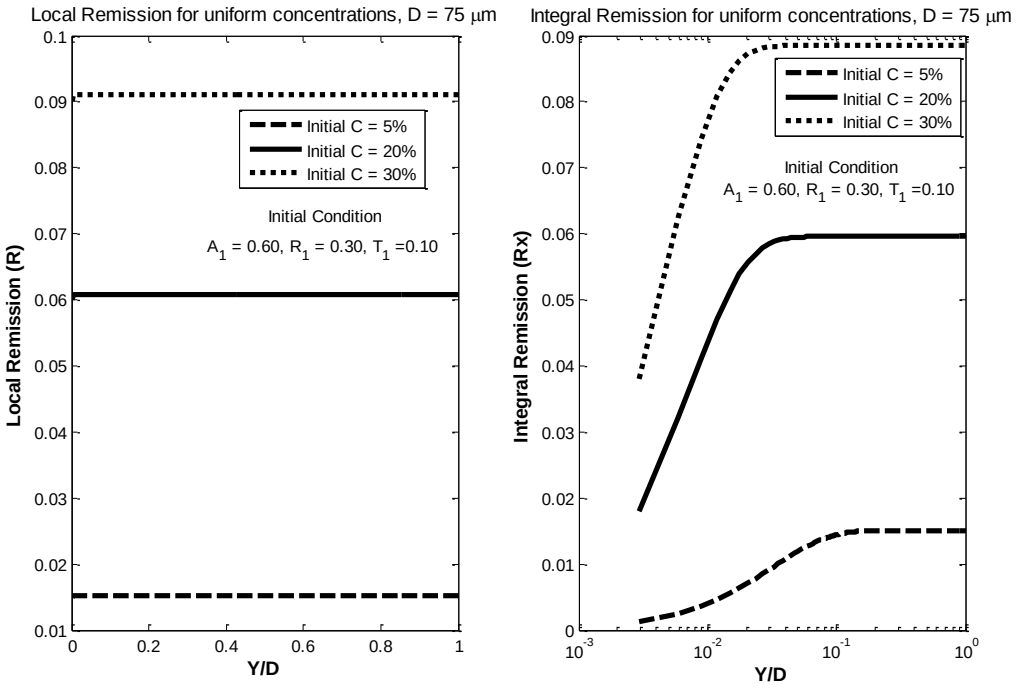

Figure 4.32 Local and integral remission fraction for the case of uniform concentrations

Figure 4.33 illustrates the transmission fraction which is plotted based on the other two fractions since the transmission fraction is dependent on the absorption and transmission fraction in the representative layer theory. The rate of decrease in the integral transmission is faster than the rate of increase in absorption and remission since the integral transmission, unlike local transmission, is not dependent to the absorption and remission. Moreover, according to Equation 3.70 the numerator of the integral transmission decreases much faster than the remission fraction. The reason stems from the function of

Ω that is much smaller than the Ψ function for the layers far from the wall. The denominator of Ψ is local remission which is very high for the regions far from the wall.

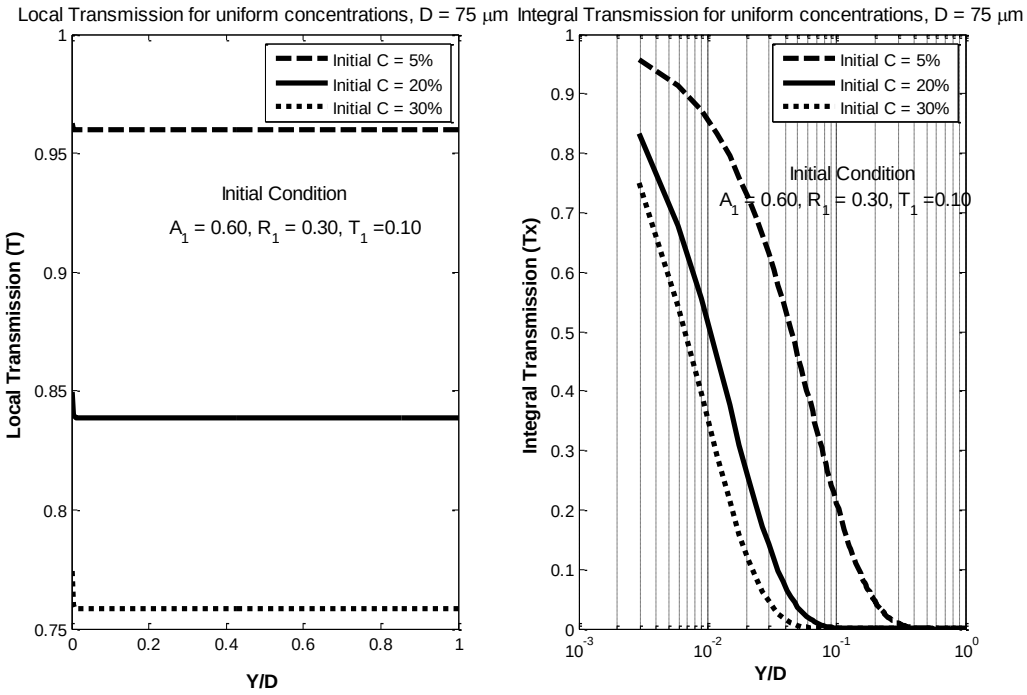

Figure 4.33 Local and integral transmission fraction for the case of uniform concentrations

Figures 4.34 to 4.36 illustrate the absorption and remission of the two linear and parabolic concentrations. In Figure 4.34, the local absorption is a strong function of the concentration profiles shown in Figure 4.30. Integral absorption fraction in Figure 4.34 illustrates that the three integral absorptions for the three concentration profiles are very close to each other. From *Y/D =0* to *Y/D* = 0.2, in the plot of the integral absorption, the discrepancy between the three concentration profiles is not considerable. In the integral absorption shown in the right side of Fogure 4.33, for the region very near the wall, from *Y/D = 0.003* to *Y/D* = 0.04, the line with equation C = -0.1(Y/D) + 0.3 has a lower absorption than the other two concentration profiles. This is reasonable because the local absorption of this line is the lowest. However, in the integral absorption region at point Y/D = 0.04 the absorption of this concentration profile jumps higher than the integral absorption of the other two profiles. This may

look unreasonable, however, by examining Equation 3.70 one can find the reason. In representative layer theory, the integral absorption is dependent to the integral remission and transmission through this equation: $A_x = 1 - T_x - R_x$. By looking at integral remission in Figure 4.35 we may conclude that the integral remission for this linear concentration is the lowest, hence, the integral absorption will increase more than the parabolic and other linear concentrations.

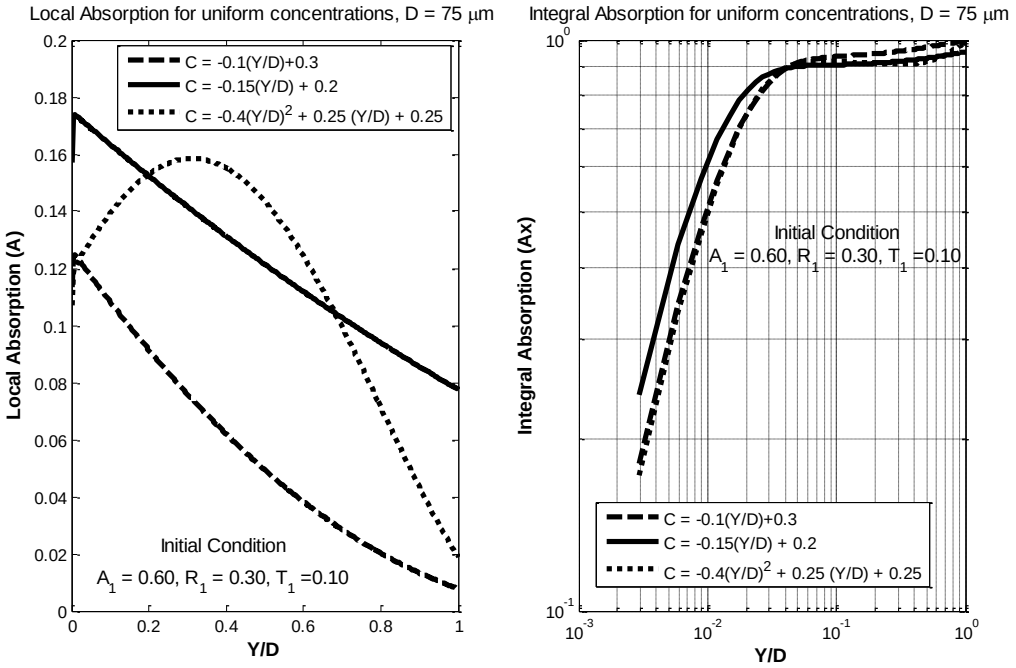

Figure 4.34 Local and integral Absorption fraction for the case of arbitrary linear and parabolic concentration profiles

Figure 4.35 shows that the integral remission has the same behavior as the local remission. In Figure 4.36, the transmission is decreasing very fast at the beginning of the sample when light first encounters the first layer and then after that it is almost zero.

Studying Figures 4.31 to 4.36 suggests that the absorption which occurs for the case of uniform concentrations is different from the behavior of linear concentrations.

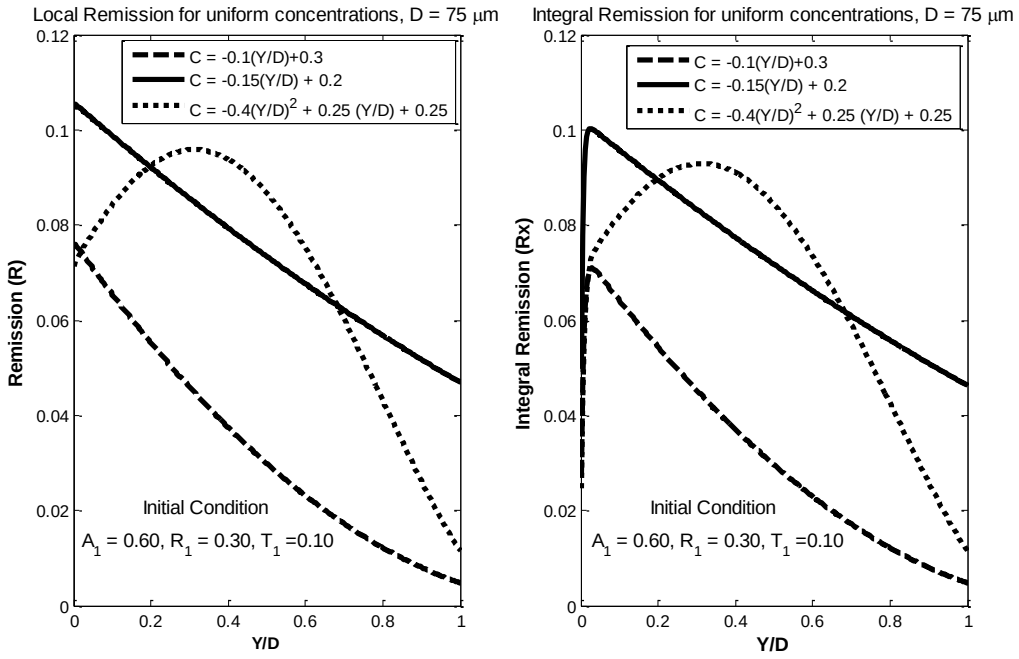

Figure 4.35 Local and integral remission fraction for the case of arbitrary linear and parabolic concentration profiles

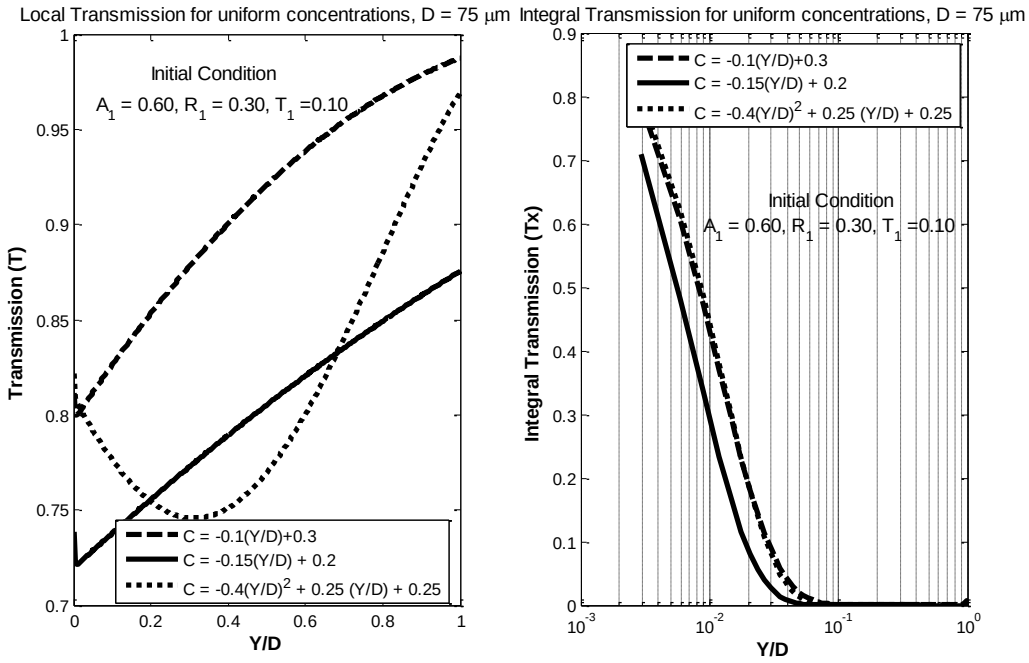

Figure 4.36 Local and integral transmission fraction for the case of arbitrary linear and parabolic concentration profiles

According to Figure 4.31 the curves reach the highest value of absorption at two different points. The points Y/D = 0.2 and Y/D = 0.04 are the ones at which the integral absorption first reaches the maximum. Therefore, the absorption for different initial conditions is different. According to Figure 4.34 the Y/D is equal to 0.04 even if the concentration is changed. This model predicts the absorption fraction much more accurately than continuum theories. Remission is a very important factor in predicting the light travel into the sample of slurry. The remission (Figure 4.32) is also increasing layer by layer. The only parameter that decreases is the transmission. The transmission reaches zero at about 0.07 of the cross-sectional diameter. Therefore, this sample with the mentioned initial fraction of light is saturated at about Y/D = 0.1. One can conclude the penetration depth of light is somewhere between *Y/D* = 0.06 to *Y/D* = 0.2. If the pipe diameter is D = 0.0254, the depth of penetration will be in the range between 0.15 cm to 0.5 cm.

Modeling for CFD Concentrations

CFD results are shown in the following different cases in Table 4.6. In addition to the data presented below, other particle sizes were simulated in this thesis. Some of the following cases are discussed in this section. Since there are many cases, only the cases of Re_D = 140000 are plotted here.

Table 4.6 Different cases of CFD results

CFD Concentrations	*Pipe Reynolds number, $Re_D = 140000$*				*Pipe Reynolds number, $Re_D = 280000$*			
	Particle diameter d_p (μm)	***Concentration (C)***			***Particle diameter d_p(μm)***	***Concentration (C)***		
	38	0.05	0.2	0.3	38	0.05	0.2	0.3
	75	0.05	0.2	0.3	75	0.05	0.2	0.3
	150	0.05	0.2	0.3	150	0.05	0.2	0.3

Figure 4.37 illustrates the CFD concentration profiles for three particle sizes ranging from 38 microns to 150 microns.

This Figure is plotted for 5% initial concentration. Here, the cases for 5% concentrations are discussed, while the 20% and 30% concentrations are presented in Appendix A.

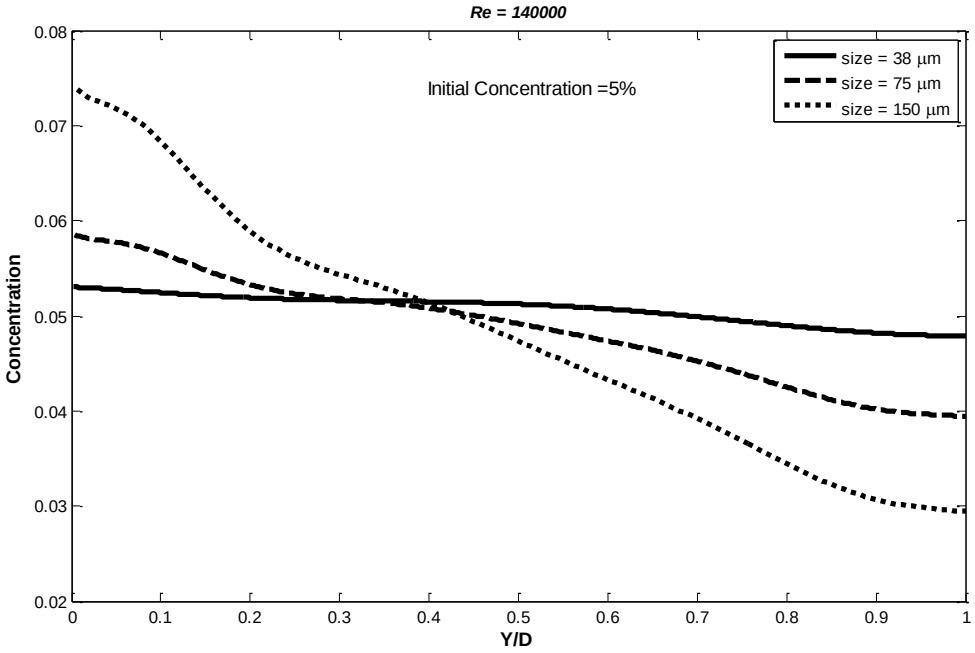

Figure 4.37 CFD concentration profiles

From Figures 4.38 to 4.40, one can conclude that the local fractions of light are functions of concentration profiles. Figure 4.38 illustrates the local absorption of light for three different particle sizes. One can notice that the three absorption curves have not passed through one point such as Figure 4.37. This may be because of the effect of concentration on absorption. The absorption is a strong function of particle size. The little jumps in the near wall regions are due to the previously mentioned effects of absorption coefficient and the numerical convergence criterion. This coefficient is adjusted for the whole model but since it is sensitive to absorption, one can see the effects of convergence in the very near wall region only for absorption fraction. Figure 4.38 describes the remission for the three particle sizes. The remission is also influenced by the concentration profiles, however, there are some small differences between Figure 4.37 and Figure 4.39 in the shape of the curves.

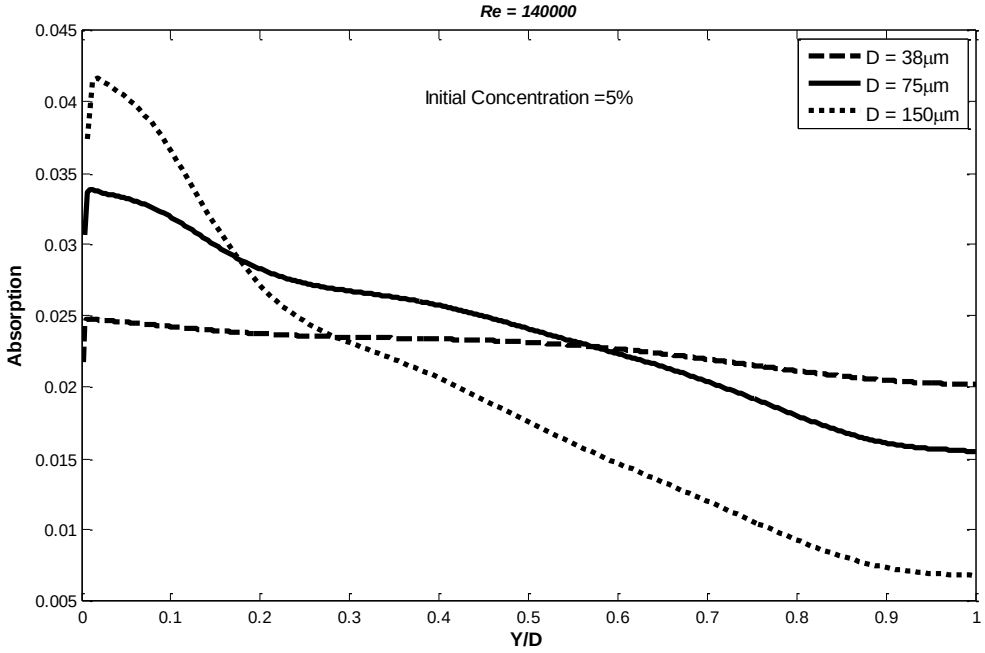

Figure 4.38 Local absorption fraction for particles with initial concentration of 5% in three different sizes of 38μm, 75 μm, and 150 μm

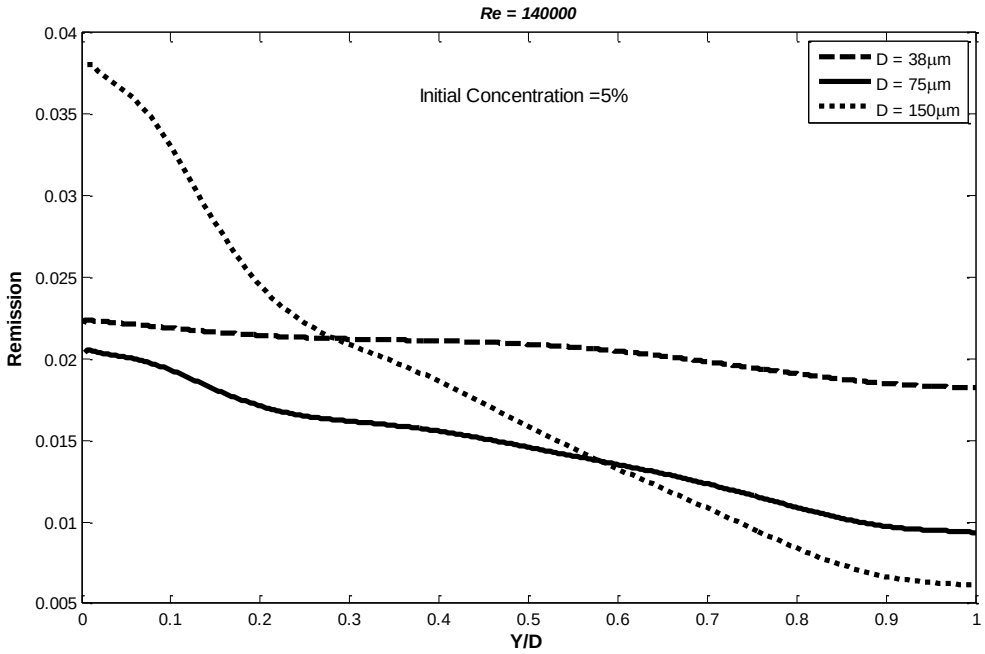

Figure 4.39 Local remission fraction for particles with initial concentration of 5% in three different sizes of 38μm, 75 μm, and 150 μm

Figure 4.40 presents local transmission for the same initial concentration and particle sizes. It shows different trends than local remission and absorption and it increases for any isolated representative layer inside the sample.

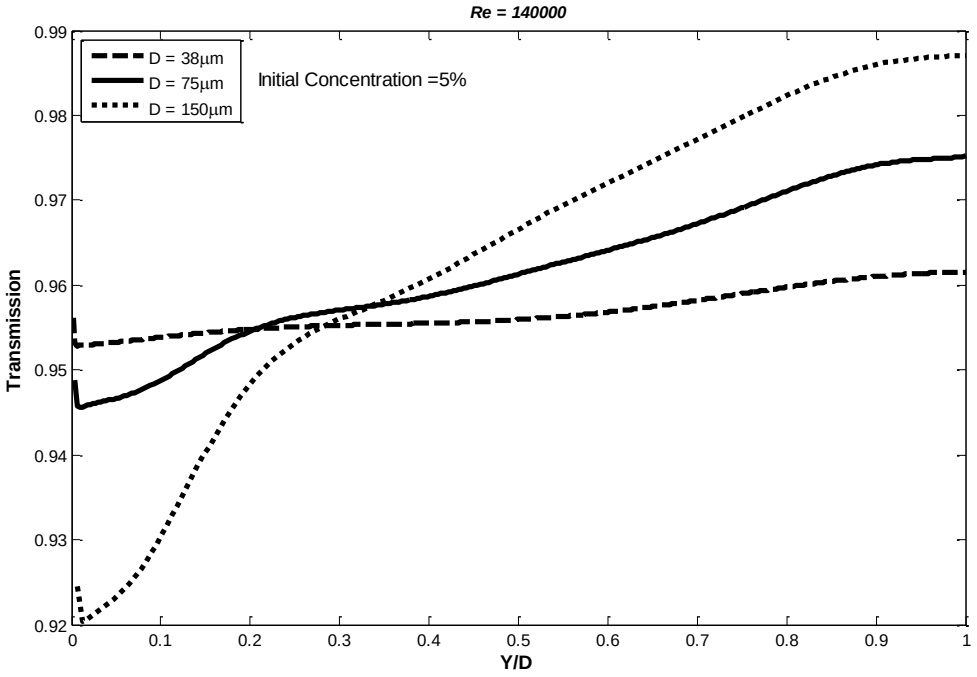

Figure 4.40 Local transmission fraction for particles with initial concentration of 5% in three different sizes of 38 μm, 75 μm, and 150 μm

Figures 4.41 to 4.43 illustrate the integral fraction of light through the sample. According to Figure 4.41, the two-phase mixture of xylene and ADP absorbs light from very near the light until the point that the light leaves the sample. Unlike the local absorption which is a strong function of concentration profiles, the integral absorption illustrates that the absorption is not very big for the Y/D = 0 to Y/D = 0.1, while after this point, the values of integral absorption are considerable. What is very important in this figure is the effect of particle sizes on integral absorption. The largest particle size, 150 microns, has the lowest integral absorption, while the integral absorption of 38 micron particles is the highest. This result skews from the differences in concentrations. From Figure 4.37, although the 150 microns particles are the largest, their concentrations are the lowest compared to two particle sizes.

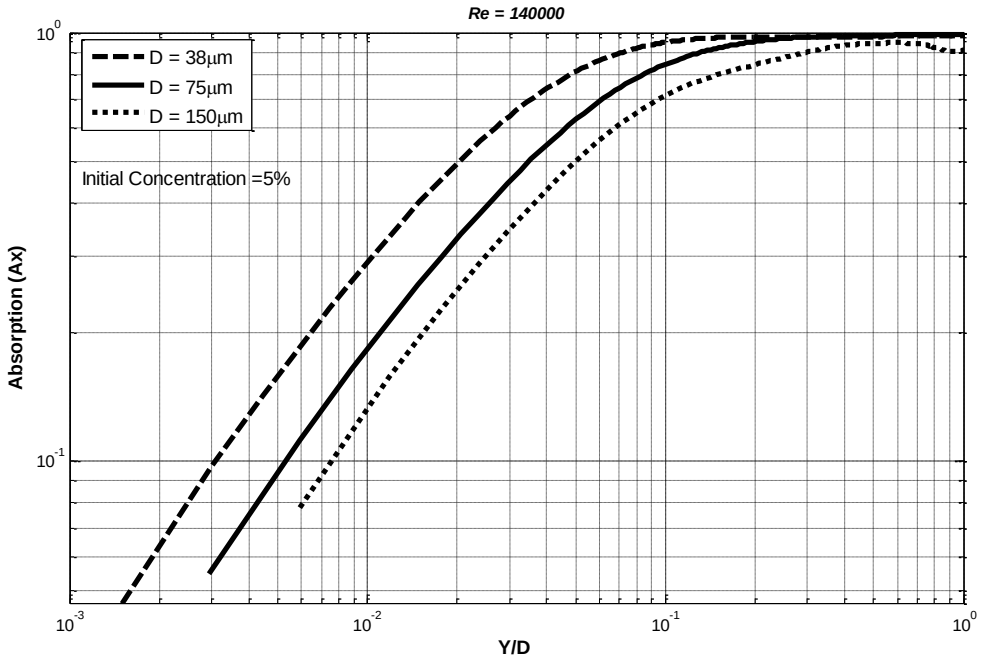

Figure 4.41 Integral absorption fraction for particles with initial concentration of 5% in three different sizes of 38μm, 75 μm, and 150 μm

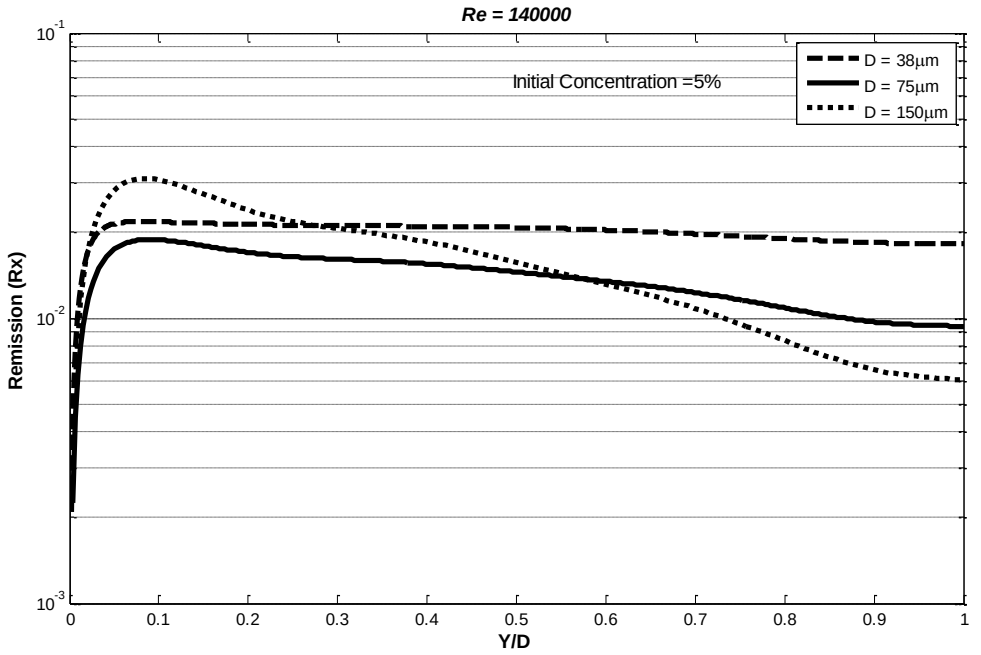

Figure 4.42 Integral remission fraction for particles with initial concentration of 5% in three different sizes of 38μm, 75 μm, and 150 μm

Surface area fraction of particles is an important parameter for remission. Remission is also influenced by concentration. Comparing Figures 4.37 and 4.39, one can see that particles with 38 microns have the lowest remission, however, the effect of concentration is stronger since 150 microns particles have the smallest remission away from the wall.

Like the hypothetical concentration profiles the integral remission is a function of concentration and it decrease through the sample. The results in Figure 4.42 are reasonable since the concentrations of particles decreased throughout the sample, therefore the remission at any distance through the sample decreases. Figure 4.43 shows the transmission through the sample. This Figure reveals logical results since the 38 micron particles which had the highest concentrations, represent the least transmission. The higher the concentrations of particles in the sample, the lower values of transmission obtained. For 38 microns particles, the transmission is zero after Y/D = 0.2 which is almost 0.5 cm into the sample depth. However, for 150 micron particles sizes, which have the lowest concentrations in the depth of the pipe, the transmission never approaches zero.

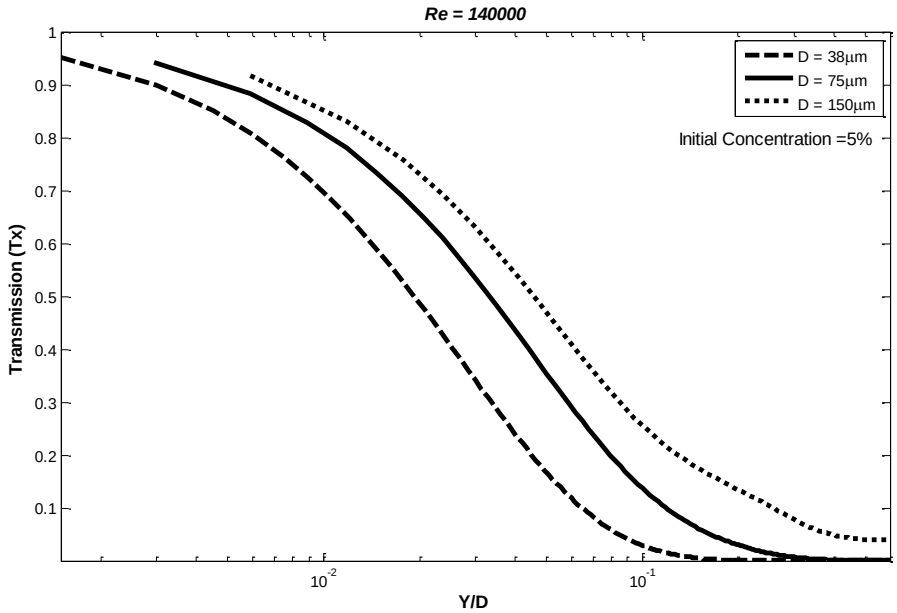

Figure 4.43 Integral transmission fraction for particles with initial concentration of 5% in three different sizes of 38 μm, 75 μm, and 150 μm

Dahm Equation and effect of voids

The Dahm equation is derived in Section 3.3.3 and designated as Equation 3.68. Figure 4.44 presents the reflectance function plotted against the ratio of absorption to remission for five different initial fractions of light. This figure illustrates the reflection of the sample against the absorption to remission function. It illustrates that by increasing the absorption of the sample the reflectance is decreased.

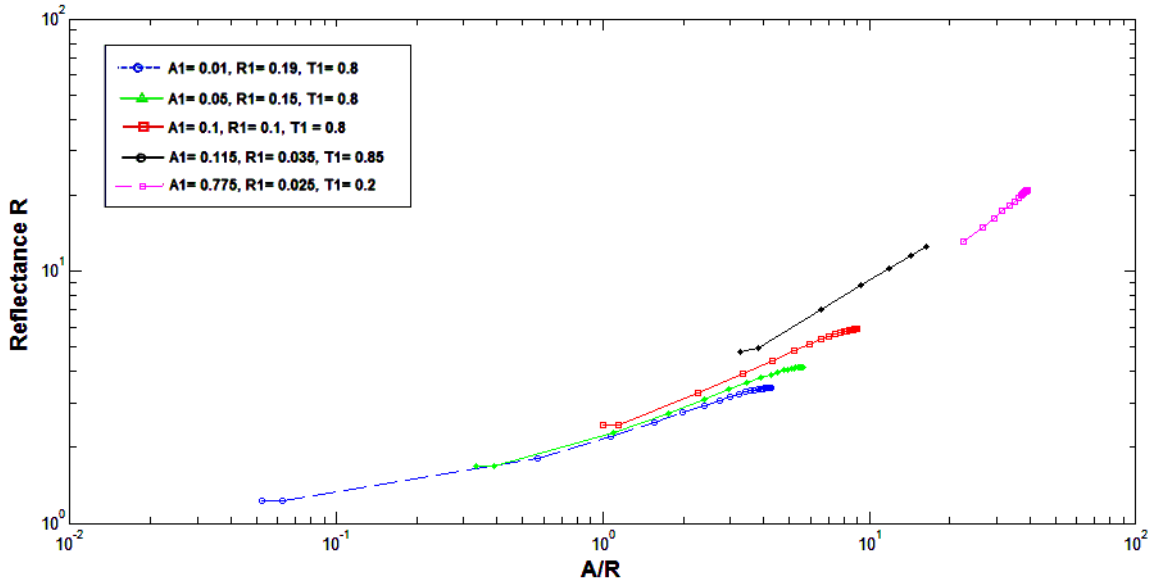

Figure 4.44 Diffuse reflectance obtained based on of Dahm equation for different absorption to remission fractions

Figure 4.45 shows a curve fit to the results in Figure 4.44. The equation is a logarithmic function which is derived by fitting a curve through all the points. This equation applies to the case of isotropic scattering. The Dahm equation is used in terms of absorption to remission function.

Figure 4.46 represents the effect of voids on the absorption/remission function. Figure 4.46 illustrates that for a given void fraction of the sample which is 1-C (concentration), when the absorption of a layer increases; the absorption to remission function also increases. Dahm and Dahm (2007) derived a similar result for the effects of voids. This effect is important since the slurry is moving and the voids change in the cross-section of the pipe.

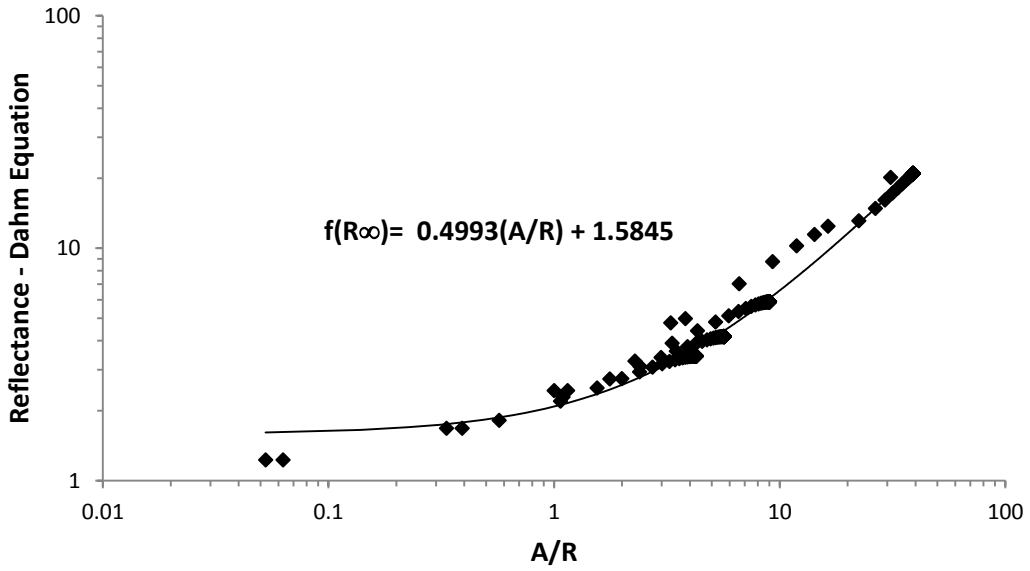

Figure 4. 45 Fitted to the reflectance derived from Dahm equation in all initial fractions showed in Figure 4.44.

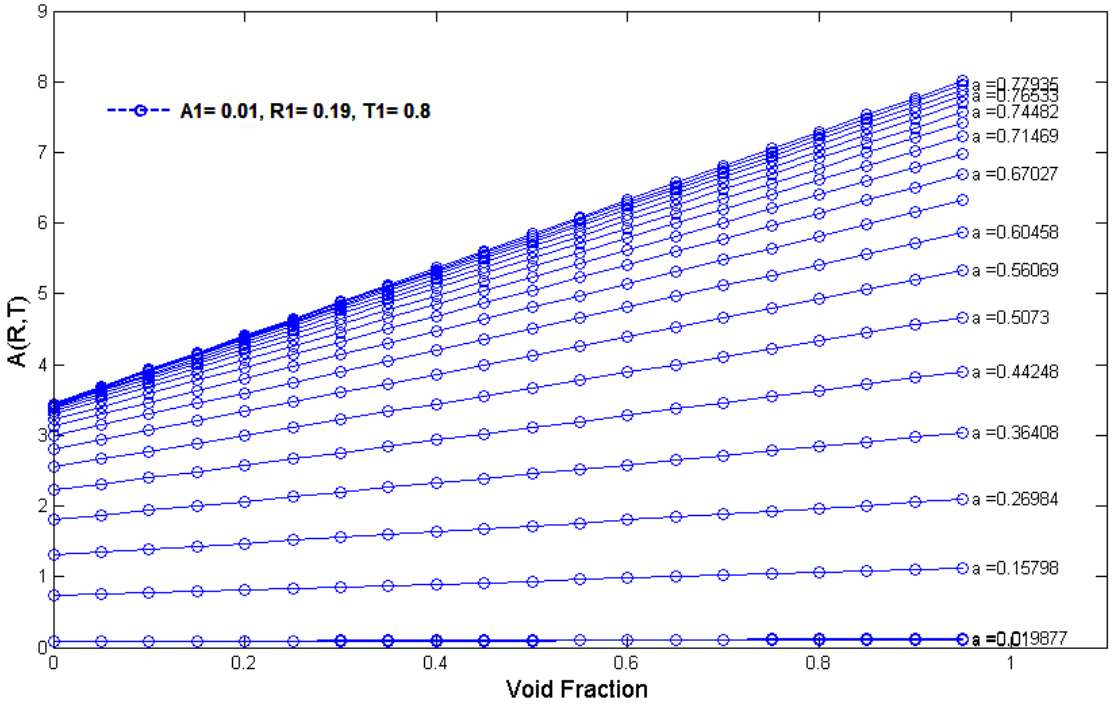

Figure 4.46 Illustration of the void fraction effects on the absorption/remission function.

The absorption/remission function is important since it is proportional to the ration of absorption to remission, therefore, the A/R is equivalent to particle size (Dahm & Dahm, 2007). One can create the voids by removing the particles; however, the concentrations of particles are changed during the time in a slurry pipe. As the void fraction of the layer goes up, the absorption and remission of the layer reduce proportionately. For example, if we remove 25% of particles, both *A* and *R* will have the value of 75% of their previous value (Dahm & Dahm, 2007). Therefore, A/R or absorption/remission function will remain constant for that particular layer. However, according to the absorption/remission function (Equation 4.6) is derived by Dahm and known as Dahm equation, the lower values of A and R will make the term $(2 - A - 2R)$ go up. Therefore, an increase in void fraction will increase the *A(R,T)*.

$$A(R,T) = \frac{(2 - A - 2R)A}{R} \tag{4.6}$$

where A is the absorption, R, remission, and T, transmission fractions. Dahm and Dahm (2007) present an example that its concept which is the effect of voids is investigated in our model. If the absorption of a single layer inside a sample is $a = 0.6$, and $r = 0.2$, then we have the following cases:

- **No voids:** $A(R,T) = \frac{(2-A-2R)A}{R} = \frac{(2-0.6-2\times0.2)0.6}{0.2} = 3$
- **For 25% voids:** $A(R,T) = \frac{(2-0.6[0.75]-2\times0.2\,[0.75])(0.6[0.75])}{0.2[0.75]} = 3.75$

Hence increasing the voids will increase the absorption to remission function. The particle size also has some effects which are discussed in Section 4.2.5 and also were investigated in Chapter Three. In Section 3.3.3, the effects of particle size on absorption/remission function are derived.

4.4 Comparison of Continuum and Discontinuum Models

As discussed by Griffiths and Dahm (2008), continuum theories make some common implicit assumptions including: **(i)** the size of particles must be infinitesimal, **(ii)** the absorption fraction of the particles inside the sample must be very small. In continuum theories the size of the finite element inside the sample is not determined by the properties of the sample, and it is required to be infinitesimal. The integration over the sample is applied by sweeping this infinitesimal thickness over the whole sample. Therefore, if there was a discontinuity in the sample composition, they will fail to predict the light interactions with the sample.

Continuum theories have some advantages and disadvantages, The advantage of using them is that their function is analytical, so integration may be used to evaluate the sample. However, one important problem is to find the boundary conditions. Since the real samples such as slurries have discontinuities, the continuum theories are not capable of predicting the light interactions in surfaces with distinct boundaries (Chalmers & Griffiths (2002). As noted in Section 4.2, continuum models are capable of predicting the samples with very small particles. This point can be observed from Figure 4.20 and 4.21 where the methods of Kubelka-Munk, Diffusion and the more accurate three flux approximation diverge in the regions with larger values of absorption to remission, corresponding to larger particles. Therefore, discontinuous mathematics has the advantage of being capable of describing real systems. The advantage of using continuum theories is related to their simpler models. They may be used for preliminary estimates before implementing the discontinuum mathematics. To clarify this, one can discuss determining the range of absorption and remission coefficients by continuum theories before applying discontinuum theories. These two coefficients must be obtained from experiments. However, when the experimental results are not available, the continuum theories can be used to estimate them before implementing in discontinuum models. These coefficients are applied to check the convergence of models such as plane parallel or representative layer theory. This

was on important advantage of using continuum theories beside discontinuum ones. The scattering of light is a discontinuous phenomena. Also, these discontinuities influence the absorption and remission fractions. Hence, these theories are not reliable in predicting the light interactions with particles.

In this thesis, after investigating the results from continuum and discontinuum theories, one can conclude that the discontinuum theories are more suitable to apply to slurries since they do not have a limiting assumption about not having discontinuity. Moreover, they can provide a relationship between the fundamental physical properties of the particles such as refractive index, volume, density, area, and shape. A few weaknesses of continuum mathematics are:

1. The Kubelka-Munk theory is not proportional to the concentration of an absorber (Dahm & Dahm, 2007). Kubleka-Munk's and also Schuster's theories assume the particles to be homogeneous and nothing is defined for non-homogeneous concentrations in this theory.
2. Kubelka-Munk's and Schuster's theorems are two flux models, and are not suitable for even the isotropic scattering assumptions (Dahm & Dahm, 2007). The small particle assumption is a limiting case applied to the continuum theories to make them applicable for dilute samples. This assumption does not match with slurries since the particle sizes and concentrations are much greater than dilute suspensions of particles.
3. In two flux models, the scattering and absorptions are not independent since the equations are solved simultaneously.

Finally, comparing the results of continuum theories to the discontinuum theories, one may be confident about using models that can predict high discontinuities that are available in a slurry sample. Discontinuum theories showed reasonable results. Using representative layer theory enables predicting the fractions of light in the layers of materials as isolated sheets. Using Stokes formulas with representative layer results, enables predicting the total fractions of light in the sample. The penetration depth of the sample was another important factor which can be predicted.

4.5 Depth of Penetration

Prediction of the depth of penetration of light inside the sample of a slurry is the goal presented in this thesis. In this section, a brief discussion about depth of penetration will be reviewed. According to the methodology reviewed by Griffiths and Dahm (2008) for applying diffuse reflection to the purposes like the quality control of a sample, investigating the actual distance that the light penetrates the sample is required. Therefore, the sample volume that is under investigation is equivalent to the radiation penetration depth or the effective sample size m_{eff} and it is essential to be calculated. Berntsson et. al (1999) presented a new method for calculating the effective sample size of pharmaceutical powders using the three flux approximation. Berntsson et. al (1999) has proposed an empirical method known as the variable layer thickness (VLT) approach. In the study, the effective sample size m_{eff} is defined as the mass per area of the sample. The diffuse reflectance of this sample $R_{\infty_{eff}}(\omega_0{}^*, \tau^*)$ is 98% of the diffuse reflectance of a corresponding optically thick sample. The procedure for obtaining this variable is not analytical since some of the parameters must be determined from experiments. The scattering and absorption coefficients are required from experiment. Then by substituting into the following equation, one can determine the albedo.

$$\omega_0 = \frac{E_a}{E_a + E_s} \tag{4.7}$$

where, ω_0 is the albedo, E_a is the radiation transfer absorption coefficient and E_s is the scattering coefficient. The optical depth is calculated from:

$$\tau = (E_a + E_s)x \tag{4.8}$$

where x is the geometrical depth of sample. Then the effective value of albedo $\omega_0{}^*$ and the optical path length are determined from the following:

$$\tau^* = \tau(1 - \omega_0 g) \tag{4.9}$$

where g is the cosine of scattering angles which was introduced in Chapter Three. Then the effectve albedo is evaluated from:

$$\omega_0{}^* = \frac{\omega_0(1-g)}{(1-\omega_0 g)} \tag{4.10}$$

The effective albedo also may be calculated from the three flux approximation using the following formula:

$$\frac{1}{\omega_0} - 1 = \frac{E_a}{E_s} = \frac{(1-R_\infty)^2}{2R_\infty}\frac{6}{5(R_\infty+4)} \tag{4.11}$$

Then, the diffuse reflectance is computed as a function of the scattering and absorption coefficients for each wavelength, for an increasing sample thickness. Then the results are compared to the diffuse reflectance of an infinitely thick sample. The sample thickness for which the above 98% limit is reached corresponds to the effective sample size m_{eff}. This method is applicable when an experimental setup is available to predict the optical properties of the sample.

4.6 Summary

In summary, for the results of the representative layer model, one can conclude that the depth of penetration of light inside the sample may be estimated from the fractions of light. The fractions of light represent the behavior of light interactions in a particulate medium like the slurry of xylene and ADP. The integral absorption, remission, and transmission fractions are analyzed with an accurate model by combining the representative layer theory with Stokes formulas. When there is no transmission in the sample, the sensor which is located in one side of the sample is not able to see the light transmitting to the other side of the sample. Also, if the reflection goes down in the sample because of the decrease in concentrations of particles, the possibilities of sensing the reflected beam will decrease. For the absorption the same procedure happens. The absorption fraction is a function of

reflectance and transmittance. Therefore, if the reflection and transmission both go down the absorption will go up. The threshold for this model is the sensitivity of the sensor. If the tolerance of the sensor is high to predict very small intensities, then the absolute zero value of the reflection and transmission generates the threshold. As discussed in Section 2.3.10, the reflection is a transmission but in the opposite direction. Therefore, the zero value for the threshold is obtainable from either remission or transmission. This zero value is obtained by transmission fraction in this Chapter. The transmission and reflections are high in the beginning of the process at which the light encounters the sample. However, after a little depth into the sample, they decrease. The reduction in the fraction may be sensible to the sensors, however, when they approach zero values, they may not able to sense the light fraction. Therefore, finding a value as a threshold that matches with the capabilities of sensor in sensing the light when it has a small intensity is a work which can be performed in the future.

CHAPTER V

CONCLUSIONS AND RECOMMENDATIONS

The present work is dedicated to the study of diffuse reflectance theories to model near-infrared phenomena in slurries to predict the depth of penetration of NIR light in the sample consisting of two-phase solid-liquid flows. The approaches are successfully developed based on optical theories that are capable of determining the light interactions with particles in a particle-laden slurry sample. The modeling was performed in MATLAB and FORTAN. The models were developed based on two major approaches in the field of optical methods; continuum and discontinuumm theories. Five theories in the field of continuum theories and three in the field of discontinuum are modeled. In this thesis, two areas of continuum and discontinuum theories were observed to have different results in modeling the light interactions with the sample. The results of the theorems focused on the fractions of light; absorption, remission, and transmission. These fractions have been found from implementing the models to the case of a slurry and then solving the model. Some of the input parameters used in these models are inherently experimental. They are different for each material. In the present work, the refractive indices, the cosine of scattering angles, and the albedo were three parameters which were chosen based on similar cases in the literature. However, for modeling of the three flux approximation, choosing the albedo from similar cases in the literature was impossible. Therefore, a range of values was defined to build the model and run the code. Hence, the results are a function of

different input parameters. There are two parameters, which are basic parameters in optical modeling; absorption coefficient and reflection or scattering coefficient. A considerable part of the models was dedicated to determining the absorption and reflection coefficient. In some of the continuum theories, such as radiative transfer approximation, three flux, Kubelka-Munk, diffusion, and Schuster's theory, they were evaluated from other inherent parameters such as absorption and reflection power of materials. However, for the theories of plane parallel mathematics, assembly of sheets and representative layer theory, a mathematical approach is built based on plane parallel layers to find the absorption and remission coefficients. Choosing the models was based on their applications in modeling NIR radiation in particulate materials and then their assumptions. In the following sections, the conclusions for the modeling approaches, as well as the recommendations to improve the models are summarized.

5.1 Conclusion of continuum theories

Continuum theories are applied to the case of slurry flow in a sample under direct illumination. Theories of Schuster, Kubleka-Munk, three flux, radiative transfer, and diffusion were chosen based upon similar applications to powdered samples.

Schuster's theory is a two-flux approach only applied to the case of homogeneous slurry fluid flow. The total reflectance from the sample depends on the boundary conditions of the differential equations, which are solved by integrating over an optically thick sample. The boundary conditions applied to the boundary of integration. The equations were solved for different boundary conditions to give information about different absorption and remission coefficients. The converged values of total reflections and the distance at which they converged differed with the boundary conditions. However, they are not very different and almost occur in the edge of the sample. Schuster's theory is powerful

for homogeneous samples. The weaknesses of this theory are that it cannot be used in a general case of a slurry sample. It can be used only for dilute suspensions of particles.

Kubelka-Munk (K-M) theory is another two-flux model, which is applied to several initial conditions to find a reciprocal reflectance, which is known as $\log\left(\frac{1}{R_\infty}\right)$. The compared diffuse reflectance matches exactly the model derived by Bull (1990). The diffuse reflection versus the absorption/remission fraction demonstrates the overall reflectance as a function of equivalent particle sizes. Hence, by knowing the particle size in our model in units of $2\tau r$, the diffuse reflectance of a uniform sample of xylene and ADP can be obtained. The information required from an experiment is only the 1/e penetration depth. This model is very powerful only in the samples without discontinuities. K-M theory has many assumptions that limit the modeling. The uniformity of the sample under consideration of K-M theory is a problem for non-uniform samples of slurries. Also, K-M theory assumes that the level of absorption in particles should be small. However, this may contradict absorption in the mixture of xylene and ADP since xylene is a good absorber and ADP particles absorb light. Therefore, Kubelka assumed that the particle sizes should be infinitesimal. However, this is a qualitative assumption, and no suggested values were found in the literature for this assumption. This is one of the weaknesses of K-M theory. Recently, many revisions to K-M theory have been proposed. The absorption and scattering coefficients should be found from experiments for use with this theory.

Radiation transfer is a fundamental theory in the field of diffuse reflectance. The approximation that is offered here has been applied to the optical modeling of human blood using near-infrared radiation. The model of Patterson (1989) suggested a procedure to find the diffuse reflection similar to Schuster's model. This procedure finds diffuse reflection for different initial conditions. This model is capable of estimating the diffuse reflection of light if the initial fractions of light and the cosines of scattering angles are given.

The three-flux approximation technique is newer than the other continuum techniques. This model successfully predicted the values of reflection as a function of absorption to reflection coefficient. The three flux model presented in this work provide results in good agreement to those of Burger et al. (1997).

The diffusion approximation is the last continuum theory. In this method the model was built based on the work presented by Kienle et al. (1998). The model results showed that the diffuse reflection decreases as the absorption increases because the reflectance decreases as the particle size increases. Moreover, this model has reasonable results.

5.2 Conclusions of discontinuum theories

Plane parallel mathematics is a fundamental model in the field of discontinuum optical theories. This model is very simple in its mathematics. However, the results show that it can be applied to the case of slurries since these materials have discontinuities. The fractions of light for absorption, remission and transmission are found by using several inputs of initial fraction of light. The absorption and remission coefficients are estimated based on the fractions of light in each layer of the sample. The results of the plane parallel model were compared to Chalmers and Griffiths (2002) and show that the this model has a good match with real samples.

The assembly of sheets model applies three equations that are developed based on plane parallel mathematics, but are more sophisticated than the equations of plane parallel theory. Moreover, the Stokes formula is used in this model to find integral fractions of light. The refractive index is an important input for this model. The absorption of this model is not sensitive to the initial fraction of light; however, remission is very small, and almost negligible. The local fraction of light is evaluated based on a technique similar to plane parallel layers. This theory is as powerful as the representative layer theory in predicting the integral fraction of light.

The last and the most important model is representative layer theory. This model has been used to predict the reflectance, transmittance, and absorbance of a series of plane parallel layers for a slurry of xylene and ADP. The representative layer model is applied to two different cases. Concentration profiles from CFD results are used to find the volume fraction that is presented by the Dahm equations. The integral fractions of light were modeled based on Stokes formulas. Arbitrary solids concentration profiles were used to test the model. The results were reasonable. The depth at which the light can penetrate into the sample may be found from the integral fractions of light.

5.3 Recommendations

The recommendations for application of the continuum and discontinuum models are discussed. For future study, the following general tasks should be performed.

- The effects of light interaction with individual particles should be studied by applying appropriate particle theories such as Mie scattering theory.
- The effects of particle motion and turbulent fluctuation on light fractions is an important stage in modeling NIR radiation through a multiphase fluid flow and should be studied.
- The effects of different particles with various shapes and polydisperse sizes on the radiation of light into the slurry fluid flow should be examined.
- The refractive index, absorbing power, remitting power, absorption coefficient, and remission coefficient of the slurry of xylene and ADP should be determined through experiments.
- A more sophisticated and numerically intensive method combining Mie scattering with Monte – Carlo simulation should be used to predict the absorption and scattering coefficients and the transport of light in the slurry.

REFERENCES

Benford, F. (1946). Radiation in a Diffusing Medium. *Journal of the Optical Society of America, 36*(9), 524-554. doi: Doi 10.1364/Josa.36.000524

Bohren, C. F., & Huffman, D. R. (1998). *Absorption and Scattering of Light by Small Particles*. New York: Wiley.

Bull, C. R. (1990). A Model of the Reflectance of Near-Infrared Radiation. *Journal of Modern Optics, 37*(12), 1955-1964. doi: Doi 10.1080/09500349014552161

Burger, T., Kuhn, J., Caps, R., & Fricke, J. (1997). Quantitative Determination Of The Scattering and Absorption Coefficients from Diffuse Reflectance and Transmittance Measurements: Application to Pharmaceutical Powders. *Applied Spectroscopy, 51*(3), 309-317. doi: Doi 10.1366/0003702971940404

Burger, T., Ploss, H. J., Kuhn, J., Ebel, S., & Fricke, J. (1997). Diffuse Reflectance and Transmittance Spectroscopy for the Quantitative Determination of Scattering and Absorption Coefficients in Quantitative Powder Analysis. *Applied Spectroscopy, 51*(9), 1323-1329.

Central Bureau of the *Comission Internationale de l'Eclairage (CIE).* (1987). *CIE International Lighting Vocabulary*, Vienna, Austria.: CIE Pub. No. 17.4

Chalmers, J. M., & Griffiths, P. R. (2002). *Handbook of Vibrational Spectroscopy (Vol. 1)*. New York: J. Wiley.

Chartier, G. (2005). *Introduction to Optics*. New York: Springer.

Chen, R.C. (1994). Analysis of Homogeneous Slurry Pipe Flow, *Journal of Marine Science and Technology*, Vol. 2, No. 1, pp. 37-45.

Crowe, C. T. (2012). *Multiphase Flows with Droplets and Particles* (2nd ed.). Boca Raton: CRC Press.

Dahm, D. J., & Dahm, K. D. (1999). Representative Layer Theory for Diffuse Reflectance. *Applied Spectroscopy, 53*(6), 647-654.

Dahm, D. J., Dahm, K. D., & Norris, K. H. (2000). Test of the Representative Layer Theory of Diffuse Reflectance Using Plane Parallel Samples. *Journal of near Infrared Spectroscopy, 8*(3), 171-181.

Dahm, D. J., & Dahm, K. D. (2007). *Interpreting Diffuse Reflectance and Ttransmittance : A Theoretical Introduction to Absorption Spectroscopy of Scattering Materials*. Chichester, U.K.: NIR Publications.

Dahm, D. J., & Dahm, K. D. (2008). Representative Layer Theory: Describing Absorption by Particulate Samples. In Z. H. Gu, L. M. Hanssen (Ed.) *Proceeding of SPIE*. Vol. 7065.

Darrigol, O. (2012). *A History of Optics from Greek Antiquity to the Nineteenth Century*. Oxford ; New York: Oxford University Press.

DiLaura, D. L. (2011). *The Lighting Handbook : Reference and Application* (10th ed.). New York, NY: Illuminating Engineering Society of North America.

Doron, P., Barnea, D. (1996). Flow Pattern Maps for Solid-Liquid Flow in Pipes, *International Journal of Multiphase Flow*, Vol 22, pp. 273-283.

Fairbairn, M. (2004). Principles of Planetary Photometry. Retrieved October 6, 2012, from http://www.astro.uvic.ca/~tatum/plphot.html

Giovanelli, R. G. (1955). Reflection by Semi-Infinite Diffusers. *Opt. Acta, 2*, 153-162.

Greivenkamp, J. E. (2004). *Field Guide to Geometrical Optics*. Bellingham, Wash.: SPIE Press.

Griffiths, P. R., & Dahm, J. D. (2008). Continuum and Discontinuum Theories of Diffuse Reflection. In D. A. Burns, & E. W. Ciurczak, (Eds.), *Handbook of near-infrared analysis* (pp. 21-64). Boca Raton: CRC Press.

Guenther, R. D. (1990). *Modern Optics*. New York: Wiley.

Hecht, E. (2002). *Optics* (4th ed.). Reading, Mass.: Addison-Wesley.

Hossain, A., Naser, J., & Imteaz, M. A. (2011). CFD Investigation of Particle Deposition in a Horizontal Looped Turbulent Pipe Flow. *Environmental Modeling & Assessment, 16*(4), 359-367.

Kienle, A., Patterson, M. S., Dognitz, N., Bays, R., Wagnieres, G., & van den Bergh, H. (1998). Noninvasive Determination of the Optical Properties of Two-Layered Turbid Media. *Applied Optics, 37*(4), 779-791. doi: Doi 10.1364/Ao.37.000779

Kortüm, G. (1969). *Reflectance Spectroscopy. Principles, Methods, Applications*. Berlin, Heidelberg, New York,: Springer.

Kubelka P., and Munk F., Ein Beitrag Zur Optik der Farbanstriche, *Zeitschrift fur technische Physik* 12 (1931) 593-601.

Kuhn, J., Korder, S., Arduini-Schuster, M. C., Caps, R., & Fricke, J. (1993). Infrared Optical Transmission and Reflection Measurements on Loose Powders. *American Institute of Physics*, *64*(9), 2523. doi: doi: 10.1063/1.1143914

Juds, S. M. (1988). *Photoelectric Sensors and Controls : Selection and Application*. New York: M. Dekker.

Lahiry, S., Ghanta, K.C. (2010). Slurry Flow Modeling by CFD, *Chemical Industry and Chemical Engineering Quarterly*, Vol. 16, pp. 295-308.

Ling, J., Skudarnov, P.V., Lin, C.X., Ebadian, M.A. (2003). Numerical Investigation of Liquid-Solid Slurry Flows in a Fully Developed Turbulent Flow Region, *International Journal of Heat and Fluid Flow*, Vol. 24, pp. 389-398.

Mandelis, A., Boroumand, F., & Bergh, H. V. (1990). Diffuse Reflectance Spectroscopy of Large Powders: The Melamed Model Revisited. *Applied Optics*,*29*(19), 2853-2860.

Martin C. Johnson. (1924). Scattering and Absorption in the Atmospheres of Emission-Line Stars. *Monthly Notices of the Royal Astronomical Society*, *85*, 56.

McCluney, R. (1994). *Introduction to Radiometry and Photometry*. Boston: Artech House.

Measurement, Vegetation, and Health. (2006). *Near Infrared and the Electromagnetic Spectrum.* Retrieved October 15, 2012, from http://mvh.sr.unh.edu/mvhtools/near_ir.htm

Meeten, G. H., & Wood, P. (1993). Optical-Fiber Methods for Measuring the Diffuse Reflectance of Fluids. *Measurement Science & Technology*, *4*(6), 643-648.

Mielenz, K. D., Velapoldi, R. A., Mavrodineanu, R., & Institute for Materials Research (U.S.). Analytical Chemistry Division. (1977). *Standardization in Spectrophotometry and Luminescence Measurements : Proceedings of a Workship Seminar Held at the National Bureau of Standards, Gaithersburg, Maryland, November, November 19-20, 1975*. Washington: U.S. Dept. of Commerce, National Bureau of Standards : for sale by the Supt. of Docs., U.S. Govt. Print. Off.

Mudgett, P. S., & Richards, L. W. (1971). Multiple Scattering Calculations for Technology. *Applied Optics*, *10*(7), 1485-&. doi: Doi 10.1364/Ao.10.001485

Mouroulis, P., & Macdonald, J. (1997). *Geometrical Optics and Optical Design*. New York ; Oxford: Oxford University Press.

Nobbs, J. H. (1985). Kubelka—Munk Theory and the Prediction of Reflectance. *Review of Progress in Coloration*, *15*(1), 66-75.

Palmer, J. M., & Grant, B. G. (2010). *The Art of Radiometry*. Bellingham, Wash.: SPIE Press.

Patterson, M. S., Schwartz, E., & Wilson, B. C. (1989). Quantitative Reflectance Spectrophotometry for the Noninvasive Measurement of Photosensitizer Concentration in Tissue During Photodynamic Therapy. *SPIE Photodynamic Therapy: Mechanism, 1065*, 115-122.

Pedrotti, F. L., Pedrotti, L. M., & Pedrotti, L. S. (2007). *Introduction to Optics* (3rd ed.). Upper Saddle River, N.J.: Pearson/Prentice Hall.

Rabhi, M., Masion, A., Roze, C., Dussouillez, P., & Bottero, J. Y. (2010). Optical Size and Concentration Monitoring of Slurries: Comparison Between Measurements and Monte Carlo Simulation. *Journal of Instrumentation, 5*. doi: Artn P04002

Rea, M. S. (2000). *The IESNA Lighting Handbook : Reference and Application* (9th ed.). New York, NY: Illuminating Engineering Society of North America.

Refractive Index Database. (n.d.). *Refractive Index Info*. Retrieved May 24, 2012, from http://refractiveindex.info/

Schuster, A. (1904). *An Introduction to theTheory of Optics*. London,: E. Arnold.

Siegel, R., & Howell, J. R. (1981). *Thermal Radiation Heat Transfer* (2d ed.). Washington: Hemisphere Pub. Corp.

SPECAC Limited. (n.d.). *Reflectance Spectroscopy*. Retrieved September 11, 2012, from http://www.specac.com

Theissing, H. H. (1950). Macrodistribution of Light Scattered by Dispersions of Spherical Dielectric Particles. *Journal of Optical Society of America,40*(4), 232-242.

Venkatram, N., Rao, D. N., & Akundi, M. A. (2005). Nonlinear Absorption, Scattering and Optical Limiting Studies of Cds Nanoparticles. *Optics Express, 13*(3), 867-872. doi: Doi 10.1364/Opex.13.000867

Wendlandt, W. W., & Hecht, H. G. (1966). *Reflectance Spectroscopy*. New York,: Interscience Publishers.

Wetzel, D. L. (1983). Near-Infrared Reflectance Analysis - Sleeper among Spectroscopic Techniques. *Analytical Chemistry, 55*(12), 1165A-1176A.

Workman, J., & Weyer, L. (2008). *Practical Guide to Interpretive Near-Infrared Spectroscopy*. Boca Raton: CRC Press.

APPENDICES

There are two different codes in this Appendix. In Section A.1 the code for Continuum theories are modeled based on Matlab 2010. In Appendix A.2 the scripts of representative layer model is illustrated.

A.1 MATLAB Script for continuum models and theory for assembly of sheets


```
% ########################################################################
%       Continuum Theories of Diffuse Reflection + Assembly of Sheets
% ########################################################################

clear
clc
close all
state = 7
iter = 100;

%###################### Plane Parallel Mathematics ##########################

% Initial Conditions ****************************************************

T(1,1) = 0.9; R(1,1) = 0.06; A(1,1) = 0.04;
T(1,2) = 0.85; R(1,2) = 0.1; A(1,2) = 0.05;
T(1,3) = 0.7; R(1,3) = 0.2; A(1,3) = 0.1;
T(1,4) = 0.55; R(1,4) = 0.25; A(1,4) = 0.2;
```

```
T(1,5) = 0.35; R(1,5) = 0.35; A(1,5) = 0.3;
T(1,6) = 0.2; R(1,6) = 0.4; A(1,6) = 0.4;
T(1,7) = 0.1; R(1,7) = 0.45; A(1,7) = 0.45;

% ****************** Three Flux approximation (with albedo) ***************
% My Model
Albedo = 0.01:0.01:1;
EaOEs = 1./Albedo -1;
KOS_3flux = (8/3)*EaOEs;
KOS_3flux = 5.54*EaOEs;
R_3flux_dir = (-(4*EaOEs + 6/5)+ 2*(4*EaOEs.^2 + 3*EaOEs).^0.5)./(2*EaOEs-6/5);
RHS = (1-R_3flux_dir)^2/(2*R_3flux_dir)*(6/5)/(R_3flux_dir+4);
w0_s = 1/(RHS+1);

R_3flux_dif = 1 + KOS_3flux - (KOS_3flux.^2 + 2*KOS_3flux).^0.5;

% Kuhn Model
data1 = load('3FluxKuhn.mat','albedo_kuhn');albedo_kuhn(:,1) = data1.albedo_kuhn;
data2 = load('3FluxKuhn.mat','R_inf_dir');R_inf_dir(:,1) = data2.R_inf_dir;
data3 = load('3FluxKuhn.mat','R_inf_dif');R_inf_dif(:,1) = data3.R_inf_dif;
data4 = load('3FluxKuhn.mat','EaOEs_Gio_dir');EaOEs_Gio_dir(:,1) = data4.EaOEs_Gio_dir;
data5 = load('3FluxKuhn.mat','EaOEs_Gio_dif');EaOEs_Gio_dif(:,1) = data5.EaOEs_Gio_dif;
data6 = load('3FluxKuhn.mat','EaOEs_3flux_dir');EaOEs_3flux_dir(:,1) = data6.EaOEs_3flux_dir;
data7 = load('3FluxKuhn.mat','EaOEs_3flux_dif');EaOEs_3flux_dif(:,1) = data7.EaOEs_3flux_dif;
EaOEs_Kuhn = 1./albedo_kuhn -1;


%########################## Beer-Lambert Approach ####################

for j = 1:state

    % ######################################################################
    %                       Initialization of Models
    % ######################################################################
    %########################## Bull (1990) ##############################

    F(1,j) = (-A(1,j)/R(1,j)) + ((A(1,j)/R(1,j))^2 + 1)^0.5;      % Initial Remission function
    U(1,j) = log10(1/F(1,j));                                     % Initial reciprocal reflectance
    Z(1,j) = A(1,j)/R(1,j);                                       % Absorption to Remission ratio
```

```
    %########################## Beer-Lambert Approach ####################

    Layer(1,j) = 0.001;                                          % Thickness of first layer
    K(1,j)= A(1,j)/Layer(1,j);                                   % Initial Absorption Coefficient
    S (1,j) = R(1,j)/Layer(1,j);
    Absorb(1,j) = 1-exp(-(K(1,j)).* Layer(1,j));                 % Absorption fraction (Beer-Lambert law)
    Kd(1,j) = (K(1,j)).* Layer(1,j);                             % Absorption fraction of Beer_Lambert law
times the thickness of that specific layer
    Trans(1,j)= exp(-Kd(1,j));                                   % Transmission of the Beer_Lambert law
    thick_sum(1,j) = Layer(1,j);                                 % this is a variable that sum up all the
layers to give us sample overall thickness

    %########################## Three Flux Approximation ####################

    alpha_O_sigma(1,j) = (3/5)*((1-R(1,j))^2)/(R(1,j)*(R(1,j)+4));
    Alpha_O_sigma(1,j) = 0.5*(A(1,j)/R(1,j));
    R_3flux(1,j) = (-(4*Alpha_O_sigma(1,j)+(6/5))+ 2*
(4*(Alpha_O_sigma(1,j)^2)+3*Alpha_O_sigma(1,j))^0.5)/((2*Alpha_O_sigma(1,j))-(6/5));

    %########################## Diffusion Theory ############################

    R_diffusion(1,j) = 1/(1+ 3*Alpha_O_sigma(1,j)+(5/3)*(3*(Alpha_O_sigma(1,j))^2 +
3*Alpha_O_sigma(1,j))^0.5);

    %########################## Schuster's Theory ###########################

    R_Schu(1,j) = (1-(K(1,j)/(K(1,j)+2*S(1,j)))^0.5)/((1+(K(1,j)/(K(1,j)+2*S(1,j)))^0.5));
    KoS(1,j) = K(1,j)/S(1,j);
    alphosig (1,j) = 0.5 * KoS(1,j);

%     %########################## Radiative Transfer ##########################

    refract = 1.5054;
    g = 0;
    rd = -1.44*refract^(-2)+0.71*refract^(-1)+0.668+0.0636*refract;
    ap(1,j) = (1 - g)*S(1,j)/(K(1,j) + (1-g)*S(1,j));
    kk = (1 + rd)/(1 - rd);
    R_rte(1,j) = ap(1,j)/(1+2*kk(1,j)*(1-refract) + (1+2*kk/3)*(3*(1-ap(1,j)))^0.5);
```

```
    R_rte_2(1,j) = 1/(1 + 1.5 * KoS(1,j) + (5/3)*(0.75*(KoS(1,j))^2 + 1.5 * KoS(1,j))^0.5);

    %######################### Theory for Sheets and an assembly of sphere

    n0 = 1.00027417;                    % The refractive index of air
    n1 = 1.52424;                       % The refractive index of ADP
    n2 = 1.49582;                       % The refractive index of Xylene
    r0 = ((n1-n2)^2)/(n1+n2)^2;
    B0 = 2*r0/(1-r0);
    B(1,j) = R(1,j)/Layer(1,j);
    k(1,j) = (K(1,j)+(B(1,j)-B0)*(1-r0^2))*(1-r0^2);
    X(1,j) = Layer(1,j);
    R1(1,j) = r0 + (1-r0)^2 * r0 * exp(-2*k(1,j)*Layer(1,j))/(1-exp(-2*k(1,j)*Layer(1,j))*(r0)^2);
    T1(1,j) = (1-r0)^2 * r0 * exp(-k(1,j)*Layer(1,j))/(1-exp(-2*k(1,j)*Layer(1,j))*(r0)^2);
    A1(1,j) = 1 - R1(1,j) - T1(1,j);
    Delta(1,j) = ((1+R1(1,j)+T1(1,j))*(1+R1(1,j)-T1(1,j))*(1 - R1(1,j)+ T1(1,j))*(1 - R1(1,j) -
T1(1,j)))^0.5;
    Omega(1,j) = (1+R1(1,j)+(T1(1,j))^2+Delta(1,j))/(2*R1(1,j));
    Psi(1,j) = (1+R1(1,j)+(T1(1,j))^2+Delta(1,j))/(2*T1(1,j));
    Tx(1,j) = (Omega(1,j)-(1/Omega(1,j)))/(Omega(1,j)*Psi(1,j)^X(1,j) - (1/(Omega(1,j)*Psi(1,j)^X(1,j))));
    Rx(1,j) = (Psi(1,j).^X(1,j) - (1/Psi(1,j).^X(1,j)))/(Omega(1,j)*Psi(1,j).^X(1,j) -
(1/(Omega(1,j)*Psi(1,j).^X(1,j))));
    Ax(1,j) = 1 - Tx(1,j) - Rx(1,j);

    %######################### Dahm_1 Equation1 ##############################

    Dahm_1(1,j) = (2-A(1,j)-2*R(1,j))*A(1,j)/(2*R(1,j));       % (1-R)^2/R = Dahm_1
    Delt(1,j) = (Dahm_1(1,j)+2)^2 - 4;
    R_Dahm_1(1,j)= ((Dahm_1(1,j)+2) + (Delt(1,j))^0.5)/2;      %  R_Dahm_1 = ((Dahm_1(1,j)+2) -
(Delt(1,j))^0.5)/2;
    aOr(1,j) = (1-F(1,j))^2/(F(1,j)*(2-A(1,j)-R(1,j)));
    K_M(1,j) = (1-F(1,j))^2/F(1,j);

    %######################### Kubelka - Munk ##############################

    % 1:-------------- To find the T and R from differential equation

    S(1,j) = 1-A(1,j);  % scattering
    kappa(1,j) = (K(1,j)*(K(1,j) + 2*S(1,j)))^0.5;
```

```
    Beta(1,j) = kappa(1,j)/(K(1,j) + 2*S(1,j));
    T_diff(1,j) = (4*Beta(1,j))/((1+(Beta(1,j))^2)*exp(kappa(1,j)* Layer(1,j)));
    R_diff(1,j)= (1 - Beta(1,j)^2)*(exp(kappa(1,j)* Layer(1,j))-exp(-kappa(1,j)*
Layer(1,j)))/((1+Beta(1,j))^2*exp(kappa(1,j)* Layer(1,j))-(1-Beta(1,j))^2*exp(-kappa(1,j)* Layer(1,j)));
    d_diff(1,j) = log((2*Beta(1,j) + (Beta(1,j).^4.*T(1,j)^2 - 2*Beta(1,j)^2*T(1,j).^2 + 4*Beta(1,j).^2 +
T(1,j)^2).^(1/2))/(T(1,j).*Beta(1,j).^2 + 2*T(1,j).*Beta(1,j) + T(1,j))./kappa(1,j);


% 2:-------------- To find Thickness where J=0 by trial and error

    samp_thick = 0.0127;
    A_const_O_I0(1,j) = - (1 - Beta(1,j))* exp(-kappa(1,j) * samp_thick) / ((1 + Beta(1,j))^2 *
exp(kappa(1,j) * samp_thick) - (1-Beta(1,j))^2 * exp(-kappa(1,j) * samp_thick));
    B_const_O_I0(1,j) = + (1 + Beta(1,j))* exp(+kappa(1,j) * samp_thick) / ((1 + Beta(1,j))^2 *
exp(kappa(1,j) * samp_thick) - (1-Beta(1,j))^2 * exp(-kappa(1,j) * samp_thick));
    Ix(1,j) = A_const_O_I0(1,j) * (1 - Beta(1,j))* exp(+kappa(1,j)*X(1,j)) + B_const_O_I0(1,j) * (1 +
Beta(1,j))* exp(-kappa(1,j)*X(1,j));
    Jx(1,j) = A_const_O_I0(1,j) * (1 + Beta(1,j))* exp(+kappa(1,j)*X(1,j)) + B_const_O_I0(1,j) * (1 -
Beta(1,j))* exp(-kappa(1,j)*X(1,j));

    % ************************************************************************

    for i = 1:iter
        T(i+1,j) = (T(i,j) * T(1,j))/(1-  R(i,j)*R(1,j));
        R(i+1,j) = R(i,j) + ((T(i,j))^2)*R(1,j)/(1 - R(1,j)*R(1,j));
        A(i+1,j) = 1 - T(i+1,j) - R(i+1,j);
        Layer(i+1,j) = (Layer(i,j)).*1.001;
        K(i+1,j) = A(i+1,j)/(Layer(i+1,j));
        S(i+1,j) = R(i+1,j) / Layer(i+1,j);
        F(i+1,j) = (1+A(i+1,j)/R(i+1,j)) - ((1+A(i+1,j)/R(i+1,j))^2 - 1)^0.5;
        U(i+1,j) = log10(1/F(i+1,j));
        Z(i+1,j) = A(i+1,j)/R(i+1,j);
        Absorb(i+1,j) = 1-exp(-(K(i+1,j))* Layer(i+1,j));
        Kd(i+1,j) = (K(i+1,j))* Layer(i+1,j);
        Trans(i+1,j)= exp(-Kd(i+1,j));
        thick_sum(i+1,j) = Layer(i+1,j)+ thick_sum(i,j);

        %######################## Schuster's Theory ############################
```

```
        R_Schu(i+1,j) = (1-
(K(i+1,j)/(K(i+1,j)+2*S(i+1,j)))^0.5)/((1+(K(i+1,j)/(K(i+1,j)+2*S(i+1,j)))^0.5));
        KoS(i+1,j) = K(i+1,j)/S(i+1,j);
        alphosig (i+1,j) = 0.5 * KoS(i+1,j);

        %######################## Radiative Transfer ##########################

        refract = 1.5054;
        g = 0.8;
        rd = -1.44*refract^(-2)+0.71*refract^(-1)+0.668+0.0636*refract;
        ap (i+1,j) = (1 - g)*S(i+1,j)/(K(i+1,j) + (1-g)*S(i+1,j));
        kk = (1 + rd)/(1-rd);
        R_rte(i+1,j) = ap(i+1,j)/(1+2*kk*(1-refract) + (1+2*kk/3)*(3*(1-ap(i+1,j)))^0.5);

        R_rte_2(i+1,j) = 1/(1 + 1.5 * KoS(i+1,j) + (5/3)*(0.75*(KoS(i+1,j))^2 + 1.5 * KoS(i+1,j))^0.5);

        %*************** Theory for Sheets and an assembly of sphere*******

        n0 = 1.00027417;                    % The refractive index of air
        n1 = 1.52424;                       % The refractive index of ADP
        n2 = 1.49582;                       % The refractive index of Xylene
        r0 = ((n1-n2)^2)/(n1+n2)^2;
        B0 = 2*r0/(1-r0);
        B(i+1,j) = R(i+1,j)/Layer(1,j);
        k(i+1,j) = (K(i+1,j)+(B(i+1,j)-B0)*(1-r0^2))*(1-r0^2);

        X(i+1,j) = X(i,j) + Layer(i+1,j);
        R1(i+1,j) = r0 + (1-r0)^2 * r0 * exp(-2*k(i+1,j)*Layer(i+1,j))/(1-exp(-
2*k(i+1,j)*Layer(i+1,j))*(r0)^2);
        T1(i+1,j) = (1-r0)^2 * r0 * exp(-k(i+1,j)*Layer(i+1,j))/(1-exp(-2*k(i+1,j)*Layer(i+1,j))*(r0)^2);
        A1(i+1,j) = 1 - R1(i+1,j) - T1(i+1,j);
        Delta(i+1,j) = ((1+R1(i+1,j)+T1(i+1,j))*(1+R1(i+1,j)-T1(i+1,j))*(1 - R1(i+1,j)+ T1(i+1,j))*(1 -
R1(i+1,j) - T1(i+1,j)))^0.5;
        Omega(i+1,j) = (1+R1(i+1,j)+(T1(i+1,j))^2+Delta(i+1,j))/(2*R1(i+1,j));
        Psi(i+1,j) = (1+R1(i+1,j)+(T1(i+1,j))^2+Delta(i+1,j))/(2*T1(i+1,j));

        Tx(i+1,j) = (Omega(i+1,j)-(1./Omega(i+1,j)))/(Omega(i+1,j)*Psi(i+1,j).^X(i+1,j) -
(1/(Omega(i+1,j)*Psi(i+1,j).^X(i+1,j))));
```

```
        Rx(i+1,j) = (Psi(i+1,j).^X(i+1,j) - (1/Psi(i+1,j).^X(i+1,j)))/(Omega(i+1,j)*Psi(i+1,j).^X(i+1,j) -
(1/(Omega(i,j)*Psi(i+1,j).^X(i+1,j))));
        Ax(i+1,j) = 1 - Tx(i+1,j) - Rx(i+1,j);

        %******************Dahm_1 Equation ******************************
        Dahm_1(i+1,j) = (2-A(i+1,j)-2*R(i+1,j))*A(i+1,j)/(2*R(i+1,j));       % (1-R)^2/R = Dahm_1
        Delt(i+1,j) = (Dahm_1(i+1,j)+2)^2 - 4;
        R_Dahm_1(i+1,j)= ((Dahm_1(i+1,j)+2) + (Delt(i+1,j))^0.5)/2;
        aOr(i+1,j) = (1-F(i+1,j))^2/(F(i+1,j)*(2-A(i+1,j)-R(i+1,j)));
        K_M(i+1,j) = (1-F(i+1,j))^2/F(i+1,j);
        Alpha_O_sigma(i+1,j) = 0.5*(A(i+1,j)/R(i+1,j));
        R_3flux(i+1,j) = (-(4*Alpha_O_sigma(i+1,j)+(6/5))+ 2*
(4*(Alpha_O_sigma(i+1,j)^2)+3*Alpha_O_sigma(i+1,j))^0.5)/((2*Alpha_O_sigma(i+1,j))-(6/5));
        R_diffusion(i+1,j) = 1/(1+ 3*Alpha_O_sigma(i+1,j)+(5/3)*(3*(Alpha_O_sigma(i+1,j))^2 +
3*Alpha_O_sigma(i+1,j))^0.5);



        %######################### Kubelka-Munk theory ######################
        % 1:-------------- To find the T and R from differential equation
        S(i+1,j) = 1-A(i+1,j);  % scattering
        kappa(i+1,j) = 0.1*(K(i+1,j)*(K(i+1,j) + 2*S(i+1,j)))^0.5;
        Beta(i+1,j) = kappa(i+1,j)/(K(i+1,j) + 2*S(i+1,j));
        T_diff(i+1,j) = (4*Beta(i+1,j))/((1+(Beta(i+1,j))^2)*exp(kappa(i+1,j)* Layer(i+1,j)));
        R_diff(i+1,j)= (1 - Beta(i+1,j)^2)*(exp(kappa(i+1,j)* Layer(i+1,j))-exp(-kappa(i+1,j)*
Layer(i+1,j)))/((1+Beta(i+1,j))^2*exp(kappa(i+1,j)* Layer(i+1,j))-(1-Beta(i+1,j))^2*exp(-kappa(i+1,j)*
Layer(i+1,j)));
        d_diff(i+1,j) = log((2*Beta(i+1,j) + (Beta(i+1,j)^4.*T(i+1,j).^2 - 2*Beta(i+1,j).^2*T(i+1,j).^2 +
4*Beta(i+1,j).^2 + T(i+1,j)^2).^(1/2))/(T(i+1,j)*Beta(i+1,j).^2 + 2*T(i+1,j).*Beta(i+1,j) +
T(i+1,j)))/kappa(i+1,j);
        % 2:-------------- To find Thickness where J=0 by trial and error
        samp_thick = .1;
        A_const_O_I0(i+1,j) = - (1 - Beta(i+1,j))* exp(-kappa(i+1,j) * samp_thick) / ((1 + Beta(i+1,j))^2 *
exp(kappa(i+1,j) * samp_thick) - (1-Beta(i+1,j))^2 * exp(-kappa(i+1,j) * samp_thick));
        B_const_O_I0(i+1,j) = + (1 + Beta(i+1,j))* exp(+kappa(i+1,j) * samp_thick) / ((1 + Beta(i+1,j))^2 *
exp(kappa(i+1,j) * samp_thick) - (1-Beta(i+1,j))^2 * exp(-kappa(i+1,j) * samp_thick));
        Ix(i+1,j) = A_const_O_I0(i+1,j) * (1 - Beta(i+1,j))* exp(+kappa(i+1,j)*X(i+1,j)) +
B_const_O_I0(i+1,j) * (1 + Beta(i+1,j))* exp(-kappa(i+1,j)*X(i+1,j));
        Jx(i+1,j) = A_const_O_I0(i+1,j) * (1 + Beta(i+1,j))* exp(+kappa(i+1,j)*X(i+1,j)) +
B_const_O_I0(i+1,j) * (1 - Beta(i+1,j))* exp(-kappa(i+1,j)*X(i+1,j));
```

```
        if (abs(K(i+1,j)-K(i,j)) < 0.0001)
            break
        end
    end
    x(j) = i;
end
```

A.2 MATLAB scripts for the Representative Layer Theory

First, the main code for the representative layer model is illustrated. This code calls three other codes that belong to the three particle sizes corresponding to 38, 75, and 150 microns. In this section three MATLAB m-files which take the CFD concentrations and import them to the main code is illustrated.

A.2.1 Main code of representative layer model


```
close all
clear
clc
format short g

D = 0.0254;                     % D: Diameter of pipe
rhop = 1480;                    % rhop: Density of ADP
rhof = 870;                     % rhof: Density of Xylene
L = 2;                       % L: Length of the pipe
n_38 = round(0.0254/(38*10^-6));% n: Number of layers
n_75 = round(0.0254/(75*10^-6));
n_150 = round(0.0254/(150*10^-6));
thk_38 = D/n_38;
thk_75 = D/n_75;
thk_150 = D/n_150;

inicon = [5 20 30];             % inicon: initial concentration
```

```
no_add = 6;                     % no_add: number of additional(assumed) concentrations to the fluent
concentrations

[Sp38_14,Sp38_28,Np_lay38_14,Np_lay38_28,dp_38,y_38] = micron38(D,rhop,rhof,L,thk_38,inicon,no_add);
[Sp75_14,Sp75_28,Np_lay75_14,Np_lay75_28,dp_75,y_75] = micron75(D,rhop,rhof,L,thk_75,inicon,no_add);
[Sp150_14,Sp150_28,Np_lay150_14,Np_lay150_28,dp_150,y_150] =
micron150(D,rhop,rhof,L,thk_150,inicon,no_add);

%% Preallocarion ************************************************************
T_38 = zeros(1,n_38-2);R_38 = zeros(1,n_38-2); A_38=zeros(1,n_38-2);k_38 = zeros(1,n_38-2); b_38 =
zeros(1,n_38-2);

A_38(1) = 0.5;
R_38(1) = 0.4;
T_38(1) = 0.1;
k_38(1) = A_38(1)/thk_38;
b_38(1) = R_38(1)/thk_38;
for i = 1:n_38-1
    T_38(i+1) = (T_38(i) * T_38(1))/(1-  R_38(i)*R_38(1));
    R_38(i+1) = R_38(i) + ((T_38(i))^2)*R_38(1)/(1 - R_38(i)*R_38(1));
    A_38(i+1) = 1 - T_38(i+1) - R_38(i+1);
    k_38(i+1) = A_38(i+1)/thk_38;
    b_38(i+1) = R_38(i+1)/thk_38;
end



A_75(1) = 0.6;
R_75(1) = 0.3;
T_75(1) = 0.1;
k_75(1) = A_75(1)/thk_75;
b_75(1) = R_75(1)/thk_75;
for i = 1:n_75-1
    T_75(i+1) = (T_75(i) * T_75(1))/(1-  R_75(i)*R_75(1));
    R_75(i+1) = R_75(i) + ((T_75(i))^2)*R_75(1)/(1 - R_75(i)*R_75(1));
    A_75(i+1) = 1 - T_75(i+1) - R_75(i+1);
    k_75(i+1) = A_75(i+1)/thk_75;
    b_75(i+1) = R_75(i+1)/thk_75;
end
```

```
T_150 = zeros(1,n_150-2);R_150 = zeros(1,n_150-2); A_150=zeros(1,n_150-2);k_150 = zeros(1,n_150-2); b_150 =
zeros(1,n_150-2);

A_150(1) = 0.5;
R_150(1) = 0.4;
T_150(1) = 0.1;
k_150(1) = A_150(1)/thk_150;
b_150(1) = R_150(1)/thk_150;

for i = 1:n_150-1
    T_150(i+1) = (T_150(i) * T_150(1))/(1-  R_150(i)*R_150(1));
    R_150(i+1) = R_150(i) + ((T_150(i))^2)*R_150(1)/(1 - R_150(i)*R_150(1));
    A_150(i+1) = 1 - T_150(i+1) - R_150(i+1);
    k_150(i+1) = A_150(i+1)/thk_150;
    b_150(i+1) = R_150(i+1)/thk_150;
end

%% Preallocation *******************************************************
A1_38u_14 = cell(1,3);R1_38u_14 = cell(1,3);T1_38u_14 = cell(1,3);
A1_38u_28 = cell(1,3);R1_38u_28 = cell(1,3);T1_38u_28 = cell(1,3);

A1_75u_14 = cell(1,3+no_add);R1_75u_14 = cell(1,3+no_add);T1_75u_14 = cell(1,3+no_add);
A1_75u_28 = cell(1,3);R1_75u_28 = cell(1,3);T1_75u_28 = cell(1,3);

A1_150u_14 = cell(1,3);R1_150u_14 = cell(1,3);T1_150u_14 = cell(1,3);
A1_150u_28 = cell(1,3);R1_150u_28 = cell(1,3);T1_150u_28 = cell(1,3);



x_38 = 1:n_38;
x_75 = 1:n_75;
x_150 = 1:n_150;

for j = 1:size(inicon,2)
    A1_38u_14{j} = Np_lay38_14{j} .*Sp38_14{j}.*(1-exp(-k_38.*dp_38));
    R1_38u_14{j} = Np_lay38_14{j}.*Sp38_14{j} .*b_38 * dp_38;
    T1_38u_14{j} = 1-A1_38u_14{j}-R1_38u_14{j};

    Omega_38u_14{j} = (1 + R1_38u_14{j} + (T1_38u_14{j}).^2 + Delta_38u_14{j})./(2*R1_38u_14{j});
    Psi_38u_14{j} = (1 + R1_38u_14{j} + (T1_38u_14{j}).^2 + Delta_38u_14{j})./(2*T1_38u_14{j});
```

```
    Rx_38u_14{j} = Omega_38u_14{j}.*(Psi_38u_14{j}.^(2*x_38)-
1)./((Omega_38u_14{j}.*Psi_38u_14{j}.^x_38).^2-1);
    Ax_38u_14{j} = 1 - Rx_38u_14{j} - Tx_38u_14{j};


    A1_38u_28{j} = Np_lay38_28{j} .*Sp38_28{j}.*(1-exp(-k_38.*dp_38));
    R1_38u_28{j} = Np_lay38_28{j}.*Sp38_28{j} .*b_38 * dp_38;
    T1_38u_28{j} = 1-A1_38u_28{j}-R1_38u_14{j};
    Delta_38u_28{j} = sqrt((1+R1_38u_28{j}+T1_38u_28{j}).*(1+R1_38u_28{j}-T1_38u_28{j}).*(1-
R1_38u_28{j}+T1_38u_28{j}).*(1-R1_38u_28{j}-T1_38u_28{j}));
    Omega_38u_28{j} = (1 + R1_38u_28{j} + (T1_38u_28{j}).^2 + Delta_38u_28{j})./(2*R1_38u_28{j});
    Psi_38u_28{j} = (1 + R1_38u_28{j} + (T1_38u_28{j}).^2 + Delta_38u_28{j})./(2*T1_38u_28{j});
    Rx_38u_28{j} = Omega_38u_28{j}.*(Psi_38u_28{j}.^(2*x_38)-
1)./((Omega_38u_28{j}.*Psi_38u_28{j}.^x_38).^2-1);
    Tx_38u_28{j} = (1./Psi_38u_28{j}.^x_38).*(Omega_38u_28{j}.^2 - 1)./(Omega_38u_28{j}.^2-
1./Psi_38u_28{j}.^(2*x_38));
    Ax_38u_28{j} = 1 - Rx_38u_28{j} - Tx_38u_28{j};


    R1_75u_14{j} = Np_lay75_14{j}.*Sp75_14{j} .*b_75 * dp_75; R1_75u_14{j+no_add-size(inicon,2)} =
Np_lay75_14{j+no_add-size(inicon,2)}.*Sp75_14{j+no_add-size(inicon,2)} .*b_75 * dp_75; R1_75u_14{j+no_add}
= Np_lay75_14{j+no_add}.*Sp75_14{j+no_add} .*b_75 * dp_75;
    T1_75u_14{j} = 1-A1_75u_14{j}-R1_75u_14{j};T1_75u_14{j+no_add-size(inicon,2)} = 1-A1_75u_14{j+no_add-
size(inicon,2)}-R1_75u_14{j+no_add-size(inicon,2)};T1_75u_14{j+no_add} = 1-A1_75u_14{j+no_add}-
R1_75u_14{j+no_add};
    Delta_75u_14{j} = sqrt((1+R1_75u_14{j}+T1_75u_14{j}).*(1+R1_75u_14{j}-T1_75u_14{j}).*(1-
R1_75u_14{j}+T1_75u_14{j}).*(1-R1_75u_14{j}-T1_75u_14{j}));Delta_75u_14{j+no_add-size(inicon,2)} =
sqrt((1+R1_75u_14{j+no_add-size(inicon,2)}+T1_75u_14{j+no_add-size(inicon,2)}).*(1+R1_75u_14{j+no_add-
size(inicon,2)}-T1_75u_14{j+no_add-size(inicon,2)}).*(1-R1_75u_14{j+no_add-
size(inicon,2)}+T1_75u_14{j+no_add-size(inicon,2)}).*(1-R1_75u_14{j+no_add-size(inicon,2)}-
T1_75u_14{j+no_add-size(inicon,2)}));Delta_75u_14{j+no_add} =
sqrt((1+R1_75u_14{j+no_add}+T1_75u_14{j+no_add}).*(1+R1_75u_14{j+no_add}-T1_75u_14{j+no_add}).*(1-
R1_75u_14{j+no_add}+T1_75u_14{j+no_add}).*(1-R1_75u_14{j+no_add}-T1_75u_14{j+no_add}));
    Omega_75u_14{j} = (1 + R1_75u_14{j} + (T1_75u_14{j}).^2 +
Delta_75u_14{j}).*(2*R1_75u_14{j});Omega_75u_14{j+no_add-size(inicon,2)} = (1 + R1_75u_14{j+no_add-
size(inicon,2)} + (T1_75u_14{j+no_add-size(inicon,2)}).^2 + Delta_75u_14{j+no_add-
size(inicon,2)}).*(2*R1_75u_14{j+no_add-size(inicon,2)});Omega_75u_14{j+no_add} = (1 + R1_75u_14{j+no_add}
+ (T1_75u_14{j+no_add}).^2 + Delta_75u_14{j+no_add}).*(2*R1_75u_14{j+no_add});
    Rx_75u_14{j} = Omega_75u_14{j}.*(Psi_75u_14{j}.^(2*x_75)-
1)./((Omega_75u_14{j}.*Psi_75u_14{j}.^x_75).^2-1);Rx_75u_14{j+no_add-size(inicon,2)} =
Omega_75u_14{j+no_add-size(inicon,2)}.*(Psi_75u_14{j+no_add-size(inicon,2)}.^(2*x_75)-
```

```
1)./((Omega_75u_14{j+no_add-size(inicon,2)}.*Psi_75u_14{j+no_add-size(inicon,2)}.^x_75).^2-
1);Rx_75u_14{j+no_add} = Omega_75u_14{j+no_add}.*(Psi_75u_14{j+no_add}.^(2*x_75)-
1)./((Omega_75u_14{j+no_add}.*Psi_75u_14{j+no_add}.^x_75).^2-1);
    Tx_75u_14{j} = (1./Psi_75u_14{j}.^x_75).*(Omega_75u_14{j}.^2 - 1)./(Omega_75u_14{j}.^2-
1./Psi_75u_14{j}.^(2*x_75));Tx_75u_14{j+no_add-size(inicon,2)} = (1./Psi_75u_14{j+no_add-
size(inicon,2)}.^x_75).*(Omega_75u_14{j+no_add-size(inicon,2)}.^2 - 1)./(Omega_75u_14{j+no_add-
size(inicon,2)}.^2-1./Psi_75u_14{j+no_add-size(inicon,2)}.^(2*x_75));Tx_75u_14{j+no_add} =
(1./Psi_75u_14{j+no_add}.^x_75).*(Omega_75u_14{j+no_add}.^2 - 1)./(Omega_75u_14{j+no_add}.^2-
1./Psi_75u_14{j+no_add}.^(2*x_75));
    Ax_75u_14{j} = 1 - Rx_75u_14{j} - Tx_75u_14{j};Ax_75u_14{j+no_add-size(inicon,2)} = 1 -
Rx_75u_14{j+no_add-size(inicon,2)} - Tx_75u_14{j+no_add-size(inicon,2)};Ax_75u_14{j+no_add} = 1 -
Rx_75u_14{j+no_add} - Tx_75u_14{j+no_add};

    A1_75u_28{j} = Np_lay75_28{j} .*Sp75_28{j}.*(1-exp(-k_75.*dp_75));
    R1_75u_28{j} = Np_lay75_28{j}.*Sp75_28{j} .*b_75 * dp_75;
    T1_75u_28{j} = 1-A1_75u_28{j}-R1_75u_28{j};
    Delta_75u_28{j} = sqrt((1+R1_75u_28{j}+T1_75u_28{j}).*(1+R1_75u_28{j}-T1_75u_28{j}).*(1-
R1_75u_28{j}+T1_75u_28{j}).*(1-R1_75u_28{j}-T1_75u_28{j}));
    Omega_75u_28{j} = (1 + R1_75u_28{j} + (T1_75u_28{j}).^2 + Delta_75u_28{j})./(2*R1_75u_28{j});
    Psi_75u_28{j} = (1 + R1_75u_28{j} + (T1_75u_28{j}).^2 + Delta_75u_28{j})./(2*T1_75u_28{j});
    Rx_75u_28{j} = Omega_75u_28{j}.*(Psi_75u_28{j}.^(2*x_75)-
1)./((Omega_75u_28{j}.*Psi_75u_28{j}.^x_75).^2-1);
    Tx_75u_28{j} = (1./Psi_75u_28{j}.^x_75).*(Omega_75u_28{j}.^2 - 1)./(Omega_75u_28{j}.^2-
1./Psi_75u_28{j}.^(2*x_75));
    Ax_75u_28{j} = 1 - Rx_75u_28{j} - Tx_75u_28{j};

    A1_150u_14{j} = Np_lay150_14{j} .*Sp150_14{j}.*(1-exp(-k_150.*dp_150));
    R1_150u_14{j} = Np_lay150_14{j}.*Sp150_14{j} .*b_150 * dp_150;
    T1_150u_14{j} = 1-A1_150u_14{j}-R1_150u_14{j};
    Delta_150u_14{j} = sqrt((1+R1_150u_14{j}+T1_150u_14{j}).*(1+R1_150u_14{j}-T1_150u_14{j}).*(1-
R1_150u_14{j}+T1_150u_14{j}).*(1-R1_150u_14{j}-T1_150u_14{j}));
    Omega_150u_14{j} = (1 + R1_150u_14{j} + (T1_150u_14{j}).^2 + Delta_150u_14{j})./(2*R1_150u_14{j});
    Psi_150u_14{j} = (1 + R1_150u_14{j} + (T1_150u_14{j}).^2 + Delta_150u_14{j})./(2*T1_150u_14{j});
    Rx_150u_14{j} = Omega_150u_14{j}.*(Psi_150u_14{j}.^(2*x_150)-
1)./((Omega_150u_14{j}.*Psi_150u_14{j}.^x_150).^2-1);
    Tx_150u_14{j} = (1./Psi_150u_14{j}.^x_150).*(Omega_150u_14{j}.^2 - 1)./(Omega_150u_14{j}.^2-
1./Psi_150u_14{j}.^(2*x_150));
    Ax_150u_14{j} = 1 - Rx_150u_14{j} - Tx_150u_14{j};
```

```
    A1_150u_28{j} = Np_lay150_28{j} .*Sp150_28{j}.*(1-exp(-k_150.*dp_150));
    R1_150u_28{j} = Np_lay150_28{j}.*Sp150_28{j} .*b_150 * dp_150;
    T1_150u_28{j} = 1-A1_150u_28{j}-R1_150u_28{j};
    Delta_150u_28{j} = sqrt((1+R1_150u_28{j}+T1_150u_28{j}).*(1+R1_150u_28{j}-T1_150u_28{j}).*(1-
R1_150u_28{j}+T1_150u_28{j}).*(1-R1_150u_28{j}-T1_150u_28{j}));
    Omega_150u_28{j} = (1 + R1_150u_28{j} + (T1_150u_28{j}).^2 + Delta_150u_28{j})./(2*R1_150u_28{j});
    Psi_150u_28{j} = (1 + R1_150u_28{j} + (T1_150u_28{j}).^2 + Delta_150u_28{j})./(2*T1_150u_28{j});
    Rx_150u_28{j} = Omega_150u_28{j}.*(Psi_150u_28{j}.^(2*x_150)-
1)./((Omega_150u_28{j}.*Psi_150u_28{j}.^x_150).^2-1);
    Tx_150u_28{j} = (1./Psi_150u_28{j}.^x_150).*(Omega_150u_28{j}.^2 - 1)./(Omega_150u_28{j}.^2-
1./Psi_150u_28{j}.^(2*x_150));
    Ax_150u_28{j} = 1 - Rx_150u_28{j} - Tx_150u_28{j};
end

%% Converting 18 cells to matrices 18*3 = 54 Matrices: ********************
A38u14_5 = cat(2,A1_38u_14{1});A38u14_20 = cat(2,A1_38u_14{2});A38u14_30 = cat(2,A1_38u_14{3});
A38u28_5 = cat(2,A1_38u_28{1});A38u28_20 = cat(2,A1_38u_28{2});A38u28_30 = cat(2,A1_38u_28{3});
A75u28_5 = cat(2,A1_75u_28{1});A75u28_20 = cat(2,A1_75u_28{2});A75u28_30 = cat(2,A1_75u_28{3});
A150u14_5 = cat(2,A1_150u_14{1});A150u14_20 = cat(2,A1_150u_14{2});A150u14_30 = cat(2,A1_150u_14{3});
A150u28_5 = cat(2,A1_150u_28{1});A150u28_20 = cat(2,A1_150u_28{2});A150u28_30 = cat(2,A1_150u_28{3});

R38u14_5 = cat(2,R1_38u_14{1});R38u14_20 = cat(2,R1_38u_14{2});R38u14_30 = cat(2,R1_38u_14{3});
R38u28_5 = cat(2,R1_38u_28{1});R38u28_20 = cat(2,R1_38u_28{2});R38u28_30 = cat(2,R1_38u_28{3});
R75u14_5 = cat(2,R1_75u_14{1});R75u14_20 = cat(2,R1_75u_14{2});R75u14_30 =
cat(2,R1_75u_14{3});R75u14_5_unif = cat(2,R1_75u_14{4});R75u14_20_unif = cat(2,R1_75u_14{5});R75u14_30_unif
= cat(2,R1_75u_14{6});R_lin20 = cat(2,R1_75u_14{7});R_lin30 = cat(2,R1_75u_14{8});R_parabolic =
cat(2,R1_75u_14{9});
R75u28_5 = cat(2,R1_75u_28{1});R75u28_20 = cat(2,R1_75u_28{2});R75u28_30 = cat(2,R1_75u_28{3});
R150u14_5 = cat(2,R1_150u_14{1});R150u14_20 = cat(2,R1_150u_14{2});R150u14_30 = cat(2,R1_150u_14{3});
R150u28_5 = cat(2,R1_150u_28{1});R150u28_20 = cat(2,R1_150u_28{2});R150u28_30 = cat(2,R1_150u_28{3});

T38u14_5 = cat(2,T1_38u_14{1});T38u14_20 = cat(2,T1_38u_14{2});T38u14_30 = cat(2,T1_38u_14{3});
T38u28_5 = cat(2,T1_38u_28{1});T38u28_20 = cat(2,T1_38u_28{2});T38u28_30 = cat(2,T1_38u_28{3});
T75u14_5 = cat(2,T1_75u_14{1});T75u14_20 = cat(2,T1_75u_14{2});T75u14_30 =
cat(2,T1_75u_14{3});T75u14_5_unif = cat(2,T1_75u_14{4});T75u14_20_unif = cat(2,T1_75u_14{5});T75u14_30_unif
= cat(2,T1_75u_14{6});T_lin20 = cat(2,T1_75u_14{7});T_lin30 = cat(2,T1_75u_14{8});T_parabolic =
cat(2,T1_75u_14{9});
T75u28_5 = cat(2,T1_75u_28{1});T75u28_20 = cat(2,T1_75u_28{2});T75u28_30 = cat(2,T1_75u_28{3});
T150u14_5 = cat(2,T1_150u_14{1});T150u14_20 = cat(2,T1_150u_14{2});T150u14_30 = cat(2,T1_150u_14{3});
T150u28_5 = cat(2,T1_150u_28{1});T150u28_20 = cat(2,T1_150u_28{2});T150u28_30 = cat(2,T1_150u_28{3});
```

```
% Preallocation *******************************************************
cumA3814_5 = zeros(1,n_38-1);cumA3814_20 = zeros(1,n_38-1);cumA3814_30 = zeros(1,n_38-1);
cumA3828_5 = zeros(1,n_38-1);cumA3828_20 = zeros(1,n_38-1);cumA3828_30 = zeros(1,n_38-1);
cumA7514_5 = zeros(1,n_75-1);cumA7514_20 = zeros(1,n_75-1);cumA7514_30 = zeros(1,n_75-1);

cumA7528_5 = zeros(1,n_75-1);cumA7528_20 = zeros(1,n_75-1);cumA7528_30 = zeros(1,n_75-1);
cumA15014_5 = zeros(1,n_150-1);cumA15014_20 = zeros(1,n_150-1);cumA15014_30 = zeros(1,n_150-1);
cumA15028_5 = zeros(1,n_150-1);cumA15028_20 = zeros(1,n_150-1);cumA15028_30 = zeros(1,n_150-1);

cumR3814_5 = zeros(1,n_38-1);cumR3814_20 = zeros(1,n_38-1);cumR3814_30 = zeros(1,n_38-1);
cumR3828_5 = zeros(1,n_38-1);cumR3828_20 = zeros(1,n_38-1);cumR3828_30 = zeros(1,n_38-1);
cumR7514_5 = zeros(1,n_75-1);cumR7514_20 = zeros(1,n_75-1);cumR7514_30 = zeros(1,n_75-1);

cumR7528_5 = zeros(1,n_75-1);cumR7528_20 = zeros(1,n_75-1);cumR7528_30 = zeros(1,n_75-1);
cumR15014_5 = zeros(1,n_150-1);cumR15014_20 = zeros(1,n_150-1);cumR15014_30 = zeros(1,n_150-1);
cumR15028_5 = zeros(1,n_150-1);cumR15028_20 = zeros(1,n_150-1);cumR15028_30 = zeros(1,n_150-1);

cumT3814_5 = zeros(1,n_38-1);cumT3814_20 = zeros(1,n_38-1);cumT3814_30 = zeros(1,n_38-1);
cumT3828_5 = zeros(1,n_38-1);cumT3828_20 = zeros(1,n_38-1);cumT3828_30 = zeros(1,n_38-1);
cumT7514_5 = zeros(1,n_75-1);cumT7514_20 = zeros(1,n_75-1);cumT7514_30 = zeros(1,n_75-1);

cumT7528_5 = zeros(1,n_75-1);cumT7528_20 = zeros(1,n_75-1);cumT7528_30 = zeros(1,n_75-1);
cumT15014_5 = zeros(1,n_150-1);cumT15014_20 = zeros(1,n_150-1);cumT15014_30 = zeros(1,n_150-1);
cumT15028_5 = zeros(1,n_150-1);cumT15028_20 = zeros(1,n_150-1);cumT15028_30 = zeros(1,n_150-1);

for m = 1:n_38-1
    cumA3814_5(m) = sum(A38u14_5(1:m));cumA3814_20(m) = sum(A38u14_20(1:m));cumA3814_30(m) =
sum(A38u14_30(1:m));
    cumA3828_5(m) = sum(A38u28_5(1:m));cumA3828_20(m) = sum(A38u28_20(1:m));cumA3828_30(m) =
sum(A38u28_30(1:m));

    cumR3814_5(m) = sum(R38u14_5(1:m));cumR3814_20(m) = sum(R38u14_20(1:m));cumR3814_30(m) =
sum(R38u14_30(1:m));
    cumR3828_5(m) = sum(R38u28_5(1:m));cumR3828_20(m) = sum(R38u28_20(1:m));cumR3828_30(m) =
sum(R38u28_30(1:m));

    cumT3814_5(m) = sum(T38u14_5(1:m));cumT3814_20(m) = sum(T38u14_20(1:m));cumT3814_30(m) =
sum(T38u14_30(1:m));
```

```
    cumT3828_5(m) = sum(T38u28_5(1:m));cumT3828_20(m) = sum(T38u28_20(1:m));cumT3828_30(m) =
sum(T38u28_30(1:m));
end

for m = 1:n_75-1
    cumA7514_5(m) = sum(A75u14_5(1:m));cumA7514_20(m) = sum(A75u14_20(1:m));cumA7514_30(m) =
sum(A75u14_30(1:m));
    cumA7528_5(m) = sum(A75u28_5(1:m));cumA7528_20(m) = sum(A75u28_20(1:m));cumA7528_30(m) =
sum(A75u28_30(1:m));

    cumR7514_5(m) = sum(R75u14_5(1:m));cumR7514_20(m) = sum(R75u14_20(1:m));cumR7514_30(m) =
sum(R75u14_30(1:m));
    cumR7528_5(m) = sum(R75u28_5(1:m));cumR7528_20(m) = sum(R75u28_20(1:m));cumR7528_30(m) =
sum(R75u28_30(1:m));

    cumT7514_5(m) = sum(T75u14_5(1:m));cumT7514_20(m) = sum(T75u14_20(1:m));cumT7514_30(m) =
sum(T75u14_30(1:m));

    cumT7528_5(m) = sum(T75u28_5(1:m));cumT7528_20(m) = sum(T75u28_20(1:m));cumT7528_30(m) =
sum(T75u28_30(1:m));
end

for m = 1:n_150-1
    cumA15014_5(m) = sum(A150u14_5(1:m));cumA15014_20(m) = sum(A150u14_20(1:m));cumA15014_30(m) =
sum(A150u14_30(1:m));
    cumA15028_5(m) = sum(A150u28_5(1:m));cumA15028_20(m) = sum(A150u28_20(1:m));cumA15028_30(m) =
sum(A150u28_30(1:m));

    cumR15014_5(m) = sum(R150u14_5(1:m));cumR15014_20(m) = sum(R150u14_20(1:m));cumR15014_30(m) =
sum(R150u14_30(1:m));
    cumR15028_5(m) = sum(R150u28_5(1:m));cumR15028_20(m) = sum(R150u28_20(1:m));cumR15028_30(m) =
sum(R150u28_30(1:m));

    cumT15014_5(m) = sum(T150u14_5(1:m));cumT15014_20(m) = sum(T150u14_20(1:m));cumT15014_30(m) =
sum(T150u14_30(1:m));
    cumT15028_5(m) = sum(T150u28_5(1:m));cumT15028_20(m) = sum(T150u28_20(1:m));cumT15028_30(m) =
sum(T150u28_30(1:m));
end
```

```
PS = [38, 75, 150];
```

A.2.2 MATLAB input script for 38 micorn

```
function [Sp_14,Sp_28,Np_lay_14,Np_lay_28,dp,y] = micron38(D,rhop,rhof,L,thk,inicon,no_add)

dp = 38*10^-6;
n_38 = round(0.0254/(dp));
thk_38 = D/n_38;
y = thk_38:thk_38:D;
wdth = D;
polyorder = 6;
vol_lay = L*thk*wdth;

cxls_Re14 = cell(size(inicon,2),1);
cxls_Re28 = cell(size(inicon,2),1);
yOD_Re14 = cell(size(inicon,2),1);
yOD_Re28 = cell(size(inicon,2),1);

data1 = load('concentration_38um.mat','cxls_Re14_5'); cxls_Re14{1} = data1.cxls_Re14_5;
data2 = load('concentration_38um.mat','cxls_Re14_20'); cxls_Re14{2} = data2.cxls_Re14_20;
data3 = load('concentration_38um.mat','cxls_Re14_30'); cxls_Re14{3} = data3.cxls_Re14_30;
data4 = load('concentration_38um.mat','cxls_Re28_5'); cxls_Re28{1} = data4.cxls_Re28_5;
data5 = load('concentration_38um.mat','cxls_Re28_20'); cxls_Re28{2} = data5.cxls_Re28_20;
data6 = load('concentration_38um.mat','cxls_Re28_30'); cxls_Re28{3} = data6.cxls_Re28_30;
data7 = load('concentration_38um.mat','yOD_Re14_5'); yOD_Re14{1} = data7.yOD_Re14_5;
data8 = load('concentration_38um.mat','yOD_Re14_20'); yOD_Re14{2} = data8.yOD_Re14_20;
data9 = load('concentration_38um.mat','yOD_Re14_30'); yOD_Re14{3} = data9.yOD_Re14_30;
data10 = load('concentration_38um.mat','yOD_Re28_5'); yOD_Re28{1} = data10.yOD_Re28_5;
data11 = load('concentration_38um.mat','yOD_Re28_20'); yOD_Re28{2} = data11.yOD_Re28_20;
data12 = load('concentration_38um.mat','yOD_Re28_30'); yOD_Re28{3} = data12.yOD_Re28_30;

% Preallocation *******************************************************
coeff_Re14 = cell(1,size(inicon,2)); coeff_Re28 = cell(1,size(inicon,2));
c_fittoxls_Re14 = cell(1,size(inicon,2)); c_fittoxls_Re28 = cell(1,size(inicon,2));
c_Re14 = cell(1,size(inicon,2)); c_Re28 = cell(1,size(inicon,2));
volp_14 = cell(1,size(inicon,2)); volp_28 = cell(1,size(inicon,2));
volf_14 = cell(1,size(inicon,2)); volf_28 = cell(1,size(inicon,2));
```

```
Np_lay_14 = cell(1,size(inicon,2)); Np_lay_28 = cell(1,size(inicon,2));
mp_14 = cell(1,size(inicon,2)); mp_28 = cell(1,size(inicon,2));
wp_14 = cell(1,size(inicon,2)); wp_28 = cell(1,size(inicon,2));
vp_14 = cell(1,size(inicon,2)); vp_28 = cell(1,size(inicon,2));
sp_14 = cell(1,size(inicon,2)); sp_28 = cell(1,size(inicon,2));
void_14 = cell(1,size(inicon,2)); void_28 = cell(1,size(inicon,2));
Vp_14 = cell(1,size(inicon,2)); Vp_28 = cell(1,size(inicon,2));
Sp_14 = cell(1,size(inicon,2)); Sp_28 = cell(1,size(inicon,2));

for i = 1:size(inicon,2)

    coeff_Re14{i} = polyfit(yOD_Re14{i},cxls_Re14{i},polyorder);
    coeff_Re28{i} = polyfit(yOD_Re28{i},cxls_Re28{i},polyorder);

    c_fittoxls_Re14{i} = polyval(coeff_Re14{i},yOD_Re14{i});        % c_fittoxls_Re14: The values of the
trendline @ Y/D values obtained from the Fluent
    c_fittoxls_Re28{i} = polyval(coeff_Re28{i},yOD_Re28{i});

    c_Re14{i} = polyval(coeff_Re14{i},y/D);                  % Particle Size = 5: fitted concentration
equation as a function of y/D
    c_Re28{i} = polyval(coeff_Re28{i},y/D);                  % Particle Size = 5: fitted concentration
equation as a function of y/D

    volp_14{i} = c_Re14{i} .* vol_lay;
    volp_28{i} = c_Re28{i} .* vol_lay;

    volf_14{i} = vol_lay.* (1-c_Re14{i});
    volf_28{i} = vol_lay.* (1-c_Re28{i});

    Np_lay_14{i} = volp_14{i}/(pi*dp^3/6);
    Np_lay_28{i} = volp_28{i}/(pi*dp^3/6);

    mp_14{i} = rhop * volp_14{i};
    mp_28{i} = rhop * volp_28{i};

    wp_14{i} = mp_14{i}./ (rhop*volp_14{i} + rhof * volf_14{i});
    wp_28{i} = mp_28{i}./ (rhop*volp_28{i} + rhof * volf_28{i});

    vp_14{i} = (wp_14{i}/(rhop))./(Np_lay_14{i}.*wp_14{i}/(rhop));          % vp: for each particle
```

```
    vp_28{i} = (wp_28{i}/(rhop))./(Np_lay_28{i}.*wp_28{i}/(rhop));

    sp_14{i} = (wp_14{i}./(rhop*dp))/(Np_lay_14{i}.*wp_14{i}/(rhop*dp));
    sp_28{i} = (wp_28{i}./(rhop*dp))/(Np_lay_28{i}.*wp_28{i}/(rhop*dp));

    void_14{i} = 1- c_Re14{i};
    void_28{i} = 1- c_Re28{i};

    Vp_14{i} = (1-void_14{i}).*vp_14{i};
    Vp_28{i} = (1-void_28{i}).*vp_28{i};

    Sp_14{i} = (1-void_14{i}).*sp_14{i};
    Sp_28{i} = (1-void_28{i}).*sp_28{i};

end
```


A.2.3 MATLAB input script for 75 micron

```
function [Sp_14,Sp_28,Np_lay_14,Np_lay_28,dp,y] = micron75(D,rhop,rhof,L,thk,inicon,no_add)

dp = 75*10^-6;
n_75 = round(0.0254/(dp));
thk_75 = D/n_75;
y = thk_75:thk_75:D;%-D/n_75;
wdth = D;
polyorder = 12;
vol_lay = L*thk*wdth;

data1 = load('concentration_75um.mat','cxls_Re14_5'); cxls_Re14{1} = data1.cxls_Re14_5;
data2 = load('concentration_75um.mat','cxls_Re14_20'); cxls_Re14{2} = data2.cxls_Re14_20;
data3 = load('concentration_75um.mat','cxls_Re14_30'); cxls_Re14{3} = data3.cxls_Re14_30;
data4 = load('concentration_75um.mat','cxls_Re14_5_unif'); cxls_Re14{4} = data4.cxls_Re14_5_unif;
% 5% uniform concentration of Excel Sheet Concentration New, Sheet 75(Re=14000) Column AG and greater
data5 = load('concentration_75um.mat','cxls_Re14_20_unif'); cxls_Re14{5} = data5.cxls_Re14_20_unif;
% 20% uniform concentration of Excel Sheet Concentration New, Sheet 75(Re=14000) Column AG and greater
```

```
data6 = load('concentration_75um.mat','cxls_Re14_30_unif'); cxls_Re14{6} = data6.cxls_Re14_30_unif;
% 30% uniform concentration of Excel Sheet Concentration New, Sheet 75(Re=14000) Column AG and greater
data7 = load('concentration_75um.mat','cxls_Re28_5'); cxls_Re28{1} = data7.cxls_Re28_5;
data8 = load('concentration_75um.mat','cxls_Re28_20'); cxls_Re28{2} = data8.cxls_Re28_20;
data9 = load('concentration_75um.mat','cxls_Re28_30'); cxls_Re28{3} = data9.cxls_Re28_30;
data10 = load('concentration_75um.mat','yOD_Re14_5'); yOD_Re14{1} = data10.yOD_Re14_5;
data11 = load('concentration_75um.mat','yOD_Re14_20'); yOD_Re14{2} = data11.yOD_Re14_20;
data12 = load('concentration_75um.mat','yOD_Re14_30'); yOD_Re14{3} = data12.yOD_Re14_30;
data13 = load('concentration_75um.mat','yOD_Re14_5_unif'); yOD_Re14{4} = data13.yOD_Re14_5_unif;
% 5% uniform concentration of Excel Sheet Concentration New, Sheet 75(Re=14000) Column AG and greater
data14 = load('concentration_75um.mat','yOD_Re14_20_unif'); yOD_Re14{5} = data14.yOD_Re14_20_unif;
% 5% uniform concentration of Excel Sheet Concentration New, Sheet 75(Re=14000) Column AG and greater
data15 = load('concentration_75um.mat','yOD_Re14_30_unif'); yOD_Re14{6} = data15.yOD_Re14_30_unif;
% 5% uniform concentration of Excel Sheet Concentration New, Sheet 75(Re=14000) Column AG and greater
data16 = load('concentration_75um.mat','yOD_Re28_5'); yOD_Re28{1} = data16.yOD_Re28_5;
data17 = load('concentration_75um.mat','yOD_Re28_20'); yOD_Re28{2} = data17.yOD_Re28_20;
data18 = load('concentration_75um.mat','yOD_Re28_30'); yOD_Re28{3} = data18.yOD_Re28_30;

data19 = load('concentration_75um.mat','cxls_lin5'); cxls_Re14{7} = data19.cxls_lin5;
data20 = load('concentration_75um.mat','cxls_lin20'); cxls_Re14{8} = data20.cxls_lin20;
data21 = load('concentration_75um.mat','cxls_parabola'); cxls_Re14{9} = data21.cxls_parabola;
data22 = load('concentration_75um.mat','yOD_lin5'); yOD_Re14{7} = data22.yOD_lin5;
data23 = load('concentration_75um.mat','yOD_lin20'); yOD_Re14{8} = data23.yOD_lin20;
data24 = load('concentration_75um.mat','yOD_parabola'); yOD_Re14{9} = data24.yOD_parabola;

% Preallocation *********************************************************
coeff_Re14 = cell(1,size(inicon,2)+no_add); coeff_Re28 = cell(1,size(inicon,2));
c_fittoxls_Re14 = cell(1,size(inicon,2)+no_add); c_fittoxls_Re28 = cell(1,size(inicon,2));
c_Re14 = cell(1,size(inicon,2)+no_add); c_Re28 = cell(1,size(inicon,2));
volp_14 = cell(1,size(inicon,2)+no_add); volp_28 = cell(1,size(inicon,2));
volf_14 = cell(1,size(inicon,2)+no_add); volf_28 = cell(1,size(inicon,2));
Np_lay_14 = cell(1,size(inicon,2)+no_add); Np_lay_28 = cell(1,size(inicon,2));
mp_14 = cell(1,size(inicon,2)+no_add); mp_28 = cell(1,size(inicon,2));
wp_14 = cell(1,size(inicon,2)+no_add); wp_28 = cell(1,size(inicon,2));
vp_14 = cell(1,size(inicon,2)+no_add); vp_28 = cell(1,size(inicon,2));
sp_14 = cell(1,size(inicon,2)+no_add); sp_28 = cell(1,size(inicon,2));
void_14 = cell(1,size(inicon,2)+no_add); void_28 = cell(1,size(inicon,2));
Vp_14 = cell(1,size(inicon,2)+no_add); Vp_28 = cell(1,size(inicon,2));
Sp_14 = cell(1,size(inicon,2)+no_add); Sp_28 = cell(1,size(inicon,2));
```

```
for i = 1:size(inicon,2)

    coeff_Re14{i} = polyfit(yOD_Re14{i},cxls_Re14{i},polyorder);
    coeff_Re28{i} = polyfit(yOD_Re28{i},cxls_Re28{i},polyorder);
    coeff_Re14{i+no_add} = polyfit(yOD_Re14{i+no_add},cxls_Re14{i+no_add},polyorder);        % This is a
curve fitt coefficient for uniform concentration
    coeff_Re14{i+no_add-size(inicon,2)} = polyfit(yOD_Re14{i+no_add-size(inicon,2)},cxls_Re14{i+no_add-
size(inicon,2)},polyorder);        % This is a curve fitt coefficient for uniform concentration


    c_fittoxls_Re14{i} = polyval(coeff_Re14{i},yOD_Re14{i});        % c_fittoxls_Re14: The values of the
trendline @ Y/D values obtained from the Fluent
    c_fittoxls_Re28{i} = polyval(coeff_Re28{i},yOD_Re28{i});
    c_fittoxls_Re14{i+no_add} = polyval(coeff_Re14{i+no_add},yOD_Re14{i+no_add});  % c_fittoxls_Re14: The
values of the trendline @ Y/D values for the uniform concentration
    c_fittoxls_Re14{i+no_add-size(inicon,2)} = polyval(coeff_Re14{i+no_add-
size(inicon,2)},yOD_Re14{i+no_add-size(inicon,2)});  % c_fittoxls_Re14: The values of the trendline @ Y/D
values for the uniform concentration

    c_Re14{i} = polyval(coeff_Re14{i},y/D);                  % Particle Size = 5: fitted concentration
equation as a function of y/D
    c_Re28{i} = polyval(coeff_Re28{i},y/D);                  % Particle Size = 5: fitted concentration
equation as a function of y/D
    c_Re14{i+no_add} = polyval(coeff_Re14{i+no_add},y/D);
    c_Re14{i+no_add-size(inicon,2)} = polyval(coeff_Re14{i+no_add-size(inicon,2)},y/D);

    volp_14{i} = c_Re14{i} .* vol_lay;
    volp_28{i} = c_Re28{i} .* vol_lay;
    volp_14{i+no_add} = c_Re14{i+no_add} .* vol_lay;
    volp_14{i+no_add-size(inicon,2)} = c_Re14{i+no_add-size(inicon,2)} .* vol_lay;

    volf_14{i} = vol_lay.* (1-c_Re14{i});
    volf_28{i} = vol_lay.* (1-c_Re28{i});
    volf_14{i+no_add} = vol_lay.* (1-c_Re14{i+no_add});
    volf_14{i+no_add-size(inicon,2)} = vol_lay.* (1-c_Re14{i+no_add-size(inicon,2)});

    Np_lay_14{i} = volp_14{i}/(pi*dp^3/6);
    Np_lay_28{i} = volp_28{i}/(pi*dp^3/6);
    Np_lay_14{i+no_add} = volp_14{i+no_add}/(pi*dp^3/6);
```

```
    Np_lay_14{i+no_add-size(inicon,2)} = volp_14{i+no_add-size(inicon,2)}/(pi*dp^3/6);

    mp_14{i} = rhop * volp_14{i};
    mp_28{i} = rhop * volp_28{i};
    mp_14{i+no_add} = rhop * volp_14{i+no_add};
    mp_14{i+no_add-size(inicon,2)} = rhop * volp_14{i+no_add-size(inicon,2)};
%
    wp_14{i} = mp_14{i}./ (rhop*volp_14{i} + rhof * volf_14{i});
    wp_28{i} = mp_28{i}./ (rhop*volp_28{i} + rhof * volf_28{i});
    wp_14{i+no_add} = mp_14{i+no_add}./ (rhop*volp_14{i+no_add} + rhof * volf_14{i+no_add});
    wp_14{i+no_add-size(inicon,2)} = mp_14{i+no_add-size(inicon,2)}./ (rhop*volp_14{i+no_add-
size(inicon,2)} + rhof * volf_14{i+no_add-size(inicon,2)});

    vp_14{i} = (wp_14{i}/(rhop))./(Np_lay_14{i}.*wp_14{i}/(rhop));          % vp: for each particle
    vp_28{i} = (wp_28{i}/(rhop))./(Np_lay_28{i}.*wp_28{i}/(rhop));
    vp_14{i+no_add} = (wp_14{i+no_add}/(rhop))./(Np_lay_14{i+no_add}.*wp_14{i+no_add}/(rhop));          %
vp: for each particle
    vp_14{i+no_add-size(inicon,2)} = (wp_14{i+no_add-size(inicon,2)}/(rhop))./(Np_lay_14{i+no_add-
size(inicon,2)}.*wp_14{i+no_add-size(inicon,2)}/(rhop));          % vp: for each particle

    sp_14{i} = (wp_14{i}./(rhop*dp))/(Np_lay_14{i}.*wp_14{i}/(rhop*dp));
    sp_28{i} = (wp_28{i}./(rhop*dp))/(Np_lay_28{i}.*wp_28{i}/(rhop*dp));
    sp_14{i+no_add} = (wp_14{i+no_add}./(rhop*dp))/(Np_lay_14{i+no_add}.*wp_14{i+no_add}/(rhop*dp));
    sp_14{i+no_add-size(inicon,2)} = (wp_14{i+no_add-size(inicon,2)}./(rhop*dp))/(Np_lay_14{i+no_add-
size(inicon,2)}.*wp_14{i+no_add-size(inicon,2)}/(rhop*dp));

    void_14{i} = 1- c_Re14{i};
    void_28{i} = 1- c_Re28{i};
    void_14{i+no_add} = 1- c_Re14{i+no_add};
    void_14{i+no_add-size(inicon,2)} = 1- c_Re14{i+no_add-size(inicon,2)};

    Vp_14{i} = (1-void_14{i}).*vp_14{i};
    Vp_28{i} = (1-void_28{i}).*vp_28{i};
    Vp_14{i+no_add} = (1-void_14{i+no_add}).*vp_14{i+no_add};
    Vp_14{i+no_add-size(inicon,2)} = (1-void_14{i+no_add-size(inicon,2)}).*vp_14{i+no_add-size(inicon,2)};

    Sp_14{i} = (1-void_14{i}).*sp_14{i};
    Sp_28{i} = (1-void_28{i}).*sp_28{i};
    Sp_14{i+no_add} = (1-void_14{i+no_add}).*sp_14{i+no_add};
    Sp_14{i+no_add-size(inicon,2)} = (1-void_14{i+no_add-size(inicon,2)}).*sp_14{i+no_add-size(inicon,2)};
```

```
end
```

A.2.4 MATLAB input script for 150 micron

```
function [Sp_14,Sp_28,Np_lay_14,Np_lay_28,dp,y] = micron150(D,rhop,rhof,L,thk,inicon,no_add)

dp = 150*10^-6;
n_150 = round(0.0254/(dp));
thk_150 = D/n_150;
y = thk_150:thk_150:D;%-D/n_150;

% wdth = 2*((D^2/4 - (y-D/2).^2).^0.5);
wdth = D;
% lgth = 1.778;
polyorder = 12;
vol_lay = L*thk*wdth;

data1 = load('concentration_150um.mat','cxls_Re14_5'); cxls_Re14{1} = data1.cxls_Re14_5;
data2 = load('concentration_150um.mat','cxls_Re14_20'); cxls_Re14{2} = data2.cxls_Re14_20;
data3 = load('concentration_150um.mat','cxls_Re14_30'); cxls_Re14{3} = data3.cxls_Re14_30;
data4 = load('concentration_150um.mat','cxls_Re28_5'); cxls_Re28{1} = data4.cxls_Re28_5;
data5 = load('concentration_150um.mat','cxls_Re28_20'); cxls_Re28{2} = data5.cxls_Re28_20;
data6 = load('concentration_150um.mat','cxls_Re28_30'); cxls_Re28{3} = data6.cxls_Re28_30;
data7 = load('concentration_150um.mat','yOD_Re14_5'); yOD_Re14{1} = data7.yOD_Re14_5;
data8 = load('concentration_150um.mat','yOD_Re14_20'); yOD_Re14{2} = data8.yOD_Re14_20;
data9 = load('concentration_150um.mat','yOD_Re14_30'); yOD_Re14{3} = data9.yOD_Re14_30;
data10 = load('concentration_150um.mat','yOD_Re28_5'); yOD_Re28{1} = data10.yOD_Re28_5;
data11 = load('concentration_150um.mat','yOD_Re28_20'); yOD_Re28{2} = data11.yOD_Re28_20;
data12 = load('concentration_150um.mat','yOD_Re28_30'); yOD_Re28{3} = data12.yOD_Re28_30;

% Preallocation *****************************************************
coeff_Re14 = cell(1,size(inicon,2)); coeff_Re28 = cell(1,size(inicon,2));
c_fittoxls_Re14 = cell(1,size(inicon,2)); c_fittoxls_Re28 = cell(1,size(inicon,2));
c_Re14 = cell(1,size(inicon,2)); c_Re28 = cell(1,size(inicon,2));
volp_14 = cell(1,size(inicon,2)); volp_28 = cell(1,size(inicon,2));
volf_14 = cell(1,size(inicon,2)); volf_28 = cell(1,size(inicon,2));
Np_lay_14 = cell(1,size(inicon,2)); Np_lay_28 = cell(1,size(inicon,2));
mp_14 = cell(1,size(inicon,2)); mp_28 = cell(1,size(inicon,2));
```

```
wp_14 = cell(1,size(inicon,2)); wp_28 = cell(1,size(inicon,2));
vp_14 = cell(1,size(inicon,2)); vp_28 = cell(1,size(inicon,2));
sp_14 = cell(1,size(inicon,2)); sp_28 = cell(1,size(inicon,2));
void_14 = cell(1,size(inicon,2)); void_28 = cell(1,size(inicon,2));
Vp_14 = cell(1,size(inicon,2)); Vp_28 = cell(1,size(inicon,2));
Sp_14 = cell(1,size(inicon,2)); Sp_28 = cell(1,size(inicon,2));

for i = 1:size(inicon,2)

    coeff_Re14{i} = polyfit(yOD_Re14{i},cxls_Re14{i},polyorder);
    coeff_Re28{i} = polyfit(yOD_Re28{i},cxls_Re28{i},polyorder);

    c_fittoxls_Re14{i} = polyval(coeff_Re14{i},yOD_Re14{i});        % c_fittoxls_Re14: The values of the
trendline @ Y/D values obtained from the Fluent
    c_fittoxls_Re28{i} = polyval(coeff_Re28{i},yOD_Re28{i});

    c_Re14{i} = polyval(coeff_Re14{i},y/D);                  % Particle Size = 5: fitted concentration
equation as a function of y/D
    c_Re28{i} = polyval(coeff_Re28{i},y/D);                  % Particle Size = 5: fitted concentration
equation as a function of y/D

    volp_14{i} = c_Re14{i} .* vol_lay;
    volp_28{i} = c_Re28{i} .* vol_lay;

    volf_14{i} = vol_lay.* (1-c_Re14{i});
    volf_28{i} = vol_lay.* (1-c_Re28{i});

    Np_lay_14{i} = volp_14{i}/(pi*dp^3/6);
    Np_lay_28{i} = volp_28{i}/(pi*dp^3/6);

    mp_14{i} = rhop * volp_14{i};
    mp_28{i} = rhop * volp_28{i};

    wp_14{i} = mp_14{i}./ (rhop*volp_14{i} + rhof * volf_14{i});
    wp_28{i} = mp_28{i}./ (rhop*volp_28{i} + rhof * volf_28{i});

    vp_14{i} = (wp_14{i}/(rhop))./(Np_lay_14{i}.*wp_14{i}/(rhop));          % vp: for each particle
    vp_28{i} = (wp_28{i}/(rhop))./(Np_lay_28{i}.*wp_28{i}/(rhop));
```

```
    sp_14{i} = (wp_14{i}./(rhop*dp))/(Np_lay_14{i}.*wp_14{i}/(rhop*dp));
    sp_28{i} = (wp_28{i}./(rhop*dp))/(Np_lay_28{i}.*wp_28{i}/(rhop*dp));

    void_14{i} = 1- c_Re14{i};
    void_28{i} = 1- c_Re28{i};

    Vp_14{i} = (1-void_14{i}).*vp_14{i};
    Vp_28{i} = (1-void_28{i}).*vp_28{i};

    Sp_14{i} = (1-void_14{i}).*sp_14{i};
    Sp_28{i} = (1-void_28{i}).*sp_28{i};

end
```

VITA

Reza Mohammadi Ziazi

Candidate for the Degree of

Master of Science

Thesis: COMPUTATIONAL APPROACHES TO OPTICAL MODELING NIR RADIATION PHENOMENA IN SLURRIES WITH ARBITRARY SOLIDS CONCENTRATION PROFILES

Major Field: Mechanical and Aerospace Engineering

Biographical:

Education:

Completed the requirements for the Master of Science in Mechanical and Aerospace Engineering at Oklahoma State University, Stillwater, Oklahoma in December, 2012.

Completed the requirements for the Bachelor of Science in Aerosapace Engineering at Amirkabir University of Technology (Tehran Polytechnic), Tehran, Iran in 2009.

Experience:

Research Assistant, Oklahoma State University (Dec. 2010- May 2012)

Professional Memberships:

Student Member, American Institute of Aeronautics and Astronautics (AIAA) – Sep. 2011

Student Member, American Society of Mechanical Engineers (ASME) – Sep. 2011

Member of Golden Key International Honor Society – Dec. 2011

Student Member, International Automation Society (IAS) – Sep. 2012

Member of the Honor Society of Phi Kappa Phi– Nov. 2012